Assessing Lanthanide-Dependent Methanol Dehydrogenase Activity and the Syntheses of Citrate-Based Siderophores

Manh Tri Phi

aus

Hanoi, Vietnam

2024

Dành tặng cho gia đình tôi.

„Wirkliches Neuland in einer Wissenschaft kann wohl nur gewonnen werden, wenn man an einer entscheidenden Stelle bereit ist, den Grund zu verlassen, auf dem die bisherige Wissenschaft ruht, und gewissermaßen ins Leere zu springen.“

Werner Heisenberg

Danksagung

Ich möchte mich als allererstes bei *Prof. Dr. Lena Daumann* bedanken. Ich danke dir für die Freiheiten und Möglichkeiten, die ich bei dir haben durfte und die daraus resultierende super lehrreiche und spannende Zeit. Es hat sich viel seit meinem Start in der Gruppe getan und ich bin froh, dass nicht nur ich, sondern wir alle die Veränderungen aktiv mitgestalten konnten und du unsere Meinungen bei deinen Entscheidungen berücksichtigt hast.

Prof. Dr. Konstantin Karaghiosoff danke ich für die Übernahme des Zweitgutachtens.

Ich bedanke mich bei den Mitgliedern der Prüfungskommission, *Prof. Dr. Alena Khmelinskaia, Prof. Dr. Anne Schütz, Prof. Dr. Thomas M. Klapötke* und *Dr. Pavel Kielkowski*, für die Mitwirkung an der mündlichen Prüfung.

Prof. Dr. N. Cecilia Martinez-Gomez, Dr. Nathan Good und *Alexa Zytnick* danke ich für die langjährige Kooperation. Ich bedanke mich bei *Prof. Paul V. Bernhardt* für die Möglichkeit ein Forschungsaufenthalt an der University of Queensland zu absolvieren und *Dr. Palraj Kalimuthu* für die praktische Einführung in die Protein-Elektrochemie. Ebenfalls bedanke ich mich bei *Dr. Sabine Schneider* und *Felix Zäh* für die Unterstützung bei der Proteinaufreinigung.

Bei *Lida Holowatyj, Beate Scholz* und *Birgit Carell* möchte ich mich für die Unterstützung und gewissenhafte Durchführung aller kleinen und großen bürokratischer Aufgaben bedanken.

Ich möchte mich ebenfalls bei den Personen am Department bedanken, die die Infrastruktur aufrechterhalten. Ohne deren Unterstützung, Einsatzbereitschaft und Wissen würden viele tägliche Abläufe nicht annähernd so einfach und unkompliziert ablaufen. Namentlich möchte ich vor allem *Brigitta Breitenstein* (NMR), *Heidi Buchholz* (Chemikalienausgabe), *Michael Gayer* (Entsorgung), *Jelina Geng* (Poststelle) und *Ronald Schürer* (Versorgung Gase und Reparatur Pumpen) hervorheben.

Des Weiteren bedanke ich mich bei meinem Praktikanten *Daniel Bejko*, Bachelorandin *Isabella Heinzelmann* und wissenschaftlichen Hilfskraft *Alishbah Maqsood* für die Unterstützung im Labor, die motivierte Arbeit, und anregenden sowie bereichernden Unterhaltungen über die Forschung und das Leben.

Ein besonderer Dank gilt dem Labor D3.062 mit seinen ehemaligen Mitgliedern Dr. Henning Widmann, Dr. Bérénice Jahn, Dr. Helena Singer und Michael Mertens für die lustige und amüsante Zeit im Labor. Natürlich geht auch ein Dank an alle ehemaligen und aktuellen Laborkollegen und -kolleginnen Ioana Ciubotaru, Philippe de Bary, Sophie Gutenthaler-Tietze, Rachel Janßen, Dr. Niko Lindlar, Annika Menke, Doreen Reuter und Dr. Violeta Vetsova: Vielen Dank für die tolle Zeit im Arbeitskreis, die täglichen

Diskussionen über wirklich alle möglichen Themen, die Kaffee- und Kuchenpause, die gemeinsamen Spieleabenden, Partys, Bierpong-Matches, Gossip- und Ranting-Austauschrunden, und fachlichen sowie privaten Ratschlägen in und für alle Lebenssituationen.

Der btS – Life Science Studierendeninitiativen e.V. und deren Mitgliedern möchte ich mich für den Ausgleich zur Promotion bedanken. Ich habe in den letzten, vor allem letzten zwei Jahren, unglaublich viel im studentischen Ehrenamt gelernt und viele neue Freundschaften in ganz Deutschland geschlossen. Ein großes Danke geht an das BV-Team 2022 und 2023. Trotz vieler Herausforderungen hat es mir sehr viel Spaß gemacht mit euch den Verein zu leiten und voranzubringen.

Ich danke meinen langjährigen Freunden sowohl in Dresden als auch in München, die ich teilweise schon über die Hälfte meines Lebens kenne. Vielen Dank für die beruhigenden Worte während herausfordernden Zeiten, dass ihr immer ein offenes Ohr hattet und wusstet wie ihr mich aufheitern konntet. Besonders möchte ich meinen Freunden in Dresden danken, die ich seit der Schulzeit kenne. Ihr habt mir sowohl während des Studiums als auch in meiner Promotionszeit immer das Gefühl gegeben, dass ich jederzeit bei euch willkommen bin. Ich hatte bei meinen Besuchen nie das Gefühl, dass ich jemals aus Dresden weggezogen bin und dafür bin ich euch unendlich dankbar.

Lời cảm ơn đặc biệt gửi đến gia đình tôi. Nếu không có quyết định dũng cảm của bố mẹ khi chuyển đến một quốc gia mà ở đó không nói được ngôn ngữ để tạo ra một tương lai tốt hơn cho con cái mình, thì con đã không thể ở đây. Sự kiên trì, sự hy sinh và lạc quan của bố mẹ chỉ là một số ít các phẩm chất mà con đã học được từ bố mẹ. Con rất vui vì có bố mẹ và hy vọng bố mẹ tự hào về con. Huy, danke, dass du meine Späße mitmachst und immer für mich da bist.

Meine liebste Charlotte, vielen Dank, dass du mich in jeder Lebenssituation unterstützt und immer für mich da bist. Ich freue mich sehr auf unsere gemeinsame Zukunft.

Publications

Publications released as part of this thesis:

Activity assays of methanol dehydrogenases

Sophie Marie Gutenthaler, <u>Manh Tri Phi</u>, Helena Singer, and Lena J. Daumann*

Methods in Enzymology **2021**, *650*, 57–79, DOI: 10.1016/bs.mie.2021.01.045

Discovery and characterization of the first known biological lanthanide chelator

Alexa M. Zytnick, Sophie M. Gutenthaler-Tietze, Allegra T. Aron, Zachary L. Reitz, <u>Manh Tri Phi</u>, Nathan M. Good, Daniel Petras, Lena J. Daumann*, N. Cecilia Martinez-Gomez*

bioRxiv **2022**, DOI: 10.1101/2022.01.19.476857

Assessing Lanthanide-Dependent Methanol Dehydrogenase Activity: The Assay Matters

<u>Manh Tri Phi</u>, Helena Singer, Felix Zäh, Christoph Haisch, Sabine Schneider, Huub J. M. Op den Camp, Lena J. Daumann*

ChemBioChem **2024**, *25*, e202300811, DOI: 10.1002/cbic.202300811

*Corresponding author/s

Conferences

07/2022	Poster presentation at the 16th European Biologic Inorganic Chemistry Conference (EuroBIC-16), Grenoble, France
09/2022	Poster presentation at the 31st Terrae Rarae, Leipzig, Germany
07/2023	Poster presentation at the 20th International Conference on Biological Inorganic Chemistry (ICBIC20), Adelaide, Australia

Summary

The discovery of lanthanide(Ln)-dependent and -utilizing microorganisms marked a pivotal moment in bioinorganic chemistry. More and more Ln-dependent and -utilizing bacteria have been discovered in a huge variety of ecosystems, ranging from marine environments, the phyllosphere to geothermal fields. Most of these bacteria are methylotrophs or methanotrophs and use C_1-molecules for their metabolism and energy source. A central enzyme is methanol dehydrogenase (MDH), which catalyzes the conversion of methanol into formaldehyde. Two cofactors are present in the active site of MDH: pyrroloquinoline quinone and a metal ion, which can be either Ca^{2+} or Ln^{3+}. While the Ca-containing MxaFI-MDH has been extensively studied in the last decades, Ln-containing XoxF-MDH has recently sparked a lot of interest. The Ln-MDH from extremophile *Methylacidiphilum fumariolicum* SolV is able to incorporate a variety of Lns. **The underlying enzyme mechanism is still debated in the literature and factors influencing the enzyme activity is still underexplored. Therefore, part of this work focused on the elucidation of mechanistic details and the impact of metal ion on the enzyme activity by comparing the enzyme activity of different Ln-MDHs.** SolV was used as the model organism and large-scale cultivation of SolV under laboratory conditions was established. Using fast protein liquid chromatography, eight different Ln-MDHs (Ln = La, Ce, Pr, Nd, Sm, Eu, Gd and Tb) were purified. UV/Vis spectroscopy, SDS-PAGE and ICP-MS were used to confirm functional Ln-MDH. Then, activity assays were used to assess enzyme activity. The widely used dye-coupled assay employs redox-active dyes to assess the enzyme activity. By using the native electron acceptor cytochrome c_{GJ} from Ln-MDH, a protein-coupled assay was developed to complement the dye-coupled assay. Depending on the assay, contrasting trends among the Ln-MDHs were observed, indicating that the assays measure different aspects of the mechanism. Further methods were developed to assess and compare the enzyme activity of Ln-MDHs. Isothermal titration calorimetry was successfully used to compare the enzyme activity of Pr- and Eu-MDH. Protein electrochemistry can be used to investigate the enzyme activity of Ln-MDHs. The established protocol to prepare electrodes containing Ln-MDH and cytochrome c_{GJ} was revisited to overcome previously encountered mass transport limitations. Additionally, kinetic isotope experiments with dye- and protein-coupled assay revealed intriguing contrasting results. Using the dye-coupled assay, the enzyme activity decreases with higher D_2O concentration in solution. However, the addition of D_2O to the protein-coupled assay increased the enzyme activity more than two-fold.

Methylorubrum extorquens AM1 is another Ln-utilizing bacterium that has garnered lots of interest. Recent studies have shown a TonB-ABC-like pathway for its uptake of Lns. **TonB-dependent transporters are often used by siderophores to transport essential Fe^{3+} into the cell. It was hypothesized that a lanthanide-specific chelator –lanthanophore– exists. Therefore, the goal was to**

identify and characterize a lanthanophore from AM1. Bioinformatic investigations by collaborators revealed several citrate-based siderophores as candidate for a lanthanophore. Aerobactin and rhodopetrobactin B were successfully synthesized and their affinity for Fe^{3+} and Ln^{3+} characterized by spectroscopic methods. In the end, a lanthanophore was identified which is structurally very close to rhodopetrobactin B.

Table of Content

I. Introduction

1. Rare Earth Elements in Biochemistry

The rare earth elements (REEs) are a group of 17 elements that consists of the 15 lanthanides (Lns) (Figure I-1) as well as scandium (Sc) and yttrium (Y). They are further divided into light REE (LREE, La–Eu) and heavy REE (HREE, Gd–Lu).[1] (The radioactive promethium (Pm) is extremely rare and is not included in general discussions about Lns). The name is misleading, as most of the REEs are more abundant and widely distributed in earth's crust than metals like copper or zinc but mineable concentrations are *rarer* than for other ores.[2] Under ambient conditions, the REEs exhibit similar chemical properties: they are Lewis acidic, kinetically labile, display a chemically stable +3 oxidation state and typically have coordination numbers (CN) between 8 and 12.[3] Due to the population of the 4f-electron shell, the atomic and ionic radii gradually decreases along the lanthanide (Ln) series which is known as Ln contraction. Due to the Ln contraction the Lewis acidity gradually increases along the Ln series. The REEs are indispensable for a multitude of our modern technologies and are rightfully coined the "vitamins of modern industry".[4] They are integral parts in many high-technology electronics such as TV screens, computers, smartphones and silicon chips.[4b] Furthermore, Lns are also widely used as catalysts, as part of hybrid cars batteries, in medicine as a contrast agent in magnetic resonance imaging, as part of X-ray tubes and are also employed in radiotherapy.[1, 5] The global production of rare earth oxides (REOs) has more than tripled in the past two decades from 95000 t (2003) to 350000 t (2023), clearly indicating a high demand for REE. China remains the leading country for REO production (70%) followed by US (12%) and Myanmar (11%).[6] Despite their high abundance in earth's crust, the low solubility of their oxides, phosphates and carbonates rendered them poorly bioavailable and thus the research field remained underexplored.[7]
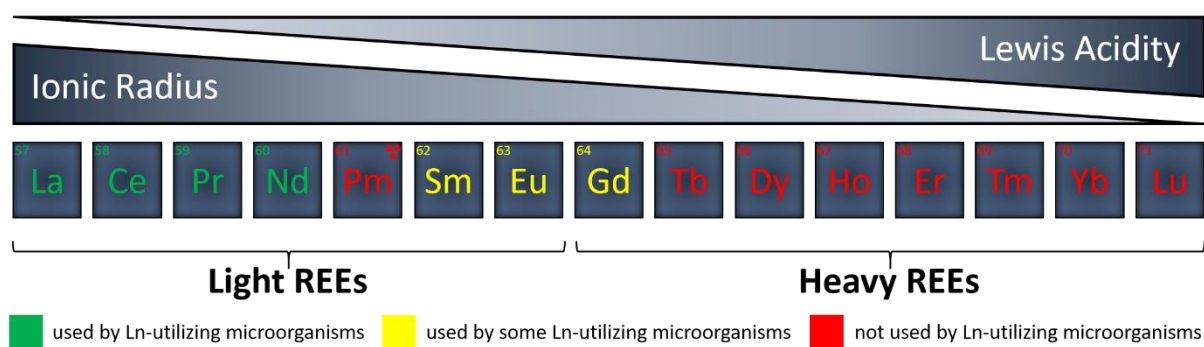
Figure I-1 Overview of the lanthanides (Lns). The Lns are divided into light (La–Eu) and heavy (Gd–Lu) rare earth elements. The ionic radius decreases across the lanthanide (Ln) series concomitant to the increase of the Lewis acidity. Most Lns display a chemical stable +3 oxidation state. Ce and Eu can also be found at +4 and +2 oxidation state.[8] Pm has no stable isotopes and is not investigated. Ln-utilizing microorganisms preferably utilize the early Lns for growth while growth with later Lns is impaired.[2a]

In 2011, Hibi *et. al* showed in a methylotrophic bacterium that La^{3+} induces the activity of a methanol dehydrogenase (MDH) which is essential for its one-carbon metabolism.[9] Shortly afterwards, the same research group reported the first strictly La^{3+}-dependent MDH that is essential for bacterial growth.[10] These findings paved the way for the new emerging research area of lanthanide metallobiochemistry.[2a] Prior to these findings, lanthanides and their spectroscopic and physical properties have been used in biochemistry for NMR studies, luminescent probes, protein coexpression probes, X-ray crystallography as well as a substitute for Ca^{2+} in metalloenzymes to characterize metal ion binding sites in enzymes.[8, 11] The trivalent Lns can replace the divalent Ca^{2+} due to their similar chemical properties. Both metal ions are similar in their ionic radii (Ca^{2+} = 1.0 Å and 1.18 Å, La^{3+} = 1.03 Å and 1.22 Å for CN 6 and 9, respectively), coordination environment, prefer the same ligands and are strong Lewis acids.[8] However, Lns have a higher CN compared to Ca^{2+} and their higher Lewis acidity make them more efficient catalysts for enzymatic hydrolysis reactions.[7] Since the discovery of the Ln-dependent MDH, the field has expanded rapidly into different research areas and it is now firmly established that Lns are biological relevant. A variety of Ln-dependent or -utilizing bacteria have been found and investigated in various ecosystems, e.g. volcanic mudpot, marine environments and the phyllosphere.[10, 12] These bacteria are mostly either methylotrophs or methanotrophs, thus utilizing C_1-molecules such as methane, methanol and methylated amines and sulfur species as their energy source.[13] Methanotrophs oxidize methane to methanol by particulate methane monooxygenase or soluble methane monooxygenase, followed by the oxidation to formaldehyde by MDH.[14] Genomic analyses have revealed two distinct variants of this MDH: the extensively studied Ca^{2+}-dependent MxaFI-MDH and the Ln^{3+}-dependent XoxF-MDH. All methanotrophs that express Ca-MDH also have the gene encoding for Ln-MDH.[13] However, studies have reported methano- and methylotrophs that solely express Ln-MDH, underscoring the broad occurrence of Ln-utilizing bacteria. Depending on the available Lns, XoxF-MDH can incorporate different Lns in the active site to attain the respective Ln-MDH. These findings are supported by a metaproteogenomic study revealing that Ln-MDH is one of the most prevalent proteins in the plant phyllosphere.[15] Moreover, phylogenetic analysis identified at least five distinct clades of XoxF with multiple divergent homologs while certain genomes only encode one MxaF copy.[16] Phylogenetic and genetic analysis across methano- and methylotrophs also suggest that Ln-MDH evolutionary precedes Ca-MDH and that most MDHs are XoxF proteins.[13, 17] If an bacterium has both Ca- and Ln-MDH, the Ca-MDH will be expressed if no Ln is available. However, even nanomolar amounts of Ln are sufficient to trigger the "lanthanide switch", leading to the preferred expression of the Ln-MDH variant even if the concentration of Ca^{2+} is 100-fold higher.[1, 18] Apart from the metal ion, the active site of the enzyme also contains the second cofactor pyrroloquinoline quinone (PQQ) that is crucial for the enzyme activity.[12b] The *xoxF* and *mxaF* gene share less than 50% sequence identity but the crucial residues for PQQ, metal binding and catalysis are

conserved in both enzymes.[15, 17] One significant difference within the active site is the additional metal-coordinating Asp residue found in Ln-MDH (Figure I-2). The Asp residue is essential for metal coordination and satisfies the higher CN preferences of Lns.
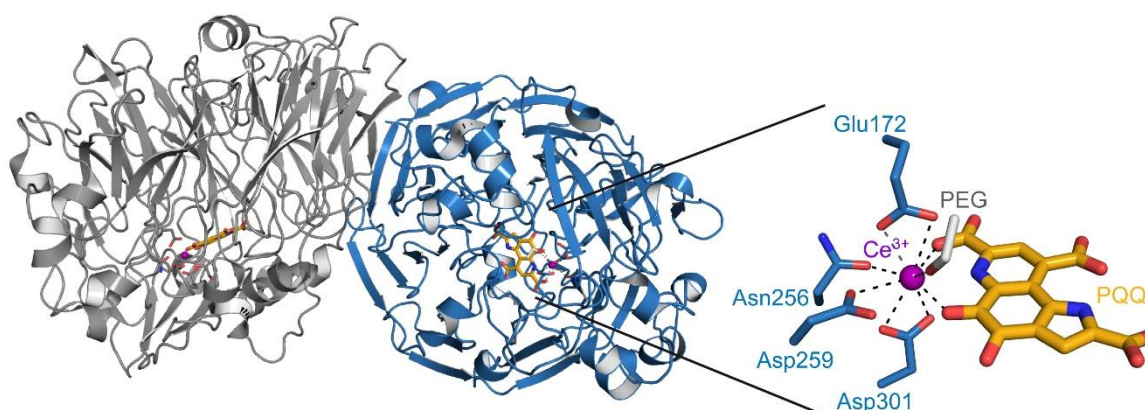
Figure I-2 The homodimeric structure and active site of Ce-MDH from *M. fumariolicum* SolV (PDB: 4MAE).[12b] The additional meta-coordinating Asp301 residue is essential for the enzyme activity of Ln-MDH. A polyethylene glycol (PEG) molecule (from the crystallization buffer) occupies the substrate binding position. Figure reprinted from Phi *et al*.[19]

Through site-directed mutagenesis, Good *et al*. exchanged this essential Asp for Ala and showed that this mutant strain is not able to grow with methanol and La^{3+}, indicating a loss of enzymatic function.[20] Two mechanisms for methanol oxidation are discussed in literature by experimental and computational research groups: the addition-elimination and hydride transfer mechanism (Figure I-3).[20b, 21]
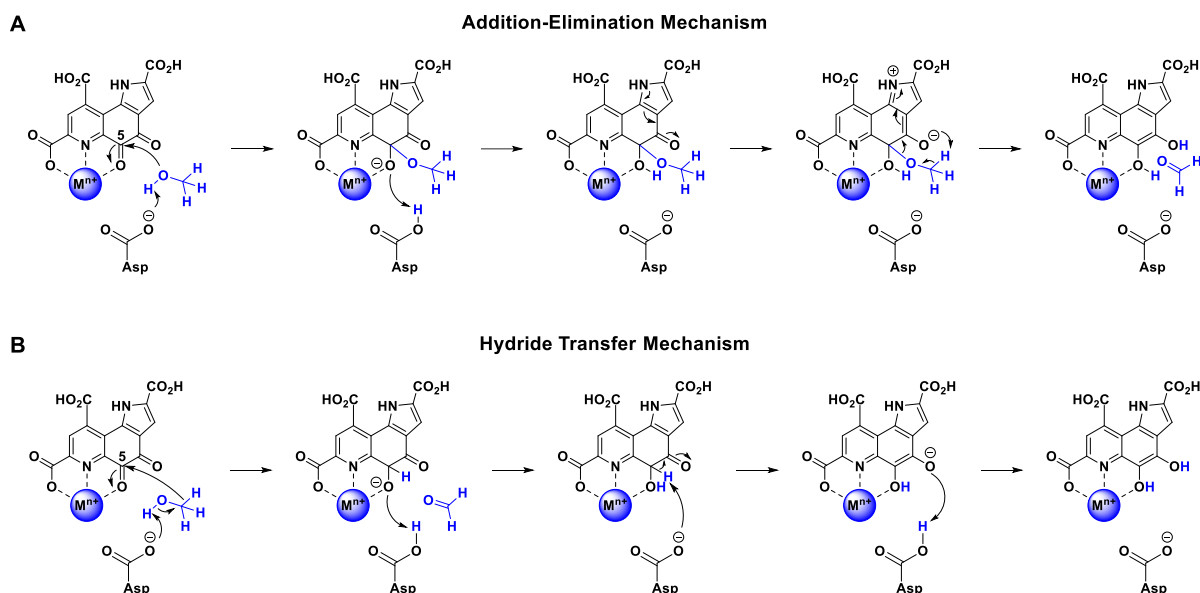
Figure I-3 The A) addition-elimination and B) hydride transfer mechanisms are discussed in the literature for the substrate oxidation in MDH.[22] C5 of PQQ was omitted after the first step for clarity. M^{n+} refers to the Lewis acid and can be Ca^{2+} or Ln^{3+}.

Both mechanisms require the activation of the PQQ C5 carbonyl bond by a Lewis acid. The hydride transfer mechanism suggests a concerted process where a hydride ion is directly transferred from the

substrate to the C5 of PQQ, along with the proton abstraction of the substrate by the catalytic Asp residue. The addition-elimination mechanism proposes that the substrate directly adds to the PQQ C5 carbonyl to form a hemiketal intermediate, followed by the release of the product.[21b, 21c] As the Lewis acidity steadily increases across the Ln series, the enzyme activity should also increase accordingly if PQQ activation by the metal ion is the sole factor impacting the substrate turnover. This assumption was disproved, as several studies that used a dye-coupled assay to assess the enzyme activity of Ln-MDH have shown that the enzyme activity for Ln-MDH containing early Lns (La–Nd) is higher than for the late Lns (Sm–Lu).[19, 20b, 23] Moreover, the same trend was observed with heterologously expressed, empty XoxF-MDH that was reconstituted with PQQ and Lns.[24]

Other biomolecules involved in Ln-uptake, transport, trafficking and storage that utilize Lns have been identified and characterized, collectively forming the lanthanome. Ln-dependent ethanol dehydrogenases have been identified and characterized in *Methylorubrum extorquens* AM1 and *Pseudomonas putida* KT2440, expanding the Ln-dependent metabolism to multicarbon sources.[18c] Lanmodulin (LanM), a highly selective Ln-binding protein consists of four metal-binding EF hand motifs, that are usually found in Ca^{2+}-binding proteins, and undergoes large conformational changes upon Ln binding. LanM responses to picomolar concentration of Lns and possess a 10^8-fold higher selectivity towards Lns over Ca^{2+}.[25] While LanM has demonstrated high potential in selective separation and recovery of REEs, its role in biological systems remains elusive.[26] Lanpepsy (LanP) is a periplasmic protein found in *Methylobacillus flagellates* that is hypothesized to be involved in Ln binding as dye competition assays and isothermal titration calorimetry have revealed multiple Ln binding sites.[27] The first lanthanophore (low-molecular Ln binding chelator) named Methylolanthanin (MLL) has been identified and isolated from *Methylorubrum extorquens* AM1. MLL has the capability to bind La^{3+}, Nd^{3+} and Lu^{3+}, scavenge Lns from the environment and significantly increases the growth yield of a mutant strain from AM1.[28]

2. Rare Earth Elements in Methylotrophy

2.1 *Methylacidiphilum Fumariolicum* SolV

Methylacidiphilum fumariolicum SolV is a fascinating and unique organism that belongs to the group of acidophilic methanotrophs. Discovered in the hot, acidic mudpots of the Solfatara, a volcano crater in Italy, this extremophile has garnered significant interest due to its ability to thrive in a harsh environment characterized by temperature reaching up to 70 °C and extremely low pH levels, dropping to as low as 1.[12b, 29] SolV uses methane as its energy source, abundantly emitted by the fumaroles around the crater at an estimated rate of 200 kg per km² daily.[30] Methane is converted to methanol by a methane monooxygenase and subsequently oxidized to formaldehyde which is either assimilated

or oxidized to CO_2.[31] The oxidation of methanol to formaldehyde, is catalyzed by a XoxF-MDH, a Ln ion and the cofactor PQQ. As a result of methanol oxidation, PQQ is reduced to pyrroloquinoline quinol ($PQQH_2$) which is re-oxidized after a step-wise single electron transfer to two separate molecules of cytochrome c_L, which itself is regenerated through an additional electron transfer to cytochrome c_H.[12b, 32] Nearly all methylotrophic bacteria possess these two periplasmic, c-type cytochromes. The cytochromes were assigned according to their isoelectronic points (p*I*), with p*I* being lower for c_L and higher for c_H. Only c_L can get reduced by MDH.[31] In SolV, the cytochrome c_L is referred to as cytochrome c_{GJ} (cyt c_{GJ}) and comprises of XoxG cytochrome coupled with the periplasmic binding protein XoxJ.[32] Cyt c_{GJ} is the first reported cytochrome from a purely Ln-dependent methylotroph and serves as the direct electron acceptor for its XoxF-MDH. Cytochromes typically exhibit a reddish-brown color in solution which is caused by their iron-containing heme groups, but cyt c_{GJ} exhibits a red-shifted absorbance spectrum leading to a yellow color in solution.[33] Further spectroscopic methods have revealed characteristic Soret and α-bands at 440 nm and 595 nm, respectively, and variable temperature variable field magnetic circular dichroism identified the presence of a low spin iron heme.[32] Kalimuthu *et al*. have also reported a temperature-dependent activity of cyt c_{GJ} in an electrochemical experiment.[34] The growth rate of SolV varies with the added Ln and its concentration in the growth medium.[12b, 19, 35] Growth rates with early Lns (La–Nd) exceed those with Gd^{3+} by more than double the amount and display a proportionally increase from 0 to 80 nM as seen with Ce^{3+}.[12b] Remarkably, SolV is also able to grow with the two actinides (Ans) americium and curium. If a mixture of equimolar amount of all Lns and these two Ans are added to the growth medium, SolV preferably takes up the early Lns, showing the highest depletion (80%) from the medium for La^{3+}. SolV can selectively extract early Lns from industrial waste and post-mining waters with minimal sample preparation, showcasing its promising platform for the bio-recovery or REE.[35]

2.2 *Methylorubrum Extorquens* AM1

The methylotrophic bacterium *M. extorquens* AM1 is another important model organism that resurfaced as a central object of investigation after the discovery of the Ln-dependent XoxF-MDH and its Ln-utilizing and -associated proteins has been extensively investigated. AM1 and its metabolism has been researched for over 60 years.[36] The function and role of the abundantly expressed *xoxF* gene in many *Methylobacteria* and other non-methylotrophic bacterial phyla has long been debated without reaching a definite conclusion.[13, 15] Only the discovery of the Ln-dependent XoxF-MDH in 2011 provided crucial insights into the function of *xoxF*.[9] Following this finding, genome sequencing revealed that AM1 is able to express both XoxF- and MxaFI-MDH and readily switches to the XoxF-MDH in the presence of just 2.5 nM Ln, achieving maximum growth rate and yield above 1 µM. AM1 is able

to grow using the early Lns (La, Ce, Pr, Nd) as well as Sm.[18a] Furthermore, a Ln-dependent ethanol dehydrogenase from AM1 was isolated and characterized as well.[18c] Comprehensive transposon mutagenesis and growth studies have elucidated the mechanism for uptake, transport and storage of Lns (for details refer to chapter 1.4), providing valuable insights into the broader implication of Ln biochemistry and how microorganisms interact with Lns. A recent study has identified and isolated the first Lanthanophore, a small molecule that binds Lns, that is most likely involved in mobilization of insoluble Lns and transport into the cell. The discovery of the highly selective Ln-binding protein LanM from AM1 has launched new methods for the selective bio-recovery of REE from electronic and industrial waste.[26a, 37]

3. Methods for Assessing Methanol Dehydrogenase Activity

The Ca-MDH has been extensively studied by Christopher Anthony and coworkers throughout the 60s to 90s.[38] They have developed dye-coupled as well as protein-coupled assays to assess the enzyme activity of Ca-MDH, extensively outlined as a chapter in the book series Methods in Enzymology (Volume 188).[39] The emergence of Ln-dependent MDH has sparked a resurgence in the field of MDHs and the need of reliable assays to accurately assess and compare enzyme activities between different Ln-MDHs was evident. We have revised these methods by Anthony and coworkers and captured the most essential developments to assess MDH activity in the last decades in Methods in Enzymology (Volume 650).[40]

In the past decades, four activity assays have been established that can be categorized in dye-coupled (Figure I-4) and protein-coupled assays (Figure I-5). The protein-coupled assays employ the physiological cytochrome of the respective MDH as electron acceptor in tandem with commercially available cytochrome *c* from equine or bovine heart to re-oxidize the physiological cytochrome. On the other hand, dye-coupled assays use small molecules as artificial electron acceptor for MDH. The most widely performed activity assay uses the artificial electron acceptors phenazine ethosulfate (PES) and 2,6-dichlorophenol indophenol (DCPIP). After oxidation of the substrate, the electrons are transferred to the redox dye DCPIP through the primary electron acceptor PES. The reduction of DCPIP leads to its discoloration and can be monitored spectroscopically. PES and DCPIP are commercially available and inexpensive. Additionally, the are unspecific electron acceptors and can be applied to any MDH irrespective of origin. The radical cation of *N,N,N',N'*-tetramethyl-*p*-phenylenediamine (TMPD) is also called Wurster's Blue (WB) and was used as electron acceptor and redox dye in the past.[41] Unlike PES/DCPIP, WB has to be prepared from its TMPD precursor by using a freshly prepared bromine solution which can be impractical for biochemistry labs.[42] Likewise, the enzyme activity can be monitored by UV/Vis spectroscopy. A common drawback for dye-coupled assays is the high light-

sensitivity of these redox dyes. Ensuring minimal light exposure at any point during preparation and measurement is crucial to obtain reliable data, adding another layer of challenge to these methods. In addition, a non-physiological pH of 9 and additives and activators like ammonia, glycine ethyl ester and potassium cyanide are added to the assay mixture which do not reflect the conditions in the cell, making data interpretation challenging.[42]
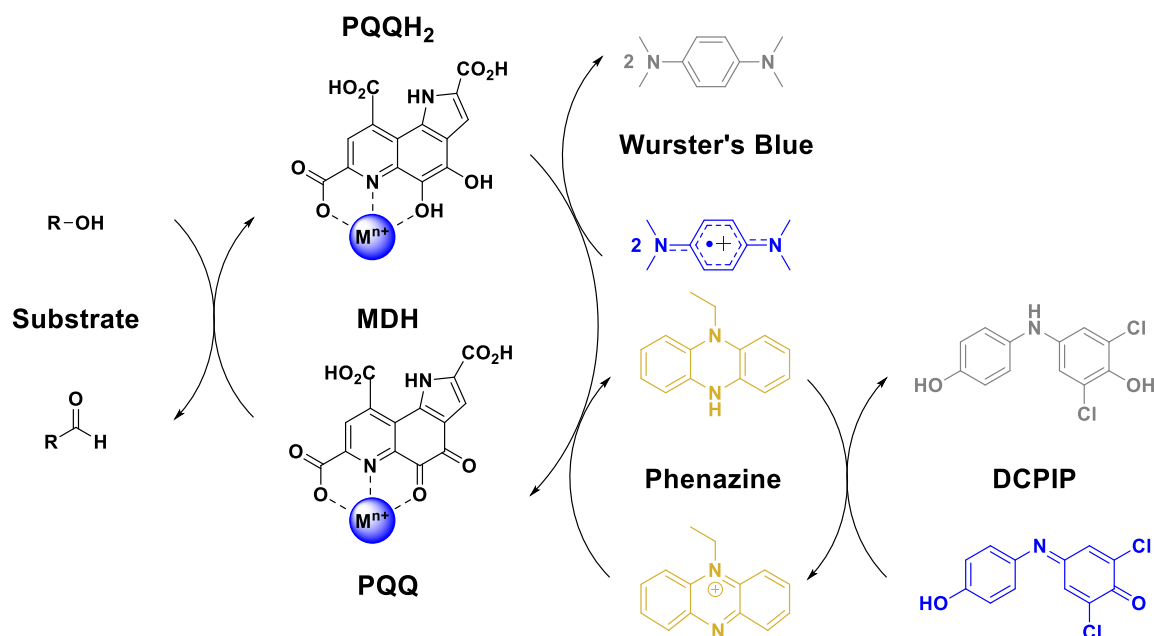
Figure I-4 Overview of the dye-coupled activity assays for methanol dehydrogenase. Wurster's Blue is reduced by PQQH$_2$, leading to its discoloration. The discoloration of DCPIP is caused by PES-mediated reduction. Adapted from Gutenthaler *et al*.[40]

Beardmore-Gray *et al.* have introduced a protein-coupled assay to assess the enzyme activity of Ca-MDH.[43] The physiological cytochrome c_L was coupled to the commercially available cytochrome *c* from equine heart to determine the enzyme activity of Ca-MDH. The reduction of cytochrome *c* by cytochrome c_L can be monitored by UV/Vis spectroscopy. Then, Kalimuthu *et al.* have developed a method to electrochemically assess the enzyme activity of Ln-MDH.[34] Here, Eu-MDH from *M. fumariolicum* SolV and its native cytochrome c_{GJ} were adsorbed with the biopolymer chitosan onto an gold electrode. Instead of a secondary cytochrome, the current was measured to determine the enzyme activity. A major challenge of the protein-coupled assays is the additional isolation and purification of the cytochrome which can require significant more time as cytochromes are usually not abundantly expressed in cells like MDH is. Another limitation is the specificity of the cytochrome to its MDH, although Beardmore-Gray *et al.* reported one instance were the cytochrome c_L from *M. extorquens* is able to interact with the Ca-MDH from two other species as well.[43] Utilizing the physiological cytochrome as electron acceptor brings the experiment closer to cellular conditions and since none of the assay components are light-sensitive, performing experiments and interpreting the data is more consistent and reliable.
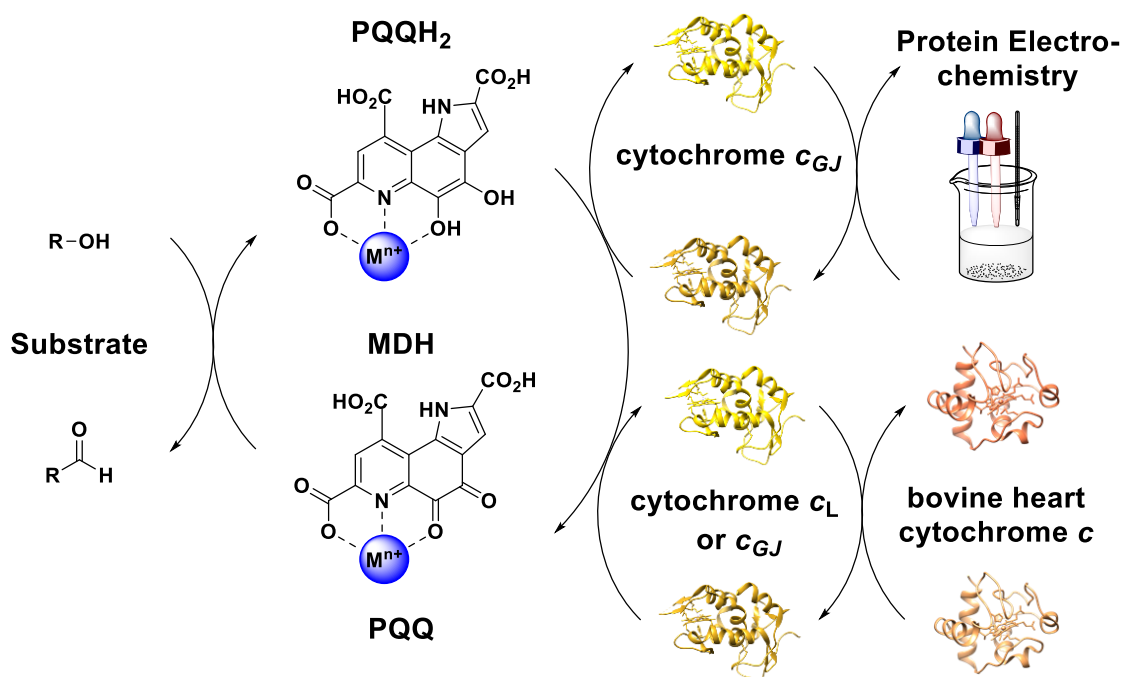
Figure I-5 Overview of the protein-coupled activity assays for methanol dehydrogenase. The physiological electron acceptor cytochrome c_{GJ} (cyt c_{GJ}) (PDB: 6ONQ) is used to re-oxidize PQQH$_2$. Cytochrome c from bovine heart (PDB: 6FF5) is used as the secondary cytochrome and spectroscopic read-out. For Ln-MDH from *M. fumariolicum* SolV and cyt c_{GJ} an electrochemical assay has been reported.[34] Protein structures were generated with Chimera. The crystal structure of cytochrome XoxG from *M. extorquens* AM1 was used for cyt c_{GJ} because no structure has been reported so far.

4. Uptake, Transport and Storage of Lanthanides and their Role in Gene Regulation

Pol *et al.* recovered the strictly Ln-dependent bacterium *M. fumariolicum* SolV from the Solfatara crater in Italy which only grew under laboratory conditions after its original, Ln-rich volcanic mudpot water was added to the growth medium.[12b] Since then, researchers have found more and more examples of strictly Ln-dependent and -utilizing microorganisms.[44] The exact mechanism of Ln-uptake, transport and storage remains largely elusive. The research groups around Cecilia Martinez-Gomez, Elizabeth Skovran, Janosch Klebensberger and Julia Vorholt found evidence that the TonB-ABC pathway is involved in the Ln-uptake, mirroring the mechanism by which siderophores, Fe^{3+}-chelating small molecules, mobilize Fe^{3+} for cellular uptake.[45] Indeed, Zytnick *et al.* have identified the first lanthanophore, a Ln^{3+}-binding small molecule, from *M. extorquens* AM1. Methylolanthanin (MLL) is able to bind La^{3+}, Nd^{3+} and Lu^{3+} and significantly increases the growth yield of an AM1 mutant strain.[28] Import of extracellular Ln into the periplasm by a TonB-dependent mechanism has long been hypothesized and was confirmed in *M. extorquens* AM1 by Roszczenko-Jasińska *et al.* using transposon mutagenesis screens and knockout strains.[46] Once the lanthanophore-bound Ln is transported into the periplasm, it is predicted to enter the cytoplasm through an inner membrane transport system. Transmission electron microscopy revealed that La^{3+} accumulates as phosphate crystals in the cytoplasm.[46] Additionally, the REE hyperaccumulator fern *Dicranopteris linearis* possesses the

transporter NREET1 that is mainly localized in the plasma membrane of the roots. NREET1 is able to selectively translocate REE from the root cell walls into the cytoplasm and demonstrating a higher preference for LREE over HREE.[47]

The Ln switch, the activation of Ln-MDH expression and suppression of Ca-MDH in the presence of Lns, was the first example of the gene regulating effect of Lns.[1, 18] Further studies have shown that the genetic regulation is more complex than initially outlined. In *Methylosinus trichosporium* OB3b, the Ln switch is completely negated by the presence copper which functions as the cofactor for particulate methane monooxygenase that facilitates the conversion of methane to methanol.[48] The co-expression of both Ca- and Ln-MDH is also possible and was observed in *M. trichosporium* OB3b and *Methylomonas* sp. strain LW13 when Ca^{2+} and Ce^{3+} were added to the growth medium.[49] Furthermore, deletion of the *xoxF* gene in *Methylobacterium aquaticum* 22A and *M. extorquens* AM1 prevented growth in the presence of Ca^{2+} due to the lack of Ca-MDH expression.[50] Zytnick *et al.* have shown that even the solubility of the Ln source can drastically impact the genetic network and growth. Almost 1500 genes of *M. extorquens* AM1 were differentially expressed when exposed to soluble $NdCl_3$ or poorly soluble Nd_2O_3.[28] Gorniak *et al.* have conducted differential gene expression analysis and reported that the gene expression of *Beijerinckiaceae* RH AL1 varies depending on the La^{3+} concentration (50 nM vs. 1 µM) and type of added Ln (La^{3+} vs. Nd^{3+} vs. Ln cocktail containing Ce^{3+}, Nd^{3+}, Dy^{3+}, Ho^{3+}, Er^{3+} and Yb^{3+}). Up to 41% of genes demonstrated altered expression levels in response to different Lns, indicating that different Lns affect different genes. The expressed genes were linked to a wide range of biological processes of the Ln-dependent metabolism but also span other cellular functions like the flagellar and chemotactic machinery, secretion and uptake system.[51]

5. Biological Role of Siderophores

Similar to Lns, iron is widely distributed in earth's crust, but often exists in insoluble forms and is not readily available. Iron is an essential element for all living organism and is involved in a broad range of metabolic processes like oxygen transport, DNA synthesis, electron transport, cofactor for enzymatic reactions and synthesis of amino acids and vitamins.[52] Siderophores are small, high-affinity Fe^{3+}-chelating molecules that are produced and secreted into the extracellular environment by microorganism and plants and play an essential role in the sequestration of insoluble Fe^{3+}. Then, the siderophore-Fe^{3+} complex is transported across the outer membrane into the host by an active transport system.[53] Since the discovery of siderophores in the 1950s, they have been extensively studied.[54] There are more than 500 known siderophores that typically form saturated hexadentate complexes with Fe^{3+}, but coordinatively unsaturated complexes are also known.[45b, 55] Pyochelin, a tetradentate dimer, and cepabactin, a bidentate monomer, both strongly bind Fe^{3+}, albeit with

generally lower stability constants compared to their coordinatively saturated counterparts.[56] The majority of siderophores can be structurally divided into four major classes (Figure I-6).
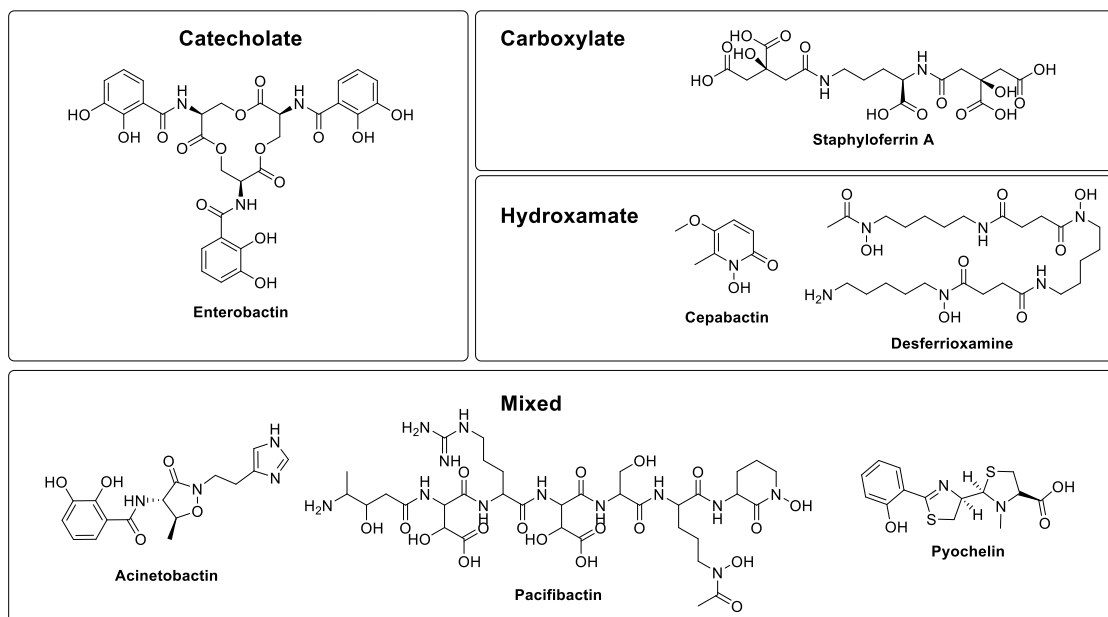
Figure I-6 Overview of the four main classes of siderophores. Siderophores are categorized based on the chemical structure of their metal-binding groups.

Although siderophores have a high affinity towards Fe^{3+}, Captain *et al.* reported a chelator-protein system consisting of the protein siderocalin and siderophore enterobactin that is able to form complexes with the lanthanide Eu^{3+} and Ans [Am^{3+}, Cm^{3+}, Th^{34} and Pu^{4+}] as well.[57] Furthermore, Hardy and Butler employed bioinformatic methods and identified the novel siderophore pacifibactin that possesses four bidentate chelating groups (two hydroxamic acid and two β-hydroxyaspartic acid groups). Out of the four chelating groups, the cyclized N^5-hydroxyornithine residue is not involved in Fe^{3+} complexation as shown by ^{13}C NMR experiments with the Fe^{3+} surrogate Ga^{3+}.[58] The remaining hydroxamate might be involved when metal ions with the preference for higher CN like Ln are present. The biological role of siderophores goes beyond "iron acquisition". Sideromycins, which consists of a siderophore and an antibiotic moiety, are secreted by bacteria to invade other microorganisms, disrupt their cell membrane and gain competitive advantage. [59]

II.   The Syntheses of Citrate-Based Siderophores

1. Introduction

In the last decades, siderophores and their essential biological role as low-molecular weight scavenger for Fe^{3+} for microorganism have been extensively investigated and are critical in facilitating the uptake and transport of this essential metal under iron-limiting conditions.[53] Since the discovery of the first strictly Ln-dependent bacterium, more and more species have emerged as Ln-utilizing microorganisms. The first studies have given insights into uptake, trafficking and storage of Lns. Research group around Cecilia Martinez-Gomez, Elizabeth Skovran and Janosch Klebensberger provided evidence that a TonB-ABC-like pathway is involved in the Ln-uptake which resembles the transport of Fe^{3+} into the cell by siderophores.[46, 60] A new class of polydentate ligands –lanthanophore– is proposed to selectively mobilize Lns from poorly soluble sources for the receptor-mediated uptake into Ln-utilizing microorganisms. In collaboration with Alexa Zytnick from the Martinez-Gomez Lab and Dr. Zachary Reitz from the Medema Lab, the existence of a lanthanophore in *M. extorquens* AM1 was investigated. The first bioinformatic investigations revealed a biosynthetic gene cluster in close proximity to the Ln-dependent MDH gene cluster. This nearby biosynthetic gene cluster was assigned to the biosynthesis of a chelator similar to aerobactin (AB), indicating that AB, a siderophore commonly utilized by bacteria, may be involved in the uptake process of Lns. This finding suggests a new function for AB beyond its role in Fe^{3+}-transport, extending its function to the acquisition and trafficking of Lns into the bacterial cell.

Our goal was to follow through with this lead and synthesize AB as well as evaluate its binding affinity and binding specificity for Lns. After characterization, *in vivo* growth studies with AB will provide insights into its ability to transport Lns into the cell and its impact on bacterial growth. These experiments will help us explore the potential of AB as a lanthanophore and elucidate our understanding of Ln-uptake mechanism.

2. Synthesis of Aerobactin

AB was first isolated by Gibson and Magrath in 1969 and then synthesized by Maurer and Miller in 1982.[61] AB is a dihydroxamate-based siderophore that is broadly used by terrestrial and marine bacteria.[62] The siderophore consists of two N^6-acetyl-N^6-hydroxy-L-lysine (ahLys) building blocks that are linked to the terminal carboxyl groups of citric acid through an amide bond (Figure II-1).
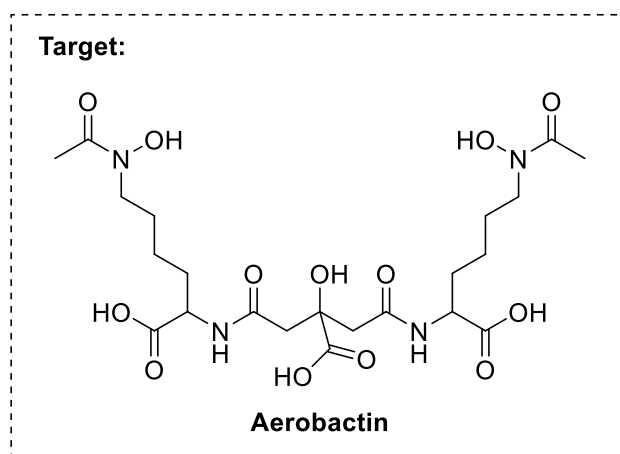
Figure II-1 Chemical structure of aerobactin.

With its two hydroxamate groups and the central α-hydroxyl carboxylate of citric acid, AB acts as a hexadentate chelator for Fe^{3+}. The preparation of AB was based on the modified procedures by Ho *et al*.[62] The citric acid derivative was obtained after three steps (Scheme II-1). Citric acid, a tricarboxylic acid, has two primary and one tertiary carboxylic acid groups and thus requires a selective method to obtain the citric acid dimethyl ester **1**. Initially, The selective synthesis involved transforming the terminal carboxyl groups into esters by acid-catalyzed Fischer esterification but the tedious work-up process led to the swap to the Dowex-H$^+$/NaI approach.[63] This alternative method resulted in a comparable yield of 20–24% but with a less laborious work-up procedure. Then, the α-carboxyl group was protected with *tert*-butyl acetate. The reaction was completed after three days and **2** was subsequently subjected to saponification with NaOH to yield the desired *tert*-butyl citric acid building block **3**.
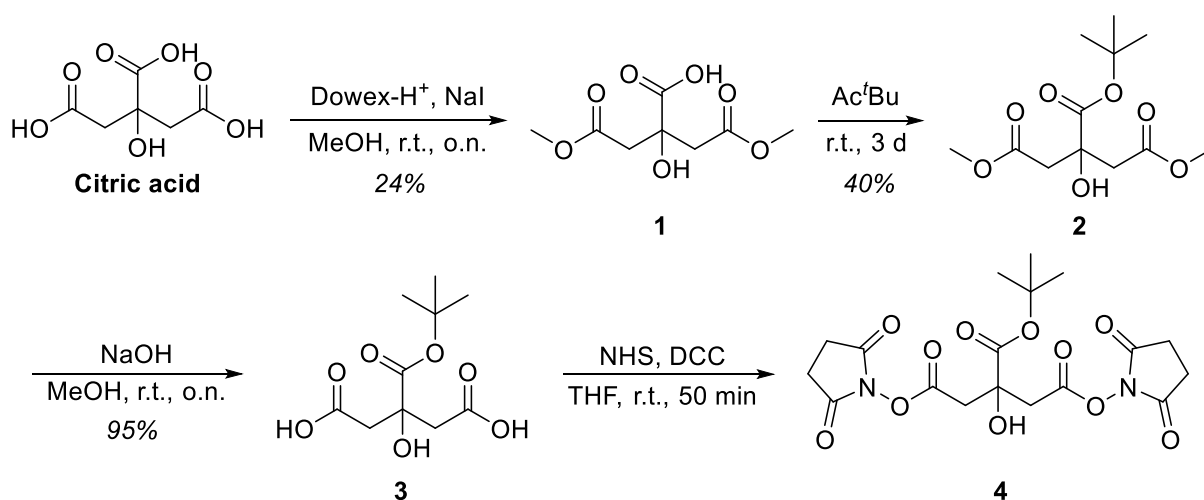
Scheme II-1 Synthesis of the citric acid building block.

The L-lysine building block was synthesized starting with commercially available N^{ε}-Boc-N^{α}-Cbz-L-lysine **5** (Scheme II-2). First, esterification of the carboxyl group was achieved using thionyl chloride and EtOH.

Conveniently, the Boc group was removed with this step as well, eliminating the need for a separate deprotection step, obtaining **6**. Then, conversion of the ε-amino group of **6** to **7** was achieved in two steps through *N*-oxidation and acetylation utilizing benzoyl peroxide and acetic anhydride (Scheme II-2, B), respectively.
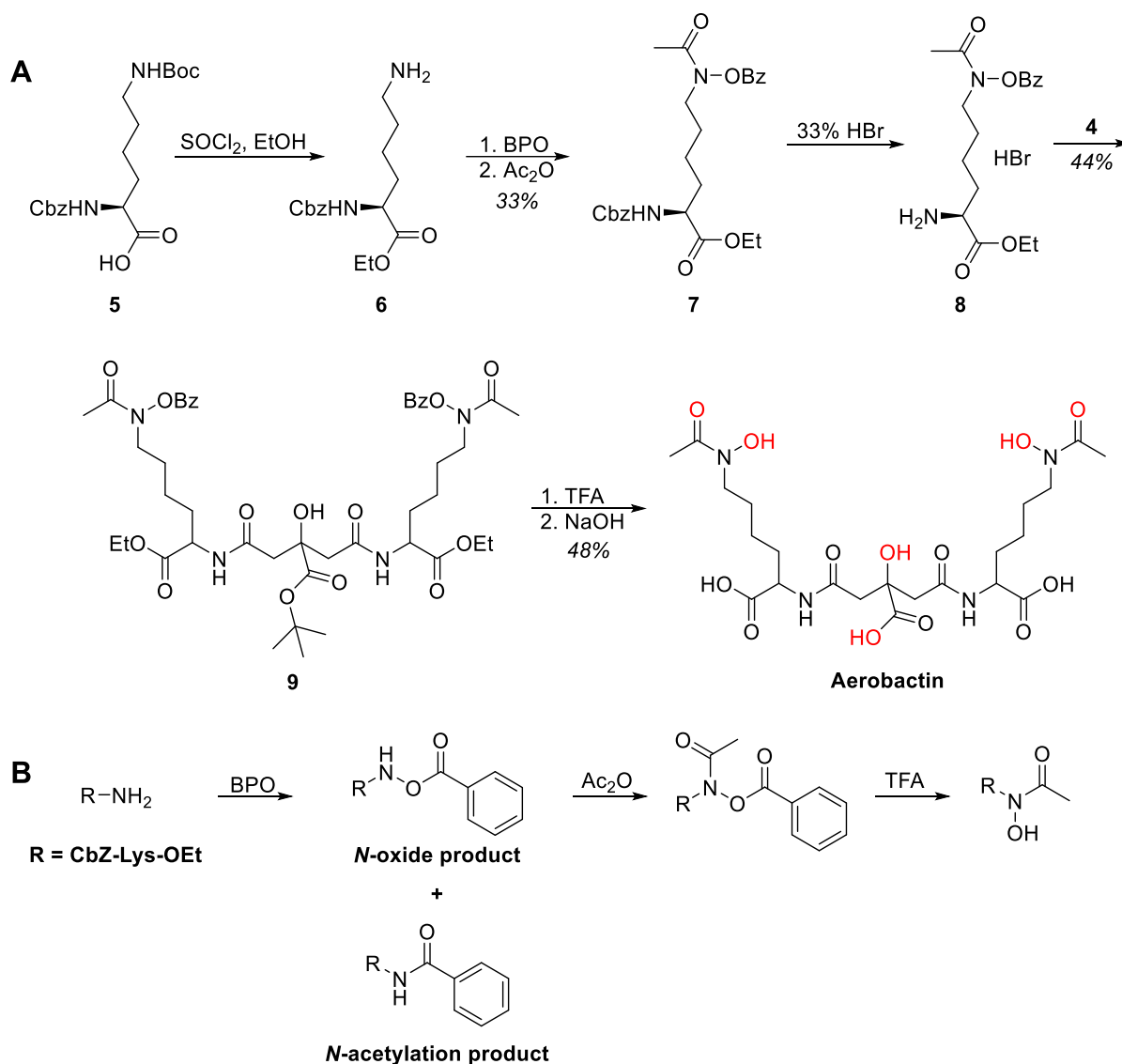
Scheme II-2 A) Synthesis of the ahLys building block **8** and coupling to the activated citric acid NHS-ester **4**. Aerobactin was purified with semi-preparative HPLC. The functional groups that are involved in Fe^{3+} complexation are colored red. (B) Conversion of Lys-NH$_2$ to the hydroxamate group.

A crucial condition to achieve the desired *N*-oxide product in satisfying yield is an optimal buffer system.[64] The biphasic solvent system consists of dichloromethane (DCM) and an aqueous NaHCO$_3$ solution that has to be adjusted to pH 10.5 to quench benzoic acid as it forms from benzoyl peroxide. As a result, the formation of the desired *N*-oxide product is favored over the production of the undesired *N*-acetylation byproduct (amide). The yield improved from 17% at pH 10.0 to 35% yield at pH 10.5. The reaction conditions (30 mL of solvent per mmol starting material) for the subsequent acetylation of the *N*-oxide product with acetic anhydride by Ho *et al.* produced dissatisfactory yields of

around 10%. However, conducting the reaction directly in acetic anhydride without any additional solvent significantly increased the yield to 95%. After Cbz-deprotection with HBr, the key step involves the conjugation of the L-lysine building block **8** to the activated *tert*-butyl citrate moiety **4**. The condensation reactions of the L-lysine building blocks were facilitated utilizing *N,N'*-dicyclohexylcarbodiimide (DCC) and *N*-hydroxysuccinimide (NHS) as the coupling reagents. Following the condensation reaction, the last step involves the global deprotection of the protecting groups of **9** which was carried out in subsequent steps by trifluoracetic acid and then NaOH. Lastly, the crude product was purified *via* semi-preparative high-performance liquid chromatography (HPLC, method: A: H_2O + 0.1% TFA and B: MeCN + 0.1% TFA, $0 \rightarrow 25\%$ in 40 min, R_t = 26 min) to isolate pure AB as a white powder in 7% overall yield. The purified AB was forwarded to the Martinez-Gomez Lab, where *in vivo* growth studies with *M. extorquens* AM1 were conducted.

3. Synthesis of Deoxyschizokinen

As *in vivo* studies involving AB and *M. extorquens* AM1 continued, cultivation and isolation of secondary metabolites from AM1 by our group member Dr. Ignacio Sottorff revealed indications of another siderophore that could possible function as a lanthanophore: deoxyschizokinen (DS). Hu and Boyer were the first to isolate and characterize DS from the bacteria *Bacillus megaterium* ATCC 19213 in 1995.[65] DS belongs to the family of Schizokinen and shares structural similarities to AB, notable its citrate-based core and the presence of a hydroxamate group. Instead of a lysine-based derivative as additional metal-binding moieties, the side chains of DS are based on 1,3-diaminopropane. Thus, the DS linker length of the side chain is one methylene group shorter but the presence of the hard O-donor groups remains critical for the coordination of Fe^{3+} (Figure II-2).
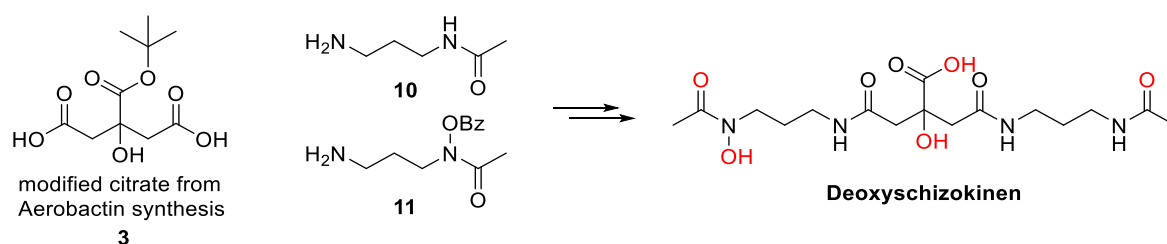
Figure II-2 Retrosynthetic analysis of Deoxyschizokinen. Deoxyschizokinen consists of a citrate moiety and two 1,3-diaminopropane derivatives. The functional groups that are involved in the complexation of Fe^{3+} are colored red.

To further investigate this lead, the synthesis of DS was pursued. Although the synthesis of Schizokinen was reported several times, no procedure for the synthesis of DS is published to the best of our knowledge.[66] Conveniently, the required central citrate moiety was already available from the synthesis of AB. DS features two asymmetric side chains: one with a hydroxamate moiety and the other

one being solely *N*-acetylated. The two distinct side chains could both be synthesized from commercially available 1,3-diaminopropane (Scheme II-3).
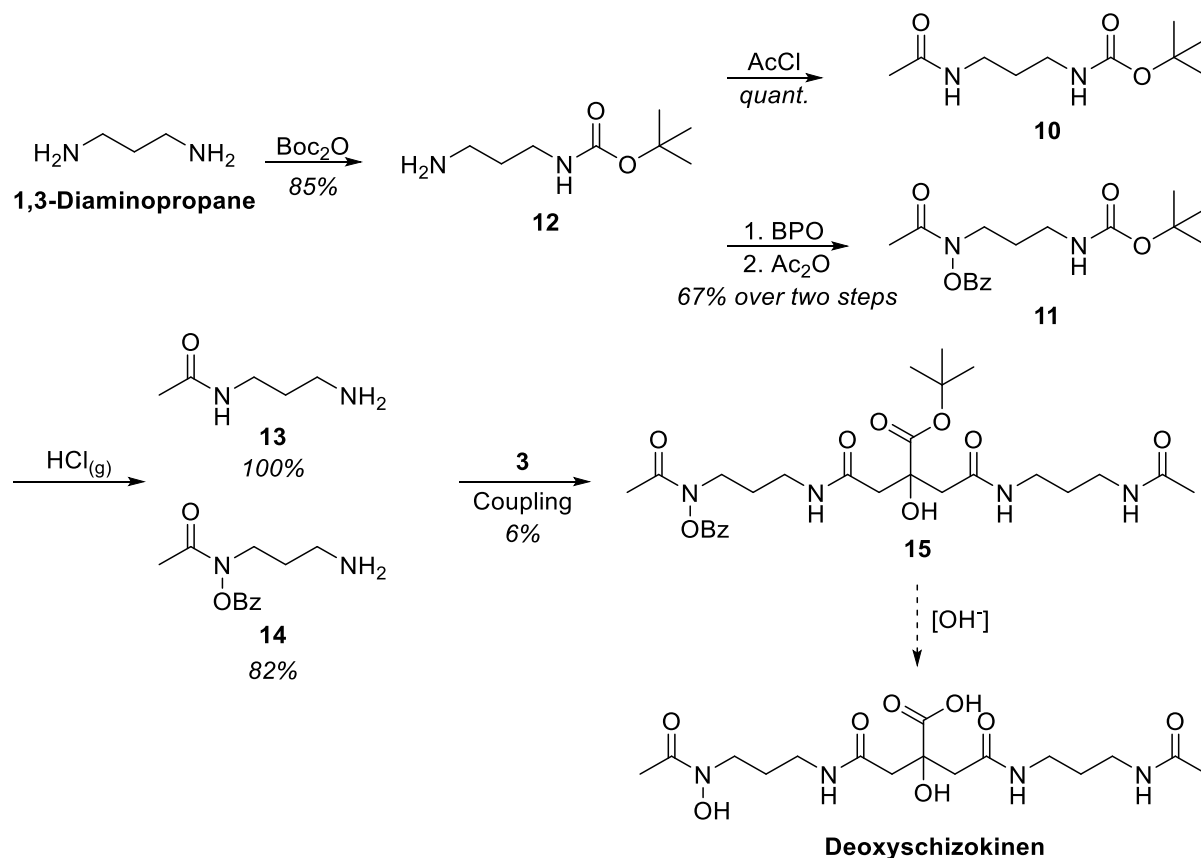
Scheme II-3 Schematic overview towards the synthesis of Deoxyschizokinen.

1,3-Diaminopropane was mono-Boc protected by Boc-anhydride to obtain **12**. Then, one side chain was subjected to *N*-acetylation while the other was treated with benzoyl peroxide for the *N*-oxidation, followed by the *N*-acetylation. Subsequently, both side chains **10** and **11** were subjected to HCl gas for Boc deprotection. The *ex situ* generated HCl gas was produced by the addition of concentrated H_2SO_4 to NaCl which was directly inserted into a solution of **10** or **11** (Figure II-3).[67] Excess amount of HCl gas was quenched by a solution of NaOH. After an exposure of 1–2 h, the respective HCl salts are formed and precipitate in Et_2O that was used as the solvent. After completion of the reaction, the solvent was removed under reduced pressure and the product is obtained as a solid. The most challenging task was to keep the highly hygroscopic HCl salts of **13** and **14** dry during the next step.
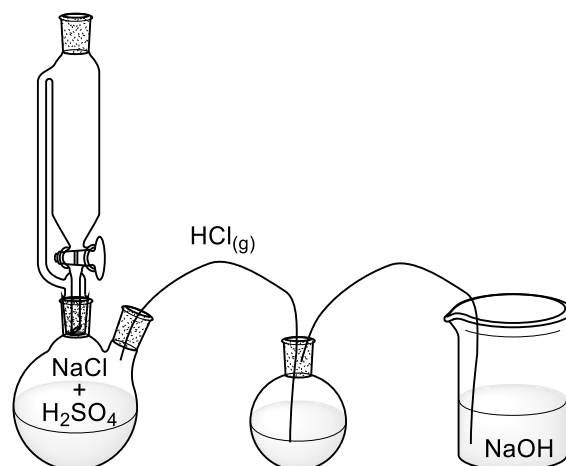
Figure II-3 Setup for the Boc deprotection of **10** and **11** by *ex situ* generated HCl gas.[67]

Then, the next step involves the coupling of both side chains to the central citrate moiety. A major challenge is the asymmetry of the side chains which require a careful approach to avoid undesired results. Two methods are possible, either a more laborious sequential two-step coupling protocol which allows for a more controlled coupling of each side chain or a quicker one-pot coupling reaction which would also lead to two possible but undesired symmetrical byproducts (Figure II-4) diminishing the yield of the reaction.
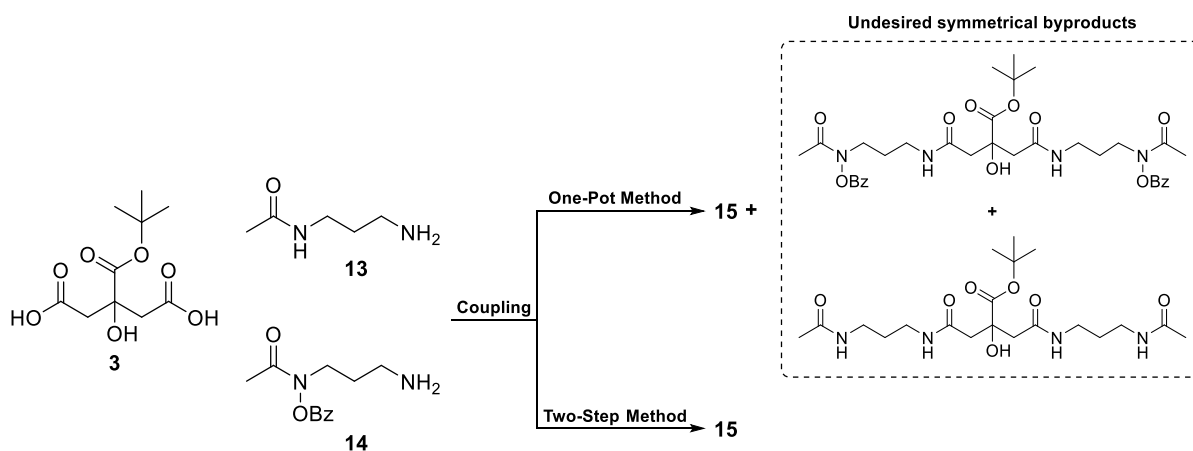
Figure II-4 The one-pot coupling procedure could lead to the generation of symmetrical coupled but undesired byproducts in addition to the desired asymmetrical coupled product **15**.

The first approach was to test the sequential two-step coupling protocol based on Fadeev *et al.*[68] The protocol involves an intramolecular cyclization of **3** to obtain **16** which was facilitated by DCC. Subsequently, side chain **14** was added first to the cyclic citric acid, inducing the ring-opening and formation of the first amide bond. Then, the second side chain **13** was conjugated to **17**, facilitated by DCC in combination with NHS to obtain **15** (Scheme II-4).
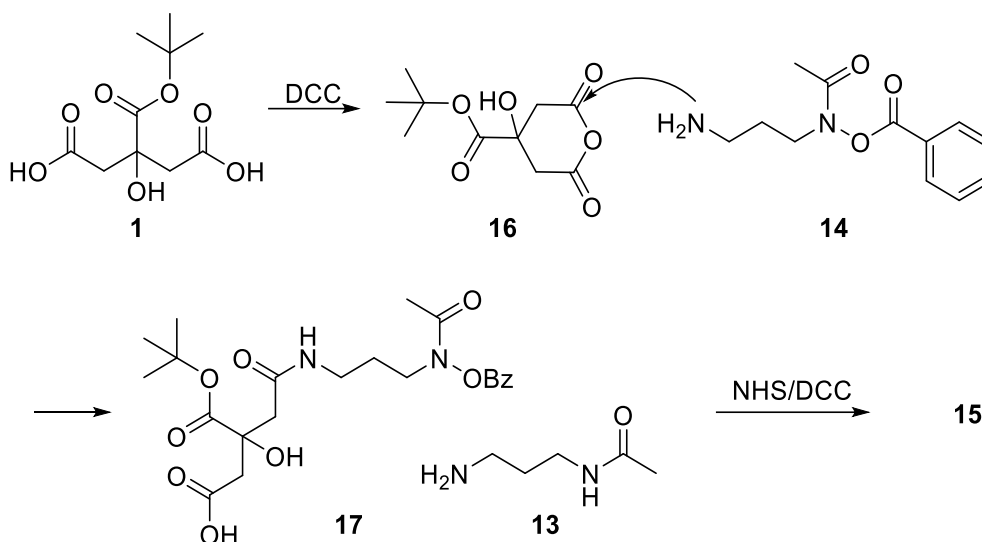
Scheme II-4 Sequential two-step procedure for generation of **15**.[68]

Following the sequential two-step protocol, a total yield of 6% was obtained. Due to the low yield, only liquid chromatography-mass spectrometry (LC-MS) could be used for product verification. The repetition or modification of the two-step protocol to improve the yield were not successful nor produced sufficient amount of product to verify product formation by ^{1}H and ^{13}C NMR.

Now, the focus was shifted towards the one-pot protocol for the simultaneous coupling of both side chains **13** and **14** to the citrate moiety. Again, DCC and NHS was used to facilitate the formation of the amide bonds. Product formation could be verified by taking a sample of the reaction mixture and submitting to LC-MS, however this method did not allow for isolation of any product **15** and subsequent analysis by NMR was not possible. Other coupling reagents like 2-mercaptothiazoline or DCC and 1,1'-carbonyldiimidazole did not yield any sufficient amount of product either.

To summarize, efforts were made to synthesize another citrate-based siderophore Deoxyschizokinen, which was also hypothesized to function as a lanthanophore. The two asymmetric 1,3-diaminopropane-based side chains contain a hydroxamate functional group and a *N*-acetylated functional group, respectively, were successfully synthesized. The key step, coupling of both side chains to the central citrate moiety could not be achieved in sufficient quantities with neither a sequential two-step nor one-pot reaction protocol. Various coupling reagents were tested to pre-activate the citrate moiety but no improvements were observed.

4. Characterization of Aerobactin

After the purification of AB by semi-preparative HPLC, the acquired ^{1}H and ^{13}C NMR data are in accordance with the existing data found in the literature.[62] Then, analysis of AB using high resolution mass spectrometry (HR-MS) revealed the [M-4H+Fe^{3+}]$^-$ fragment (616.1318) as the major peak (Figure

II-5, A). These results were obtained without addition of any Fe^{3+} source and showcases that AB is able to scavenge Fe^{3+} from its surrounding environment (most likely from the injection port of the HR-MS) and its the impressive binding affinity to Fe^{3+}. To probe if AB is capable to form a complex with Lns as well, a 10-fold excess of $LaCl_3$ and $LuCl_3$ were added to AB, respectively, and both samples were submitted to HR-MS. In the sample containing La^{3+}, the AB-La^{3+} complex remained undetected, but the AB-Fe^{3+} was detected again. However, the sample with Lu^{3+}, the major peak was identified as the $[M-2H+Lu^{3+}]^+$ fragment (737.1505), verifying the formation of the AB-Lu^{3+} complex (Figure II-5, B).
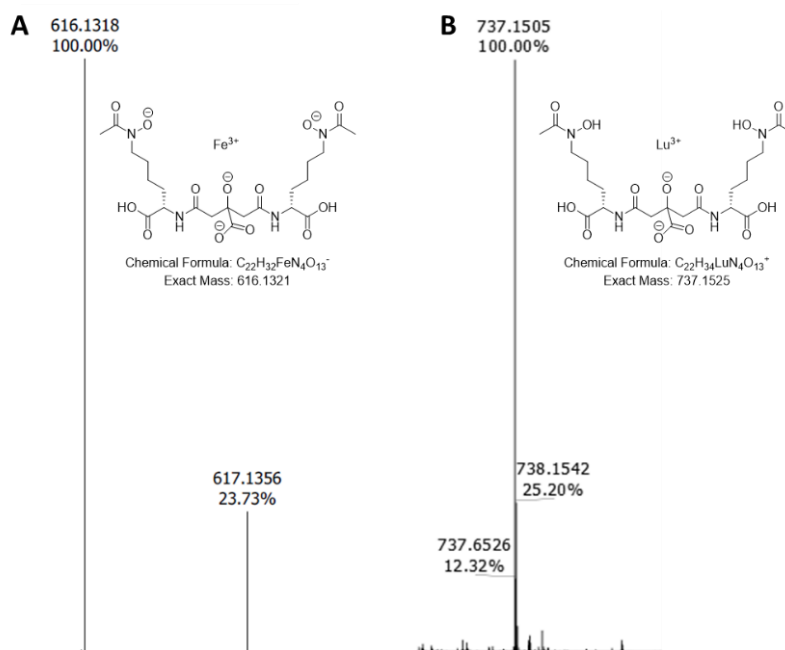
Figure II-5 High resolution mass spectrometry results from aerobactin with A) Fe^{3+} and B) Lu^{3+}.

Notably, the charge of the AB-Lu^{3+} complex was found in the positive and negative channel with an overall positive or negative charge of +1 and -1, respectively. The differences in charge for AB-Fe^{3+} and AB-Lu^{3+} could be indicative of a different binding interaction of AB with Fe^{3+} and Lu^{3+}, respectively, and suggests that there might be different coordination environments for the two complexes. In addition, the variation in charge could also impact the stability, solubility and biological function of these complexes under physiological conditions. This charge variation could be a "recognition signal" for receptors or import channels to distinguish between Fe^{3+} and Lns^{3+} and thus for siderophores and lanthanophores, respectively.

Next UV/Vis spectroscopy was used for further investigation of AB. AB itself is spectroscopic silent and does not show any distinct features (Figure II-6, A). Then, an increasing amount of Fe^{3+} was added to the solution. The sample containing equimolar amount of Fe^{3+} shows a broad absorption band spanning a range from 400 to 500 nm and a distinct absorption maximum (λ_{max}) at 296 nm is observed at 10 equivalents of Fe^{3+} (Figure II-6, A).
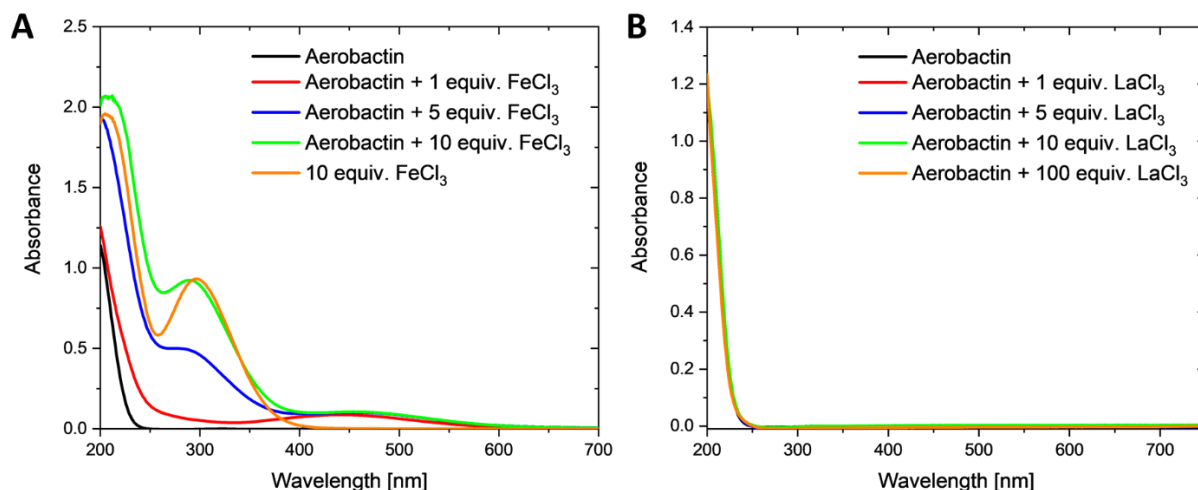
Figure II-6 A) UV/Vis spectra of 50 µM FeCl$_3$ and 50 µM Aerobactin with 1–10 equivalents of FeCl$_3$ in H$_2$O. B) UV/Vis spectra of 50 µM Aerobactin with 1–100 equiv. of LaCl$_3$ in H$_2$O. Samples were incubated for 1 h.

The λ$_{max}$ around 300 nm is characteristic for the α-hydroxycarboxylate-to-Fe^{3+} ligand-to-metal-charge transfer (LMCT) and the broad absorption band at 400 nm is typical for hydroxamate-to-Fe^{3+} LMCT.[58] The same experiment was repeated with the addition of La^{3+} to AB instead of Fe^{3+} but no remarkable changes are detected by UV/Vis spectroscopy, even upon addition of 100 equivalents of La^{3+} (Figure II-6).

Due to the spectroscopic silence of AB and La^{3+} in these experiments, complexation could only be monitored through changes of the LMCT bands of the AB-Fe^{3+} complex. In addition to the α-hydroxycarboxylate, two hydroxamate groups are involved in metal complexation. Harris *et al.* noted that the acidic carboxylate are deprotonated at a pH below 5, while the more basic hydroxamate groups are deprotonated between pH 7 and 10.[69] The deprotonation of these groups could be crucial for complexation, thus a buffer system with a pH set to 8 was used for the next experiment. Adjusting the buffer to a higher pH would more likely lead to precipitation of insoluble Fe(OH)$_3$ and Ln(OH)$_3$, thereby interfering with the measurements. Before proceeding with the experiment, desferrioxamine B (DFO) (Figure II-7) was employed as a proxy for AB. DFO is an aliphatic trihydroxamate siderophore but does not have a central citrate moiety. DFO is commercially available and capable of binding Fe^{3+} and Lns^{3+} which allows for gauging and adjusting of experimental conditions before AB is used.[70]
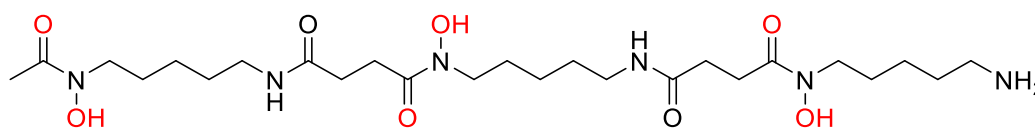
Figure II-7 Chemical structure of desferrioxamine B (DFO). The functional groups that are involved in Fe^{3+} complexation are colored red.

Titration experiments were conducted to investigate the affinity of DFO and AB fors Lns^{3+}. Similar to AB, DFO is spectroscopic silent but exhibits a broad peak around 400 nm characteristic for the hydroxamate-to-Fe^{3+} LMCT.[71] First, DFO was incubated with equimolar amounts of Fe^{3+} before an increasing amount of La^{3+} or Lu^{3+} were added to the solution. The same procedure was repeated for AB and the results are shown in (Figure II-8).
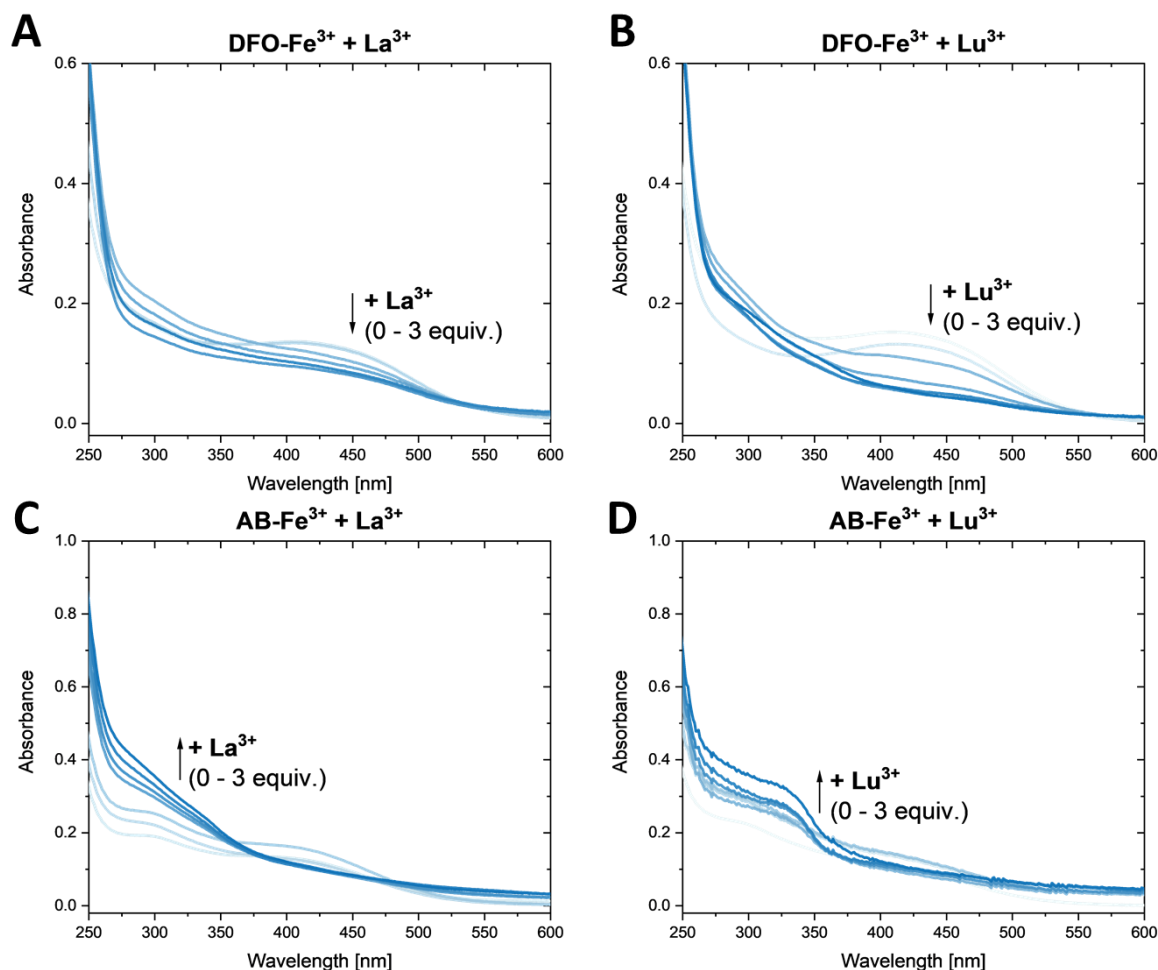
Figure II-8 UV/Vis spectra of titration experiments with DFO and AB. A solution containing 100 µM DFO and 100 µM FeCl$_3$ was incubated for 10 min before 0–3 equiv. of A) LaCl$_3$ or B) LuCl$_3$ was added. A solution containing 100 µM AB and 100 µM FeCl$_3$ was incubated for 10 min before 0–3 equiv. of C) LaCl$_3$ or D) LuCl$_3$ was added. Samples were measured after 2 h of incubation. Solvent: 10 mM HEPES, 100 mM KCl, pH 8.05, equivalent of LnCl$_3$ increases from light to dark blue.

Similar to the previous measurements with AB, the DFO-Fe^{3+} complex also shows the characteristic broad absorption from 400 to 500 nm that is indicative of the hydroxamate-to-Fe^{3+} LMCT. Since DFO has no citrate moiety, the α-hydroxycarboxylate-to-Fe^{3+} LMCT around 300 nm is not visible. The increasing addition of La^{3+} to DFO-Fe^{3+} resulted in a reduction of the hydroxamate-to-Fe^{3+} LMCT signal, implying that the amount of DFO-Fe^{3+} decreases in favor of forming the DFO-La^{3+} complex. The same trend is observed for the addition of Lu^{3+} to the DFO-Fe^{3+} solution, but the decrease of the hydroxamate-to-Fe^{3+} LMCT is more pronounced in comparison to the titration of La^{3+} to DFO-Fe^{3+}. This suggests that under these conditions, more DFO-Lu^{3+} is formed than DFO-La^{3+}. The AB-Fe^{3+} complex

shows the previously observed signals at 300 and 400 to 500 nm. After titration of La^{3+} to the AB-Fe^{3+} complex, the hydroxamate-to-Fe^{3+} LMCT signal decreases while the absorption maximum at 300 nm increases but simultaneously flattens losing its distinct sharp peak. These results indicate a decrease of the AB-Fe^{3+} complex in favor of formation of the AB-La^{3+} complex. Again, the observed change is more pronounced when Lu^{3+} is added. The hydroxamate-to-Fe^{3+} LMCT signal flattens while a new absorption maximum at 325 nm replaces the characteristic α-hydroxycarboxylate-to-Fe^{3+} LMCT around 300 nm. Overall, introducing La^{3+} or Lu^{3+} to the DFO-Fe^{3+} and AB-Fe^{3+} complexes resulted in the decrease of the typical LMCT signals of these complexes, indicating the formation of new La^{3+} and Lu^{3+} complexes. These results further support the ability of AB to form complexes with Lns and that La^{3+} and Lu^{3+} are able to compete with Fe^{3+} for binding.

Dye-based assays are another spectroscopic method to investigate the binding capabilities of ligands. The chrome azurol S (CAS) assay, developed by Schwyn and Neiland, is a widely used qualitative method to detect and determine siderophores and was later optimized for Lns by Gladilovich et al.[72] The classic assay solution of Schwyn and Neiland inlcudes CAS (Figure II-9), Fe^{3+}, hexadecyltrimethylammonium bromide (HDTMA) and sulphosalicyclic acid, with latter serving as a weak chelator for Fe^{3+} to keep it in a soluble form.
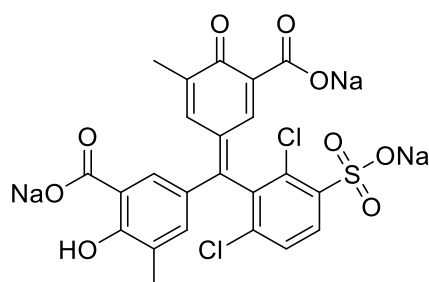
Figure II-9 Chemical structure of chrome azurol S.

The modified CAS assay for lanthanophores contains only CAS, HDTMA and Ln^{3+} before AB was added.[73] Free CAS has a distinct λ_{max} at 425 nm while the CAS-Ln^{3+} complex exhibits two absorption maxima at 500 and 625 nm that will decrease upon addition of a stronger ligand for Lns than CAS.[74] The ligand exchange can be represented by the following equation:

$$\textbf{CAS-Ln}^{3+} \quad + \quad \textbf{AB} \quad \longrightarrow \quad \textbf{CAS} \quad + \quad \textbf{AB-Ln}^{3+}$$

The change in λ_{max} can be monitored by UV/Vis spectroscopy and can also be visually perceived as a change in color. Before proceeding to examine the complexation of AB with Lns (La^{3+}, Nd^{3+} and Lu^{3+}), the modified CAS assay was assessed with DFO. Previous experiments have shown that deprotonation of the functional groups that are involved in metal binding are important for complexation, thus metal binding was assessed across the pH range of 6.4–8.1, and the results are shown in Figure II-10.
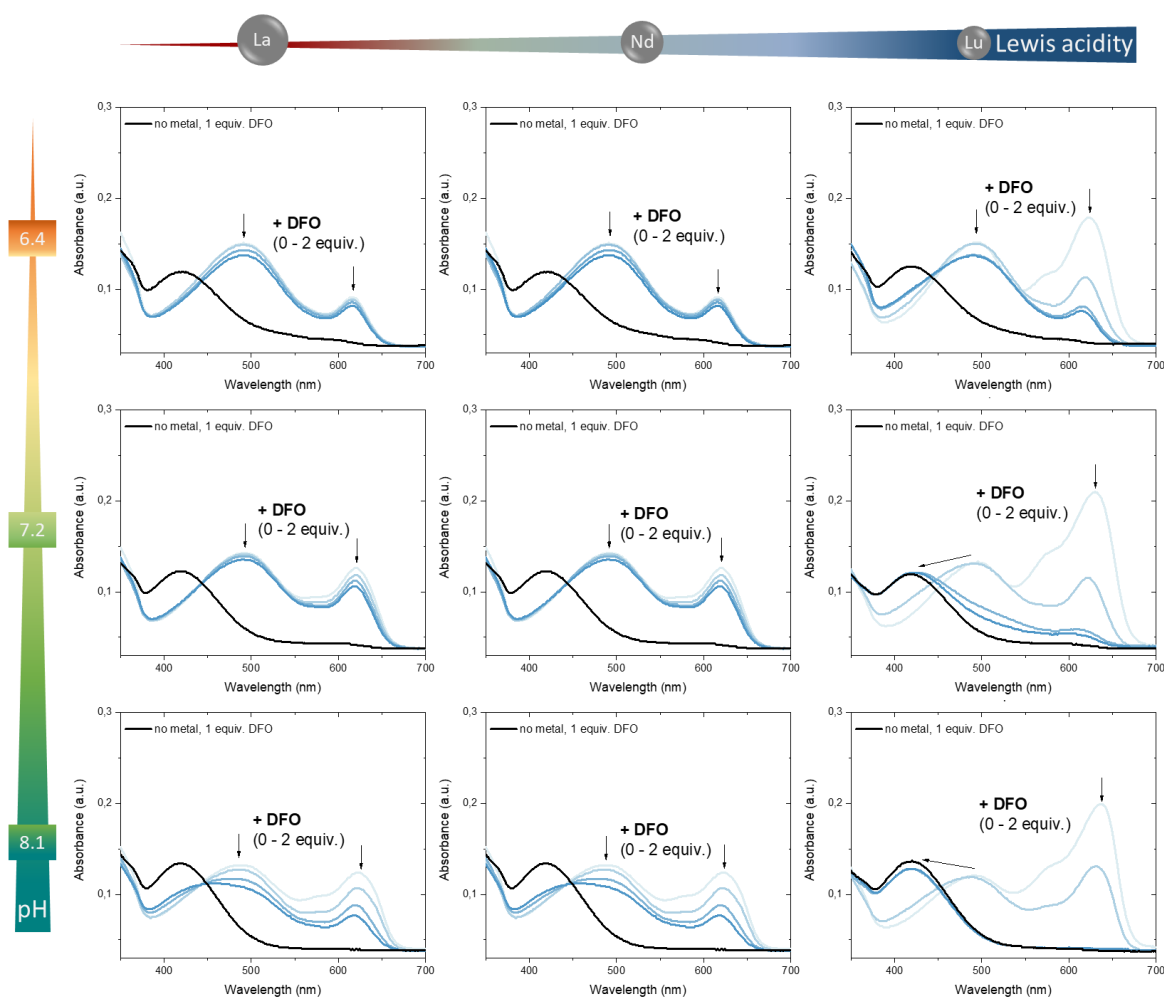
Figure II-10 Chrome azurol S assay with desferrioxamine B (DFO) at three different pH values with $LaCl_3$, $NdCl_3$ and $LuCl_3$. Conditions: MOPSO/HEPES buffer (1.5 mM each), 18.75 μM CAS, 50 μM HDTMA, 18.75 μM $LnCl_3$ and 0–3 equiv. 0–37.50 μM DFO, equivalents of DFO increases from light to dark blue.

Each column corresponds to a different Ln and the rows represent the pH at which the assay was performed. For the La^{3+} column, the addition of DFO merely decreases the λ_{max} of the CAS-La^{3+} complex at pH 6.4 but gradually increases towards higher pH. This indicates that DFO requires higher pH for binding of La^{3+}. The same trend is observed for the Nd^{3+} column. Only at higher pH, the formation of the DFO-Nd^{3+} complex is observed. However, the higher Lewis acidity of Lu^{3+} leads to formation of DFO-Lu^{3+} complex even at a pH of 6.4 which was not observed for La^{3+} and Nd^{3+}. At pH 8.1 using two equivalents of DFO, the observed spectrum overlaps with the negative control sample (no metal, one equivalent of DFO and one equivalent of CAS), resembling the spectra of free CAS. This suggests the absence of the CAS-Lu^{3+} complex, implying that all Lu^{3+} have been bound by DFO resulting in the formation of the DFO-Lu^{3+} complex. These results underscore the previous observation that DFO binds Lu^{3+} more readily than the earlier lanthanides La^{3+} and Nd^{3+}.

Since the proof-of-concept worked, the CAS assay was repeated with AB to assess its ability to bind Lns under various pH conditions (Figure II-11).
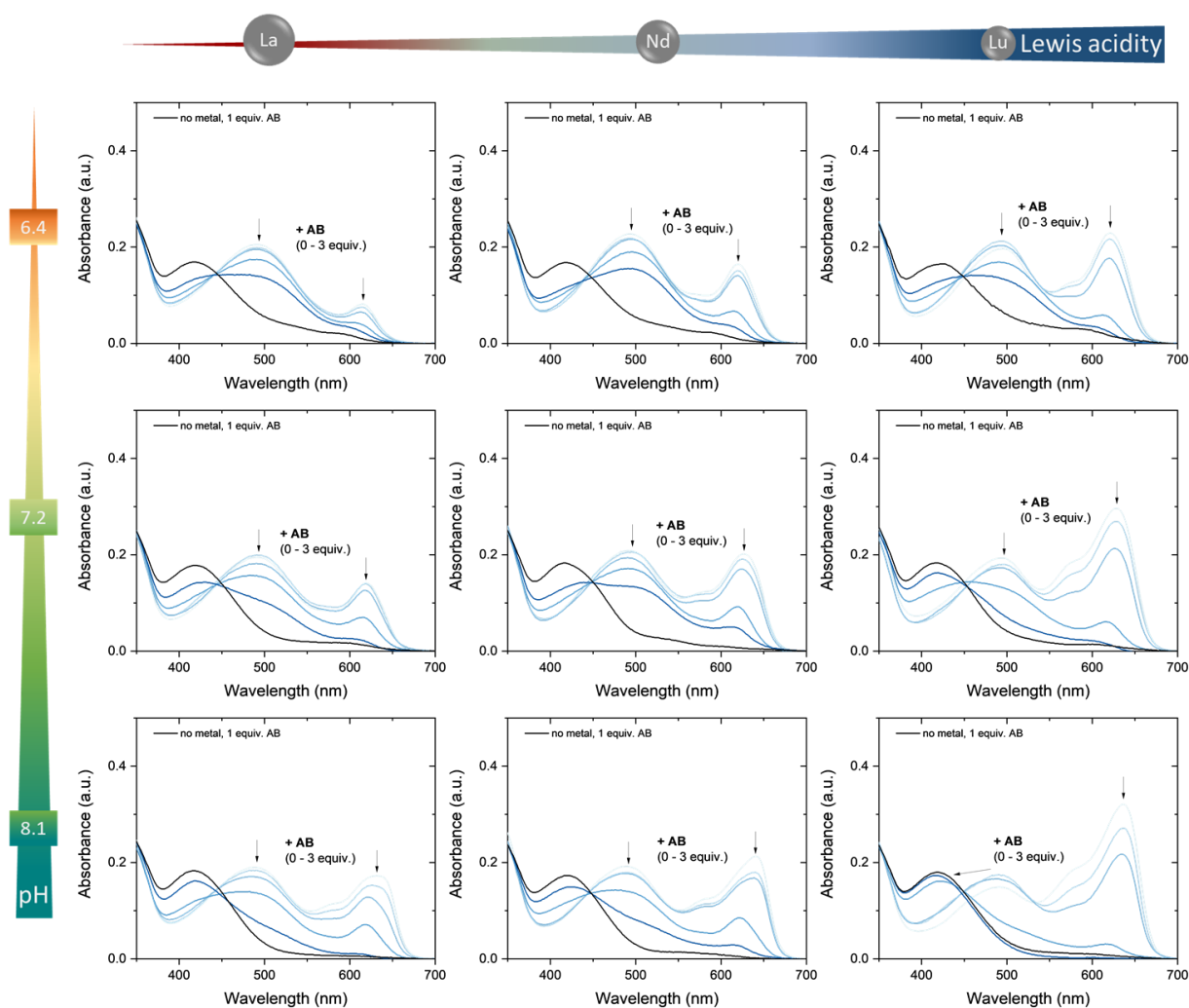
Figure II-11 Chrome azurol S assay with aerobactin (AB) at three different pH values with LaCl3, NdCl3 and LuCl3. Conditions: MOPSO/HEPES buffer (1.5 mM each), 18.75 μM CAS, 50 μM HDTMA, 18.75 μM LnCl3 and 0–3 equiv. 0–56.25 μM AB, equivalents of AB increases from light to dark blue.

In line with the results from the CAS assay with DFO, a pH- and Ln-dependent complex formation of the AB-Ln^{3+} is observed and correlates with the amount of AB added to the assay solution. A higher pH leads to greater decrease of the characteristic λ_{max} of the CAS-Ln^{3+} complex, implying that deprotonation events are likely playing a significant role in the formation and stability of the AB-Ln^{3+} complex. Furthermore, the interaction between AB and Lns is also affected by the Lewis acidity of the metal. Lu^{3+}, the strongest Lewis acid among these three, exhibits a tendency to form a complex with AB more readily. This is indicated by the higher decline of λ_{max} even at lower equivalents of AB in the assay solution, similar to the results of the CAS assay with DFO. The consistent absorbance pattern of the AB-Lu^{3+} complex also suggest that this complex is the most stable across the tested pH range, reflecting a potentially stronger and more stable interaction compared to the complex formed with La^{3+} and Nd^{3+}, respectively.

To investigate whether AB is a lanthanophore, *in vivo* growth studies with *M. extorquens* AM1 were conducted by Alexa Zytnick from the Martinez-Gomez group. Since AM1 is able to switch, depending

on availability of Lns, between Ln-MDH and Ca-MDH for its metabolism and growth, a knock-out strain of AM1 lacking the gene for the expression of Ca-MDH was generated. This mutant strain, called ΔmxaF, has a growth defect and barely grows without the addition of Lns. Only with addition of Lns, Ln-MDH can be expressed and the growth of the mutant strain is restored. A series of growth studies were conducted with the ΔmxaF mutant strain. To assess whether the availability of Lns are influencing the growth, $NdCl_3$ and Nd_2O_3 salts were used as a soluble and poorly soluble source of Lns, respectively. Due to the better solubility in aqueous solution and thus better availability of Nd^{3+} when using $NdCl_3$, the growth should, at least initially, be higher compared to Nd_2O_3. In addition, the Ln-limiting condition when using Nd_2O_3 could trigger or increase the biosynthetic production and secretion of the lanthanophore thus increasing the growth rate at a later time point. Furthermore, samples that either contained or lacked AB were prepared to examine if AB is able to additionally support the growth. If AB is an efficient lanthanophore, the supply of AB to the mutant strain grown with $NdCl_3$ or Nd_2O_3 should increase the growth in comparison to the experiment without the addition of AB. The growth studies were conducted in multi-well culture plates that were continuously shaken and the cell growth was automatically monitored by a plate reader (Figure II-12) determining the optical density at 600 nm (OD_{600}). Higher Ln solubility drastically increases the growth rate of ΔmxaF, suggesting that the source of the Ln plays a crucial role for the growth which is negatively impacted by the less soluble Nd_2O_3.[73] As already shown above, AB is able to bind Lns at physiological pH and thus was supplemented to the media to investigate its effect on the growth. The addition AB did not have any significant effect on growth rate or growth yield of when using $NdCl_3$ or Nd_2O_3.

Sample	μ (hr^{-1})	Growth Yield (OD_{600})
ΔmxaF $NdCl_3$	0.030 ± 0.001	0.563 ± 0.071
ΔmxaF $NdCl_3$ + AB	0.031 ± 0.001	0.554 ± 0.083
ΔmxaF Nd_2O_3	0.011 ± 0.000	0.348 ± 0.014
ΔmxaF Nd_2O_3 + AB	0.010 ± 0.000	0.330 ± 0.034
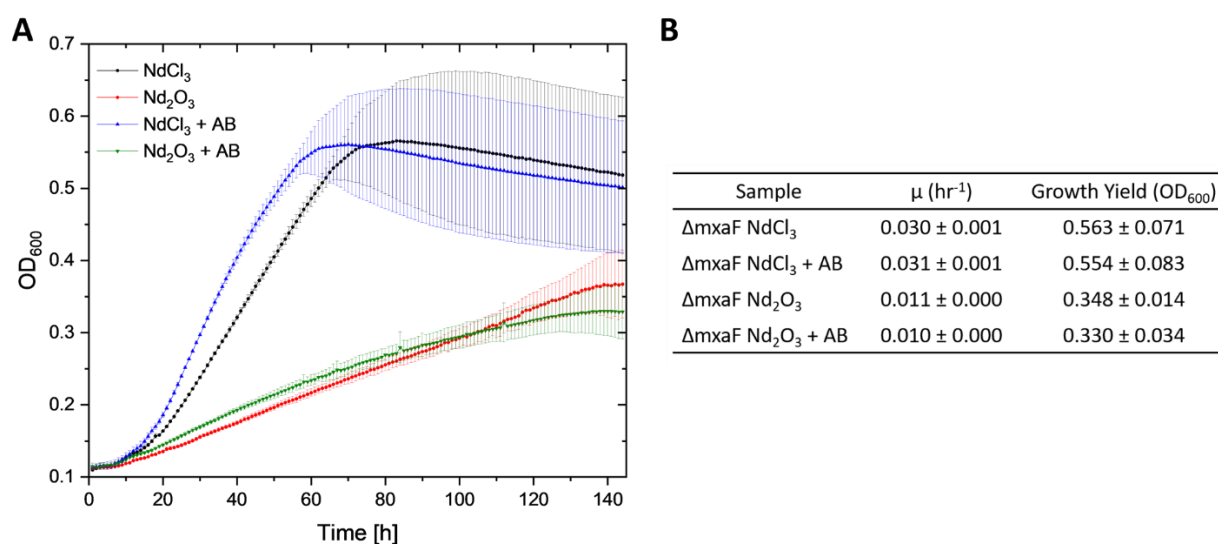
Figure II-12 A) Growth curves of ΔmxaF with $NdCl_3$ or Nd_2O_3 and the effect of 2 μM AB on the growth. Final Nd^{3+} concentration of 2 μM. Each data point represents the mean of three replicates. B) Calculated growth rates and growth yields. Raw data was kindly provided by Alexa Zytnick.

The binding affinity of AB for La^{3+}, Nd^{3+} and Lu^{3+} was assessed using various spectroscopic methods. Both show no characteristic peaks in the UV/Vis region thus confirmation of Ln complexation could

only be examined indirectly. Titration experiments and CAS assay have revealed that AB is able to bind Lns in a pH- and Ln-dependent way. The AB-Ln^{3+} complex is more readily formed at higher pH and with a stronger Lewis acid. Growth studies were conducted to examine the impact of AB on the ΔmxaF mutant strain from AM1. The exogenous addition of AB did not result in a significant enhanced growth and AB is likely not a lanthanophore.

5. Synthesis of Rhodopetrobactin B and Petrobactin

The exogenous addition of AB did not show any significant impact on growth of the ΔmxaF mutant strains of *M. extorquens* AM1 and cannot be considered a lanthanide-specific lanthanophore. This led to further bioinformatic investigation by Dr. Zachary Reitz and Alexa Zytnick. They have discovered yet another family of citrate-based siderophore that could be a lanthanophore: petrobactin. Petrobactin was first characterized by Barbeau *et al.* in 2021 and is produced by the oil-degrading marine bacterium *Marinobacter hydrocarbonoclasticus*.[75] Petrobactin consists of a central citrate moiety and two dihydroxybenzoyl groups that are connected through spermidine-based linkers. Initially defined as containing 2,3-dihydroxybenzoic acid groups, the structure was later revised and ultimately determined to comprise of 3,4-dihydroxybenzoic acid groups.[76] Further investigation revealed an acetyltransferase near its biosynthetic gene cluster pointing to the closely related rhodopetrobactin B (RPB). Rhodopetrobactin A and B, first identified by Baars *et al.* in 2018, share structural similarities with petrobactin and are both secreted by the bacterium *Rhodopseudomonas palustris*, from which the prefix "rhodo" is derived.

Intrigued by these findings, the initial focus was on synthesizing RPB.[77] Similar to petrobactin, RPB is composed of a central citrate moiety and two 3,4-dihydroxybenzoic acid groups that connected by a dibutylenetriamine-based side chain with an acetylated secondary amine (Figure II-13).
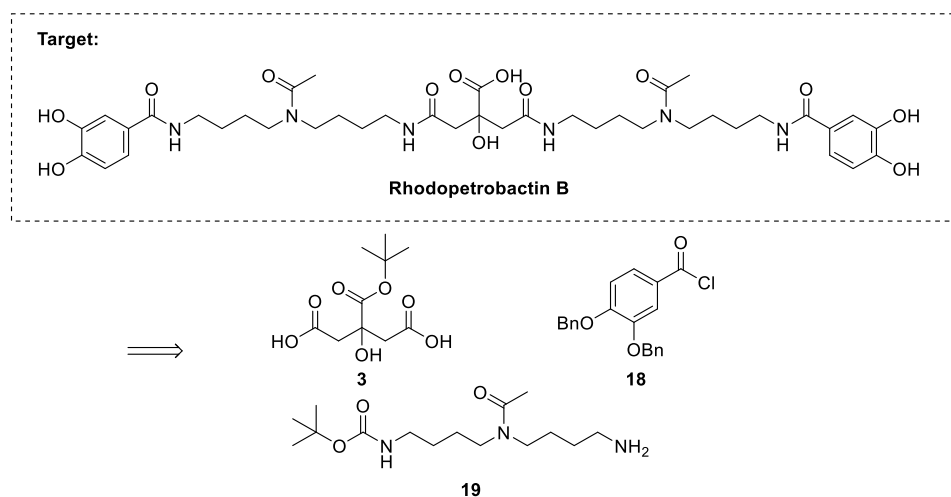
Figure II-13 Chemical structure of rhodopetrobactin B and its retrosynthetic analysis.

Starting from commercially available 3,4-dihydroxybenzoic acid, the protection of the hydroxy groups with benzyl bromide to avoid side reaction further down the synthesis route was conducted. The protection step was examined with benzyl bromide and benzyl chloride, both at 65–70 °C. After 1 d of stirring, the reaction mixtures were treated equally. Although the protection with benzyl bromide should be better due to bromide being the better leaving group, the use of benzyl chloride actually resulted in slightly higher yield (Scheme II-5) and purity. To aid amide formation with the dibutylenetriamine linker **19**, the benzoic acid was transformed to the more reactive benzoyl chloride **18** with oxalyl chloride.
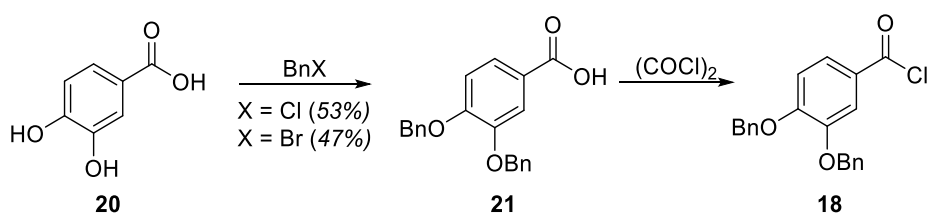
Scheme II-5 Synthetic pathway towards the benzoyl chloride **18**.

For the dibutylenetriamine side chain, commercially available 1,4-diaminobutane was used and the base-catalyzed mono-Boc protection with Boc_2O was performed. After separation from the unwanted di-Boc protected byproduct, **22** was elongated with 4-bromobutyronitrile through a S_N2 reaction to obtain **23**. After stirring for 16 h at room temperature, the secondary amine was acetylated to form 24, followed by the reduction of the nitrile group to an amine by exposure to Co^{2+}-catalyzed reduction with $NaBH_4$ (Scheme II-6).[78]
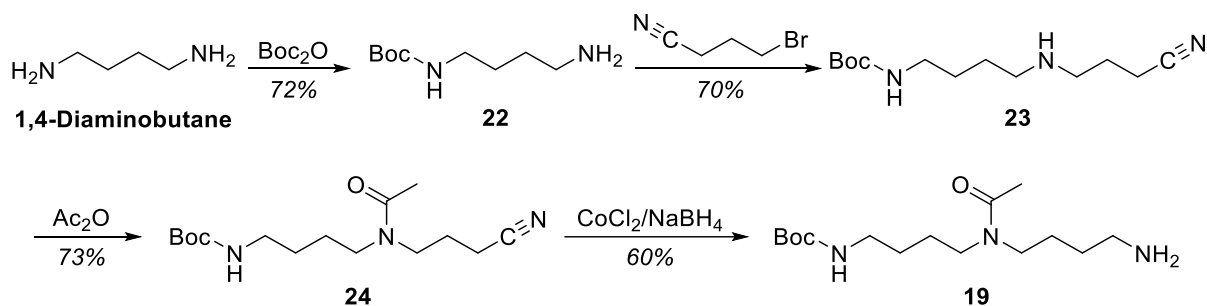
Scheme II-6 Synthetic pathway towards the dibutylenetriamine linker **19**.

Then, the amine **19** was added to the benzoyl chloride **18** (Scheme II-7). After Boc deprotection with TFA, the crude product **25** was ready for the conjugation to the citrate motif **3**. The citrate building block was activated with NHS/DCC and Boc-deprotected **25** was added dropwise to the solution to obtain **26**. In the last steps, the *tert*-butyl ester group and the benzyl groups were deprotected with HCl/AcOH and Pd/C with H_2, respectively.
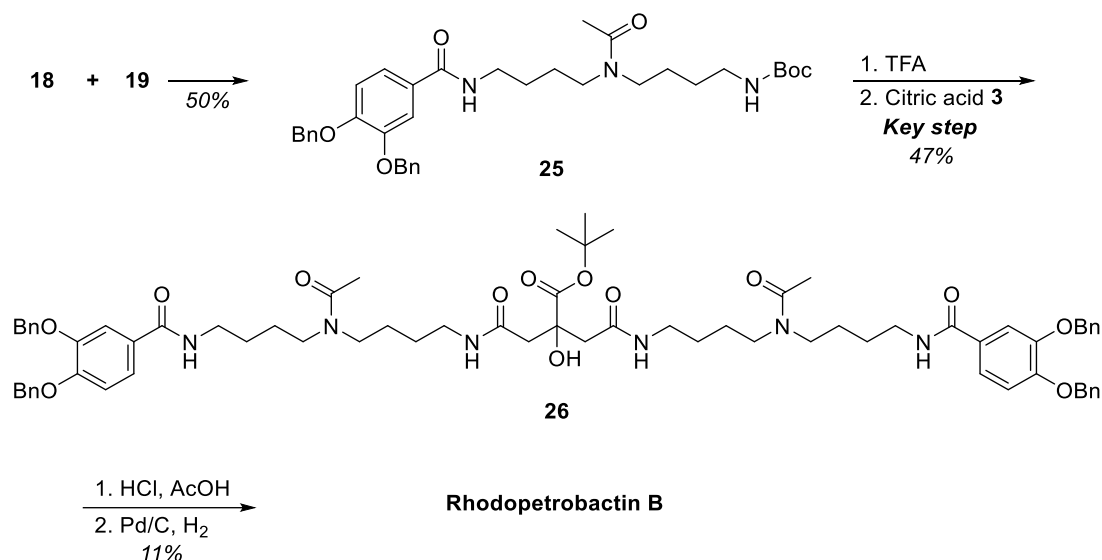
Scheme II-7 Synthetic pathway towards rhodopetrobactin B.

After removal of Pd/C with Celite and 0.45 µM syringe filters, the crude solution was subjected to purification by preparative HPLC. In contrast to the purification method by Baars *et al.* (A: H_2O + 1% MeCN and B: MeCN + 2% H_2O), the method for AB purification (A: H_2O + 0.1% TFA and B: MeCN + 0.1% TFA) was applied. Again, a reverse-phase C18-AQ column was used. The optimization of the method started with 5 to 100% B over 60 min. Various major peaks were collected and low resolution LC-MS analysis showed elution of RPB at around 30% B. The method was further optimized for time, solvent usage and separation. With the final purification method (5 to 32% B over 45 min), RPB elutes sharply at R_t = 27.7 min (Figure II-14). After removal of solvent by lyophilization, RPB was obtained as a white powder in 0.6% overall yield.
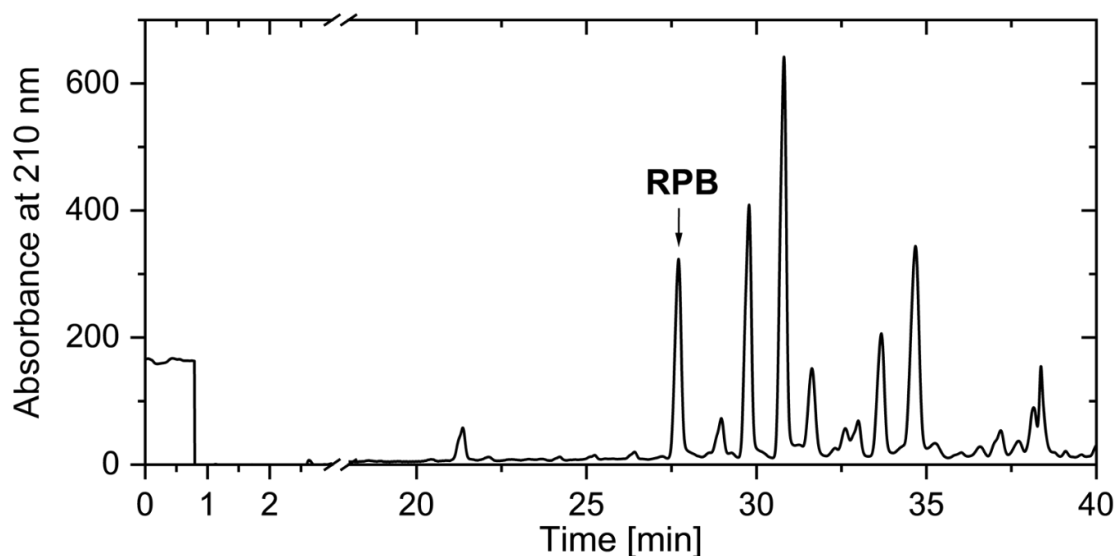
Figure II-14 HPLC chromatogram of the purification of rhodopetrobactin B. Method: 5 to 32% B over 45 min, A: H_2O + 0.1% TFA and B: MeCN + 0.1% TFA, flow: 20 mL/min, reverse-phase C18-AQ column, R_t = 27.7 min.

Building upon the synthesis methodology of RPB, the synthesis of petrobactin was approached (Figure II-15). The main distinctions are the linker length and the absence of the acetyl groups. Given that the citrate and catechol building blocks are shared between RPB and petrobactin, the main focus was on the synthesis of the side chain.
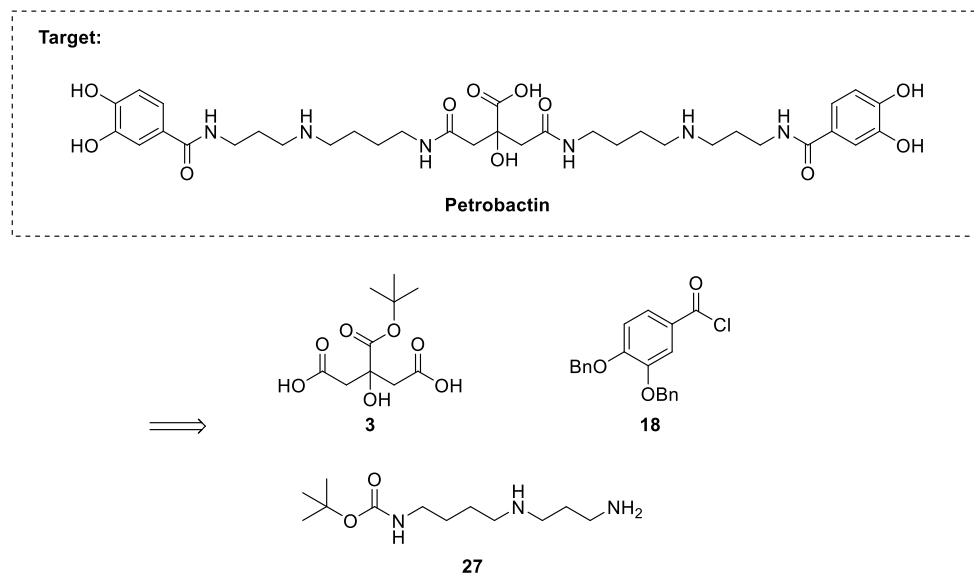
Figure II-15 Chemical structure of petrobactin and its retrosynthetic analysis.

In contrast to RPB, the linker connecting the citrate motif and the catechol moiety is based on spermidine. Furthermore, the secondary amine is not acetylated, thus reducing the synthesis by one step (Scheme II-8).
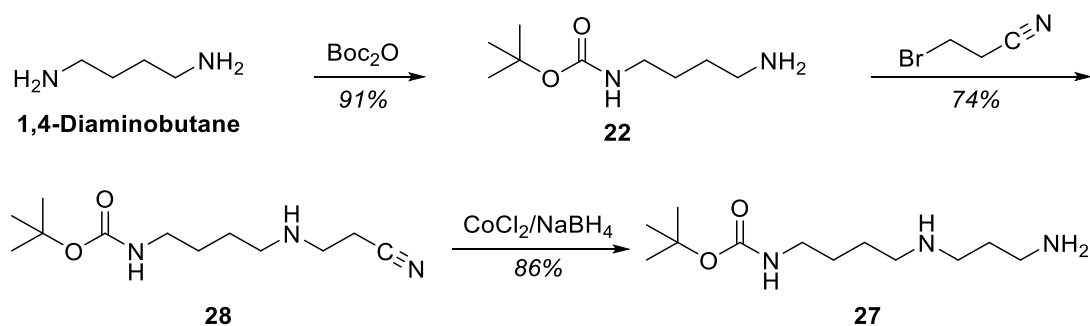
Scheme II-8 Synthetic pathway towards the spermidine-based linker **27**.

Identically to the dibutylenetriamine side chain of RPB, the synthesis started from commercially available 1,4-diaminobutane. For the mono-protection step with Boc$_2$O, the solvent was changed from MeOH with 10% TEA to DCM and without the addition of any base which resulted in an increase of yield from 72% to 91%. Insoluble byproducts could be removed by filtration and **22** was obtained after extraction without further purification by column chromatography. After mono-Boc protection, **22** was elongated by a S$_N$2 reaction and 3-bromopropanenitrile to obtain **28**. The reaction was optimized by changing the base from K$_2$CO$_3$ to triethylamine, reducing the heating temperature from 80 °C to 60 °C

and extending reaction time from 4 h to 18 h. These combined adjustments improved the yield from 20% to 74%. The nitrile group was reduced to an amine by LiAlH$_4$ as reduction with the previously used CoCl$_2$ and NaBH$_4$ yielded unsatisfactory results (improved from 40% to 86%). The amide **29** was formed with benzoyl chloride **18** and amine **27** (Scheme II-9). Subsequently, deprotection of the *tert*-butyl ester and the benzyl group of **30** followed the same procedure as in the synthesis of RPB.

Scheme II-9 Key coupling step towards petrobactin.

For the purification of petrobactin by preparative HPLC, we used the optimized method from the RPB as starting point (5 to 32% B over 45 min). Due to two unacetylated secondary amines, petrobactin should be slightly more polar than RPB thus eluting earlier with a reverse phase column. Again, major peaks were collected for low resolution LC-MS to identify petrobactin, but petrobactin was not detected in any peak. Although the mass of **30** was identified by low resolution LC-MS, the yield of the coupling step and subsequent purification by HPLC was insufficient for obtaining detectable levels of petrobactin by low resolution LC-MS.

The previously successful approach for generating the activated citrate **3** involves the use of DCC and NHS. However, coupling attempts were not successful, the coupling conditions were changed to the 1-Ethyl-3-(3-dimethylaminopropyl)carbodiimide (EDC) and 1-hydroxybenzotriazol (HOBT) system. Several attempts with EDC/HOBT only led to the mono-coupled product as detected by low resolution LC-MS (Scheme II-10).

Scheme II-10 Proposed synthetic pathway towards the coupling product **30**.

Further attempts, which included adjusting equivalents, reaction time and even re-adding new EDC/HOBT and side chain **29** to the mono-coupled product **31** also failed to yield the coupling product **30**. The assumption was made that the secondary amine of **29** might compete with the primary amine and also reacts with the activating reagents thus reducing formation of the desired product drastically. Thiazolidine-2-thione was employed to generate an activated species which is selective for primary amines (Scheme II-11).[79] Although a yellow intermediate was obtained indicating successful preparation of **33**, the isolation of thiazolidine-activated citric acid was not possible. These failed attempts led to the decision to cease the efforts towards the synthesis of petrobactin.
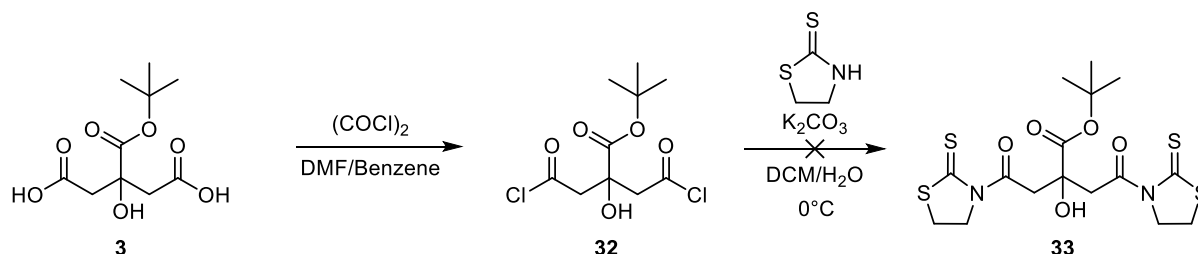
Scheme II-11 Proposed synthetic pathway towards thiazolidine-activated citric acid **33**.

6. Characterization of Rhodopetrobactin B

With RPB in hand, the binding of RPB towards Fe^{3+} and Ln^{3+} was characterized and compared. The acquired ^1H, ^{13}C and 2D-NMR data of the purified RPB are in accordance with the existing data found in the literature.[80] Quadrupole time-of-flight mass spectrometry (QTOF-MS) analysis confirmed the successful synthesis of RPB (Figure II-16). Then, complex formation of RPB with Fe^{3+} and Ln^{3+} was assessed by QTOF-MS as previous measurements with AB showed that the respective complexes can be detected. Samples containing RPB with excess of Fe^{3+} as well as Lns (La^{3+} and Lu^{3+}) were prepared and analyzed by QTOF-MS, but the mass of these complexes could not be detected.

Chemical Formula: $C_{40}H_{59}N_6O_{13}^+$
Exact Mass: 831.4135
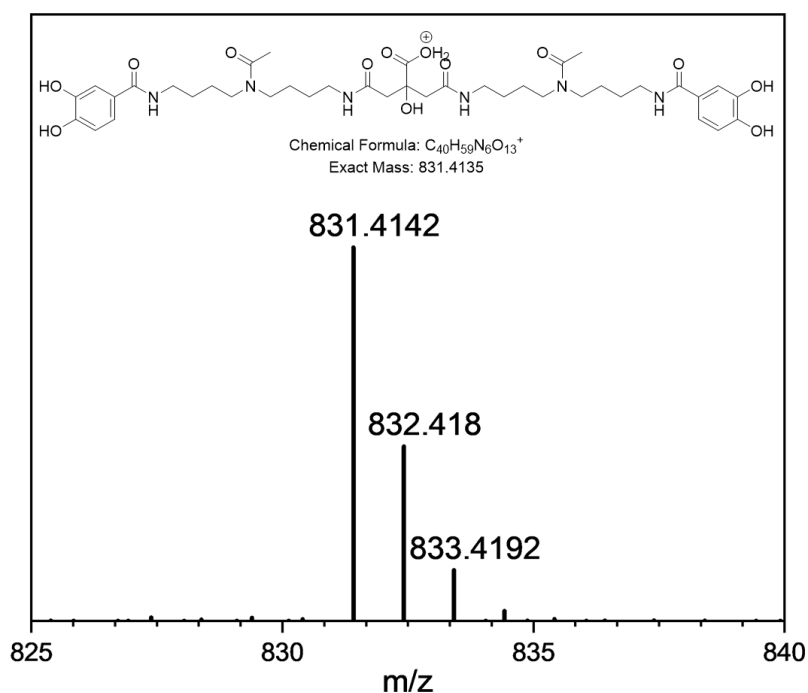
Figure II-16 High resolution mass spectrometry results from rhodopetrobactin B with its isotope pattern.

Despite the QTOF-MS results, further binding studies were conducted. The impact of the two acetyl groups are especially interesting since their role in coordination of Fe^{3+} and Ln^{3+} is still elusive. They could be involved in coordination with their oxygen atoms which would result in up to eight donor groups for the possible preferential coordination of Ln^{3+} over Fe^{3+}. On the other hand, they could restrict the whole molecule to form certain geometry due to the sterically hindrance they create. Before proceeding with the experiments, DFO was employed as a proxy for RPB.

UV/Vis spectra of RPB in H_2O was measured. This was followed by the acquisition of two additional spectra with $FeCl_3$ and $LaCl_3$ as Fe^{3+} and La^{3+} source, respectively. The samples were measured immediately after addition of the metal salt, after 1 h and after 24 h incubation in the dark at room temperature (Figure II-17).
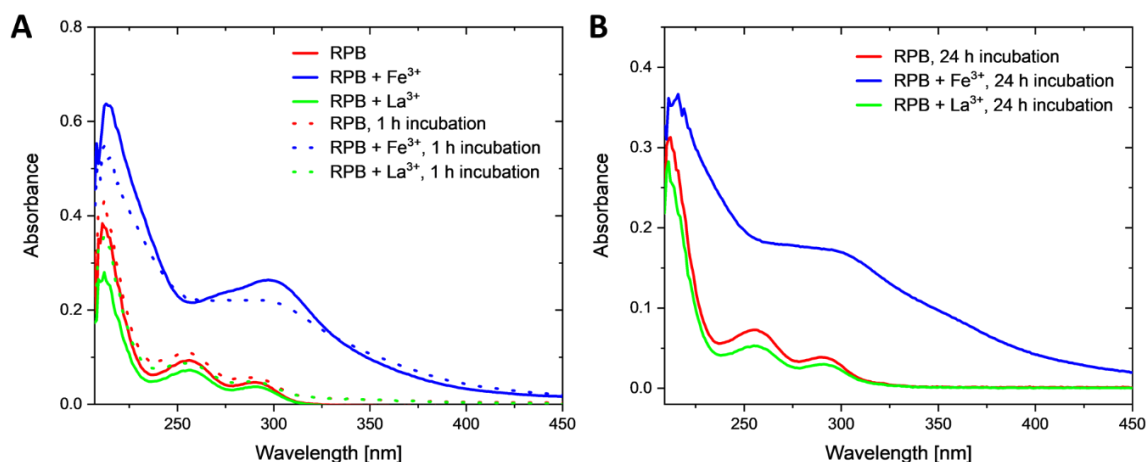
Figure II-17 UV/Vis spectra of rhodopetrobactin B with Fe^{3+} and La^{3+} (0.1 mM each, 1:1). Samples were measured A) directly (solid line), after 1 h incubation (dotted line) or B) after 24 h. Solvent: H_2O, incubation: in the dark at room temperature.

RPB shows two distinct absorption at 255 nm and 290 nm which originate from the 3,4-dihydroxybenzoic acid groups (Figure II-17A, red solid line).[80] After the addition of equimolar amount of Fe^{3+} and immediate measurement, the observed spectra changed and one single absorption peak at 300 nm was observed indicating the formation of a complex (Figure II-17A, blue solid line). On the other hand, the addition of La^{3+} did not led to any major changes in the spectrum (Figure II-17A, green solid line). Then, all samples were incubated for 1 h in the dark at room temperature and measured again. After incubation, only the sample containing Fe^{3+} exhibited a slight change, characterized by a less sharp absorption peak compared to before, suggesting precipitation of the complex. After 24 h incubation in the dark at room temperature (Figure II-17B), the absorption peaks remained unchanged indicating that the addition of equimolar amount of La^{3+} to RPB did not led to complexation as no change was observed compared to the control sample. As no complexation of La^{3+} in H_2O was observed, UV/Vis experiments in a buffer solution were conducted (Figure II-18).
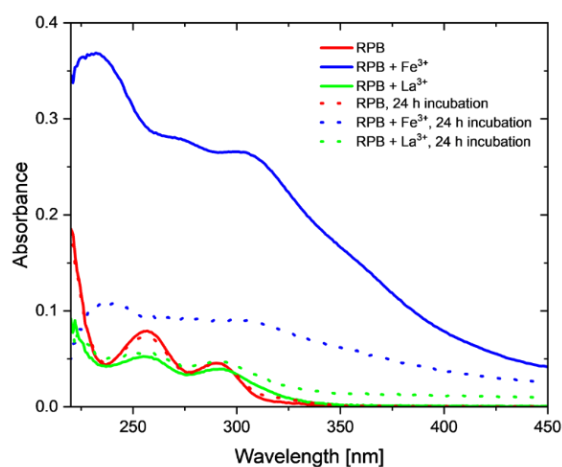
Figure II-18 UV/Vis spectra of rhodopetrobactin B with Fe^{3+} and La^{3+} (0.1 mM each, 1:1). Samples were measured directly (solid line) or after 24 h incubation (dotted line). Solvent: 10 mM MOPSO, 100 mM KCl, pH 6.6, incubation: in the dark at room temperature.

Similar results are observed in buffer solution. RPB remains stable over a period of 24 h, showing no significant change in the UV/Vis spectra (Figure II-18, red lines). Again, the spectra of RPB-Fe^{3+} (Figure II-18, blue lines) shows a drastic decrease of signal after 24 h indicating that the complex precipitates in buffer too. The spectrum of RPB-La^{3+} is unchanged which is similar to the results in H_2O, suggesting that no La^{3+} is bound after 24 h in buffer.

Then, the CAS assays was used to investigate the binding of RPB to Lns (Figure II-19). The default conditions across the pH range of 6.4–8.1 with three $LnCl_3$ ($LaCl_3$, $NdCl_3$ and $LuCl_3$) that were previously used for the assessment of DFO and AB were applied.
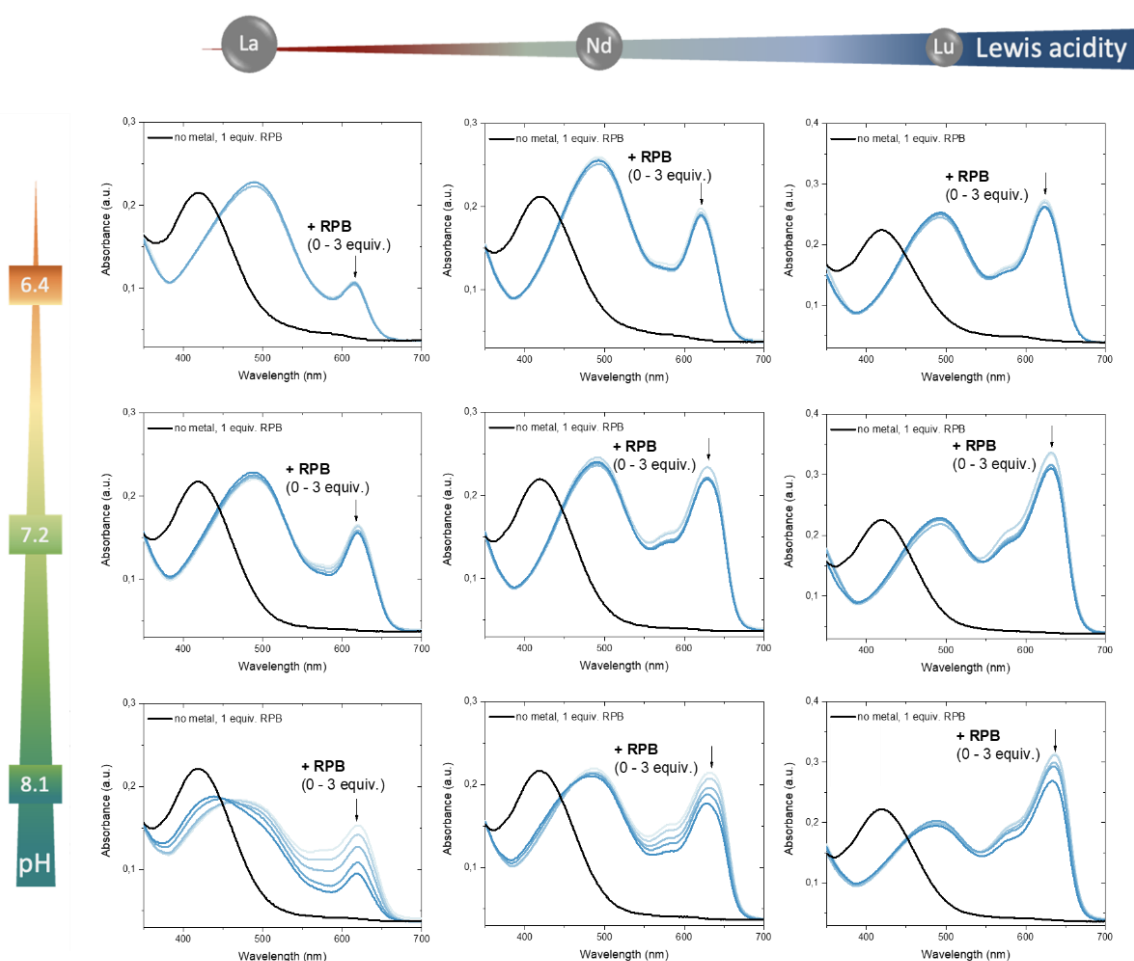
Figure II-19 Chrome azurol S assay with rhodopetrobactin B (RPB) at three different pH values with $LaCl_3$, $NdCl_3$ and $LuCl_3$. Conditions: MOPSO/HEPES buffer (1.5 mM each), 18.75 µM CAS, 50 µM HDTMA, 18.75 µM $LnCl_3$ and 0–3 equiv. 0–56.25 µM RPB, equivalents of RPB increases from light to dark blue.

Akin to the results with AB and DFO, a pH- and Lewis acidity-dependent binding is observed with RPB: an increase in pH correlates with enhanced complexation of the Lns, as evidenced by a reduction in λ_{max} at 625 nm. This trend is also apparent in relation to Lewis acidity, where the highest decrease in λ_{max} at 625 nm is observed for Lu^{3+}, the strongest Lewis acid. These results suggest that RPB is able to compete with CAS for Lns and can strip off Lns from CAS. Although the CAS assay is not a quantitative method, the smaller reduction of λ_{max} at 625 nm with RPB compared to DFO (Figure II-10) and AB

(Figure II-11), implies that RPB binds to Lns less strongly than DFO and AB do. This is also supported by the mass spectrometry data.

In vivo growth studies with RPB did not led to significant increased growth of ΔmxaF but concurrent analysis of the influence of Ln solubility on gene networks revealed that nearly 1500 genes are differently expressed between growth on $NdCl_3$ or Nd_2O_3.[28] A gene cluster, which was among the most upregulated genes, is homologous to a biosynthetic gene cluster expressing the transport, regulation and biosynthesis of citrate-based siderophores rhodopetrobactin and petrobactin. With molecular networking and structural analysis of ΔmxaF supernatants by ultra high performance liquid chromatography tandem mass spectrometry revealed a chemical structure that matches RPB minus two oxygen atoms.[28] Isolation and extensive NMR analysis of the molecule disclosed two doublets in the aromatic region, indicating the para substitution of the hydroxybenzoic acid group. The lanthanophore, which was named methylolanthanin (MLL, Figure II-20) is able to bind La^{3+}, Nd^{3+} and Lu^{3+} as shown by mass spectrometry. The addition of MLL to ΔmxaF significantly increases the growth yield but is not essential for the growth.[28]

Rhodopetrobactin B
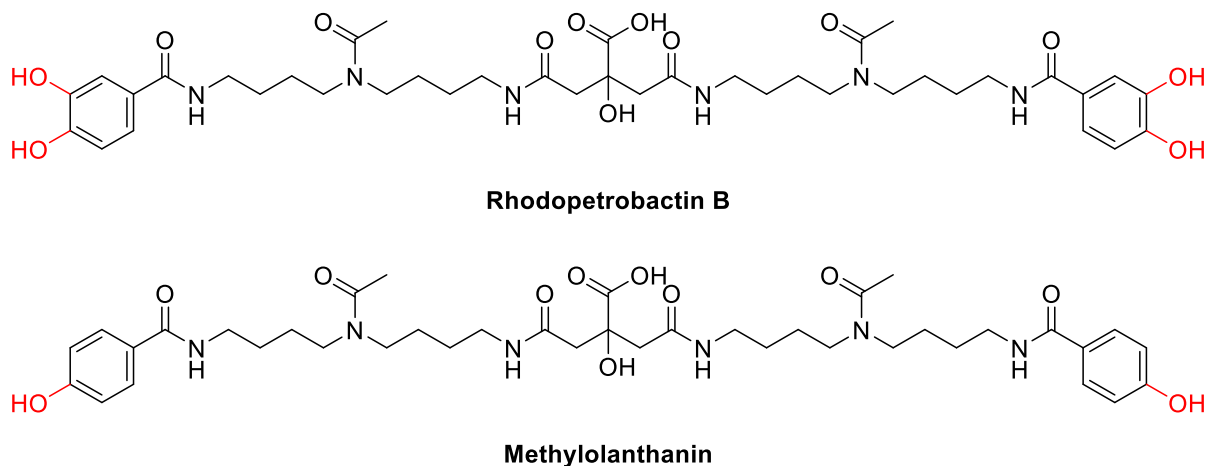
Methylolanthanin

Figure II-20 Chemical structure of lanthanophore methylolanthanin and the related siderophore rhodopetrobactin B.

In summary, the successful synthesis of RPB was confirmed by NMR analysis and mass spectrometry. Then, the ability of RPB to form a complex with Fe^{3+} and La^{3+} in H_2O and MOPSO buffer using UV/Vis spectroscopy was investigated. RPB exhibits absorption maxima at 290 nm and 255 nm, which is characteristic for the 3,4-dihydroxybenzoic acid moieties of RPB and remains stable in H_2O and buffer after 24 h in the dark and at room temperature. A distinct maximum around 320 nm arises upon Fe^{3+} addition but no change is observed for the addition of La^{3+}. CAS assay with RPB across the pH range of 6.4–8.1 using La^{3+}, Nd^{3+} and Lu^{3+} reinforce previously finding that complexation of these Lns with RPB increase with higher pH and a stronger Lewis acid. Finally, *in vivo* growth studies have shown that RPB does not significantly increases the growth of ΔmxaF. But further bioinformatic investigation, molecular networking, structural and functional analysis have revealed methylolanthanin as a

lanthanophore. MLL is capable of binding La^{3+}, Nd^{3+} and Lu^{3+} and significantly increases the growth yield of ΔmxaF.

7. Conclusion and Outlook

Fe^{3+} is an essential element that is indispensable for a wide range of cellular functions. Siderophores are important low-molecular and high-affinity Fe^{3+} chelators that are produced and secreted by microorganism for uptake and transport of Fe^{3+} into the host. Since the discovery of Ln-utilizing enzymes and associated proteins, it was hypothesized that a similar Ln-specific chelator (lanthanophore) was produced by Ln-utilizing microorganisms. The discovery of a TonB-ABC-like pathway, which is commonly used by siderophore-Fe^{3+} complexes to enter the cell, near the gene cluster for Ln-dependent MDH mainly supported this hypothesis.[46] Bioinformatic investigations have led to several citrate-based siderophores (Figure II-21) that could be a lanthanophore.

Aerobactin

Deoxyschizokinen

Petrobactin

Rhodopetrobactin B
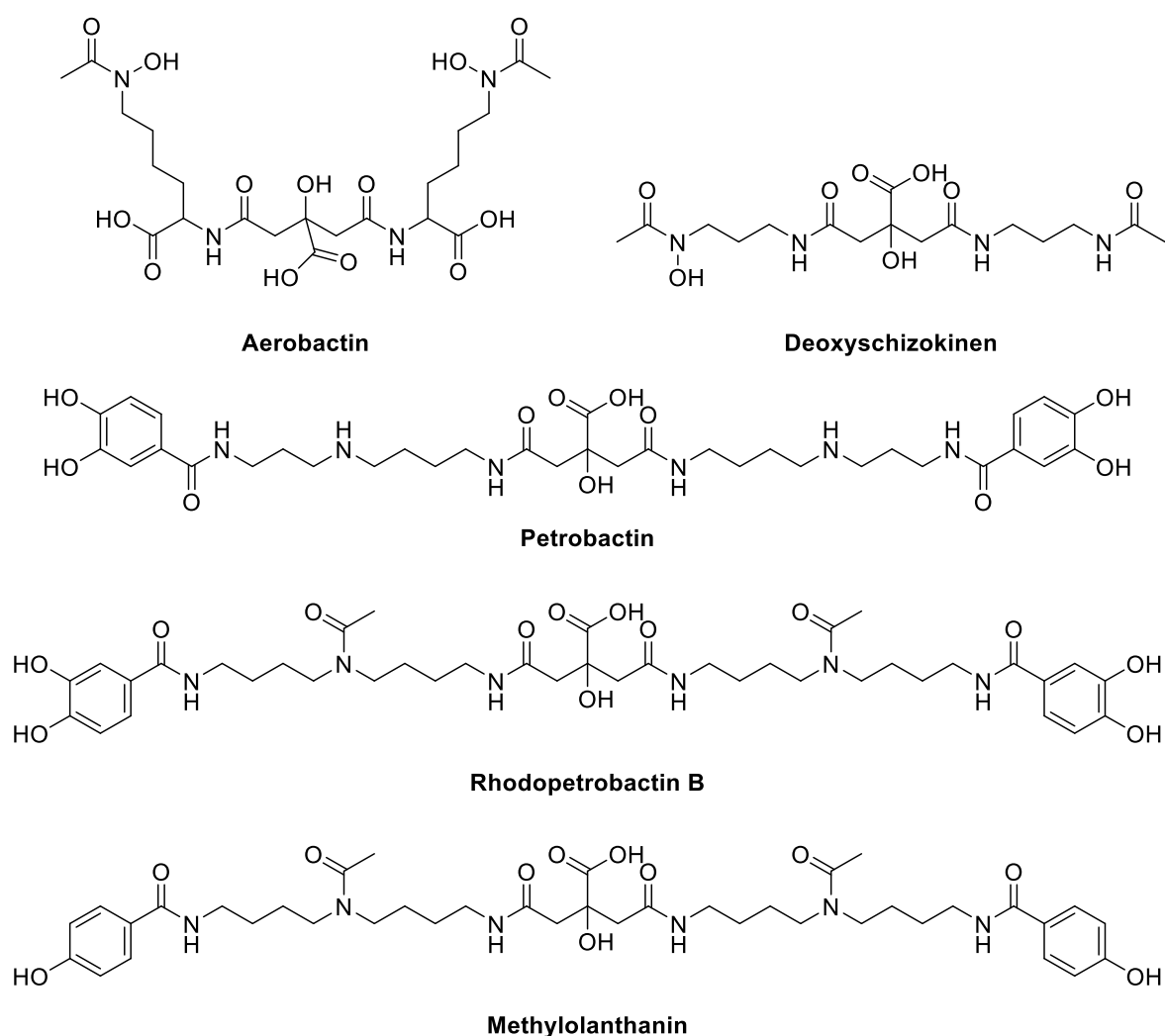
Methylolanthanin

Figure II-21 Overview of citrate-based siderophores that were considered to be a lanthanophore. Only aerobactin and rhodopetrobactin B were successfully synthesized and examined for binding towards Fe^{3+} and Ln^{3+}. Methylolanthanin was isolated from *M. extorquens* AM1 and identified as a lanthanophore.[28]

The syntheses of four citrate-based siderophores were attempted. Deoxyschizokinen and petrobactin could not be synthesized due to synthetic challenges, particularly in the crucial coupling step of the side chains to the central citrate moiety. However, aerobactin (AB) and rhodopetrobactin B (RPB) were synthesized successfully. To provide insights into their capability to form complexes, their binding abilities with Fe^{3+} and Lns^{3+} were further characterized by various spectroscopic methods, including UV/Vis spectroscopy and colorimetric assays. The results suggest pH- and Lewis acid-dependent binding of AB and RPB. The complex formation increases with higher pH as well as stronger Lewis acidity ($Lu^{3+} > Nd^{3+} > La^{3+}$). It should be mentioned that a higher pH will inevitably lead to formation of $Fe(OH)_3$ and $Ln(OH)_3$, distorting the results. These *in vitro* studies were complemented with *in vivo* studies of a mutant strain from *M. extorquens* AM1. The ∆mxaF strain can only grow if Lns are available. The addition of Nd^{3+} restored the growth defect of ∆mxaF and addition of AB or RPB should further enhance the growth. However, in some preliminary experiments growth rates and growth yields did not significantly increase with the addition of AB or RPB, indicating that these siderophores may not function as lanthanophores. Molecular networking and structural analysis of the ∆mxaF supernatant by ultra high performance liquid chromatography tandem mass spectrometry revealed a chemical structure that matches RPB minus two oxygen atoms.[28] Following the isolation, NMR analysis showed that the newly identified molecule has para-substituted hydroxybenzoic acid groups and is able to form complexes with various Lns. The lanthanophore was named methylolanthanin (MLL) and significantly improves the growth rate and growth yield of ∆mxaF. The structural resemblance of MLL to RPB offers intriguing evidence for the possibility of more lanthanophores that share structural similarities with siderophores. Uncovering additional lanthanophores will advance our understanding of the complex biochemical processes of the Ln metabolism. Considering the critical role of Lns in today's industry, the insights obtained may pave the way for innovative strategies for REE separation and application in medicine.

III.   Assessing Ln-Dependent Methanol Dehydrogenase Activity

1. Introduction

The acidophilic methanotroph *M. fumariolicum* SolV was first isolated from a mudpot near the Solfatara volcano by the research group of Op den Camp.[12b, 29] Despite the location and its harsh environmental conditions like temperatures up to 70 °C and a pH of 1, SolV is able to thrive and can therefore be classified as an extremophilic bacterium. Initial attempts to grow SolV in a laboratory setup were not successful. Only the addition of the water from the volcanic mudpot to the cultivation media led to growth. Inductively coupled plasma mass spectrometry (ICP-MS) analysis of the mudpot water revealed an unusual high concentration of Ce^{3+}. After addition of Ce^{3+} to the growth medium, Pol *et al.* were able to grow SolV. Growth studies showed a concentration-dependent growth rate and that the growth rate also highly depends on the supplemented Ln (Ln = La, Ce, Nd, Pr, Sm, Eu and Gd) which is higher with the early Lns.[12b] The cultivation of SolV is a challenging task, as a gas phase with 10% CH_4 and 5% CO_2 as well as a constant temperature of 55 °C is required for optimal growth. They were able to successfully purify Ce-MDH and resolve the crystal structure. Other groups have obtained Ln-MDHs by heterologous expression in *E. coli*, isolation by affinity chromatography using His- and Strep-tags. Once isolated, the holo-enzyme was reconstituted by addition of the cofactor PQQ and the desired Ln.[24] This strategy allowed to obtained Ln- and An-containing MDHs but the metalation of the active site was not determined. Others could successfully reconstitute partial apo-enzymes with the addition of Lns.[20b, 81] Although these methods allowed to obtain Ln-MDH, the cyt c_{GJ} could not be obtained by heterologous expression. A so far unknown modification at or near the heme complex makes the heterologous expression of cyt c_{GJ} not possible and native purification is the only method to obtain cyt c_{GJ}.[32] Versantvoort *et al.* were able to purify and characterize cyt c_{GJ} directly from SolV.[32] UV/Vis spectroscopy confirmed the interaction between Ln-MDH and cyt c_{GJ}. The addition of substrate and Ln-MDH caused the reduction of cyt c_{GJ}, evident by the shift from the oxidized to the reduced state (434 nm to 440 nm).

Our goal was to cultivate SolV with as many as possible Lns and isolate the respective Ln-dependent MDH. Due to the relatively high amount of Ln-MDH in SolV, native purification of Ln-MDH is possible. Additionally, the cyt c_{GJ} was purified as well to develop protein-coupled activity assays based on the methods developed by Anthony and coworkers.[39] Then, the enzyme activity was systematically investigate to further elucidate the mechanism of Ln-MDH (Figure III-1).

Figure III-1 Graphical overview of the workflow. *M. fumariolicum* SolV was grown in a large-scale bioreactor, followed by the purification of Ln-MDH and cyt c_{GJ}. After confirmation by UV/Vis spectroscopy, SDS-PAGE and determination of the metal content in the active site, the enzyme activity of Ln-MDHs were determined by activity assays. This figure was created with Biorender.com

2. Large-Scale Cultivation of *Methylacidiphilum Fumariolicum* SolV

The large-scale cultivation of SolV was carried out in a custom-made 3.7 L bioreactor (Figure III-2A). The bioreactor features an external controlled heating system for precise temperature control of its inbuilt heating jacket, inverted reflux condensers with an external cooling system to minimize evaporation of the growth medium and gas inlets for CH_4, CO_2 and air equipped with gas diffusion stones that create small bubbles to improve the solubility of the gases.
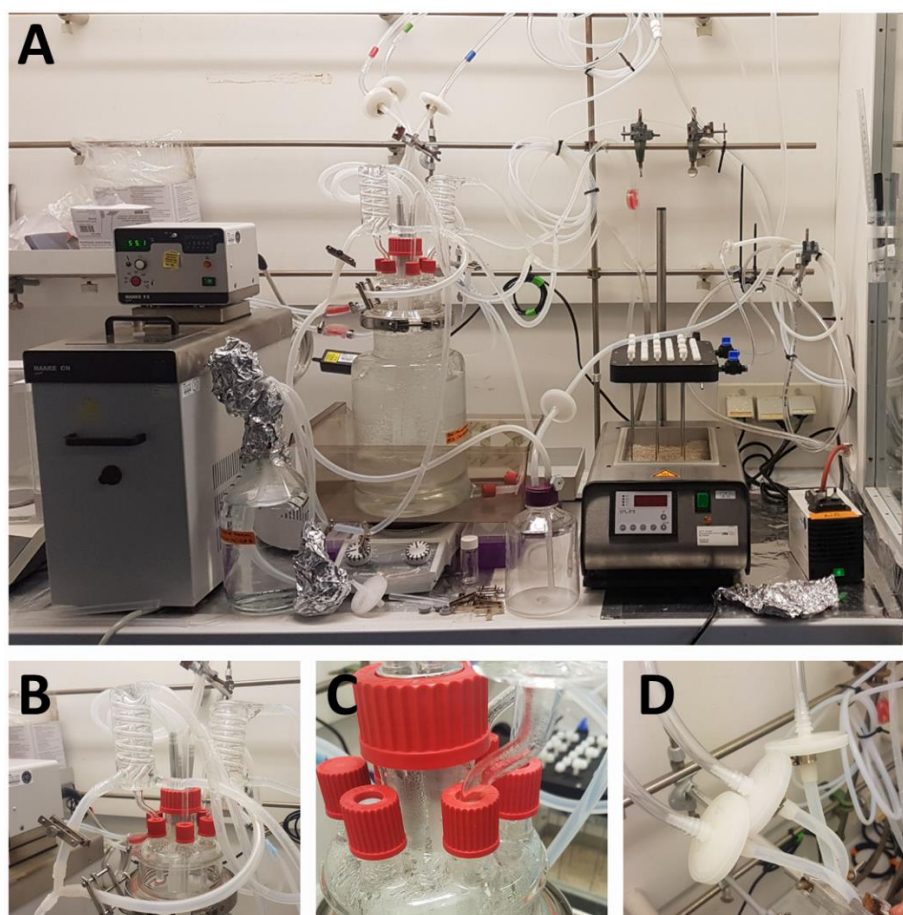
Figure III-2 Pictures of the 3.7 L bioreactor for the large-scale cultivation of *M. fumariolicum* SolV. A) The bioreactor during operation is heated to 55 °C by an external heating system and supplied with air, CH_4 and CO_2 (CH_4 and CO_2 gas bottles are not shown). B) Two inverted reflux condensers are connected to the inlet ports and ensure minimal loss of medium due to evaporation. The condensers are filled with water and cooled by an external cooling system. C) Multiple inlet ports allow to

facilitate sample taking and refilling of medium. D) Large 0.2 µm filter units were used to keep purity of gases high (purity CH_4 ≥ 99.9 vol% and CO_2 99.9 vol%). More details can be found in Ref. [35]

Additional inlet ports allow for the convenient addition of new cultivation medium and an additional outlet facilitates sample taking.[35] The cultivation of SolV follow the procedures reported by Singer *et al*.[35] For the inoculation of the bioreactor, SolV with the desired Ln was initially grown in small polypropylene plastic cultivation flasks. Once SolV reached a high cell density, the inoculant was transferred to the bioreactor until a starting OD_{600} of around 0.05 was reached. Continuous monitoring of the bacterial growth was achieved through regular measurement of the OD_{600}. Bacterial growth typically adheres to a classic growth curve pattern: an initial lag-phase characterized by minimal growth, followed by a phase of rapid exponential growth, transitioning to a stationary phase and subsequently entering a decline in the death phase. A total of nine separate large-scale cultivations of SolV at 55 °C and pH 2.7 with nine different Ln (Ln = La, Ce, Pr, Nd, Sm, Eu, Gd, Tb and Lu) were carried out. Exponential growth was observed for seven out of nine cultivations. The cultivation of SolV with Tb^{3+} and Lu^{3+} was discontinued after ten days, as the growth curve was only linear with these specific elements. The goal was to accumulate as much biomass as fast as possible for the subsequent isolation of the respective Ln-MDH and cyt c_{GJ}, thus prior to reaching the stationary growth phase and subsequent death phase, 2 L of SolV cells were harvested (Figure III-3).
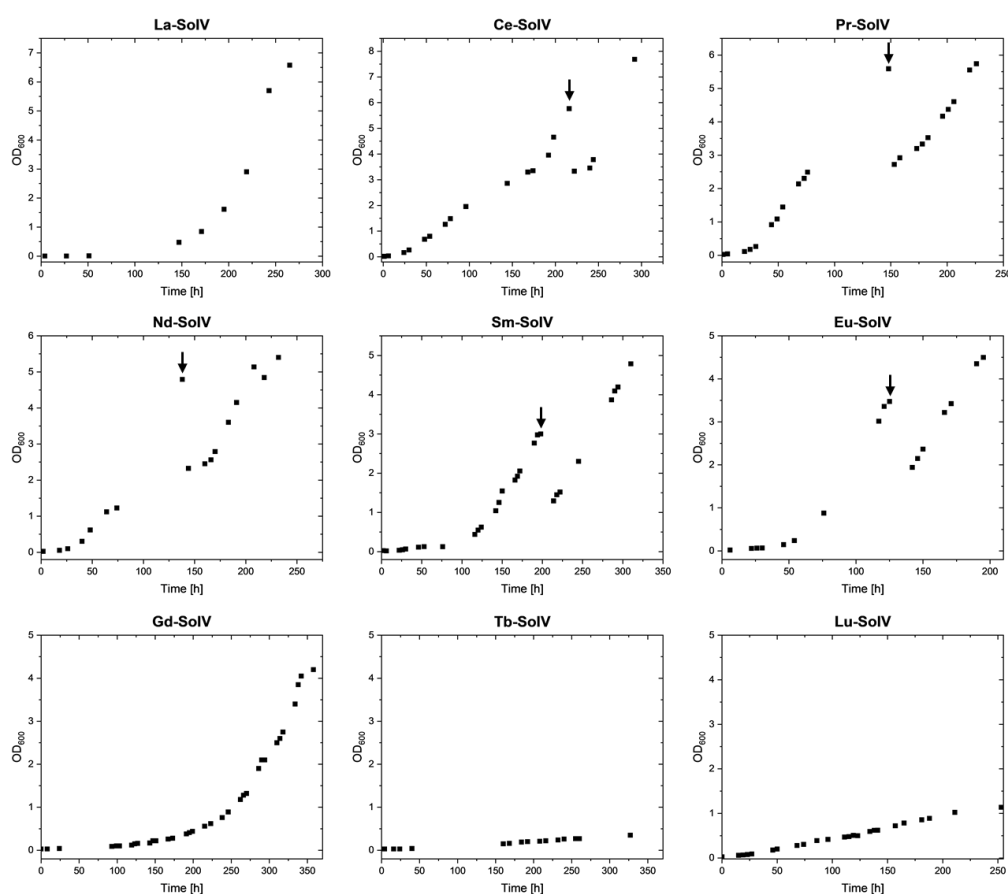
Figure III-3 Growth curves of *M. fumariolicum* SolV cultivated with different Ln (2 µM) at 55 °C and pH 2.7. The arrow indicates the time point when 2 L of SolV was harvested and refilled with new growth medium.

Then, the bioreactor was refilled with new growth medium to benefit from the exponential growth phase, effectively creating a continuous cell culture system. This method was introduced after the cultivation of SolV with La^{3+} was finished, therefore refilling for La-SolV is not shown. With the exception of SolV containing Gd^{3+}, Tb^{3+} or Lu^{3+}, this approach proved effective for all other cultivations, achieving an OD_{600} of over 4 in each case. The growth curves of all cultivations up until the first harvest including the respective growth rates are shown in Figure III-4.
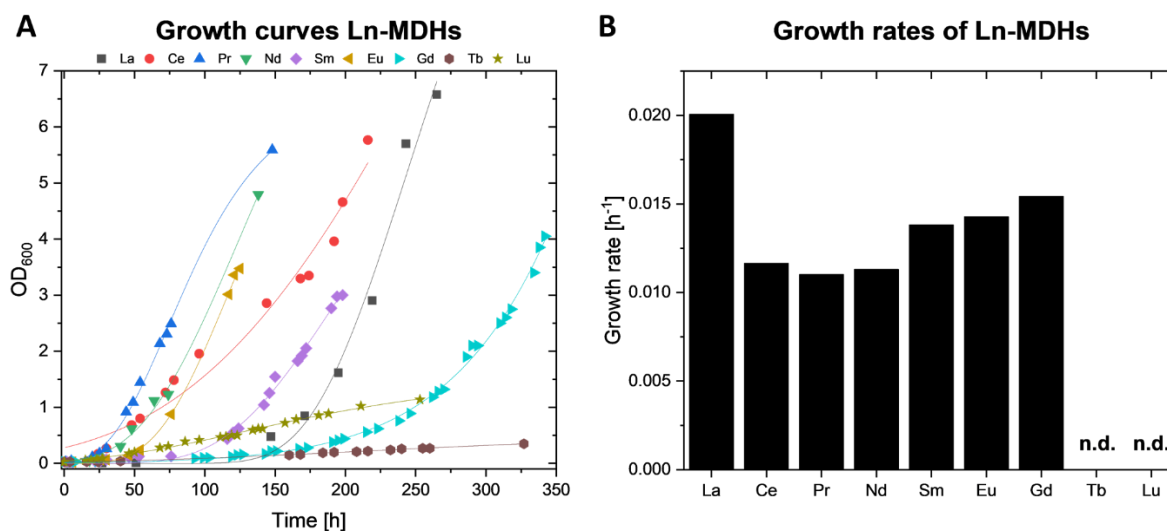
Figure III-4 A) Growth curves of all Ln-SolV cultivation until the first harvest. B) Growth rates of all Ln-SolV during exponential phase. Growth rates of Tb- and Lu-Solv were not determined (n.d.) due to the absence of an exponential growth phase.

Pol *et al.* showed similar growth rates with La^{3+}, Ce^{3+}, Pr^{3+} and Nd^{3+} while the SolV cultivation with Sm^{3+} and Eu^{3+} was less effective.[17] In our bioreactor, La-SolV also demonstrates the highest growth rate but Sm-, Eu- and Gd-SolV have a slightly higher growth rate than SolV grown with Ce^{3+}, Pr^{3+} and Nd^{3+}, contrasting their results. Pr-SolV showed the lowest growth rate. Tb- and Lu-SolV, both not grown by Pol *et al.*, remained in the slow-growing lag phase. Even after ten days, Tb- and Lu-SolV showed no exponential growth. Although more Lns were supplemented to the growth medium than Pol *et al.* (2 µM in comparison to 0.25 µM Ln), our growth rates are much lower than reported by them (e.g. La: 0.085 h^{-1} vs. 0.020 h^{-1}).[12b] This is attributed to the use of their advanced, commercially available 10 L bioreactor that enables better monitoring of the cultivation process and tighter control of parameters such as gas flow and temperature. It is important to point out that each cultivation encountered unique challenges ranging from variations in initial OD_{600}, temporary reduction or interruptions in gas supply, to fluctuations in temperature (48–55 °C) and varying timepoints of harvest and refilling of medium. After each cultivation cycle, the procedures and operations of the bioreactor were improved to overcome these issues. Therefore, the reported growth rates are likely not representative.

After harvesting, the liquid cell culture was centrifuged, the supernatant discarded, the cell pellet was resuspended with PIPES buffer containing 1 mM MeOH and flash-frozen in liquid nitrogen. The buffer

containing 1 mM MeOH is imperative to stabilize the Ln-MDH in the following purification process and also reduces the loss in enzyme activity while being stored long-term at -80 °C. Furthermore, commonly used phosphate buffer should not be used as resuspension buffer nor as storage buffer and should be completely avoided when working with Ln-dependent proteins. Due to the formation of insoluble $LnPO_4$ with the Ln in the active site of the enzyme, phosphate buffer can drastically impair the enzyme activity.

3. Cell Lysis and Protein Purification

3.1 Purification and Characterization of Lanthanide-Dependent Methanol Dehydrogenases

Once the cell pellet was resuspended, the cells were subjected to cell lysis. Cell lysis is a critical step that involves breaking down of the cell membrane to release the intracellular components like proteins and DNA. An effective cell lysis can help maximizing the yield and purity of the desired target protein. Various methods for cell lysis are available and are generally categorized into mechanical (e.g. high pressure homogenizer or glass beads) and non-mechanical lysis which is further divided into physical, chemical and biological methods like heating, use of detergents and enzymatic digestion, respectively.[82] Commonly, a combination of methods is applied to ensure effective lysis. For lysis of SolV, the combination of freeze/thaw, chemical and enzymatic lysis was employed. A commercially available protein extraction reagent for chemical cell lysis was added to the frozen sample and incubated until thawn. Then, lysozyme was added to further facilitate the breakdown of the cell membrane, followed by DNAse to degrade unwanted DNA. Lastly, the protein-containing supernatant was separated from the cell debris by centrifugation. To optimize the isolation of Ln-MDH and cyt c_{GJ}, the protocol of Pol *et al.* was modified.[12b] Fast protein liquid chromatography (FPLC) was conducted using the ÄKTA Go system, employing a cation exchange column for the purification. A 10 mM PIPES buffer solution containing 1 mM MeOH (pH 7.2) as buffer A was used to ensure enzyme activity remains high throughout the purification process. The elution buffer B consists of the same buffer with the addition of 1 M NaCl. Initially, bound proteins were eluted with a linear gradient of 0 to 100% buffer B (Figure III-5).
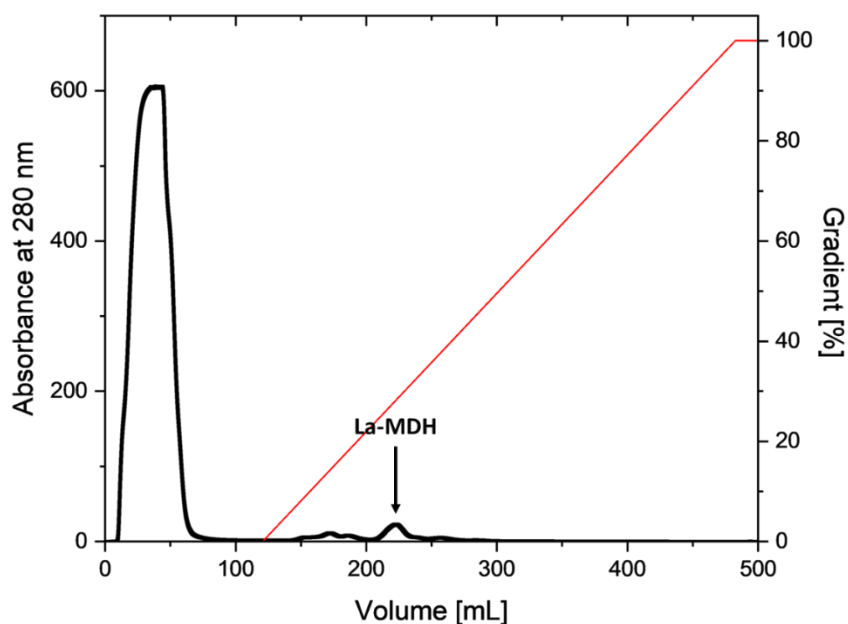
Figure III-5 Chromatogram of La-SolV purification. Buffer A: 10 mM PIPES with 1 mM MeOH (pH 7); buffer B: 10 mM PIPES with 1 mM MeOH and 1 M NaCl (pH 7). Gradient: 0 to 100% B. Flow: 5 mL/min.

Three major peaks were collected and analyzed by UV/Vis spectroscopy and sodium dodecyl sulfate polyacrylamide gel electrophoresis (SDS-PAGE) (Figure V-25). The UV/Vis spectra displayed the characteristic A_{280} protein band for all samples indicating the presence of proteins. Peak 3 also demonstrates an absorbance at 355 nm which is characteristic for the cofactor PQQ implying the presence of Ln-MDH.[12b, 20b] SDS-PAGE analysis of peak 3 shows a prominent band around 63 kDa corresponding to Ln-MDH. Peak 1 has a prominent band around 25 kDA which aligns with the size of cyt c_{GJ}.[32] Another faint band can be observed around 35 kDA which is suggested be a hydroxylamine oxidoreductase. These results show that cyt c_{GJ} elutes at 2% B and Ln-MDH at 25 to 30% B. Further optimizations have led to a time- and solvent-saving protocol (see Table III-1 and Figure III-6) that allows to simultaneously isolate c_{GJ} and pure Ln-MDH in a single process.

Table III-1 Optimized purification method for the purification of Ln-MDH and cyt c_{GJ}. CV, column volume (20 mL).

Step #	Elution buffer B	Comment
1	0–2% for 1 CV	Remove unbound proteins
2	2% for 3 CV	Elution of cyt c_{GJ}
3	2–45% for 10 CV	Elution of Ln-MDH at 25–30% B
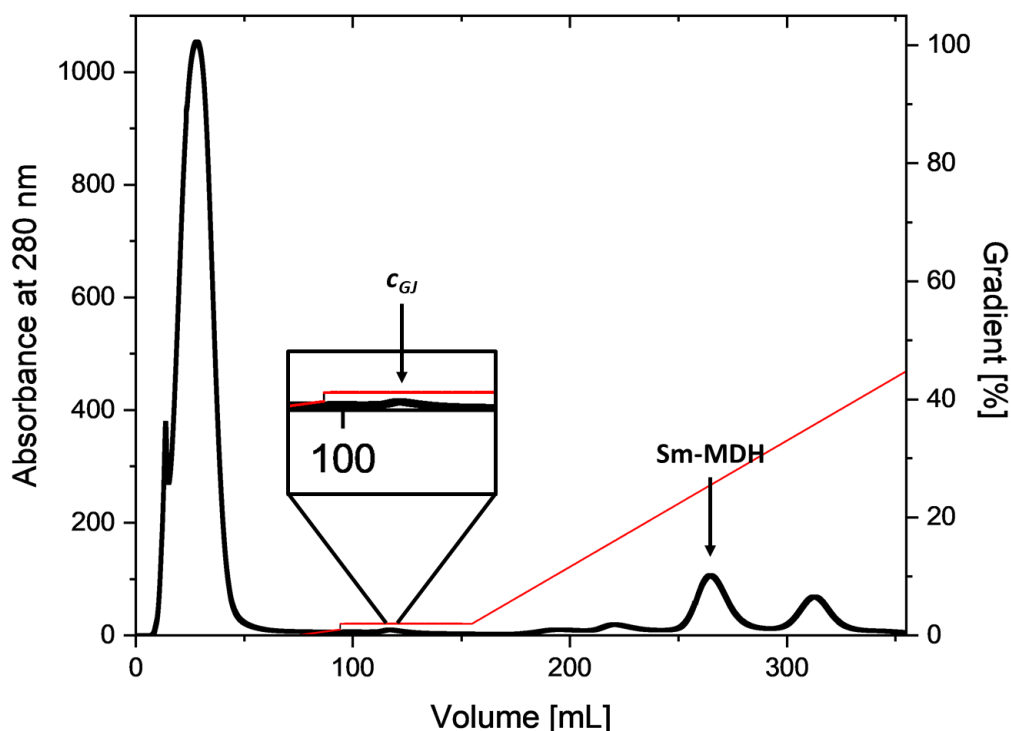
Figure III-6 Chromatogram of Sm-SolV purification. Buffer A: 10 mM PIPES with 1 mM MeOH (pH 7); buffer B: 10 mM PIPES with 1 mM MeOH and 1 M NaCl (pH 7). Gradient: 0 to 2% B, then 0 to 45% B. Flow: 5 mL/min.

The purification for Ln-MDH from each Ln-SolV was consistent and the results were reproducible. In total, nine different Ln-MDHs were obtained. Previous ICP-MS experiments have shown that the active site of Ln-MDHs is not fully occupied with Lns, thus determination of the metal content of the enzyme is indispensable.[20b] Good *et al*. noticed that the enzyme activity of La-MDH with a metal content of 39% only displays half the enzyme activity compared to previous studies.[20a] Each batch of purified Ln-MDH should be analyzed separately and considered as an individual enzyme batch because variability in metal content is possible, i.e. one batch of Pr-MDH has a metal content of 50%, whereas another batch of Pr-MDH has 40%. To determine the metal content, the ratio between total protein amount and Ln^{3+} concentration is required. The total protein concentration of each sample was determined by A_{280} measurement with UV/Vis spectroscopy and the concentration of Ln^{3+} of each sample was measured by ICP-MS after digestion of the sample with HNO_3 at 90 °C for 1 h. ICP-MS measurements reveal only the total metal content of a sample without specifying active site metalation, which can be a challenge when Ln-MDH co-purifies with other Ln-binding proteins like LanM, as noted by Featherston *et al*.[23] This would make ICP-MS measurement ineffective, but time-resolved laser-induced fluorescence spectroscopy (TRLFS) is able to distinguish between Eu^{3+} in the active site and in solution. TRLFS analysis validated the metal content of Eu-MDH that was previously determined by ICP-MS measurement, affirming the reliability of ICP-MS as an analytical method to determine the metal content.[83] The metal content of one batch of each Ln-MDH is shown in Table III-2.

Table III-2 Metal content of one batch of each Ln-MDH. Results of protein determination by UV/Vis spectroscopy and Ln^{3+} concentration determination by ICP-MS measurement (n = 2) were used to calculate the metal content. n.d., not detected.

Ln-MDH	La	Ce	Pr	Nd	Sm	Eu	Gd	Tb	Lu
Metal content [%]	42.7	42.4	43.8	47.8	41.9	34.3	19.2	11.3	n.d.

The metal content is higher for the early Lns up to Sm^{3+} (42–48%) but decreases rapidly afterwards. Tb-MDH showed the lowest occupancy with 11.3% and measurements of Lu-MDH did not detect sufficient amount of Lu^{3+}, although preliminary analysis by SDS-PAGE clearly showed the Ln-MDH at 63 kDa (Figure V-26). Still, Ln-MDH obtained from Lu-SolV was precluded for further experiments. For the remaining eight Ln-MDHs, the SDS-PAGE analysis depicted in Figure III-7 demonstrates that none of the samples contain any major protein impurities.
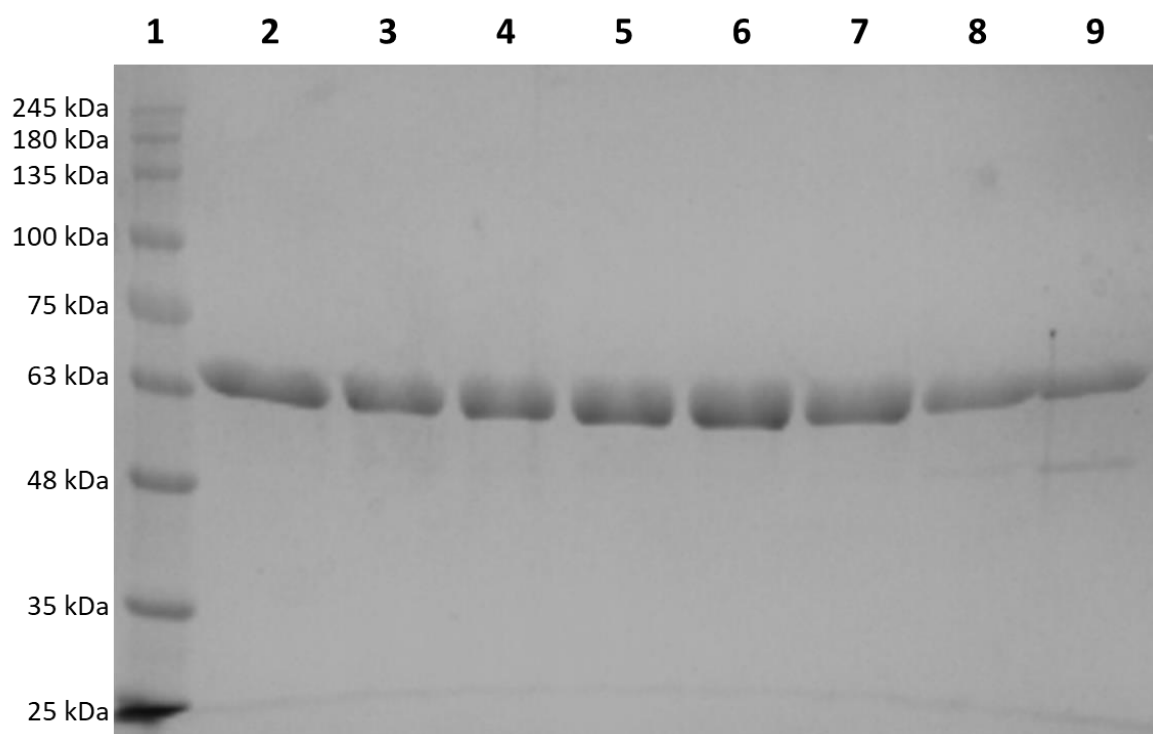
Figure III-7 SDS-PAGE analysis (12% w/v acrylamide) of purified XoxF-MDHs (1: marker, 2: La-MDH, 3: Ce-MDH, 4: Pr-MDH, 5: Nd-MDH, 6: Sm-MDH, 7: Eu-MDH, 8: Gd-MDH, 9: Tb-MDH). BlueEye prestained protein ladder (Jena Bioscience) was used as the marker.

In summary, SolV was cultivated using nine different Lns, with seven displaying exponential growth curves, while Tb- and Lu-supplemented SolV only demonstrated linear growth curves. A purification protocol was established to reliably purify the respective Ln-MDH. Due to the variability in the active site metalation of the enzyme, ICP-MS analysis is indispensable to accurately measure the metal content to determine the amount of active enzyme of each enzyme batch. ICP-MS analysis showed that Lu-MDH did not contain any Lu^{3+} in the active site and was thus omitted for further experiments. Therefore, eight pure Ln-MDH could be isolated from the collected Ln-SolV cells. While the purification

protocol also allowed to isolate cyt c_{GJ}, an additional purification step is necessary due to the presence of an impurity.

3.2 Purification and Characterization of Cytochrome c_{GJ}

In comparison to Ln-MDH, the amount of cyt c_{GJ} isolated from SolV is rather low. The inbuilt UV/Vis monitor of the ÄKTA Go also indicates overlapping protein signals in cyt c_{GJ}-containing fractions thus impurities by other proteins are expected. Contaminating proteins could interfere with the protein assay components and also distort the protein concentration measurement of cyt c_{GJ}, compromising the results and validity of the quantitative assay. Size exclusion chromatography (SEC) was employed for the second purification of cyt c_{GJ} to remove protein impurities by differentiating based on the protein size. The SEC protocol from Versantvoort *et al.* was modified by changing the buffer to 10 mM PIPES with 200 mM NaCl (pH 7.2).[32] The purification was conducted on a ÄKTA Pure system with its inbuild multi-wavelength UV/Vis monitor to facilitate identification of cyt c_{GJ} fractions based on its characteristic A_{434} band.[32] Initial procedures were performed using a solvent flow of 1 mL/min but overlapping fractions of cyt c_{GJ} and the impurity led to reduction of the solvent flow to 0.3 mL/min to increase the resolution of the separation. Reducing the flow further would not necessarily be beneficial, as diffusion effects could negatively affect the resolution. With the help of the multi-wavelength UV/Vis monitor, fractions containing cyt c_{GJ} could be clearly identified (Figure III-8). Pure cyt c_{GJ} was obtained as shown by SDS-PAGE analysis and UV/Vis spectroscopy (Figure III-9).
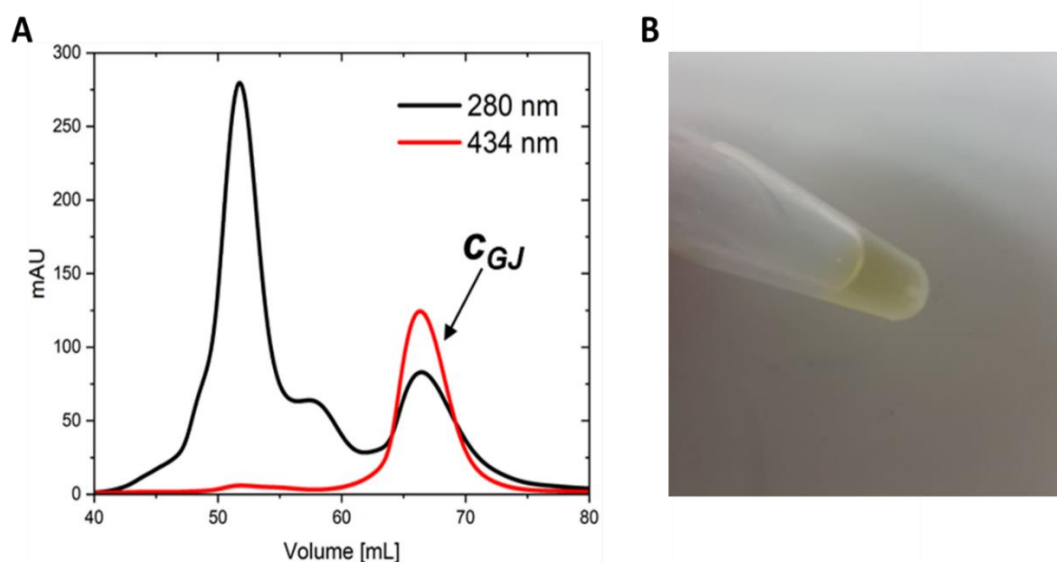
Figure III-8 A) Chromatogram of cyt c_{GJ} purification by size exclusion chromatography (SEC). Conditions: 10 mM PIPES with 0.2 M NaCl, pH 7.2 at 4 °C. B) Picture of purified cyt c_{GJ}.

Due to the unknown modification at or near the heme complex of cyt c_{GJ} and associated difficulties to conduct heterologous expression of cyt c_{GJ}, obtaining cyt c_{GJ} is highly laborious. Furthermore, the

protein-coupled assay requires high amount of cyt c_{GJ} (typically 1–10 μM for a single measurement). For the isolation of around 1 mg pure cyt c_{GJ}, roughly 150 mL SolV cells (OD$_{600}$ > 3) are required which takes at least 10 days to grow and 10 days to purify. A single enzyme activity measurement using the protein-coupled assay at 100 μL assay volume and 5 μM cyt c_{GJ} requires 15 μg. Given eight Ln-MDH and conducting three measurement for each Ln-MDH, 400–500 μg of cyt c_{GJ} is required to comfortably perform one experiment. Thus, alternative methods to decrease the time-consuming procedure were investigated.
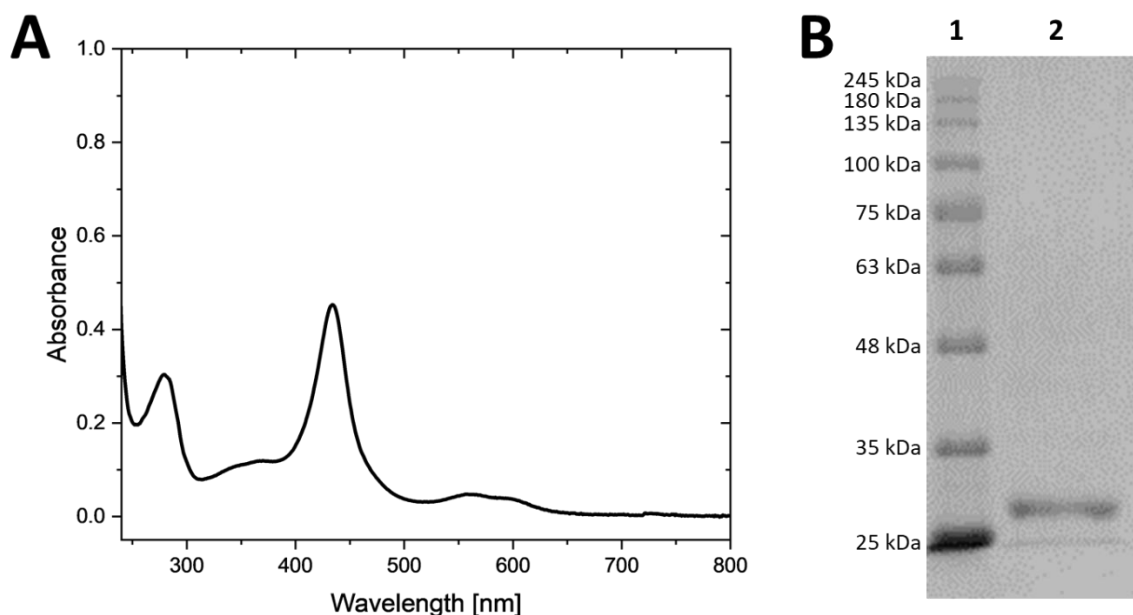
Figure III-9 A) V/Vis spectrum of cyt c_{GJ} after purification by size exclusion chromatography. B) SDS-PAGE analysis (12% w/v acrylamide) of the purified cyt c_{GJ} after size exclusion chromatography (1: marker, 2: cyt c_{GJ}). BlueEye prestained protein ladder (Jena Bioscience) was used as the marker.

In the first place, the activity and stability of cyt c_{GJ} after long-term storage was investigated. The activity of previously purified cyt c_{GJ} sample, which were stored at -80 °C, were assessed. Three different cyt c_{GJ} samples, stored for varying durations, were analyzed: a five-year-old sample (cyt c_{GJ} 1), a 2.5-year-old sample (cyt c_{GJ} 2) and a one-month old sample (cyt c_{GJ} 3). The protein-coupled activity assay based on Gutenthaler *et al.* was used to assess the enzyme activity with Pr-MDH.[40] In addition, various ratios of Ln-MDH to cyt c_{GJ} were evaluated for their effect (Figure III-10).
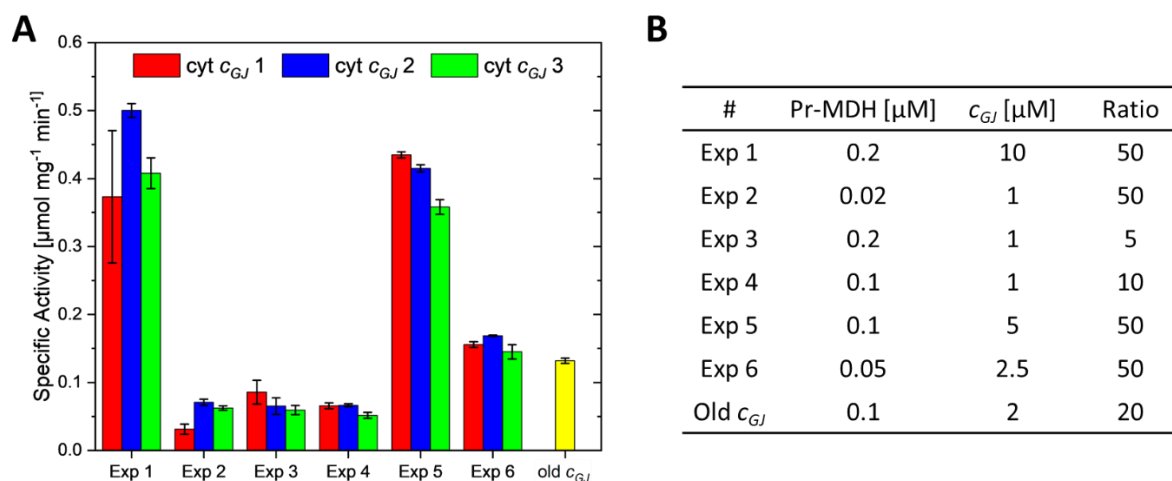
Figure III-10 Specific activity (n = 2) of 20–200 nM Pr-MDH with 1–10 µM cyt c_{GJ}. Cyt c_{GJ} 1, cyt c_{GJ} 2 and cyt c_{GJ} 3 were stored at -80 °C for 5 years, 2.5 years and 1 month, respectively. The old cyt c_{GJ} sample was stored at 4 °C for two years. Conditions: 10 mM PIPES pH 7.2, 50 µM cyt c from equine heart, 20 mM MeOH, 45 °C.

Albeit belonging to different „generations", all three cyt c_{GJ} samples exhibited comparable enzyme activity across all experimental conditions. It is crucial to note that simply maintaining a specific ratio of cyt c_{GJ} to Ln-MDH is not sufficient but the absolute concentration of the proteins matters as well. For example, both Exp 1 and Exp 2 have a Ln-MDH to cyt c_{GJ} ratio of 50, but the enzyme activity in Exp 1 is an order of magnitude higher due to the higher protein concentration in solution. When experiments with the same amount of Ln-MDH and different amount of cyt c_{GJ} are compared (Exp 1 vs. Exp 3 or Exp 4 vs. Exp 5), the experiments with higher cyt c_{GJ} concentration yield higher enzyme activity. These results are expected as reactions typically proceed at a faster rate in more concentrated solution. Valuable information is found when comparing the conditions of Exp 1 and Exp 5 which is frequently used for the protein-coupled activity assays. Both are in the same order of magnitude, have the same ratio and also display comparable enzyme activity but Exp 5 only requires half the amount of cyt c_{GJ} for each measurement. Henceforward, the conditions of Exp 5 were used for protein-coupled activity assay which will enables more efficient use of cyt c_{GJ} over time.

Next, the recovery and activity of cyt c_{GJ} from assay mixtures from past experiments was evaluated. These assay mixtures, comprising of Ln-MDH, cyt c_{GJ}, cyt c from equine or bovine heart and MeOH, were stored at 4 °C for at least two years. The assay mixture was injected without further preparation into the ÄKTA Go system and cyt c_{GJ} was isolated from the remaining assay components by cation exchange chromatography (Figure V-27). Then, protein-coupled activity assay with 100 nM Pr-MDH and 2 µM cyt c_{GJ} was conducted and a specific enzyme activity of 0.13 µmol mg^{-1} min^{-1} was reached. Even after over two years of storage at 4 °C, the old cyt c_{GJ} sample remains stable and relatively active. The activity of this cyt c_{GJ} sample is comparable to Exp 4 and Exp 5 (both were conducted with 100 nM Pr-MDH). The ratio of this cyt c_{GJ} sample (20) falls between the ratios of Exp 4 (10) and Exp 5 (50), which is correspondingly reflected in its specific enzyme activity, also falling between those two

experiments. Therefore, assay mixtures can be retained for future use and cyt c_{GJ} can be recovered without significant loss in activity.

After a second purification step, cyt c_{GJ} could be successfully purified by size exclusion chromatography. The low abundance of cyt c_{GJ} in SolV and laborious isolation protocol required the optimization of handling cyt c_{GJ}. Optimal reaction conditions for the protein-coupled assay were found and will save half the amount of required cyt c_{GJ} per measurement. Additionally, cyt c_{GJ} is highly stable and remains active when stored for five years at -80 °C. Recycling of cyt c_{GJ} from previous protein-coupled assay mixtures is possible even after storage for more than two years at 4 °C. The the activity stays relatively high, but it remains open how often this recycling procedure can be done before cyt c_{GJ} losses its function.

4. Determination of Methanol Dehydrogenase Enzyme Activity

4.1 Publication: Activity Assays of Methanol Dehydrogenases

Sophie Marie Gutenthaler, Manh Tri Phi, Helena Singer, and Lena J. Daumann*

Contributions: HS, MTP and SMG wrote section 1, 2 and 3/4, respectively. LJD conceptualized, acquired funding and reviewed. All authors approved of the final version.

Keywords: methanol dehydrogenase, lanthanides, assay, cytochrome, electron acceptor

This work was published as a chapter in the 650th volume of the "Methods in Enzymology" book series, edited by Prof. Dr. Joseph A. Cotruvo Jr. This volume summarizes the latest developments in lanthanide-dependent processes within methylotrophs, covering aspects such as the isolation of these methylotrophs, genetic methodologies, protein expression and purification of lanthanide-utilizing proteins and activity assays for lanthanide-dependent alcohol dehydrogenases and model chemistry.[84] Our work is an update of the Methods in Enzymology article by Day and Anthony, focusing on the recent improvements of the widely used artificial dye-coupled and protein-coupled activity assays to investigate the enzyme activity of lanthanide-dependent methanol dehydrogenases.[39] We update these methods with insights into a new protein-coupled assay using the physiological *c*-type cytochrome and explore the impact of activators, additives and buffers on these systems.

CHAPTER THREE

Activity assays of methanol dehydrogenases

Sophie M. Gutenthaler, Manh Tri Phi, Helena Singer, and Lena J. Daumann*

Department of Chemistry, Ludwig-Maximilians-Universität München, München, Germany
*Corresponding author: e-mail address: lena.daumann@lmu.de

Contents

Abstract

The field of methanol dehydrogenases (MDHs) has experienced revival in the recent decade due to the observation of lanthanide-dependent MDH, in addition to widely known calcium-MDH. With the advent of lanthanide-dependent alcohol dehydrogenases, the need for reliable assays to evaluate and compare activities between different MDHs is obvious: from extremophilic to neutrophilic organisms, or with different lanthanide ions in the active site. Here we outline four assays that have been reported for Ln-MDH, discussing the advantages and disadvantages of the assays and their components. It should be noted, in 1990 Day and Anthony produced a comprehensive summary in Methods in Enzymology on the available methods for Ca-MDH assays at the time (Day & Anthony, 1990). This chapter is an updated appraisal of the most important developments in the last 30 years.

1. Assays based on artificial electron acceptors

Pyrroloquinoline quinone-dependent MDHs are responsible for the oxidation of primary alcohols such as methanol to formaldehyde in many bacteria, utilizing a specific cytochrome as an electron acceptor (EA). For kinetic investigations of MDH, the physiological electron acceptor cytochrome can be replaced with artificial components. One of the most widely used artificial dye-coupled assays is based on a protocol by Anthony from the early 1960s. The experimental conditions have been optimized and adjusted for use in physiological environments over the decades. Using only artificial components for enzymatic activity determination has two major advantages over physiological cytochrome EAs: they are commercially available, and can be used independent of the organism and its specific cytochrome (Scheme 1).

Alkylated phenazines, such as phenazine ethosulfate (PES) or phenazine methosulfate (PMS), are used as artificial primary EAs for the regeneration of the redox cofactor pyrroloquinoline quinone (PQQ) in the active site of MDH (Scheme 1) (Anthony, 2000). The oxidation of substrates can be visualized spectrophotometrically by the final EA: 2,6-dichlorophenol indophenol (DCPIP), which decolorizes on reduction at 600 nm; or with the redox dye Wurster's Blue (WB) at 610 nm (Jahn et al., 2020; Myers, 1990).
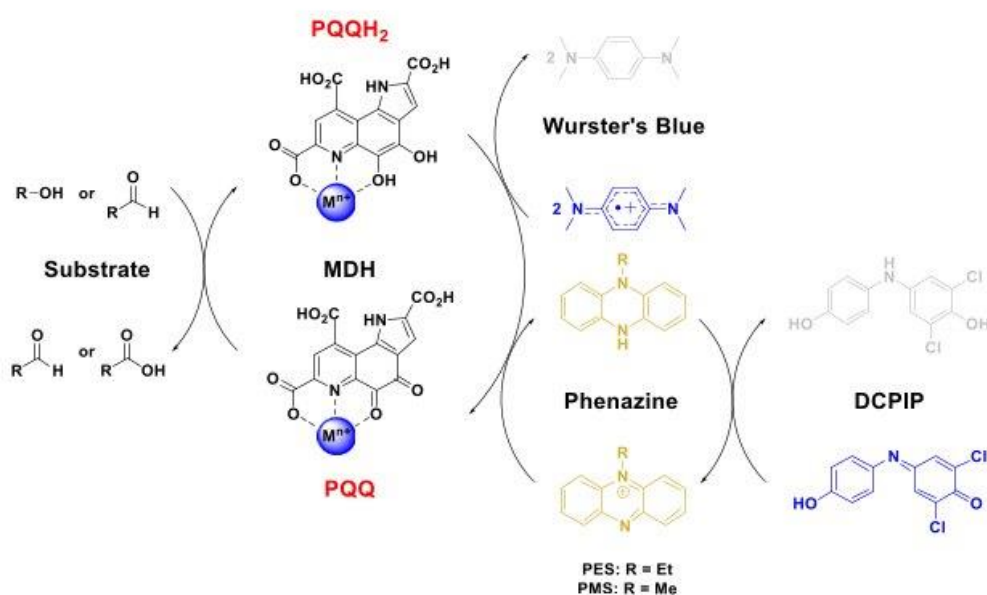
Scheme 1 Overview of the artificial dye assays for methanol dehydrogenases (Jahn et al., 2020).

If WB is used, no further EA is required since the redox indicator WB acts as both an EA and a redox dye (Anthony, 2000; Jahn et al., 2020).

Besides monitoring the enzymatic activity with exclusively artificial components, an additional method is described using the physiological electron acceptor, cytochrome c_L, coupled to the spectrophotometric output of DCPIP (Cox, Day, & Anthony, 1992). To quantify the enzymatic activity of MDH and to enable comparison between MDHs, the specific activity can be determined. Besides the amount of enzyme used, further parameters and values need to be identified to calculate the enzyme unit, U. The extinction coefficient ε_{600nm} for DCPIP or ε_{610nm} for WB depends on the pH as well as the temperature and buffer system. As various values for ε can be found in the literature (Jahn et al., 2020), determination of this value is recommended for each respective system based on the Beer–Lambert law. The pathlength of the cell and the volume of assay are set by the equipment and device. The initial rate of slope should be calculated after the addition of substrate; a period of 1–5 min is optimal.

$$specific\ activity\ \left[\mu mol\ min^{-1}\ mg^{-1}\right] = \frac{enzyme\ unit\ U\ \left[\mu mol\ min^{-1}\right]}{amount\ of\ enzyme\ \left[mg\right]}$$

$$enzyme\ unit\ U\ \left[\mu mol\ min^{-1}\right] = \frac{-1 \cdot initial\ rate\ of\ slope\ of\ measurement}{\varepsilon\ \left[cm^{-1}M^{-1}\right] \cdot pathlength\ of\ cell\ \left[cm\right]} \cdot 10^6 \cdot volume\ of\ assay\ \left[L\right]$$

A note on the equipment: As the assay should be carried out under light exclusion for elimination of unwanted side-reactions, even if the instrument is room-light immune, measurements with an open compartment are not recommended. Performing the assay is possible with double-beam, as well as with single-beam spectrophotometers. However, diode array spectrophotometers have the distinct disadvantage that they induce phenazine dye side-reactions and decomposition. Here, no individual wavelength is selected for running enzyme kinetics, but rather the entire spectrum from, e.g., 200–800 nm interacts with the sample in the cuvette (Lente & Espenson, 2004). Furthermore, since enzymatic activity of MDH is dependent on temperature, temperature control during the measurement is indispensable for accurate and reproducible results: a thermostatted cell holder based on a Peltier element provides a convenient option. To enable the acquisition of several samples simultaneously, a microplate spectrophotometer can be used. Here, if possible, a temperature gradient of 1–2 °C should be set to prevent condensation of assay mix vapors on the microplate lid. Some plate reader instruments have a condensation control feature already

built in. If this is not possible, the measurements can as well be performed without a lid, given that the assay temperatures are below 30 °C. When performing the measurements in a cuvette, the solution should be thoroughly mixed at all times. This can be obtained by using a cuvette equipped with a stirring bar. When using a plate reader for the activity determination, a shaking step should be implemented after the addition of each component.

1.1 Phenazine and DCPIP assay

A note on phenazines: Alkylated phenazines are used in the dye-coupled assay to replace the physiological EA cytochrome. Mainly phenazine ethosulfate (PES) and methosulfate (PMS) are mentioned in the literature (Ghosh & Quayle, 1979). However, PES is the preferred EA during enzymatic activity determination due to reduced radical formation, and lower tendency for dealkylation and phenazine formation (Ghosh & Quayle, 1979; Jahn et al., 2020). PMS decomposes more easily into phenazine when additives such as KCN or ammonia are added, lowering the concentration of accessible EA and increasing the amount of potential substrates for MDH similar to the PMS degradation side product of formaldehyde due to dealkylation (Jahn et al., 2020). In particular, light-induced degradation of the phenazine dyes as well as the connected radical formation poses challenges. Therefore, the preparation of EA stock solutions should be carried out under the exclusion of light, followed by a short heating of the assay mix (DCPIP and PES) to reduce radical auto-bleaching (Vu et al., 2016). The radical formation is not only light-dependent, but is also more pronounced at elevated temperatures and in an alkaline environment (Jahn et al., 2020). Furthermore, preparation of EA stock solutions in water instead of buffer and storage on ice minimizes this unwanted side-reaction (Jahn et al., 2020).

A note on DCPIP: In the absence of the enzyme or after complete consumption of the substrate, over time a slight increase of absorbance can be observed, most likely due to re-oxidation of reduced DCPIP under aerobic conditions (Naumann, Mayer, & Bannasch, 1985). Jahn et al. also reported a higher enzymatic activity of MDH as well as a reduced bleaching of the dye itself when the assay was performed under oxygen exclusion, supporting this presumption (Jahn et al., 2020). Since DCPIP is a weak acid, with a pK_a of 5.90, change of pH has an impact on the absorbance maximum of the dye and on the extinction coefficient ε (see Fig. 1A) (Armstrong, 1964). This can be visualized by comparing the absorbance
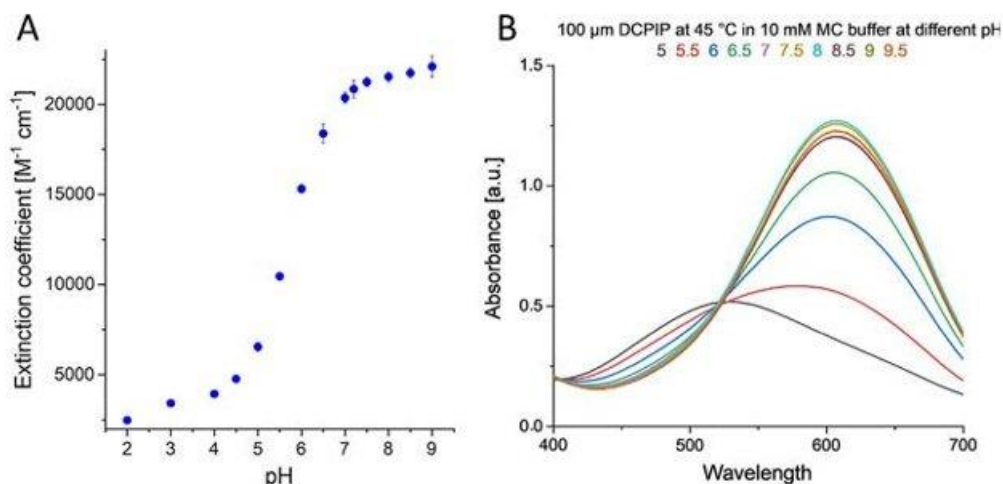
Fig. 1 (A) Extinction coefficient of DCPIP in 10 mM MC buffer (2.5 mM citrate, 2.5 mM Bis-Tris, 2.5 mM Tris, 2.5 mM CHES) at different pH. Measurements were carried out with a plate reader at 45 °C in triplicates. (B) Absorbance spectra of 100 μM DCPIP in 10 mM MC buffer at different pH at 45 °C. Spectra were collected after 2 min equilibrium time at 45 °C in a stirred quartz cuvette using a Cary 60 spectrophotometer.

spectra of DCPIP at different pHs. While spectra at pH 7–9.5 reveal a maximum at 600 nm, the maximum declines with decreasing pH value and shifts to lower wavelengths (see Fig. 1B). As a result, vastly varying extinction coefficients for DCPIP can be found in the literature, both for different buffer systems and even for similar conditions. In addition, optimal conditions for each MDH characterization need to be adjusted individually for new assay conditions (e.g., choosing a suitable buffer system, determining the pH optimum and testing if additives are required). Therefore, it is recommended to determine the extinction coefficient for the investigated system under the specific assay conditions. Furthermore, low color stability of DCPIP with ongoing storage was described which suggests that DCPIP solution should be freshly prepared (Jahn et al., 2020).

1.1.1 Protocol

Conditions: 1 mL assay volume, 1 mM PES, 100 μM DCPIP, 200 nM MDH, 50 mM MeOH (temperature, pH/buffer system of choice and optional: 15 mM NH$_4$Cl). Depending on the organism from which MDH is purified, the temperature for the enzymatic activity determination may vary. For example, for MDH isolated from *Methylacidiphilum fumariolicum* SolV (*M. fumariolicum* SolV) a pH of 7 and 45 °C is a reasonable compromise between enzyme stability and activity (Pol et al., 2014), while the activity of MDH from *Methylorubrum extorquens* AM1 (*M. extorquens* AM1) is

monitored at pH 9 and 30 °C (Vu et al., 2016). Again, the ideal enzyme concentration depends on various factors such as the initial enzyme activity. For Eu-MDH isolated from *M. fumariolicum* SolV, 200 nM was used (Lumpe, Pol, Op den Camp, & Daumann, 2018). Light exposure should be reduced to a minimum during preparation.

1. Prepare separate fresh stock solutions of 100 mM PES (CAS: 10510-77-7, 334.39 g/mol, 33.44 mg/mL) and 2 mM DCPIP (2,6-Dichlorophenol-indophenol sodium salt dihydrate, CAS: 10510-77-7, 326.11 g/mol, 0.65 mg/mL) in ultrapure water (type 1) in amber reaction tubes and store them on ice. For a 10 mL final assay mixture at least 200 μL PES and 1 mL DCPIP are needed.

2. Prepare additive stock solutions if required; for instance, NH_4Cl should be dissolved to give a 500 mM (CAS: 12125-02-9, 53.49 g/mol, 26.74 mg/mL) solution in ultrapure water (type 1). For a 10 mL final assay mixture at least 600 μL NH_4Cl are needed.

3. For the preparation of 10 mL of assay mix solution, dilute PES to a concentration of 2 mM by adding 200 μL of the 100 mM PES solution. Add DCPIP to a concentration of 200 μM by adding 1 mL of the 2 mM DCPIP solution to the respective buffer in an amber reaction tube. If NH_4Cl or other additives are required, add them to this mixture. Then, increase the volume to 10 mL with addition of buffer. Afterward, heat the assay mixture for at least 15 min at the temperature which is specified for the assay later (e.g., 30 or 45 °C), then vortex and store on ice.

4. For the spectrophotometric readout, mix 500 μL assay mixture with 400 μL of buffer in a cuvette (e.g., 1 cm pathlength, 1400 μL volume) and let it equilibrate at the required temperature (e.g., 30 or 45 °C) for at least 2 min in the dark.

5. For 200 nM final enzyme concentration add 50 μL of MDH (4 μM in the buffer system that is used for the assay) to the cuvette and monitor the absorbance at 600 nm for 2 min. As reported by various groups, MDH reveals enzymatic activity in the absence of additional substrate, caused by the "endogenous substrate" which is not fully understood at this time. Thus, it has to be assessed for each system individually.

6. Add 50 μL of 1 M MeOH to the cuvette to yield a final concentration of 50 mM and to start the measurement. Monitor the absorbance at 600 nm. For the calculation of the enzymatic activity, the initial rate (gradient/slope) after the addition of should be determined.

1.2 Wurster's Blue assay

For the method described above, two artificial components are required for the enzymatic investigations of MDH, but kinetic measurements also can be performed by solely using the radical cation Wurster's Blue; the main advantage is that WB acts simultaneously as EA and dye. Synthesized by Wurster in 1879 (Wurster & Schobig, 1879), Duine and co-workers reported WB as potential EA for the characterization of MDH (Duine, Frank, & Westerling, 1978), 10 years after the first reported characterization of MDH isolated from *M. extorquens* AM1 by Anthony based on the DCPIP/PES assay (Anthony & Zatman, 1964). Despite the reduced number of components for the spectrophotometrical investigation of MDH when using WB, the enzymatic activity is to this day mainly monitored with the two-component system DCPIP/PES. The restrained use of the one-electron receptor could potentially be due to the fact that it previously had to be synthesized by a procedure described in the literature (Michaelis & Granick, 1943), while DCPIP and the phenazine dyes were commercially available. Since this is not the case anymore and Jahn et al. have had a closer look at the unwanted side-reactions during the assay procedure, including how to avoid them, WB might be a good alternative to the DCPIP/PES assay for investigating MDH enzymes (Jahn et al., 2020).

As described for DCPIP, it is recommended that the extinction coefficient of WB be determined for the used assay conditions, as again various coefficients can be found in the literature. Absorbance spectra collected of WB reveal two maxima at 560 and 610 nm, with the latter being commonly used for monitoring the specific activity (Fig. 2) (Frank, Dijkstra, Duine, & Balny, 1988).

The stability of WB under different storage conditions, temperatures and at various pH values was previously examined (Jahn et al., 2020). A reduced stability in alkaline buffers was reported, while at acidic pH and in water WB was confirmed to be stable. Michaelis and Granick also described the highest radical concentration at pH 4.62 (Michaelis & Granick, 1943). Since most MDH activity assays are performed at pH 9, the low stability of WB under these conditions might interfere with the kinetic investigations. To circumvent the problem of fast radical degradation, the stock solution of WB in water should be added shortly before the spectrophotometric investigations. Furthermore, the radical yield is greatly reduced with longer storage time as well as with light exposure and increasing temperature. Therefore, it is recommended that the stock solution of WB be prepared in water, immediately before the activity determination, in an amber tube and stored on ice until needed.
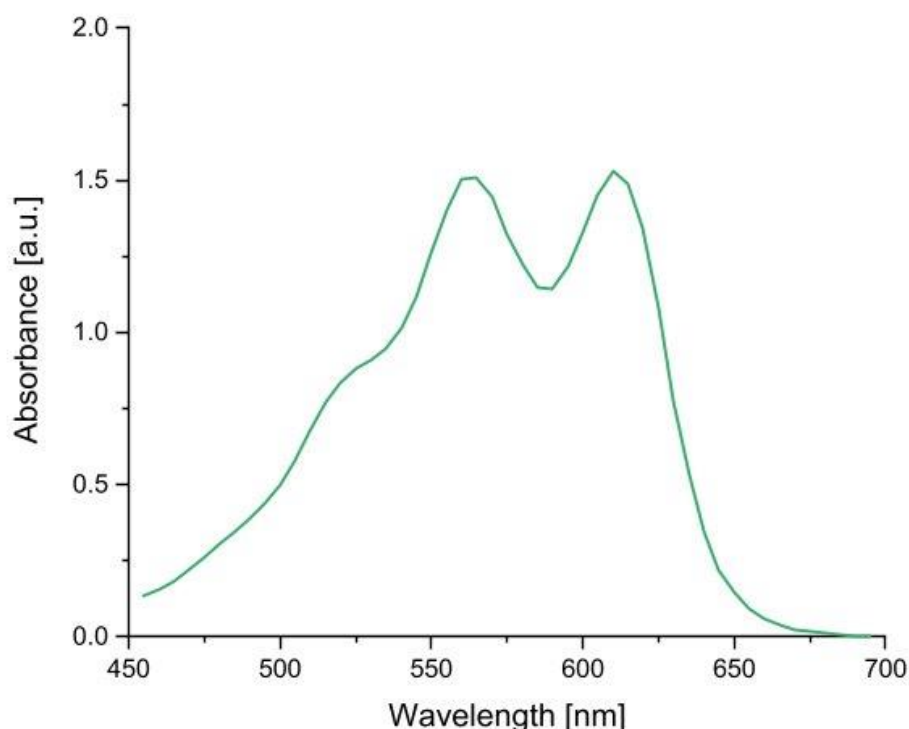
Fig. 2 Absorbance spectra of 200 μM WB in 100 mM MC buffer (2.5 mM citrate, 2.5 mM Bis-Tris, 2.5 mM Tris, 2.5 mM CHES) at pH 9 at 25 °C. Spectra were collected after 2 min equilibration time in a stirred quartz cuvette with a Cary 60 spectrophotometer.

1.2.1 Protocol

Conditions: 1 mL assay volume, 200 μM WB, 200 nM MDH, 50 mM MeOH (temperature and pH/buffer system of choice and optional: 15 mM NH_4Cl). Please see above for a discussion of temperature and pH conditions for the assay. Light exposure should be reduced to a minimum during preparation.

1. Prepare a fresh 1 mM solution of WB (Wuster's blue perchlorate, CAS: 34527-55-4, 263.69 g/mol, 0.26 mg/mL) in ultrapure water (type 1) in an amber tube. Make sure that all of the solid is dissolved by vortexing and ultrasonicating the solution and then store it on ice.

2. Prepare additive stock solutions if required, for instance NH_4Cl should be dissolved to give a 500 mM (CAS: 12125-02-9, 53.49 g/mol, 26.74 mg/mL) solution in ultrapure water (type 1). For 10 mL final assay mixture at least 600 μL of NH_4Cl are needed.

3. For the spectrophotometric readout, mix 200 μL of the 1 mM WB solution with potentially required additives and buffer to yield a final volume of 900 μL immediately before starting the activity determination and incubate for 2 min at the required temperature (e.g., 30 or 45 °C) in the dark.

4. For 200 nM final enzyme concentration, add 50 μL of MDH (4 μM in the buffer system that is used for the assay) and monitor the absorbance

at 610 nm for 2 min. As reported by various groups, MDH reveals enzymatic activity in the absence of additional substrate, caused by the "endogenous substrate" which is not fully understood at the present time. Thus, it has to be assessed for each system individually.

5. Add 50 μL of 1 M MeOH to yield a final concentration of 50 mM to start the measurement. Monitor the absorbance at 610 nm. For calculation of enzymatic activity, initial rate (gradient/slope) after substrate addition should be determined.
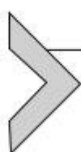
2. Assays based on the native cytochrome electron acceptor

In addition to the artificial assay, Anthony and co-workers introduced in the early 1980s the methanol cytochrome c oxidoreductase activity assay for Ca-MDH (Beardmore-Gray, O'Keeffe, & Anthony, 1983).

2.1 Spectrophotometric assay with cytochrome c_L

In contrast to the artificial assay, Ca–MDH activity is assessed by coupling its native cytochrome c_L to a secondary cytochrome c from bovine or equine heart. Its reduction is followed spectroscopically at 550 nm (Beardmore-Gray et al., 1983; Dijkstra, Frank, & Duine, 1989). They noted that cytochrome c_L from *Methylophilus methylotrophus* and *Paracoccus denitrificans* only interact with their respective native Ca-MDH while cytochrome c_L from AM1 is able to interact with the Ca-MDH from all three species (Beardmore-Gray et al., 1983). After further optimization, the assay mixture contained the native cytochrome c_L, secondary cytochrome c (from bovine or equine heart) and methanol as substrate. The assay was initiated by the addition of MDH. Recently, Chistoserdova and co-workers showed in *Methylomonas* sp. strain LW13 that a XoxG(4) protein acts as the specific native electron acceptor for its Ln-MDH (Zheng, Huang, Zhao, & Chistoserdova, 2018). Based on these findings, several groups adjusted Anthony and co-workers' previous protocol. In *M. extorquens* AM1, the native cytochrome c_L partner for Ln-MDH is referred to as XoxG which was biochemically and structurally characterized by Featherston et al. (2019). The native cytochrome c_L in *M. fumariolicum* SolV is a fusion protein and is denominated as c_{GJ}. The fusion protein consists of a XoxG cytochrome and periplasmic binding protein XoxJ. Protein-based activity assays for MDH from *M. extorquens* AM1 and *M. fumariolicum* SolV have been reported and consist of MDH, secondary cytochrome c (from bovine or equine heart), methanol as substrate and are initiated by addition of their respective native cytochrome (Fig. 3)
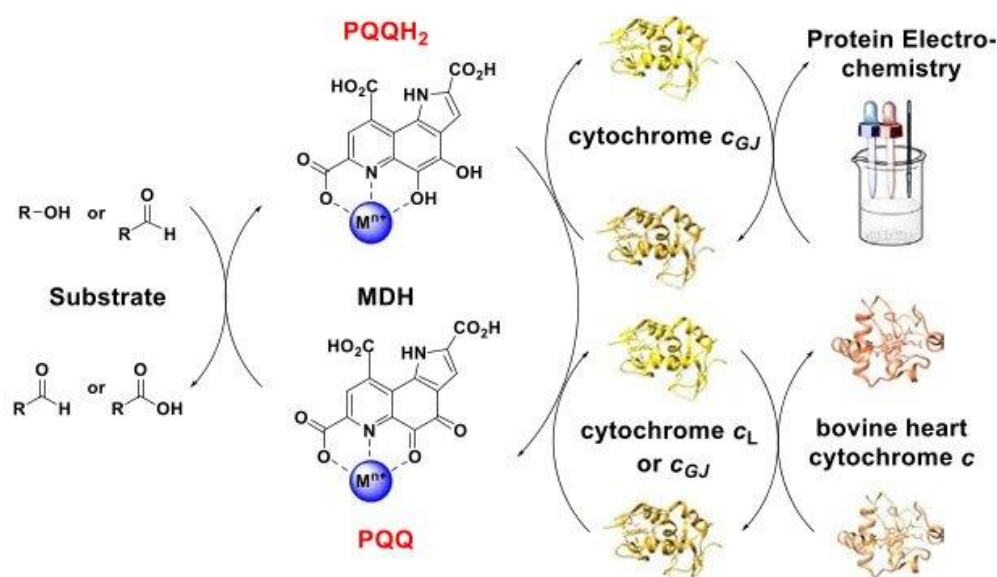
Fig. 3 Overview of assay methods involving the natural electron acceptor of MDH. Lower assay shows the spectrophotometric method where cytochrome reduction is coupled to a second cytochrome from equine or bovine heart. For the MDH/cytochrome c_{GJ} pair of *M. fumariolicum* SolV an assay using protein electrochemistry has also been reported. The protein structures depicted here were generated with Chimera (Pettersen et al., 2004), PDB 6ONQ and 6FF5. Please note, for cytochrome c_{GJ} from *M. fumariolicum* SolV no crystal structure has been reported so far and the structure of the cytochrome from *M. extorquens* AM1 has been used in its place.

(Featherston et al., 2019; Kalimuthu, Daumann, Pol, Op den Camp, & Bernhardt, 2019; Versantvoort et al., 2019). Independently of strain, the native cytochrome c_L is re-oxidized by the secondary electron acceptor equine/bovine heart cytochrome *c*, whose α-band intensity increases upon reduction by cytochrome c_L. The reduction can thus be followed spectrophotometrically at 550 nm. The amount of reduced cytochrome *c* per minute is assessed by subtracting the absorbance of the oxidized form from the fully reduced cytochrome to obtain an extinction coefficient of $19.5 \, \text{mM}^{-1} \, \text{cm}^{-1}$ at pH 7.2 (Day & Anthony, 1990; Versantvoort et al., 2019). Cytochrome *c* can be fully reduced by the addition of 100 equivalents of sodium dithionite.

Note on salt content and additives: The electron transfer from MDH to cytochrome c_L is based on electrostatic interaction between lysine residues on MDH and carboxyl residues on cytochrome c_L (Cox et al., 1992). It is known that this single "docking" site is affected by the ionic strength of the buffer. Anthony and co-workers have shown that increasing the concentration of NaCl from 0 to 50 mM drastically decreases the affinity of cytochrome c_L to Ca-MDH which is reflected by a sixfold increase of the

K_M value. The effect of NaCl can be reversed by increasing the concentration of cytochrome c_L (Cox et al., 1992). Furthermore, they observed that ethylenediaminetetraacetic acid (EDTA) and other tetracarboxylates (e.g., EGTA and CDTA) could interfere with the protein–protein interaction by interaction of their carboxy groups with lysine residues on the "docking" site of MDH. Recent work by Op den Camp and co-workers support these findings and showed that the activity readout of MDH (assessed with the cytochrome assay) decreases by 50% when a NaCl concentration of higher than 100 mM is used (Versantvoort et al., 2019). Since protein purifications often involve high NaCl gradient for elution of the target protein, buffer exchange or dialysis step of MDH and cytochrome c_L before usage in protein-based activity assays is recommended.

2.1.1 Protocol

Conditions: 100 μL assay volume (in 96 well-plate), 100 nM of XoxF-MDH, 50 μM cytochrome c from equine or bovine heart, 20 mM MeOH and 0–10 μM cytochrome c_L (pH 7.0–7.2, buffer system of choice). The appropriate amount of cytochrome c_L can vary across different systems. The K_M value of XoxF-XoxG needs to be considered when designing these assays. The reaction was incubated for 20 min at 30 °C for XoxG (*M. extorquens* AM1) and for 2 min at 45 °C for c_{GJ} (*M. fumariolicum* SolV) before absorbance was measured at 550 nm.

1. Prepare a fresh stock solution of 0.5 mM cytochrome c from equine heart (CAS: 9007-43-6, 12,384 g/mol, 6.2 mg/mL) in buffer in reaction tubes. Store on ice until needed. For 1 mL final assay mix at least 100 μL cytochrome c are needed.

2. Prepare a stock solution of 1 M MeOH (32.04 g/mol, 40 μL/mL) in ultrapure water (type 1) in reaction tubes. For 1 mL final assay mixture at least 10 μL MeOH are needed.

3. For the preparation of 90 μL assay mixture, combine 68 μL of buffer, 10 μL of 0.5 mM cytochrome c from equine heart, 10 μL of a 1 μM MDH solution (in the used buffer system) and 2 μL of a 1 M MeOH solution. Store on ice until needed. It is recommended to pre-heat the plate in the plate reader and to store the buffer at room temperature.

4. If a final concentration of 1 μM c_L is required, the 10 μL cytochrome c_L mixture is prepared by diluting cytochrome c_L to a concentration of 10 μM in buffer. Store on ice until needed.

5. Incubate both mixtures in separate wells of a 96-well plate. The assay is initiated by addition of the cytochrome c_L solution to the assay mixture.

The average gradient (slope) after cytochrome c_L addition is used to calculate the rate of reduction. The pathlength of the well plate has to be measured as well.

$$\textit{specific activity} \left[\mu mol \min^{-1} mg^{-1}\right] = \frac{\textit{enzyme unit U} \left[\mu mol \min^{-1}\right]}{\textit{amount of enzyme} \left[mg\right]}$$

$$\textit{enzyme unit U} \left[\mu mol \min^{-1}\right] = \frac{\textit{initial rate of slope of measurement}}{\varepsilon \left[cm^{-1} M^{-1}\right] \bullet \textit{pathlength of cell} \left[cm\right]} \bullet 10^6 \bullet \textit{volume of assay} \left[L\right]$$

2.2 Electrochemical assay

Kalimuthu et al. developed a method that allows the co-adsorption of Eu–MDH and its cytochrome c_{GJ} from *M. fumariolicum* SolV with the biopolymer chitosan onto an Au working electrode (Kalimuthu et al., 2019). The Au electrode replaces the bovine/equine heart cytochrome c as the secondary electron acceptor and the activity is determined by measuring the current. With that electrode in hand the effect of ammonium ions, methanol concentration, formaldehyde concentration, pH and temperature can be assayed electrochemically. Here, activating agents such as ammonium ions or glycine ethyl ester (GEE) are not necessary, nor is the addition of cyanide as protecting agent. The transformation of a quasi-reversible wave of c_{GJ} into a sigmoidal wave upon addition of either methanol or formaldehyde and MDH displays a homogeneous (Eu–MDH to cytochrome c_{GJ}) and heterogeneous (cytochrome c_{GJ} to Au electrode) electron transfer process. Screening across the pH range of 5.4–9.5 identified the pH optimum at pH 7.3, which is in accordance with results from dye-linked assays. With similarities to the dye-linked assays, Eu–MDH and c_{GJ} display increased activity with higher temperature. To the best of our knowledge, there are no additional publications on bioelectrochemistry of Ln-MDHs. For a precise procedure we refer the reader to Kalimuthu et al. (2019).
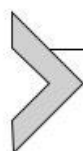
3. Role of activators, additives, and buffers
3.1 Ammonium salts

Ammonium chloride is usually needed as activator in MDH assays with artificial electron acceptors (Afolabi et al., 2001; Anthony, 2000; Day & Anthony, 1990; Frank et al., 1988; Goodwin & Anthony, 1996; Harris & Davidson, 1993). It acts as an activator at low concentrations by increasing

V_{max} (Goodwin & Anthony, 1996), while an inhibitory effect can be observed at higher concentrations (Afolabi et al., 2001; Harris & Davidson, 1993). Anthony and Zatman suggested in 1964 that the free base ammonia and not the ammonium ion is the active form as they observed that at pH 9 the activation was more effective than at pH 7, even if higher amounts of ammonium chloride were added at neutral pH (Anthony & Zatman, 1964). The conclusion is based on the fact that the pK_a of NH_3/NH_4^+ in water is 9.21 which means that the predominant species at pH 7 is ammonium and at pH 9 more free base is available (Hall, 1957). Thus, to completely shift the equilibrium to ammonia, pH values higher than pH 9.21 would be needed.

The inhibitory effect of added ammonium chloride was suggested by molecular modeling to be due to the ammonium ion, preventing methanol from binding properly to the active site of MDH (Reddy & Bruice, 2004). However, the full mechanism of activation by ammonia is still not fully understood. It was proposed that ammonia acts by activating the reduction of PQQ by the substrate (Afolabi et al., 2001; Frank et al., 1988; Goodwin & Anthony, 1996). Furthermore, Reddy and Bruice suggested in 2004, based on molecular modeling, that the formation of an MDH-PQQ-(NH)-methanol intermediate might be involved (Reddy & Bruice, 2004). Moreover, it must be noted that ammonia can induce the decomposition of artificial electron acceptors such as PMS and PES leading to phenazine which is problematic as the concentration of the electron acceptor is decreased and formaldehyde is formed as a side product which can act as a substrate for the studied MDH system. To circumvent this problem, it is recommended that PES be used rather than PMS (as this behavior is less pronounced for PES), to keep the light-exposure to a minimum, to prepare the stock solution in water instead of buffer and to heat them briefly at the temperature used for the assay prior to use in order to minimize the mentioned side-reactions (Jahn et al., 2020; Vu et al., 2016).

If the assay is performed in the presence of natural electron acceptors (the respective cytochrome c_L or c_{Gj}), no ammonia needs to be added as an activator, and the assay can be performed at lower pH (Anthony, 2000; Day & Anthony, 1990; Featherston et al., 2019; Kalimuthu et al., 2019; Versantvoort et al., 2019). Furthermore, not all MDHs require the addition of an activator. For example, the Ln-MDH isolated from *M. fumariolicum* SolV doesn't need ammonia as activator (albeit the activity with it is slightly higher) and can as well be assayed at neutral pH with artificial EAs (Pol et al., 2014).

3.2 Glycine ethyl ester (GEE)

As alternative activator to ammonium salts, amines such as methylamine or esters of glycine and alanine have been proposed in the literature (Anthony, 1986). Martinez-Gomez and coworkers reported that methylamine was an even better activator than ammonia for the ethanol dehydrogenase (ExaF) isolated from *M. extorquens* (Good et al., 2016). Hothi et al. stated in 2005 that GEE might be a more beneficial activator for PQQ-dependent MDHs as they observed higher activity with GEE at lower concentrations than with ammonium chloride and a less pronounced inhibition at higher concentrations (Hothi, Sutcliffe, & Scrutton, 2005). However, it should be considered that GEE can degrade under assay conditions depending on the used pH, temperature and activator concentration (e.g., at pH 8.6 ethanol is rapidly produced in a 10 mM solution, Fig. 4); since esters are known to hydrolyze under acidic or basic conditions producing a carboxylic acid and an alcohol. Therefore, it is recommended that the stability of the used GEE be checked (e.g., by ^{1}H NMR spectroscopy) under assay conditions in the absence of MDH as the substrate ethanol might be generated.

3.3 Potassium cyanide (KCN)

KCN is routinely added to MDH assays as it was found to suppress the endogenous MDH activity and the reduction of the used artificial electron acceptor as well as to prevent enzyme inactivation (Duine & Frank, 1980). Endogenous activity refers to the activity observed for MDHs in the absence of added substrate, which is believed to be caused by low concentrations of contaminating aldehydes and alcohols presumably present at low concentrations in used reagents (Anthony & Zatman, 1964; Day & Anthony, 1990; Duine et al., 1978; Duine & Frank, 1980). However, depending on the used assay conditions, it should be kept in mind that the main species in the solution under investigation might not be cyanide but HCN. The pK_a of HCN is 9.21 (Beck, 1987), which means that at pH 7.2 the predominant species is HCN which can outgas of the solution, especially if the assay is performed at elevated temperatures (e.g., at 45 °C used for investigating the Ln-MDH of *M. fumariolicum* SolV (Jahn et al., 2020)) (Arun et al., 2005). At pH 9 the predominant species is still HCN, but to a much lesser extent. Above pH 9.21 the predominate species is cyanide. Depending on the chosen assay conditions (high temperature, neutral pH, high KCN concentration), HCN (highly toxic!) might outgas of the investigated solution. The assay should therefore be performed in a well-ventilated area. It should further be noted that the KCN can also induce the decomposition of PMS and PES (compare

A 10 mM GEE in deuterium oxide; pH 8.6; r.t.

glycine ethyl ester

ethanol

B 10 mM GEE in deuterium oxide; pH 6.5; r.t.
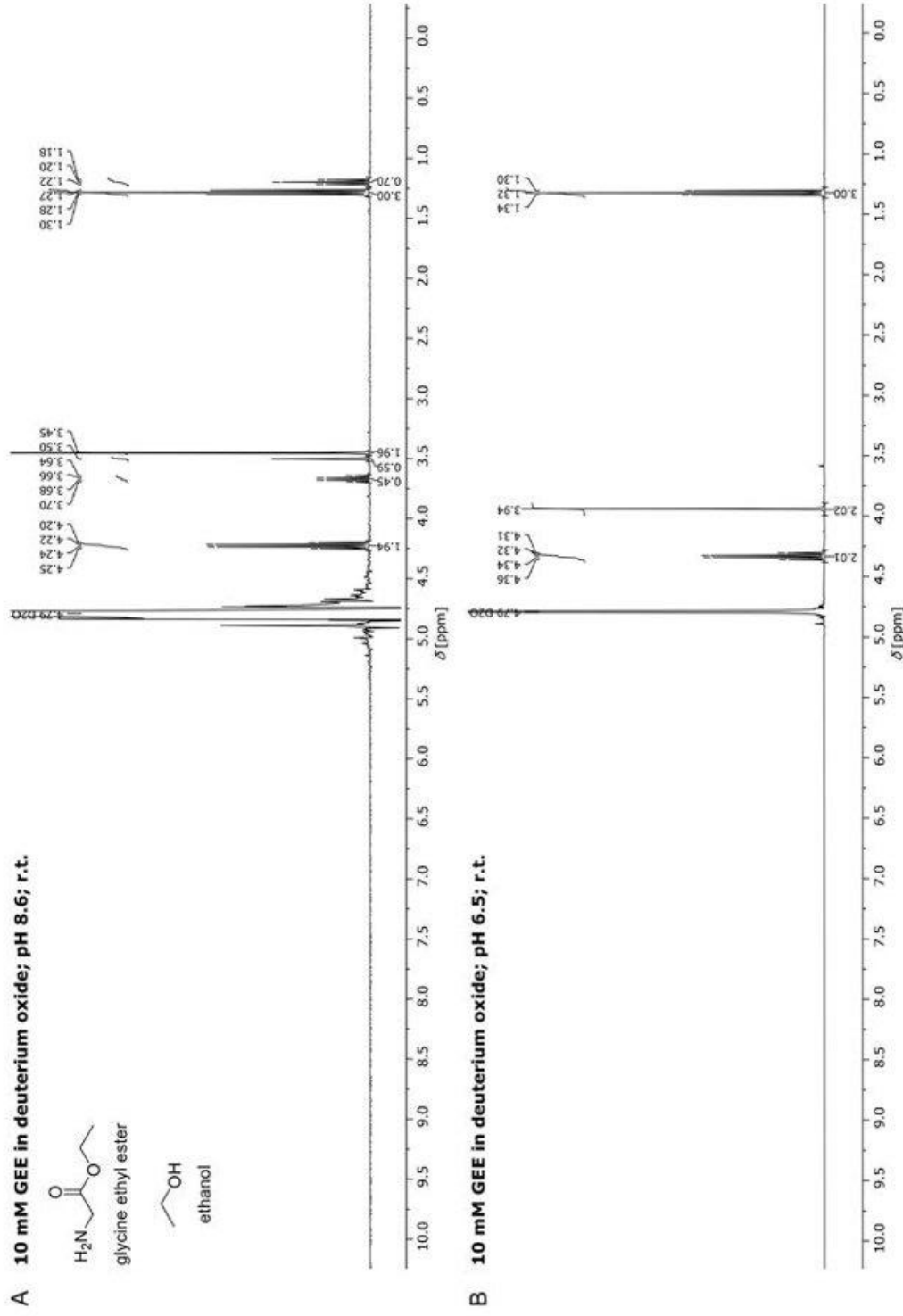
Fig. 4 (A) ^{1}H NMR spectrum of a GEE sample that was immediately measured after the pH adjustment to 8.6. In addition to the signals of GEE (δ [ppm] = 4.23 (q, 2H), 3.45 (s, 2H), 1.28 (t, 3H)), signals that can be assigned to ethanol (δ [ppm] = 3.67 (q, 2H), 1.20 (t, 3H)) are observed as well. (B) ^{1}H NMR spectrum of a GEE sample that was adjusted to pH 6.5 and measured after 24 h storage at room temperature. No ethanol could be detected in this sample; the different shifts for the NMR signals of the GEE are due to the different pH value. All samples were measured on a Bruker 400 MHz instrument.

with ammonia), leading to the same troublesome side products phenazine and formaldehyde (Jahn et al., 2020). The same recommendations, as stated above, apply.

3.4 Lanthanide salts

If assaying Ln-dependent alcohol dehydrogenases (ADHs), sometimes $LnCl_3$ are added for the saturation of the apo-enzyme (concentrations $0-20\,\mu M$ were used for MDH isolated from *M. fumariolicum* SolV, and up to $100\,\mu M$ for ethanol dehydrogenase isolated from *M. extorquens* AM1) (Good et al., 2016; Lumpe et al., 2018). However, it should be noted that this can impact the electrostatic interaction of MDH with its cytochrome. Additionally, when preparing $LnCl_3$ stock solutions it should be kept in mind that $LnCl_3$ readily hydrolyzes at alkaline pH forming $Ln(OH)_3$ precipitates and can also react with carbon dioxide to form $Ln_2(CO_3)_3$ precipitates. Due to the hygroscopic nature of $LnCl_3$ salts, the water content of the used $LnCl_3 \times n\ H_2O$ salt for preparing the stock solutions should be determined regularly by, e.g., elemental analysis. All things considered, it is recommended to prepare the stock solutions freshly and use them for a maximum of 1 week, stored in plastic containers (contamination with other ions can occur if stored in glass) at a low pH (addition of, e.g., HCl to prevent hydrolysis, not necessary if the stock is used freshly) and at fairly high concentrations (e.g., $1-10\,mM$) (Evans, 1990). The stock solutions should always be checked for precipitates before use.

3.5 Pyrroloquinoline quinone (PQQ)

In some reports, PQQ is added to ethanol dehydrogenase assay mixtures to restore activity (Good et al., 2016). Whether this works for MDHs is currently unknown and the literature on reconstitution is scarce. However, it should be noted in any case, that PQQ can readily precipitate with lanthanides in aqueous solutions (Lumpe et al., 2020). This might be disadvantageous, if $LnCl_3$ salts are added as well, for the saturation of the apo-Ln-MDH.

3.6 Buffers

As there is no such thing as a perfect buffer, the pros and cons of every buffer system should be precisely considered in respect to the envisioned experimental setting. For example, if the redox chemistry of a system is under investigation (MDHs assay) the usage of PIPES and HEPES might be inadvisable as both buffers are known for radical formation. In Table 1 an

Table 1 Selected considerations of different buffers frequently used in MDH assays.

Buffer	pH change upon heating	Metal binding ability	Known side reaction/other issues
Acetate	Yes* (Fukada & Takahashi, 1998)	Yes, e.g., Y(III), Cu(II), Zn(II), Cd(II), Pb(II) and Ln(III) (Kolat & Powell, 1962)	
Citrate	None (Ellis & Morrison, 1982)	Yes, e.g., alkaline earth metal ions; transitions metal ions (Wyrzykowski & Chmurzyński, 2010; Wyrzykowski, Czupryniak, Ossowski, & Chmurzyński, 2010) and Ln(III) (Nikonorov, 2010)	
Phosphate	Yes* (Fukada & Takahashi, 1998)	Yes, e.g., alkali and alkaline earth metal ions (Van Wazer & Callis, 1958)	Possible precipitation of Ln(III) (Jordan et al., 2018; Liu & Byrne, 1997)
Bis–Tris	Yes** (Ellis & Morrison, 1982)	Yes, e.g., alkali, alkaline earth and transition metal ions (Sigel, Scheller, & Prijs, 1982) and Ln(III) (Jin Oh et al., 1998)	
HEPES	Yes** (Fukada & Takahashi, 1998)	Yes, mostly weak binding of e.g. Cu(II) (Sokołowska & Bal, 2005), Zn(II), Pb(II), Cd(II) (Zeinab Mohamed Anwar, 2005) and Ln(III) (Anwar & Azab, 2001; Soares & Conde, 2000) some reports do not observe any complexation of Zn(II) and Cd(II) → opinion in the literature not unified	Radical formation, not suitable for redox-active systems (Grady, Chasteen, & Harris, 1988)

Table 1 Selected considerations of different buffers frequently used in MDH assays.—cont'd

Buffer	pH change upon heating	Metal binding ability	Known side reaction/other issues
PIPES	Yes* (Fukada & Takahashi, 1998)	Yes, e.g., Ln(III), (Azab, Al–Deyab, Anwar, Abd El-Gawad, & Kamel, 2011) Co(II) and Ni(II) (Wyrzykowski, Pilarski, Jacewicz, & Chmurzyński, 2013)	Radical formation, not suitable for redox-active systems (Grady et al., 1988)
Tris	Yes*** (Ellis & Morrison, 1982)	Yes, alkali, alkaline earth metal ions (Sigel et al., 1982), some transition metals (Xiao et al., 2020), Eu(III) and Tb(III) (Pfefferlé & Bünzli, 1989)	Imine condensations with aldehydes (Hoffman, Frey, Smith, & Auble, 2015)
CAPS	Yes*** (Fukada & Takahashi, 1998)	Yes, weak binding of, e.g., Cu(II), Pb(II), Cd(II) and Zn(II) (Ferreira, Pinto, Soares, & Soares, 2015)	
MOPS	Yes** (Fukada & Takahashi, 1998)	Yes, mild or weak binding of e.g. Cu(II), Pb(II), Zn(II), Cd(II) (Xiao et al., 2020)	
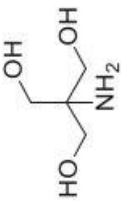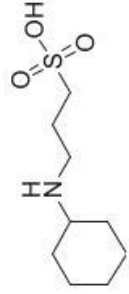
All Values from Fukada and Takahashi (1998) were obtained in 0.1 M KCl and from Ellis and Morrison (1982) with ionic strength 0.1. * = pH change per 5 °C change <0.05, ** = 0.10 > pH change per 5 °C change >0.05, *** = pH change per 5 °C change >0.10; pH change refers to the temperature range from 20 to 45 °C.

overview of different buffers, frequently used in MDH assays, and some selected considerations, e.g., about susceptibility to pH change upon temperature changes or potential metal complexation, are given without claim of completeness. For a comprehensive overview of different buffer systems we refer the reader to Ferreira et al. (2015).
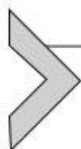
4. Safety considerations

Potassium cyanide and likewise its acid, HCN, are potent inhibitors of cellular respiration and thus highly toxic. Appropriate care should be taken when handling and disposing of cyanide containing stock solutions. The Wurster's blue radical cation usually contains a perchlorate counterion. Perchlorates can potentially form explosive mixtures with metal salts or organic compounds. Appropriate care should be taken when handling the Wurster's blue salt.

References

Afolabi, P. R., Mohammed, F., Amaratunga, K., Majekodunmi, O., Dales, L., Gill, R., et al. (2001). Site-directed mutagenesis and X-ray crystallography of the PQQ-containing quinoprotein methanol dehydrogenase and its electron acceptor, cytochrome cL. *Biochemistry, 40*(33), 9799–9809. https://doi.org/10.1021/bi002932l.

Anthony, C. (1986). Bacterial oxidation of methane and methanol. In A. H. Rose, & D. W. Tempest (Eds.), *Vol. 27. Advances in microbial physiology* (pp. 113–210). Academic Press.

Anthony, C. (2000). Methanol dehydrogenase, a PQQ-containing quinoprotein dehydrogenase. In A. Holzenburg, & N. S. Scrutton (Eds.), *Enzyme-catalyzed electron and radical transfer: Subcellular biochemistry* (pp. 73–117). Boston, MA: Springer US.

Anthony, C., & Zatman, L. J. (1964). Microbial oxidation of methanol. 2. The methanol-oxidizing enzyme of Pseudomonas sp. M27. *Biochemical Journal, 92*, 614–621.

Anwar, Z. M. (2005). Complexation equilibria of Zn(II), Pb(II) and Cd(II) with reduced glutathione (GSH) and biologically important zwitterionic buffers. *Journal of the Chinese Chemical Society (Taipei, Taiwan), 52*(5), 863–871. https://doi.org/10.1002/jccs.200500121.

Anwar, Z. M., & Azab, H. A. (2001). Ternary complexes formed by trivalent lanthanide ions, nucleotides, and biological buffers. *Journal of Chemical and Engineering Data, 46*(3), 613–618. https://doi.org/10.1021/je000187+.

Armstrong, J. M. (1964). The molar extinction coefficient of 2,6-dichlorophenol indophenol. *Biochimica et Biophysica Acta, 86*, 194–197.

Arun, P., Moffett, J. R., Ives, J. A., Todorov, T. I., Centeno, J. A., Namboodiri, M. A. A., et al. (2005). Rapid sodium cyanide depletion in cell culture media: Outgassing of hydrogen cyanide at physiological pH. *Analytical Biochemistry, 339*(2), 282–289. https://doi.org/10.1016/j.ab.2005.01.015.

Azab, H. A., Al-Deyab, S. S., Anwar, Z. M., Abd El-Gawad, I. I., & Kamel, R. M. (2011). Comparison of the coordination tendency of amino acids, nucleobases, or mononucleotides toward the monomeric and dimeric lanthanide complexes with biologically important compounds. *Journal of Chemical and Engineering Data, 56*(5), 2613–2625. https://doi.org/10.1021/je200099n.

Beardmore-Gray, M., O'Keeffe, D. T., & Anthony, C. (1983). The methanol: Cytochrome c oxidoreductase activity of methylotrophs. *Microbiology*, *129*(4), 923–933.

Beck, M. T. (1987). Critical survey of stability constants of cyano complexes. *Pure and Applied Chemistry*, *59*(12), 1703–1720. https://doi.org/10.1351/pac198759121703.

Cox, J. M., Day, D. J., & Anthony, C. (1992). The interaction of methanol dehydrogenase and its electron acceptor, cytochrome cL in methylotrophic bacteria. *Biochimica et Biophysica Acta, Protein Structure and Molecular Enzymology*, *1119*(1), 97–106. https://doi.org/10.1016/0167-4838(92)90240-E.

Day, D. J., & Anthony, C. (1990). Methanol dehydrogenase from methylobacterium extorquens AM1. In M. E. Lidstrom (Ed.), *Vol. 188*. *Methods in enzymology* (pp. 210–216). Academic Press.

Dijkstra, M., Frank, J., Jr., & Duine, J. A. (1989). Studies on electron transfer from methanol dehydrogenase to cytochrome cL, both purified from Hyphomicrobium X. *Biochemical Journal*, *257*(1), 87–94. https://doi.org/10.1042/bj2570087.

Duine, J. A., & Frank, J., Jr. (1980). Studies on methanol dehydrogenase from Hyphomicrobium X. Isolation of an oxidized form of the enzyme. *Biochemical Journal*, *187*(1), 213–219. https://doi.org/10.1042/bj1870213.

Duine, J. A., Frank, J., & Westerling, J. (1978). Purification and properties of methanol dehydrogenase from Hyphomicrobium X. *Biochimica et Biophysica Acta (BBA)—Enzymology*, *524*(2), 277–287. https://doi.org/10.1016/0005-2744(78)90164-X.

Ellis, K. J., & Morrison, J. F. (1982). Buffers of constant ionic strength for studying pH-dependent processes. *Methods in Enzymology*, *87*, 405–426. https://doi.org/10.1016/s0076-6879(82)87025-0.

Evans, C. H. (1990). *Biochemistry of the lanthanides*. New York: Springer Science & Business Media.

Featherston, E. R., Rose, H. R., McBride, M. J., Taylor, E., Boal, A. K., & Cotruvo, J. J. (2019). Biochemical and structural characterization of XoxG and XoxJ and their roles in activity of the lanthanide-dependent methanol dehydrogenase, XoxF. *ChemBioChem*, *20*, 2360–2372. https://doi.org/10.1002/cbic.201900184.

Ferreira, C. M. H., Pinto, I. S. S., Soares, E. V., & Soares, H. M. V. M. (2015). (Un)suitability of the use of pH buffers in biological, biochemical and environmental studies and their interaction with metal ions—A review. *RSC Advances*, *5*(39), 30989–31003. https://doi.org/10.1039/C4RA15453C.

Frank, J., Dijkstra, M., Duine, J. A., & Balny, C. (1988). Kinetic and spectral studies on the redox forms of methanol dehydrogenase from Hyphomicrobium X. *European Journal of Biochemistry*, *174*(2), 331–338. https://doi.org/10.1111/j.1432-1033.1988.tb14102.x.

Fukada, H., & Takahashi, K. (1998). Enthalpy and heat capacity changes for the proton dissociation of various buffer components in 0.1 M potassium chloride. *Proteins: Structure, Function, and Bioinformatics*, *33*(2), 159–166. https://doi.org/10.1002/(sici)1097-0134(19981101)33:2<159::Aid-prot2>3.0.Co;2-e.

Ghosh, R., & Quayle, J. R. (1979). Phenazine ethosulfate as a preferred electron acceptor to phenazine methosulfate in dye-linked enzyme assays. *Analytical Biochemistry*, *99*, 112–117.

Good, N. M., Vu, H. N., Suriano, C. J., Subuyuj, G. A., Skovran, E., & Martinez-Gomez, N. C. (2016). Pyrroloquinoline quinone ethanol dehydrogenase in *Methylobacterium extorquens* AM1 extends lanthanide-dependent metabolism to multicarbon substrates. *Journal of Bacteriology*, *198*(22), 3109–3118. https://doi.org/10.1128/jb.00478-16.

Goodwin, M. G., & Anthony, C. (1996). Characterization of a novel methanol dehydrogenase containing a Ba2+ ion at the active site. *Biochemical Journal*, *318*(2), 673–679. https://doi.org/10.1042/bj3180673.

Grady, J. K., Chasteen, N. D., & Harris, D. C. (1988). Radicals from "good's" buffers. *Analytical Biochemistry*, *173*(1), 111–115. https://doi.org/10.1016/0003-2697(88)90167-4.

Hall, H. K. (1957). Correlation of the base strengths of amines. *Journal of the American Chemical Society*, *79*(20), 5441–5444. https://doi.org/10.1021/ja01577a030.

Harris, T. K., & Davidson, V. L. (1993). A new kinetic model for the steady-state reactions of the quinoprotein methanol dehydrogenase from Paracoccus denitrificans. *Biochemistry*, *32*(16), 4362–4368. https://doi.org/10.1021/bi00067a028.

Hoffman, E. A., Frey, B. L., Smith, L. M., & Auble, D. T. (2015). Formaldehyde crosslinking: A tool for the study of chromatin complexes. *Journal of Biological Chemistry*, *290*(44), 26404–26411. https://doi.org/10.1074/jbc.R115.651679.

Hothi, P., Sutcliffe, M. J., & Scrutton, N. S. (2005). Kinetic isotope effects and ligand binding in PQQ-dependent methanol dehydrogenase. *Biochemical Journal*, *388*(Pt. 1), 123–133. https://doi.org/10.1042/BJ20041731.

Jahn, B., Jonasson, N. S. W., Hu, H., Singer, H., Pol, A., Good, N. M., et al. (2020). Understanding the chemistry of the artificial electron acceptors PES, PMS, DCPIP and Wurster's Blue in methanol dehydrogenase assays. *JBIC, Journal of Biological Inorganic Chemistry*, *25*, 199–212. https://doi.org/10.1007/s00775-020-01752-9.

Jin Oh, S., Choi, Y.-S., Hwangbo, S., Chul Bae, S., Kang Ku, J., & Won Park, J. (1998). Structure and phosphodiesterase activity of Bis-Tris coordinated lanthanide (III) complexes. *Chemical Communications (Cambridge, United Kingdom)*, (20), 2189–2190. https://doi.org/10.1039/A806021E.

Jordan, N., Demnitz, M., Lösch, H., Starke, S., Brendler, V., & Huittinen, N. (2018). Complexation of trivalent lanthanides (Eu) and actinides (cm) with aqueous phosphates at elevated temperatures. *Inorganic Chemistry*, *57*(12), 7015–7024. https://doi.org/10.1021/acs.inorgchem.8b00647.

Kalimuthu, P., Daumann, L. J., Pol, A., Op den Camp, H. J. M., & Bernhardt, P. V. (2019). Electrocatalysis of a europium-dependent bacterial methanol dehydrogenase with its physiological electron-acceptor cytochrome cGJ. *Chemistry—A European Journal*, *25*(37), 8760–8768. https://doi.org/10.1002/chem.201900525.

Kolat, R. S., & Powell, J. E. (1962). Acetate complexes of the rare earth and several transition metal ions. *Inorganic Chemistry*, *1*(2), 293–296. https://doi.org/10.1021/ic50002a019.

Lente, G., & Espenson, J. H. (2004). Photoreduction of 2,6-dichloroquinone in aqueous solution: Use of a diode array spectrophotometer concurrently to drive and detect a photochemical reaction. *Journal of Photochemistry and Photobiology A: Chemistry*, *163*(1), 249–258. https://doi.org/10.1016/j.jphotochem.2003.12.005.

Liu, X., & Byrne, R. H. (1997). Rare earth and yttrium phosphate solubilities in aqueous solution. *Geochimica et Cosmochimica Acta*, *61*(8), 1625–1633. https://doi.org/10.1016/S0016-7037(97)00037-9.

Lumpe, H., Menke, A., Haisch, C., Mayer, P., Kabelitz, A., Yusenko, K. V., et al. (2020). The earlier the better: Structural analysis and separation of lanthanides with pyrroloquinoline quinone. *Chemistry—A European Journal*, *26*(44), 10133–10139. https://doi.org/10.1002/chem.202002653.

Lumpe, H., Pol, A., Op den Camp, H. J. M., & Daumann, L. J. (2018). Impact of the lanthanide contraction on the activity of a lanthanide-dependent methanol dehydrogenase—A kinetic and DFT study. *Dalton Transactions*, *47*, 10463–10472. https://doi.org/10.1039/C8DT01238E.

Michaelis, L., & Granick, S. (1943). The polymerization of the free radicals of the Wurster dye type: The dimeric resonance bond. *Journal of the American Chemical Society*, *65*(9), 1747–1755. https://doi.org/10.1021/ja01249a026.

Myers, A. (1990). Use of DCPIP in a colorimetric method to investigate electron transport in crude heart mitochondrial extracts. *Journal of Biological Education*, *24*(2), 123–127. https://doi.org/10.1080/00219266.1990.9655123.

Naumann, R., Mayer, D., & Bannasch, P. (1985). Voltammetric measurements of the kinetics of enzymatic reduction of 2,6-dichlorophenolindophenol in normal and neoplastic hepatocytes using glucose as substrate. *Biochimica et Biophysica Acta (BBA)—Molecular Cell Research*, *847*(1), 96–100. https://doi.org/10.1016/0167-4889(85)90158-2.

Nikonorov, V. V. (2010). Determination of the stability constants of lanthanide complexes with oxyacids using capillary electrophoresis. *Journal of Analytical Chemistry (Translation of Zhurnal Analiticheskoi Khimii)*, *65*(4), 359–365. https://doi.org/10.1134/S1061934810040040.

Pettersen, E. F., Goddard, T. D., Huang, C. C., Couch, G. S., Greenblatt, D. M., Meng, E. C., et al. (2004). UCSF chimera—A visualization system for exploratory research and analysis. *Journal of Computational Chemistry*, *25*, 1605–1612. https://doi.org/10.1002/jcc.20084.

Pfefferlé, J.-M., & Bünzli, J.-C. G. (1989). Interaction between the buffer Tris and the eu(III) ion: Luminescence and potentiometric investigation. *Helvetica Chimica Acta*, *72*(7), 1487–1494. https://doi.org/10.1002/hlca.19890720709.

Pol, A., Barends, T. R. M., Dietl, A., Khadem, A. F., Eygensteyn, J., Jetten, M. S. M., et al. (2014). Rare earth metals are essential for methanotrophic life in volcanic mudpots. *Environmental Microbiology*, *16*(1), 255–264. https://doi.org/10.1111/1462-2920.12249.

Reddy, S. Y., & Bruice, T. C. (2004). Mechanisms of ammonia activation and ammonium ion inhibition of quinoprotein methanol dehydrogenase: A computational approach. *Proceedings of the National Academy of Sciences of the United States of America*, *101*(45), 15887–15892. https://doi.org/10.1073/pnas.0407209101.

Sigel, H., Scheller, K. H., & Prijs, B. (1982). Metal ion/buffer interactions. Stability of alkali and alkaline earth ion complexes with triethanolamine (tea), 2-amino-2(hydroxymethyl)-1,3-propanediol (tris)and 2-[bis(2-hydroxyethyl)-amino] 2(hydroxymethyl)-1,3-propanediol (Bistris) in aqueous and mixed solvents. *Inorganica Chimica Acta*, *66*, 147–155. https://doi.org/10.1016/S0020-1693(00)85805-3.

Soares, H. M. V. M., & Conde, P. C. F. L. (2000). Electrochemical investigations of the effect of N-substituted aminosulfonic acids with a piperazinic ring pH buffers on heavy metal processes which may have implications on speciation studies. *Analytica Chimica Acta*, *421*(1), 103–111. https://doi.org/10.1016/S0003-2670(00)01028-X.

Sokołowska, M., & Bal, W. (2005). Cu(II) complexation by "non-coordinating" N-2-hydroxyethylpiperazine-N′-2-ethanesulfonic acid (HEPES buffer). *Journal of Inorganic Biochemistry*, *99*(8), 1653–1660. https://doi.org/10.1016/j.jinorgbio.2005.05.007.

Van Wazer, J. R., & Callis, C. F. (1958). Metal complexing by phosphates. *Chemical Reviews (Washington, DC, United States)*, *58*(6), 1011–1046. https://doi.org/10.1021/cr50024a001.

Versantvoort, W., Pol, A., Daumann, L. J., Larrabee, J. A., Strayer, A. H., Jetten, M. S. M., et al. (2019). Characterization of a novel cytochrome cGJ as the electron acceptor of XoxF-MDH in the thermoacidophilic methanotroph Methylacidiphilum fumariolicum SolV. *Biochimica et Biophysica Acta, Proteins and Proteomics*, *1867*(6), 595–603. https://doi.org/10.1016/j.bbapap.2019.04.001.

Vu, H. N., Subuyuj, G. A., Vijayakumar, S., Good, N. M., Martinez-Gomez, N. C., & Skovran, E. (2016). Lanthanide-dependent regulation of methanol oxidation Systems in *Methylobacterium extorquens* AM1 and their contribution to methanol growth. *Journal of Bacteriology*, *198*(8), 1250–1259. https://doi.org/10.1128/JB.00937-15.

Wurster, C., & Schobig, E. (1879). Ueber die Einwirkung oxydirender Agentien auf Tetramethylparaphenylendiamin. *Berichte der Deutschen Chemischen Gesellschaft*, *12*(2), 1807–1813. https://doi.org/10.1002/cber.187901202156.

Wyrzykowski, D., & Chmurzyński, L. (2010). Thermodynamics of citrate complexation with Mn2+, Co2+, Ni2+ and Zn2+ ions. *Journal of Thermal Analysis and Calorimetry*, *102*(1), 61–64. https://doi.org/10.1007/s10973-009-0523-4.

Wyrzykowski, D., Czupryniak, J., Ossowski, T., & Chmurzyński, L. (2010). Thermodynamic interactions of the alkaline earth metal ions with citric acid. *Journal of Thermal Analysis and Calorimetry*, *102*(1), 149–154. https://doi.org/10.1007/s10973-010-0970-y.

Wyrzykowski, D., Pilarski, B., Jacewicz, D., & Chmurzyński, L. (2013). Investigation of metal–buffer interactions using isothermal titration calorimetry. *Journal of Thermal Analysis and Calorimetry*, *111*(3), 1829–1836. https://doi.org/10.1007/s10973-012-2593-y.

Xiao, C.-Q., Huang, Q., Zhang, Y., Zhang, H.-Q., & Lai, L. (2020). Binding thermodynamics of divalent metal ions to several biological buffers. *Thermochimica Acta*, *691*, 178721. https://doi.org/10.1016/j.tca.2020.178721.

Zheng, Y., Huang, J., Zhao, F., & Chistoserdova, L. (2018). Physiological effect of XoxG(4) on lanthanide-dependent methanotrophy. *MBio*, *9*(2), e02430-02417. https://doi.org/10.1128/mBio.02430-17.

4.2 Publication: Assessing Lanthanide-Dependent Methanol Dehydrogenase Activity: The Assay Matters

Manh Tri Phi, Helena Singer, Felix Zäh, Christoph Haisch, Sabine Schneider, Huub J. M. Op den Camp,

Lena J. Daumann*

Contributions: MTP and LJD conceived the study. MTP carried out the growth studies of SolV, purification, assays and data analysis. HS helped with the growth of SolV. FZ and SS assisted with the purification of cyt c_{GJ}. CS provided access to ICP-MS. HJMOdC provided SolV. MTP and LJD wrote the manuscript. All authors approved the final version.

Keywords: lanthanide-dependent bacteria, lanthanides, methanol dehydrogenase, methylotrophy, metalloenzymes
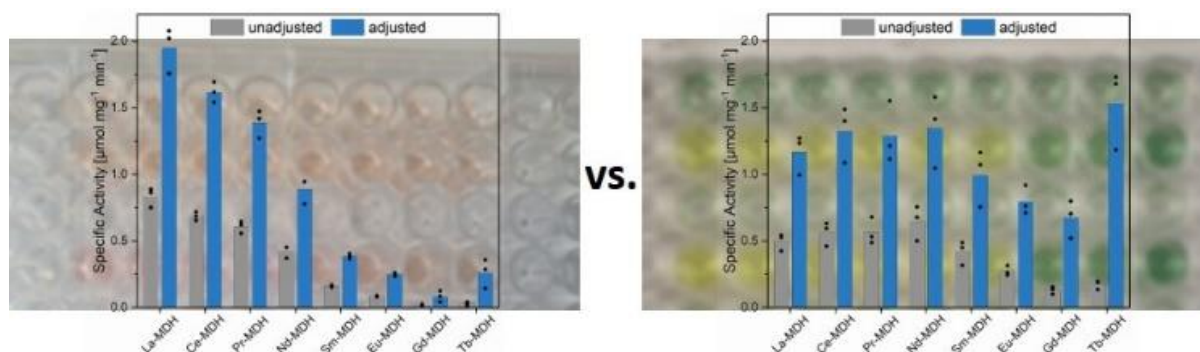
No Lu-ck with lutetium! We compare a widely used artificial dye-coupled assay to assess the enzyme activity of lanthanide-dependent methanol dehydrogenases with a protein-coupled assay and show why the assay matters. Furthermore, we explain quickly why the metal content of metalloenzymes should be determined before any experiments and how this can help to obtain accurate and reliable date.
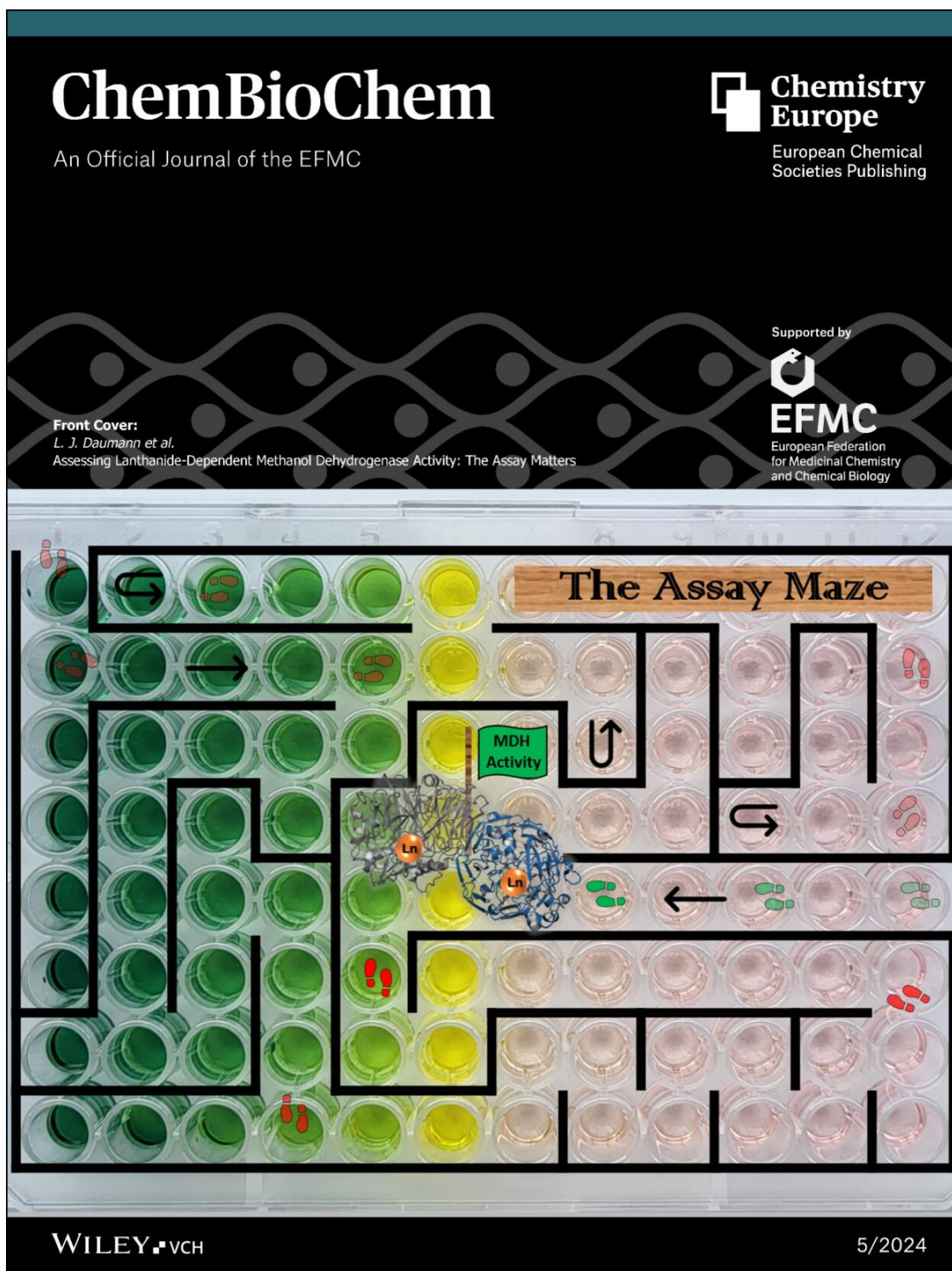
We investigate the enzyme activity of eight lanthanide-dependent methanol dehydrogenases through two different activity assays. Contrasting trends emerge from the widely used artificial dye-coupled assay (left) versus the protein coupled assay (right), underscoring the significance of why the choice of assay matters. The cover features a well plate illustrating results from both assays with a maze overlay distinguishing the misleading from the "straightforward" assay. (designed by Sophie Marie Gutenthaler-Tietze)

74

VIP *Very Important Paper*

Assessing Lanthanide-Dependent Methanol Dehydrogenase Activity: The Assay Matters

Manh Tri Phi,[a] Helena Singer,[a] Felix Zäh,[a] Christoph Haisch,[b] Sabine Schneider,[a] Huub J. M. Op den Camp,[c] and Lena J. Daumann*[a, d]

Artificial dye-coupled assays have been widely adopted as a rapid and convenient method to assess the activity of methanol dehydrogenases (MDH). Lanthanide(Ln)-dependent XoxF-MDHs are able to incorporate different lanthanides (Lns) in their active site. Dye-coupled assays showed that the earlier Lns exhibit a higher enzyme activity than the late Lns. Despite widespread use, there are limitations: oftentimes a pH of 9 and activators are required for the assay. Moreover, Ln-MDH variants are not obtained by isolation from the cells grown with the respective Ln, but by incubation of an apo-MDH with the Ln. Herein, we report the cultivation of Ln-dependent methanotroph *Meth-* *ylacidiphilum fumariolicum* SolV with nine different Lns, the isolation of the respective MDHs and the assessment of the enzyme activity using the dye-coupled assay. We compare these results with a protein-coupled assay using its physiological electron acceptor cytochrome c_{GJ} (cyt c_{GJ}). Depending on the assay, two distinct trends are observed among the Ln series. The specific enzyme activity of La-, Ce- and Pr-MDH, as measured by the protein-coupled assay, exceeds that measured by the dye-coupled assay. This suggests that early Lns also have a positive effect on the interaction between XoxF-MDH and its cyt c_{GJ} thereby increasing functional efficiency.

Introduction

In recent years, lanthanides (Ln, La–Lu) have firmly been established as biological relevant. Ln-dependent or -utilizing bacteria have been found in a variety of ecosystems, e.g. phyllosphere, pond sediment, (coastal) marine environment, shale rock, rice rhizosphere and geothermal fields.[1] Most of these bacteria are either methylotrophs or methanotrophs and use small C_1-molecules like methane, methanol, halogenated methanes, methylated amines and methylated sulfur species as their energy source.[2] Methanotrophs are able to convert

methane to carbon dioxide and play a significant role in the global carbon cycle.[1c] In the first step, methane is oxidized to methanol by particulate methane monooxygenase or soluble methane monooxygenase and subsequently oxidized to formaldehyde by methanol dehydrogenase (MDH).[3] There are two variants of this MDH: Ca-containing MxaFI-MDH and Ln-containing XoxF-MDH. All methanotrophs that possess the MxaFI-MDH variant also have the XoxF-MDH.[2,4] There are also reports of methano- and methylotrophs that exclusively possess the XoxF-MDH, highlighting the widespread prevalence of Ln-utilizing microorganisms.[1g,5]

If both types of MDH are present, MxaFI-MDH is expressed in the absence of any Ln. However, even the presence of nanomolar amounts of Ln is sufficient to initiate a transcriptional response, the "lanthanide-switch", favouring the expression of the XoxF-MDH variant even when the concentration of Ca is 100-fold higher.[9] In addition to the Ln ion, the active site contains pyrroloquinoline quinone (PQQ) as the second essential cofactor for XoxF-MDH (Figure 1).[6]

The mechanistic details of methanol oxidation by XoxF-MDH remains up for debate but two mechanisms are widely discussed by "wet-lab" and computational research groups: the addition-elimination and hydride transfer mechanism.[7,10] Pol *et al.* isolated the acidophilic methanotroph *Methylacidiphilum fumariolicum* SolV from a volcanic mudpot.[6] This bacterium is strictly dependent on Ln and exclusively possesses XoxF-MDH.[6,11] To cultivate SolV in a laboratory set-up, the extreme conditions of its natural environment have to be provided, including a Ln source, high temperature, low pH and the supply of methane and carbon dioxide.[6,12]

Most, if not all methylotrophic bacteria contain two distinct periplasmic, c-type cytochromes known as c_L and c_H. In the past, these cytochromes were designated based on their isoelectric points (p*I*), cyt c_L having the lower p*I* value and cyt c_H the higher

[a] M. T. Phi, H. Singer, F. Zäh, Prof. Dr. S. Schneider, Prof. Dr. L. J. Daumann
    Department of Chemistry
    Ludwig-Maximilians-Universität München
    Butenandtstr. 5–13, 81377 München (Germany)

[b] Prof. Dr. C. Haisch
    Faculty of Chemistry
    Technical University of Munich
    Lichtenbergstr. 4, 85748 Garching (Germany)

[c] Prof. H. J. M. Op den Camp
    Department of Microbiology
    Research Institute for Biological and Environmental Sciences
    Radboud University Nijmegen
    Heyendaalseweg 135, 6525 AJ, Nijmegen (The Netherlands)

[d] Prof. Dr. L. J. Daumann
    Chair of Bioinorganic Chemistry
    Heinrich-Heine-Universität Düsseldorf
    Universitätsstraße 1, 40225 Düsseldorf (Germany)
    E-mail: lena.daumann@hhu.de

ChemBioChem

Research Article
doi.org/10.1002/cbic.202300811

Chemistry
Europe
European Chemical
Societies Publishing
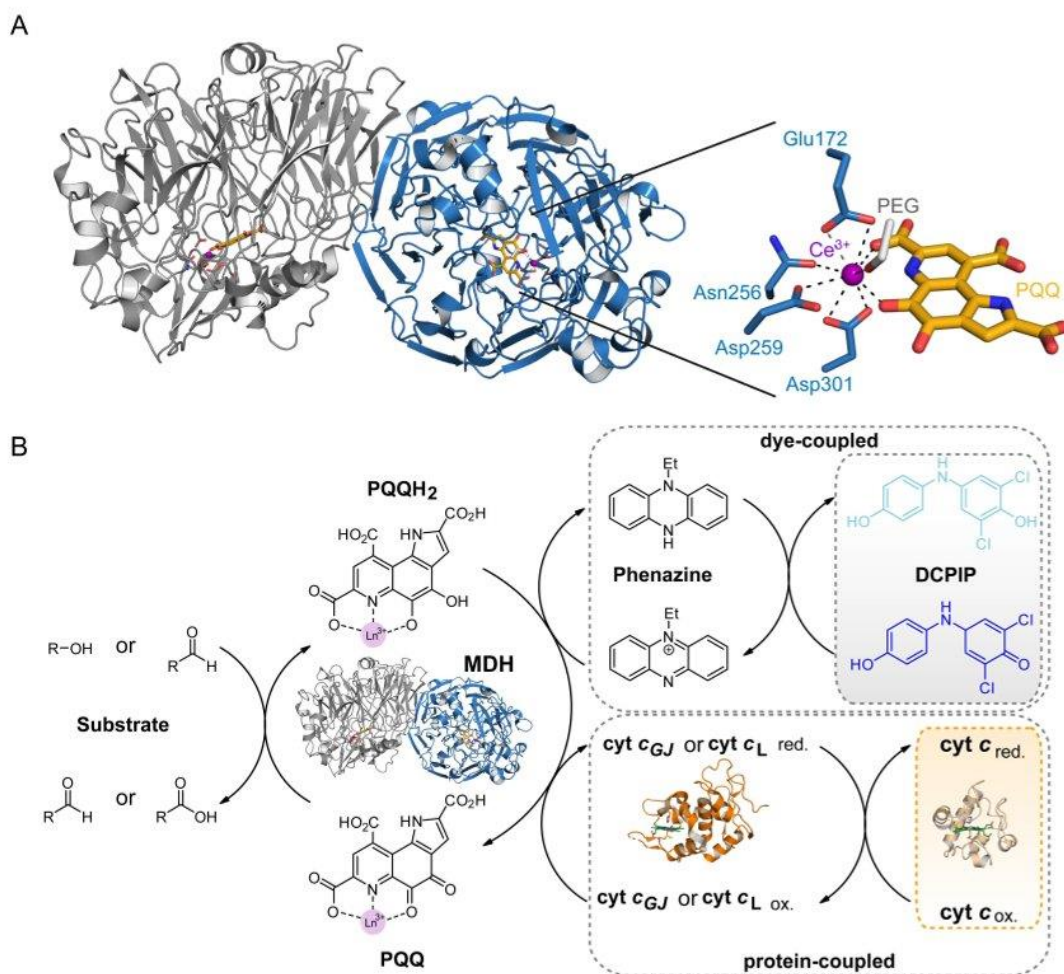
Figure 1. A) Homodimeric structure of Ce-MDH from *Methylacidiphilum fumariolicum* SolV (PDB: 4MAE)[6] and zoom in its active center. The cofactors PQQ and Ce^{3+}, as well as the coordinating amino acids are highlighted. The substrate binding coordination position of the Ce^{3+} is occupied by a polyethylene glycol (PEG) molecule from the crystallization buffer. (B) Schematic overview of the dye- and protein-coupled assay used in this study. Phenazine ethosulfate is reduced by PQQH$_2$ in MDH, leading to the reduction of DCPIP and causing its discoloration. PQQH$_2$ also reduces cyt c_{GJ} which in turn reduces equine heart cyt *c*. The change in absorbance for DCPIP and equine heart cyt *c* can be measured using UV/Vis at A$_{600}$ and A$_{550}$, respectively. The crystal structures of cytochrome c XoxG from *Methylorubrum extorquens* AM1 (PDB: 6ONQ) and equine heart cyt *c* (PDB: 1HRC) were used to illustrate this scheme. PQQ, pyrroloquinoline quinone. PQQH$_2$, pyrroloquinoline quinol. DCPIP, 2,6-dichlorophenolindophenol. Modified from Refs. [7] and [8].

value. Only the cyt c_L is able to interact with MDH.[13] The physiological electron transfer of MxaFI-MDH from substrate to its immediate cyt c_L was extensively studied by Anthony and co-workers in *Methylorubrum extorquens* AM1.[14] Fundamentally, oxidation of methanol results in a concomitant reduction of PQQ to PQQH$_2$, which is step-wise re-oxidized after two single electron transfers to two separate molecules of cyt c_L which is reduced as well. Finally, cyt c_L regeneration is achieved through an additional electron transfer to cyt c_H.[13] In case of SolV, cyt c_L is termed cyt c_{GJ} and consists of the XoxG cytochrome and a periplasmic binding protein XoxJ.[15] The interaction or "docking" of cyt c_{GJ} to XoxF-MDH involves electrostatic interaction between lysine residues on XoxF-MDH and carboxyl residues on cyt c_{GJ}. Disassembly of the reduced cyt c_{GJ} is required before XoxF-MDH can interact with the next molecule of cyt c_{GJ}. Electrostatic interactions are also involved for the electron transfer from cyt c_{GJ} to cyt c_H.[14a] The interaction between XoxF-

MDH and cyt c_{GJ} is disturbed by high salt concentration which inhibits substrate oxidation by up to 50% at 150 mM NaCl, 100 mM K$_2$SO$_4$ or 25 mM phosphate.[14a,15] Furthermore, electrochemical experiments revealed that cyt c_{GJ} itself exhibits temperature dependence, with a 20% increase in current going from 10 to 35°C.[16] Featherston *et al.* characterized the immediate cytochrome of XoxF-MDH, XoxG, from *M. extorquens* AM1 (the structure of this cytochrome is shown in Figure 1B in lieu of a structure of the native electron acceptor from SolV). By comparing the results of an artificial dye-coupled assay with a XoxG-based assay, they concluded that these assays measure distinct aspects of XoxF-MDH activity.[17]

For decades, the most commonly practiced method to determine the activity of MDHs is a dye-coupled assay using the dyes phenazine ethosulfate (PES) as primary and 2,6-dichlorophenolindophenol (DCPIP) as secondary artificial electron acceptor.[18] The reduction of DCPIP results in its discolor-

ChemBioChem

Research Article
doi.org/10.1002/cbic.202300811

Chemistry Europe
European Chemical
Societies Publishing

ation which is measured at 600 nm by UV/Vis. Based on previous work by Anthony and co-workers, protein-coupled activity assays for MDH from SolV using its physiological cyt c_{GJ} partner were developed.[8,15,19] Commercially available cyt c from equine or bovine heart is used as secondary electron acceptor.[15] Again, the reduction of the secondary electron acceptor can be monitored to determine the enzyme activity (Figure 1B). Kalimuthu *et al.* developed an electrochemical assay that allows the co-adsorption of Eu-MDH and cyt c_{GJ} onto an electrode which functions as the secondary electron acceptor. In this case, the enzyme activity is tracked by measuring the current.[16]

Previous studies mainly used the dye-coupled assay to determine the enzyme activity of XoxF-MDH because the reagents are commercially available and low-cost. Usually a pH of 9, additives and activators like ammonia, glycine ethyl ester, potassium cyanide and an excess of Ln are included in the assay mixture to optimize the conditions for the assays (these additives are not necessary for MDH from *M. fumariolicum* SolV).[8] These experimental conditions rarely reflect the physiological conditions inside the cell and are truly artificial. Furthermore, the source of the endogenous substrate that causes background reaction is still unknown.[19] Although, Featherston *et al.* compared the enzyme activity of La-, Ce- and Pr-MDH from *M. extorquens* AM1 with the dye-coupled and protein-coupled assay, the differences in buffer, pH and activator do not allow for a direct comparison.[17]

Herein, we report the cultivation of *M. fumariolicum* SolV with nine different Lns and the isolation and purification of the respective Ln-MDHs and their physiological electron acceptor cyt c_{GJ}. Using the dye- and protein-coupled assays under the same assay conditions, we evaluated the enzyme activity of the different Ln-MDHs and observed varying trends among them, depending on the assay used.

Results and Discussion

The growth rate of *M. fumariolicum* SolV is highly dependent on supplemented Ln and its concentration in the growth medium.[6,12a] Compared to the growth of SolV with early Lns La-Nd, the growth rate of SolV with late lanthanide Gd is less than half.[6] When given a mixture of equimolar amount of all Ln and two actinides (Am, Cm), SolV preferably takes up the early Ln, showing the highest (80%) depletion from the medium for La.[12a] The depletion of Gd is barely 20% which is less than Am and Cm with a depletion of around 45% each.[12a] Based on the availability, XoxF-MDH is capable to incorporate a variety of Ln in its active site to obtain the respective Ln-MDH. We conducted nine separate cultivations of SolV at 55 °C and pH 2.7 with nine different Ln (La, Ce, Pr, Nd, Sm, Eu, Gd, Tb and Lu) in a self-build customized 3.5 L bioreactor, following a previously reported protocol.[12b] We observed exponential growth for seven out of nine cultivations (Figure S1) and stopped the cultivation of SolV with Tb and Lu after 10 days as only linear growth was observed with these elements. Nonetheless, cells of all cultivations were collected for isolation of XoxF-MDHs and cyt

c_{GJ}. MDH makes up a high proportion of SolV's biomass and can be isolated without an affinity tag as previously shown.[6] The quantity of cyt c_{GJ} obtained after purification is low and makes native purification laborious. The heterologous expression of cyt c_{GJ} is desirable, but due to a so far unknown modification of or near its heme complex, native purification is, to the best of our knowledge, the only way to obtain cyt c_{GJ}.[15] Native protein purification of XoxF-MDHs and cyt c_{GJ} were performed by ion exchange chromatography and cyt c_{GJ} was additionally purified by size exclusion chromatography (SEC) (Figure S2). The addition of 1 mM MeOH to all buffer solutions is imperative to ensure stability and activity of Ln-MDHs along the purification process and for long-term storage.[6] To avoid secondary interactions of cyt c_{GJ} with the silica matrix, NaCl is added to the buffer for SEC. However, since the interaction of MDH and cyt c_{GJ} is mainly electrostatically and thus negatively affected by high salt concentrations, NaCl needs to be removed after SEC, which was done using centrifugal filter devices.[15] Ln-MDHs and cyt c_{GJ} were analyzed by SDS-PAGE (Figure S3) and the metal content of all Ln-MDHs was measured by Inductively Coupled Plasma Mass Spectrometer (ICP-MS).

ICP-MS measurement does not provide information about the metalation of the active site but rather the metal content of the sample. This can pose a challenge when XoxF-MDH co-purifies with other Ln-binding proteins such as LanM rendering the read-out ineffective, as noted by Featherston *et al.*[17] SolV does not encode LanM in its genome and the use of time-resolved laser-induced fluorescence spectroscopy (TRLFS) enables the differentiation between Eu in the active site and in solution. TRLFS confirms the previously determined metal content value of Eu-MDH obtained by ICP-MS analysis.[20] Previous studies found that XoxF-MDH from SolV is metallated on average with 60–70% of the respective Ln ions after purification.[6–7,20] Our results show that the metal content of Ln-MDH is higher in the case of early Lns (La–Nd), ranging from 42–48%. However, there is a notable decrease in metalation across the Ln series, with Tb-MDH having 11% metal content. La-XoxF1 from *M. extorquens* AM1 with a metal content of 39% displayed only half the specific activity compared to its previous studies.[21] As the metal content is highly variable depending on the batch and metal, we recommend to determine the metal content of Ln-MDHs, before conducting any experiment to ensure accurate and reliable data. Despite their similar ionic radii, these small differences influence the incorporation efficiency and retention of the Ln in the active site. MDH obtained from SolV grown with Lu did not contain detectable amounts of Lu and was omitted for further experiments. PQQ is the second indispensable cofactor in the active site of Ln-MDH. The occupancy of the cofactor was determined by measuring its absorption maximum at 355 nm.[7,10a] The cofactor was present in all samples but whether the loading is 100% cannot be taken from this method. Fully accounting for PQQ and/or metal contents continues to pose a challenge. Despite ongoing efforts, a comprehensive understanding of the exact mechanisms and factors influencing the presence and quantity of PQQ and/or metals remains elusive.

ChemBioChem

Research Article
doi.org/10.1002/cbic.202300811

Chemistry Europe
European Chemical
Societies Publishing

With eight Ln-MDHs and cyt c_{GJ} in hand, we moved on to determine the methanol oxidation activity. For decades, an artificial dye-coupled assay that utilizes redox-active dyes has been widely employed to assess the enzyme activity of MDHs derived from a vast variety of microorganisms.[1a,7,22] In addition to the non-specificity of the dye-coupled assay to MDH, the commercially available and low-cost reagents favor the usage of this assay. However, this method does not mirror the mechanism *in vivo* and conclusions drawn from the dye-coupled assay should be considered carefully. PES/DCPIP and the alternative dye-coupled method with Wurster's Blue are all photosensitive, can induce high background reactivity and should be performed vigilantly.[18b] Similar to previous work, the specific activity of the Ln-MDHs with early Lns is higher and increases towards Nd-MDH and then decline subsequently (Figure 2A). In order to account for the varying metal content among samples, we adjusted the specific activities by assuming a 100% metal content within the active site. Due to the relatively low metal content of Tb (11.3%) in the MDH sample purified from cells grown on Tb and likely even lower metalation of the active site and activation of PQQ, the adjusted

specific activity is likely to be artificially inflated, but was included for transparency. For the smaller Lns, several theoretical studies have shown that the activation of PQQ is insufficient, preventing effective oxidation.[10a,23] The low metalation of the sample leads to a substantial increase in uncertainty and will not be further discussed. Earlier studies obtained and compared the activity of different XoxF-MDHs by titrating the desired Ln to partial-apo Eu-MDH or incubating apo-MDH with Ln and PQQ.[7,10a,12a,22] To the best of our knowledge, the isolation of various Ln-MDHs from a microorganism grown with its respective Ln has not been widely practiced so far. Singer *et al.* were able to receive XoxF-MDH containing the heavier, smaller Lns by expressing an apo-XoxF-MDH in *Escherichia coli* and incubation with the respective Ln and PQQ for 72 hours.[12a] The results of their dye-coupled activity assays show that Tb-MDH is less active than Gd-MDH (although it should be noted, that metalation was not investigated here).

Computational and experimental studies also discuss the effect of the Lewis acidity of the Ln on enzyme activity.[7,10a–c] Due to the Ln contraction, the Lewis acidity increases across the Ln series. PQQ requires a Lewis acid to activate its C5 quinone C−O bond for the subsequent proton abstraction step of the substrate. Higher Lewis acidity facilitates the rate-limiting breaking of the substrate C−H bond hence increasing substrate turnover and enzyme activity but obtaining XoxF-MDH with late Ln remains challenging.

A protein-coupled activity assay is another method to investigate kinetic parameters of MDHs. Anthony and co-workers developed a protein-coupled activity assay for MxaFI-MDH from *M. extorquens* AM1.[19,24] The assay mixture is composed of MxaFI-MDH, its physiological partner cyt c_L, cyt c from equine or bovine heart and MeOH as substrate. The physiological electron acceptor cyt c_L is used to re-oxidize MxaFI-MDH and the introduction of the secondary cytochrome c from equine or bovine heart is able to re-oxidze cyt c_L without interacting with MDH (Figure 1B).[24] Versantvoort *et al.* have shown with XoxF-MDH from SolV that the rate of reduction of the secondary cytochrome depends on the concentration of the physiological partner cytochrome which appeared to be linear between 0 and 1 μM for cyt c_{GJ}.[15] This method reflects the physiological mechanism more accurately and is easier to handle without photosensitive reagents. A limitation is the MDH-specificity of the real physiological cytochrome partners although some rare cases are reported where this was still possible, e.g. the cyt c_L of AM1 is able to interact with MDH from *Paracoccus denitrificans* and *Methylophilus methylotrophus*.[24] Featherston *et al.* discussed the subtle differences of the immediate cytochromes MxaG and XoxG of MxaFI-MDH and XoxF-MDH, respectively, from *M. extorquens* AM1.[17] Both cytochromes are *c*-type cytochromes and carry the typical characteristics: covalent attachment of the heme *c* moiety to the protein *via* two thioether bonds and axial ligation of the Fe^{3+} by histidine and a second, in this case, a methionine residue.[25] The main distinctions are the loss of a helix in cyt *c* XoxG and the absence of a Ca^{2+} binding site in another helix. These differences result in more solvent-exposed heme that is
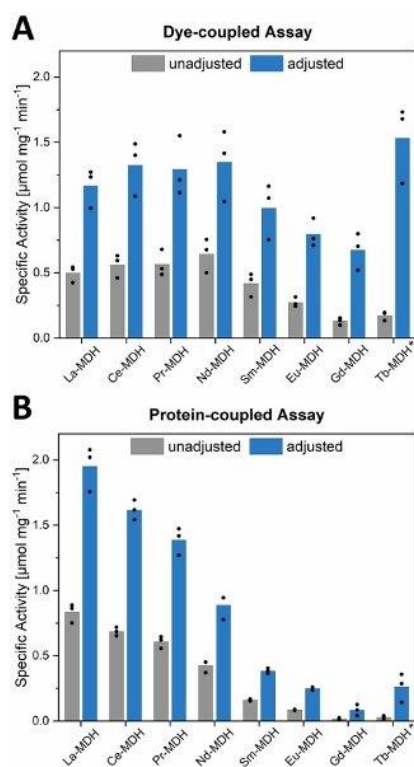
Figure 2. Results of the determination of specific enzyme activity using (A) the dye-coupled and (B) protein-coupled assay (outlined in Figure 1B). Conditions dye-coupled assay: 100 nM XoxF-MDH, 1 mM PES, 100 μM DCPIP, 50 mM MeOH in 10 mM PIPES with 1 mM MeOH, pH 7.2, 45 °C. Conditions protein-coupled assay: 100 nM XoxF-MDH, 5 μM cyt c_{GJ}, 50 μM cyt *c* from equine heart, 50 mM MeOH in 10 mM PIPES with 1 mM MeOH, pH 7.2, 45 °C. The adjusted values are calculated assuming 100% metal content in the active site. Technical replicates (n = 3) were conducted and each dot represents the result of one measurement. *The relatively low metal content of Tb-MDH (11.3%) likely inflates the adjusted value for the enzymatic activity.

ChemBioChem

Research Article
doi.org/10.1002/cbic.202300811

**Chemistry
Europe**
European Chemical
Societies Publishing

proposed to be the source of the relatively low midpoint reduction value of the XoxG-type cytochromes.[17] These subtle yet important structural changes are likely to result in different enzymatic activity of MDHs *in vivo* and cannot be properly reflected by an artificial dye-coupled assay. Thus, conclusions deduced from dye-coupled assays should be drawn carefully.

The highly laborious work to obtain adequate protein quantities required for protein-coupled activity assays is another hindrance, which should be considered. Before we conduct protein-coupled assay of XoxF-MDHs with cyt c_{GJ}, we determined the optimal concentration of cyt c_{GJ} to obtain maximum substrate turnover. Among all tested Ln-MDHs, Nd-MDH demonstrated the highest enzyme activity based on the dye-coupled assay and was chosen as the proxy for this experiment. Nd-MDH was assayed with increasing amount of cyt c_{GJ} (0–30 μM) and Michaelis-Menten kinetics were obtained by best curve fitting (Figure S4).

Based on these results, a concentration of cyt c_{GJ} above 100 μM is required to obtain v_{max}, which is a prohibitively large amount of cyt c_{GJ} for a single assay. Therefore, we decided to choose a value at the end of the linear phase and proceeded with 5 μM cyt c_{GJ} for each assay. We evaluated the enzymatic activity of eight XoxF-MDHs with the protein-coupled assay and the results are shown in Figure 2B. In order to exclude any day-to-day deviation, we used the same enzyme batch for both methods and conducted the experiments on the same day. In contrast to the dye-coupled assay, we observed a gradual decrease in enzymatic activity across the Ln series. Again, Gd-MDH displays the lowest enzyme activity, while La-MDH exhibits the highest enzyme activity. Regardless of method, Gd-MDH constantly remains the least active MDH. As discussed above, Lewis acidity can have a significant impact on substrate turnover through various mechanisms. Additional functions of the Lewis acid, like substrate orientation, cofactor redox cycling and substrate activation and their effects on the enzyme activity, have been discussed.[10a,c,d,26] We found that the specific enzyme activity of La-, Ce- and Pr-MDH is higher with the protein-coupled assay compared to their activity measured with the dye-coupled assay. In contrast, Nd-, Sm-, Eu- and Gd-MDH exhibit lower specific activity with the protein-coupled assay than with the dye-coupled assay. These results indicate that, depending on the assay, distinct trends can be observed among the XoxF-MDHs, implying that different aspects of the enzyme activity are being measured. Moreover, the protein-coupled assay revealed greater specific enzyme activity for La-, Ce- and Pr-MDH suggesting that these Lns may positively affect the efficiency in cyt c_{GJ} reduction. In comparison to the dye-coupled assay, protein-protein interaction steps are involved in the protein-coupled assay to transfer the electrons from XoxF-MDH to the final electron acceptor, but the positive effect of La, Ce and Pr on the interaction still exceed this challenge. These results indicate that La, Ce and Pr are not just suitable Lewis acids that catalyze the rate-limiting step for substrate turnover, but also facilitate and enhance the electron transfer between XoxF-MDH and its cyt c_{GJ}, thereby increasing the overall functional efficiency. We cannot rule out that the use of 5 μM

cyt c_{GJ} may not be optimal and might be sufficient to reach v_{max} for one XoxF-MDH but not for another such as Nd-MDH.

Conclusions

To conclude, we have grown *M. fumariolicum* SolV with nine different Lns and were able to purify eight different XoxF-MDHs, and their physiological electron acceptor cyt c_{GJ} and assessed the enzyme activity by performing dye- and protein-coupled activity assays. ICP-MS measurements revealed that XoxF-MDH contain varying amount of Ln in their active site and that this value decreases towards Tb. ICP-MS also showed that XoxF-MDH isolated from Lu-grown SolV was not able to incorporate any Lu. Next, we determined the enzyme activity using the dye-coupled assay with PES/DCPIP and compared the results with the protein-coupled assay using cyt c_{GJ} as electron acceptor. The data obtained from each method showed a discernible and distinct pattern Ln-MDHs, providing evidence that these methods are impacted by different aspects of the Ln-dependent enzyme activity. Both methods revealed that Gd-MDH is the least active among the eight XoxF-MDHs and that the enzymes containing larger Lns have higher activity, but different trends amongst the Ln series are observed based on the method used. At first glance, the increased activity of XoxF-MDH with early Lns align with the higher growth rates of SolV when cultivated with early Lns, suggesting that the growth of SolV is mainly linked to the activity of XoxF-MDH.[6,12a] Wegner and co-workers discovered in *Beijerinckiaceae* bacterium RH AL1 that the addition of La or a Ln cocktail change the expression of nearly 41% of all genes in the genome and that different Lns affect different genes. Differentially expressed genes are associated with various biological processes of the Ln-dependent metabolism but also include secretion and uptake system, the flagellar and chemotactic machinery and other cellular functions.[27] Therefore, the influence of Lns extend beyond their catalytic role in methanol oxidation.

Using the dye-coupled assay, the enzyme activity increases towards Nd-MDH and declines afterwards. These results are in accordance with previous studies.[7,10a,12a,22] Using the protein-coupled assay, La-MDH displayed the highest enzyme activity which decreases progressively towards Gd-MDH. Although more steps are involved to transfer the electrons from XoxF-MDH to the final electron acceptor, we observed that La-, Ce- and Pr-MDH exhibit higher enzymatic activity in the protein-coupled assay than in the dye-coupled assay. This indicates that the enhancing effects of Ln are not limited to XoxF-MDH but also influence the electron transfer by its cyt c_{GJ}. When adjusting the enzyme activity by their varying metal content, the trends became more pronounced, supporting our findings. This normalization allowed us to account for any potential discrepancies in the metal content and increases the accuracy and reliability of the results. To enhance reproducibility and comparability, we propose to incorporate the determination of metal content by ICP-MS into any kinetic experiments that involves metalloenzymes. This additional step will ensure that

ChemBioChem

Research Article
doi.org/10.1002/cbic.202300811

Chemistry Europe
European Chemical
Societies Publishing

variations in metal content are accounted for, which will enable more meaningful comparisons between different experiments.

Experimental Section

Bacterial culture

The cultivation of *M. fumariolicum* SolV (La–Eu) was performed by using a modified protocol as previously reported.[12a] For the composition of the growth medium see Table S1. SolV was grown with the desired Ln (La–Eu) in single-use polypropylene plastic cultivation flasks to an optical density at 600 nm (OD_{600}) of 0.5. Around 100–200 mL of SolV culture was used to inoculate the large-scale (3.5 L) bioreactor (non-commercial, self-build) to obtain a starting OD_{600} of 0.05.[12b] Throughout the cultivation, CO_2 (600 mL/min), CH_4 (750 mL/min) and air (1000 mL/min) was sparged through the medium. The temperature was kept at 55 °C and a stirring bar was used to ensure homogeneity and even distribution of gases.

The inoculants for Gd- and Tb-grown SolV were obtained by starvation of La-grown SolV through two cycles:

Minimal medium (100 mL) and La-grown SolV was added to a 1 L cultivation flask to a starting OD_{600} of 0.05. For incubation, a gas atmosphere of 85% air, 10% CH_4 and 5% CO_2 was provided. The flask was incubated in a shaker at 55 °C and 250 rpm for 4 days until an OD_{600} of around 0.25 was reached (cycle 1). 100 mL of this starved La-grown SolV was used to repeat the same procedure once more until an OD_{600} of 0.125 was reached (cycle 2). In the third round, 100 nM $GdCl_3$ or $TbCl_3$ was added to the starved SolV culture and further incubated until the desired OD_{600} was reached and then used as inoculant for the bioreactor.

Protein Purification

M. fumariolicum SolV cells were harvested by centrifugation at 8000 rpm for 10 min (Avanti JXN-26, Beckman Coulter). The cells were resuspended in 10 mM PIPES (piperazine-*N,N′*-bis(2-ethanesulfonic acid) supplemented with 1 mM MeOH (pH 7.2) and chemically lysed by commercially available BugBuster Protein Extraction Reagent (Merck, product code 70921). 10xBugBuster Protein Extraction Reagent was diluted to 1x with 10 mM PIPES and 1 mM MeOH (pH 7.2). The reagent was added to frozen or thawed cell pellet (2 mL 1xBugBuster per 1 g resuspended cells), followed by the addition of 0.5–1.0 mg/mL lysozyme from chicken egg white (Sigma-Aldrich, CAS 12650–88-3), 0.2–0.5 mg/mL DNase I (PanReac AppliChem, product code A3778,0100) and incubated on a shaking platform for 30–45 min at room temperature. Afterwards, insoluble cell debris were removed by centrifugation (17000 rpm, 20 min, 4 °C). After filtration of the supernatant with a filter paper (VWR, 5–13 μm particle retention), the sample was applied on a HiPrep™ SP Sepharose FF 16/10 cation exchange column (Cytiva, product code 28936544). The column was equilibrated with 10 mM PIPES with 1 mM MeOH (pH 7.2) and bound proteins were eluted using 10 mM PIPES with 1 M NaCl and 1 mM MeOH (pH 7.2). Cyt c_{GJ} eluted at 2% (20 mM NaCl) and MDH at 25% (250 mM NaCl). Cyt c_{GJ} was further concentrated using an Amicon® Ultra Centrifugal Unit (Merck, product code UFC901024) with a molecular weight cut-off of 10 kDa and applied on a HiLoad™ 16/600 Superdex™ 75 pg size exclusion column (Cytiva, product code 28989333). The column was equilibrated with 10 mM PIPES and 0.2 M NaCl (pH 7.2) and cyt c_{GJ} started to elute after 65 mL at a flowrate of 0.3 mL/min recording the UV/Vis absorption at 280 nm and its Soret peak of 434 nm. The NaCl concentration was reduced to less than 1 mM with an

Amicon® Ultra Centrifugal Unit (Merck, UFC201024) with a molecular weight cut-off of 10 kDa and 10 mM PIPES (pH 7.2).

For SDS-PAGE analysis, mPAGE® 4X LDS sample buffer (Merck, product code MPSB-10 ML) containing 2% β-mercaptoethanol was added to samples and then heated at 70 °C for 5–7 min. The samples were loaded on a 12% SDS-PAGE gel (12% w/v acrylamide). The gel was stained with Coomassie Blue Stain for 1 h and subsequently treated with a destaining solution (10% (v/v) acetic acid and 20% (v/v) EtOH in ultrapure water). MDHs (63.5 kDa) and cyt c_{GJ} (29.7 kDa) appear as dominant bands (Figure S3).

Activity Assays

The activity assay with cyt c_{GJ} and artificial electron acceptors are based on the protocols reported by Gutenthaler *et al.*[8] The enzymatic activity of MDH was assessed with native cyt c_{GJ} through the reduction of equine heart cyt c (Sigma, CAS 9007-43-6). The reaction was monitored with an Epoch2 plate reader (formerly BioTek, now Agilent) at 45 °C through the increase of A_{550}. All experiments were conducted in 96-well-plates. Each well contained a total volume of 100 μL with 50 μM equine heart cytochrome *c*, 5 μM cyt c_{GJ}, 100 nM MDH and 50 mM MeOH in 10 mM PIPES with 1 mM MeOH (pH 7.2). Everything but MDH were mixed together and incubated for 2 min at 45 °C before the reaction was initiated with the addition of MDH which was also incubated for 2 min at 45 °C. The extinction coefficient of equine heart cytochrome *c* was previously determined at 19.5 $mM^{-1}\,cm^{-1}$ for 10 mM PIPES (pH 7.2).[15] The specific activity was calculated using the slope of the initial 2 min after MDH addition. The specific activity of each experiment was adjusted according to the metal content of the MDH.

$$enzyme\ unit\ U\ [\mu mol\ min^{-1}] =$$
$$\frac{initial\ rate\ of\ slope\ of\ measurement}{\varepsilon\ [cm^{-1}\ M^{-1}] \times pathlength\ of\ cell\ [cm]} \times 10^6$$
$$\times volume\ of\ assay\ [L]$$

$$specific\ activity\ [\mu mol\ min^{-1}\ mg^{-1}] =$$
$$\frac{enzyme\ Unit\ U\ [\mu mol\ min^{-1}]}{amount\ of\ enzyme\ [mg]}$$

$$specific\ activity_{adjusted}\ [\mu mol\ min^{-1}\ mg^{-1}] =$$
$$\frac{enzyme\ Unit\ U\ [\mu mol\ min^{-1}]}{amount\ of\ enzyme\ [mg] \times \frac{metal\ content\ [\%]}{100}}$$

The activity assay with the artificial electron acceptor DCPIP (2,6-Dichlorophenolindophenol sodium salt dihydrate, formerly Fluka, now Honeywell, CAS: 1266615–56-8) and PES (phenazine ethosulfate, Sigma-Aldrich, CAS 10510-77-7) was assessed through the reduction of DCPIP. The reaction was monitored with an Epoch2 plate reader (formerly BioTek, now Agilent) through the decrease of A_{600}. Each well contained a total volume of 100 μL with 1 mM PES, 100 μM DCPIP, 100 nM MDH, 50 mM MeOH in 10 mM PIPES with 1 mM MeOH (pH 7.2). Everything but MDH were mixed and incubated for 2 min at 45 °C in the dark before the reaction was initiated with addition of MDH which was also incubated for 2 min at 45 °C in the dark. The extinction coefficient of DCPIP was determined at 19.8 $mM^{-1}\,cm^{-1}$ for 10 mM PIPES (pH 7.2). The specific activity was calculated using the slope of the initial 2 min

after MDH addition. The specific activity of each experiment was adjusted according to the metal content of the MDH.

$$enzyme\ unit\ U\ [\mu mol\ min^{-1}] =$$

$$\frac{-1 \times initial\ rate\ of\ slope\ of\ measurement}{\varepsilon\ [cm^{-1}\ M^{-1}] \times pathlength\ of\ cell\ [cm]} \times 10^6$$

$$\times volume\ of\ assay\ [L]$$

$$specific\ activity\ [\mu mol\ min^{-1}\ mg^{-1}] =$$

$$\frac{enzyme\ Unit\ U\ [\mu mol\ min^{-1}]}{amount\ of\ enzyme\ [mg]}$$

$$specific\ activity_{adjusted}\ [\mu mol\ min^{-1}\ mg^{-1}] =$$

$$\frac{enzyme\ Unit\ U\ [\mu mol\ min^{-1}]}{amount\ of\ enzyme\ [mg] \times \frac{metal\ content\ [\%]}{100}}$$

The Michaelis-Menten constant K_M and the maximum turnover speed v_{max} of the cyt c_{Gj}-based activity assay (0–30 μM) with 100 nM Nd-MDH were calculated with the Michaelis-Menten equation using the slope of the initial 2 min after initiation:

$$v_0 = \frac{v_{max}[S]}{K_M + [S]}$$

With v_0 representing the initial velocity and [S] the substrate concentration. The specific activity of each experiment was adjusted according to the metal content of Nd-MDH (47.8%).

Metal analysis by ICP-MS

The Ln-content of each MDH was determined by addition of the samples to 3% nitric acid (Suprapur®, Supelco) and heating for 1 h at 90°C before analysis using an Inductively Coupled Plasma Mass Spectrometer (Nexion 350D, Perkin Elmer). Protein concentration were determined spectrophotometrically at 280 nm using an extinction coefficient of 158 cm^{-1} mM^{-1}.[6] The metal content of the Ln-MDHs (technical duplicates) used in these experiments was determined at 42.7% for La-MDH, 42.4% for Ce-MDH, 43.8% for Pr-MDH, 47.8% for Nd-MDH, 41.9% for Sm-MDH, 34.3% for Eu-MDH, 19.2% for Gd-MDH and 11.3% for Tb-MDH.

Conflict of Interests

The authors declare no conflict of interest.

Data Availability Statement

Further data available in the SI.

[1] a) T. Nakagawa, R. Mitsui, A. Tani, K. Sasa, S. Tashiro, T. Iwama, T. Hayakawa, K. Kawai, PLoS One **2012**, 7, e50480; b) S. Kato, M. Takashino, K. Igarashi, W. Kitagawa, Microbes Environ. **2020**, 35; c) B. Vekeman, D. Speth, J. Wille, G. Cremers, P. De Vos, H. J. M. Op den Camp, K. Heylen, Microb. Ecol. **2016**, 72, 503–509; d) M. Taubert, C. Grob, A. M. Howat, O. J. Burns, J. L. Dixon, Y. Chen, J. C. Murrell, Environ. Microbiol. **2015**, 17, 3937–3948; e) H. Lv, N. Sahin, A. Tani, Environ. Microbiol. **2018**, 20, 1204–1223; f) P. Roszczenko-Jasińska, T. Krucoń, R. Stasiuk, R. Matlakowska, FEMS Microbiol. Ecol. **2020**, 97; g) S. Hou, K. S. Makarova, J. H. W. Saw, P. Senin, B. V. Ly, Z. Zhou, Y. Ren, J. Wang, M. Y. Galperin, M. V. Omelchenko, Y. I. Wolf, N. Yutin, E. V. Koonin, M. B. Stott, B. W. Mountain, M. A. Crowe, A. V. Smirnova, P. F. Dunfield, L. Feng, L. Wang, M. Alam, Biol. Direct **2008**, 3, 26.

[2] L. Chistoserdova, Environ. Microbiol. **2011**, 13, 2603–2622.

[3] a) H. In Yeub, L. Seung Hwan, C. Yoo Seong, P. Si Jae, N. Jeong Geol, C. In Seop, K. Choongik, K. Hyun Cheol, K. Yong Hwan, L. Jin Won, J. Microbiol. Biotechnol. **2014**, 24, 1597–1605; b) A. S. Hakemian, A. C. Rosenzweig, Annu. Rev. Biochem. **2007**, 76, 223–241; cT. J. Kang, E. Y. Lee, J. Ind. Eng. Chem. **2016**, 35, 8–13.

[4] a) R. A. Schmitz, N. Picone, H. Singer, A. Dietl, K.-A. Seifert, A. Pol, M. S. M. Jetten, T. R. M. Barends, L. J. Daumann, H. J. M. O. d. Camp, M. W. Ribbe, mBio **2021**, 12, e01708–01721; b) L. Chistoserdova, M. G. Kalyuzhnaya, Trends Microbiol. **2018**, 26, 703–714.

[5] a) C. Mackenzie, M. Choudhary, F. W. Larimer, P. F. Predki, S. Stilwagen, J. P. Armitage, R. D. Barber, T. J. Donohue, J. P. Hosler, J. E. Newman, J. P. Shapleigh, R. E. Sockett, J. Zeilstra-Ryalls, S. Kaplan, Photosynth. Res. **2001**, 70, 19–41; b) G. Bosch, T. Wang, E. Latypova, M. G. Kalyuzhnaya, M. Hackett, L. Chistoserdova, Microbiology **2009**, 155, 1103–1110.

[6] A. Pol, T. R. M. Barends, A. Dietl, A. F. Khadem, J. Eygensteyn, M. S. M. Jetten, H. J. M. Op den Camp, Environ. Microbiol. **2014**, 16, 255–264.

[7] B. Jahn, A. Pol, H. Lumpe, T. R. M. Barends, A. Dietl, C. Hogendoorn, H. J. M. Op den Camp, L. J. Daumann, ChemBioChem **2018**, 19, 1147–1153.

[8] S. M. Gutenthaler, M. T. Phi, H. Singer, L. J. Daumann, in Methods Enzymology, Vol. 650 (Ed.: J. A. Cotruvo), Academic Press, **2021**, pp. 57–79.

[9] a) H. N. Vu, G. A. Subuyuj, S. Vijayakumar, N. M. Good, N. C. Martinez-Gomez, E. Skovran, J. Bacteriol. **2016**, 198, 1250–1259; b) F. Chu, M. E. Lidstrom, J. Bacteriol. **2016**, 198, 1317–1325; c) W. Gu, M. Farhan Ul Haque, A. A. DiSpirito, J. D. Semrau, FEMS Microbiol. Lett. **2016**, 363; d) S. Masuda, Y. Suzuki, Y. Fujitani, R. Mitsui, T. Nakagawa, M. Shintani, A. Tani, mSphere **2018**, 3, 10.1128/msphere.00462-00417.

[10] a) H. Lumpe, A. Pol, H. J. M. Op den Camp, L. J. Daumann, Dalton Trans. **2018**, 47, 10463–10472; b) M. Prejanò, N. Russo, T. Marino, Chem. Eur. J. **2020**, 26, 11334–11339; c) M. Prejanò, T. Marino, N. Russo, Chem. Eur. J. **2017**, 23, 8652–8657; d) M. Leopoldini, N. Russo, M. Toscano, Chem. Eur. J. **2007**, 13, 2109–2117; e) C. Anthony, Arch. Biochem. Biophys. **2004**, 428, 2–9.

[11] A. Pol, K. Heijmans, H. R. Harhangi, D. Tedesco, M. S. M. Jetten, H. J. M. Op den Camp, Nature **2007**, 450, 874–878.

[12] a) H. Singer, R. Steudtner, A. S. Klein, C. Rulofs, C. Zeymer, B. Drobot, A. Pol, N. C. Martinez-Gomez, H. J. M. Op den Camp, L. Daumann, Angew. Chem. Int. Ed. **2023**, 62, e202303669; b) H. Singer, R. Steudtner, I. Sottorff, B. Drobot, A. Pol, H. J. M. Op den Camp, L. J. Daumann, Chem. Commun. **2023**, 59, 9066–9069.

[13] C. Anthony, Biochim. Biophys. Acta **1992**, 1099, 1–15.

[14] a) J. M. Cox, D. J. Day, C. Anthony, Biochim. Biophys. Acta **1992**, 1119, 97–106; b) C. Anthony, in Enzyme-Catalyzed Electron and Radical Transfer: Subcellular Biochemistry (Eds.: A. Holzenburg, N. S. Scrutton), Springer US, Boston, **2000**, pp. 73–117; c) P. R. Afolabi, F. Mohammed, K. Amaratunga, O. Majekodunmi, L. Dales, R. Gill, D. Thompson, B. Cooper, P. Wood, M. Goodwin, C. Anthony, Biochemistry **2001**, 40, 9799–9809.

[15] W. Versantvoort, A. Pol, L. J. Daumann, J. A. Larrabee, A. H. Strayer, M. S. M. Jetten, L. van Niftrik, J. Reimann, H. J. M. Op den Camp, Biochim. Biophys. Acta **2019**, 1867, 595–603.

[16] P. Kalimuthu, L. J. Daumann, A. Pol, H. J. M. Op den Camp, P. V. Bernhardt, *Chem. Eur. J.* **2019**, *25*, 8760–8768.

[17] E. R. Featherston, H. R. Rose, M. J. McBride, E. M. Taylor, A. K. Boal, J. A. Cotruvo Jr., *ChemBioChem* **2019**, *20*, 2360–2372.

[18] a) R. Ghosh, J. R. Quayle, *Anal. Biochem.* **1979**, *99*, 112–117; b) B. Jahn, N. S. W. Jonasson, H. Hu, H. Singer, A. Pol, N. M. Good, H. J. M. O. den Camp, N. C. Martinez-Gomez, L. J. Daumann, *J. Biol. Inorg. Chem.* **2020**, 199–212.

[19] D. J. Day, C. Anthony, in *Methods Enzymology, Vol. 188*, Academic Press, **1990**, pp. 210–216.

[20] N. A. Danaf, J. Kretzschmar, B. Jahn, H. Singer, A. Pol, H. J. M. Op den Camp, R. Steudtner, D. C. Lamb, B. Drobot, L. J. Daumann, *Phys. Chem. Chem. Phys.* **2022**, *24*, 15397–15405.

[21] N. M. Good, M. Fellner, K. Demirer, J. Hu, R. P. Hausinger, N. C. Martinez-Gomez, *J. Biol. Chem.* **2020**.

[22] M. Wehrmann, P. Billard, A. Martin-Meriadec, A. Zegeye, J. Klebensberger, X. Zhang, D. K. Newman, *mBio* **2017**, *8*, e00570–00517.

[23] S. Tsushima, *Phys. Chem. Chem. Phys.* **2019**, *21*, 21979–21983.

[24] M. Beardmore-Gray, D. T. O'Keeffe, C. Anthony, *Microbiology* **1983**, *129*, 923–933.

[25] a) I. Bertini, G. Cavallaro, A. Rosato, *Chem. Rev.* **2006**, *106*, 90–115; b) J. Liu, S. Chakraborty, P. Hosseinzadeh, Y. Yu, S. Tian, I. Petrik, A. Bhagi, Y. Lu, *Chem. Rev.* **2014**, *114*, 4366–4469.

[26] a) C. Anthony, P. Williams, *Biochim. Biophys. Acta Proteins Proteomics* **2003**, *1647*, 18–23; b) J. A. Bogart, A. J. Lewis, E. J. Schelter, *Chem. Eur. J.* **2015**, *21*, 1743–1748.

[27] a) C.-E. Wegner, M. Westermann, F. Steiniger, L. Gorniak, R. Budhraja, L. Adrian, K. Küsel, *Appl. Environ. Microbiol.* **2021**, *87*, e03144–03120; b) < L. Gorniak, J. Bechwar, M. Westermann, F. Steiniger, C.-E. Wegner, *Microbiol. Spectr.* **2023**, *11*, e00867–823.

4.3 Assessing Enzyme Activity with Isothermal Titration Calorimetry

Isothermal titration calorimetry (ITC) is a powerful method to obtain kinetic as well as thermodynamic parameters from a chemical reaction. Every reaction produces or consumes energy which is reflected by the generated heat. Modern calorimeters are able to measure and compensate the generated heat and translate the required thermal power to the reaction rate of the chemical reaction.[85] The instrument can compensate an exothermic reaction by reducing the supplied thermal power or an endothermic reaction by supplying more thermal power to return to the baseline. ITC typically consists of a sample and reference cell as well as a syringe (Figure III-11). The sample cell contains one reactant, while the reference cell contains only the buffer solution. The syringe is filled with the other reactant that is gradually injected into the sample cell. The required thermal power to compensate for the heat effect, the differential power (DP) between the reference and the sample cell, are used to calculate the thermodynamic parameters of the reaction. The application of ITC is versatile and is widely used to study binding interactions in various systems: protein-small molecule, protein-protein, RNA-RNA, protein-metal, small molecule-metal, enzyme-substrate etc. The method is label-free and does not require additional fluorophores, dyes or modification of the reactants which allows for the study of interactions between native states.
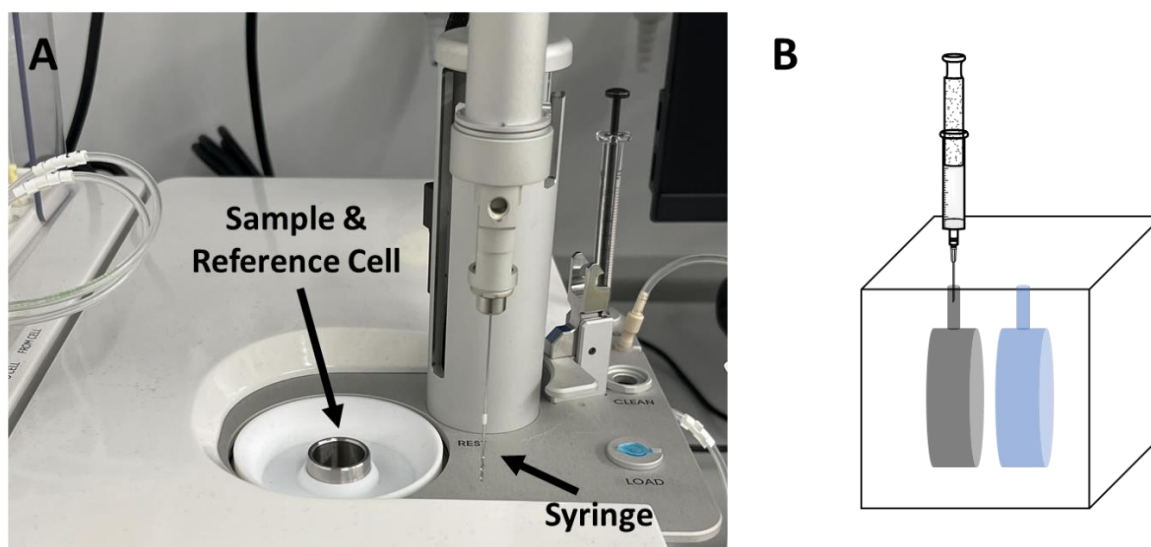
Figure III-11 A) Picture of a MicroCal PEAQ-ITC (Malvern Panalytical) with the sample and reference cell as well as syringe. B) Simplified graphical representation of the sample and reference cell inside the casing. Syringe containing the substrate is injected into the sample cell.

In addition to the dye- and protein-coupled assay, ITC was used as a new method to investigate and compare the enzyme activity of Ln-MDHs from SolV. Initial experiments were conducted using the components and conditions of the dye-coupled assay. The cell was filled with Pr-MDH, PES, DCPIP and the syringe with MeOH as substrate. These experiments were unsuccessful as only the heat generated solely by the injection of the substrate into the cell (dilution effect) was observed and not from the enzymatic reaction itself. Thus, the conditions of the protein-coupled assay were applied: the cell was

filled with Pr-MDH, cyt *c* and MeOH, while the syringe contained cyt c_{GJ} to initiate the reaction. Using this setup, reproducibility was a major issue. The injection of cyt c_{GJ} to the sample cell caused formation of bubbles, a challenge encountered in the protein-coupled assay using microwell plates as well, which subsequently burst spontaneously creating irreproducible measurements. By filling the syringe with Pr-MDH and mixing cyt c_{GJ} into the sample cell, reliable results were obtained (Figure III-12). For the control run, cyt c_{GJ} was omitted from the sample cell. The measured data with the adjusted baseline superimposed onto its control experiment is shown in Figure III-12A and Figure III-12B shows the results after normalization of the signal. Approximately 4 min after injection, the signal returns to the baseline indicating the end of the enzymatic reaction and that the substrate is fully converted.
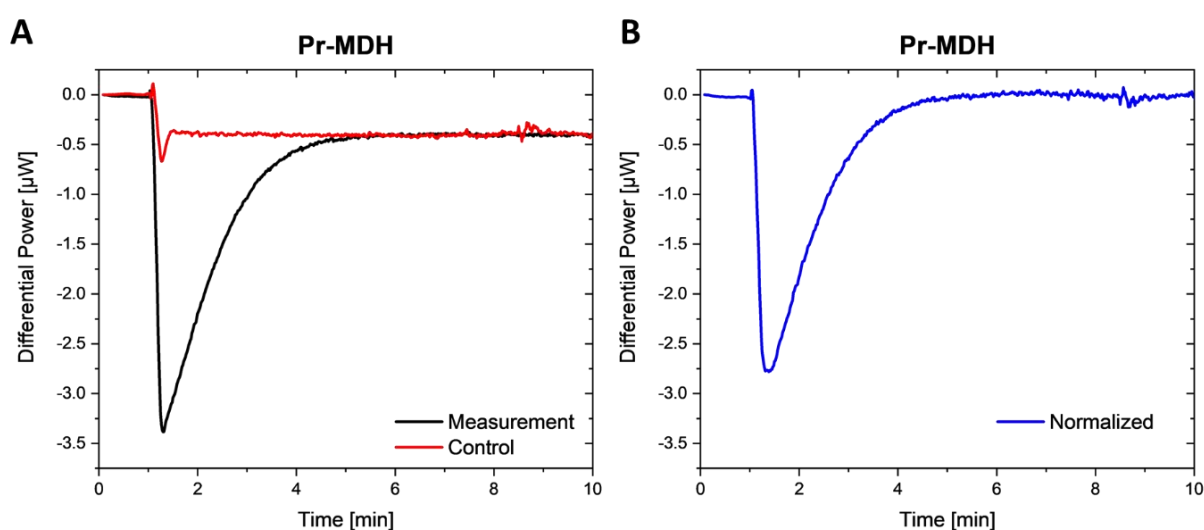
Figure III-12 Raw data of a single injection assay. A) Injection of Pr-MDH into the assay mixture containing cyt c_{GJ}, cyt c, and MeOH. Cyt c_{GJ} was omitted for the control injection. B) Results after normalization. Conditions: 5 µL of a 10 µM Pr-MDH solution was injected over 10 s into 5 µM cyt c_{GJ}, 50 µM cyt *c*, 20 mM MeOH in 10 mM PIPES (pH 7.2), at 45 °C.

The same experimental conditions were used, but the syringe was filled with Eu-MDH to assess its enzyme activity in comparison to Pr-MDH and the results are shown in Figure III-13. Again, Figure III-13A shows the data with adjusted baseline superimposed onto the control data and Figure III-13B shows the results after normalization. The signal returns approximately 10 min after injection back to baseline.
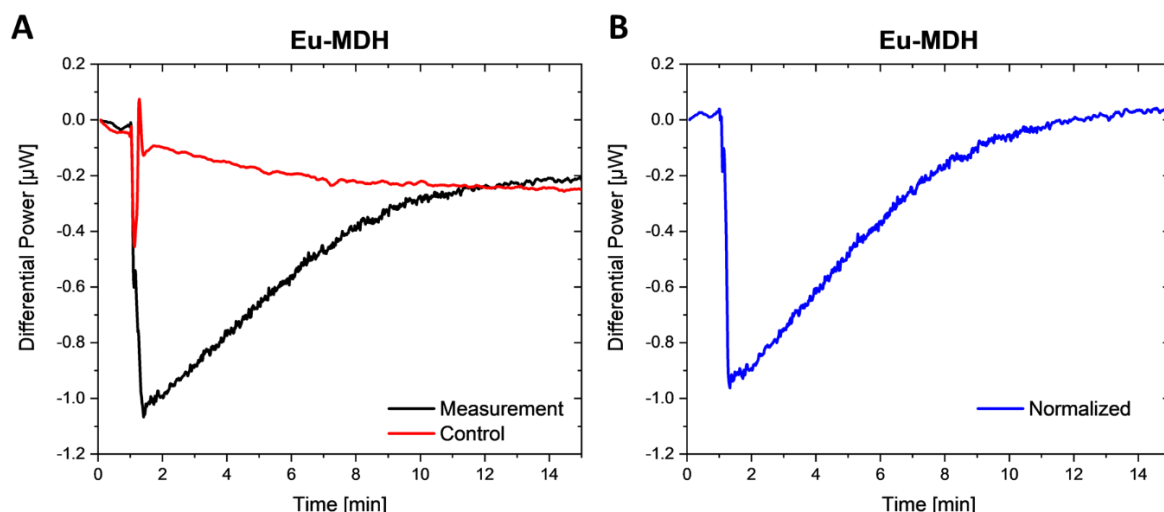
Figure III-13 Raw data of a single injection assay. A) Injection of Eu-MDH into the assay mixture containing cyt c_{GJ}, cyt c, and MeOH. Cyt c_{GJ} was omitted for the control injection. B) Results after normalization. Conditions: 5 µL of a 10 µM Eu-MDH solution was injected over 10 s into 5 µM cyt c_{GJ}, 50 µM cyt c, 20 mM MeOH in 10 mM PIPES (pH 7.2), at 45 °C.

Figure III-14 displays the results for both Pr-MDH and Eu-MDH side by side, highlighting notable differences: the maximum DP change is barely reaching -1.0 µW for Eu-MDH while the experiment with Pr-MDH shows a maximum DP change of -2.75 µW. In addition, the return to baseline after injection, thus complete substrate turnover, takes Eu-MDH around 10 min, more than twice as long as Pr-MDH. Despite these differences, the negative DP values for both enzymes classifies them as an exothermic reaction.
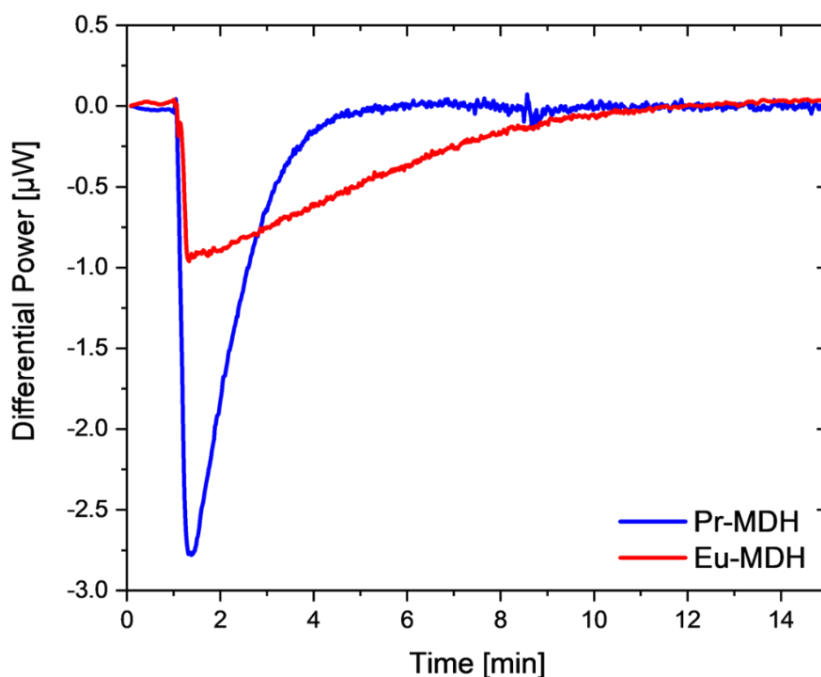
Figure III-14 Results from isothermal titration calorimetry experiments of Pr- and EuMDH using the single injection mode. 5 µL of 10 µM Pr- or EuMDH was injected into 5 µM cyt c_{GJ}, 50 µM cyt c and 20 mM MeOH in 10 mM PIPES (pH 7.2) at 45 °C.

The higher DP value of Pr-MDH can be interpreted as that more exothermic energy from the chemical reaction in a shorter timeframe is released in comparison to Eu-MDH which could be the result of higher substrate turnover of Pr-MDH in comparison to Eu-MDH. Even if the same mechanism is expected for both enzymes, thermodynamic factors like substrate affinity and enthalpy, which stem from the slightly structural environment of the active site, could influence the DP value. Also, the metal content of both enzymes was not determined and thus the differences could also originate from the varying amounts of active enzymes. The difference in the time each Ln-MDH takes to return to baseline indicates a difference in their reaction rates. Pr-MDH requires a shorter time compared to Eu-MDH, suggesting a faster rate of substrate turnover for Pr-MDH. Again, given the unknown metal content of the enzymes, this outcome should be considered with caution. Nevertheless, this result aligns with the findings of the dye- and protein-coupled assay supporting the hypothesis that the metal ion in the active site has an essential impact on the activity of the enzyme. Although both Ln-MDHs display distinctive thermograms, they exhibit comparable ΔH (total heat generated) values. This similarity in ΔH is evident from the integrated area under the curve in the respective experiments (Figure III-15). This observation makes sense as the same amount of substrate is present in both experiments and both are able to turnover all of the substrate.
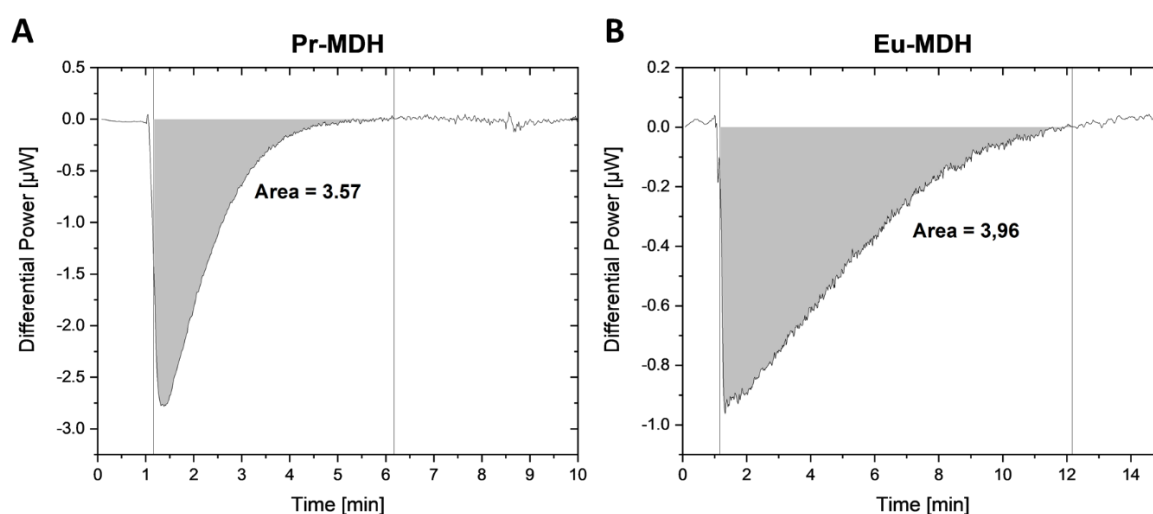
Figure III-15 Calculated area under the curve reflects the total heat (ΔH) generated by the enzymatic reaction. Calculated with the integration tool from Origin.

Taken together, the conditions of the protein-coupled assay was applied to assess and compare the enzymatic activity of Eu-MDH and Pr-MDH with a calorimeter. The crucial step was to reverse the default settings and fill the syringe with the enzyme instead of the substrate. According to the data, Pr-MDH exhibits at least twice the substrate turnover rate of Eu-MDH. This demonstrates that the enzyme activity of Pr-MDH is higher than Eu-MDH and is consistent with the data obtained by dye- and protein-coupled assays. Therefore, ITC proves to be a viable method for assessing the enzyme activity of the Ln-MDHs. This introduces a novel approach to investigate the enzyme activity of Ln-MDHs. These

experiments should be repeated with the inclusion of all other Ln-MDHs to gain a more comprehensive understanding of the enzyme activity. Furthermore, the metal content of the Ln-MDHs should be determined in advance as this what not the case for these set of experiments. This will lead to a more reliable and complete conclusion.

4.4 Electrochemical Assay

The electrochemical assay is another method to assess the enzyme activity of Ln-MDHs with its native cyt c_{GJ}.[40] In 2019, Bernhardt and coworkers developed a workflow that enables the concurrent adsorption of Eu-MDH and cyt c_{GJ} with the biopolymer chitosan on a mercaptoundecanol(MU)-modified gold (Au) working electrode for a mediated electron transfer.[34] It is crucial to constrain the proteins beneath a semipermeable dialysis membrane close to the electrode surface. The Au electrode, substituting for the cyt c as the secondary electron acceptor, enables the assessment of the enzyme activity by measuring the current. The effect of various additives that are frequently required for the dye-coupled assay were investigated as well as a range of pH and temperature were screened to optimize the enzyme activity. Upon addition of MeOH as substrate, the quasi-reversible wave of cyt c_{GJ} changes into a sigmoidal wave displaying both homogeneous (Eu-MDH to cyt c_{GJ}) and heterogeneous (cyt c_{GJ} to Au electrode) electron transfer processes. Experiments focusing on the effect of increasing substrate concentration showed that the Michaelis constant K_M obtained from the electrochemical assay is an order of magnitude higher than the value obtained from solution assays, indicating that the mass transport of the substrate across the membrane is a limiting factor in this assay. During the research stay at the lab of Prof. Paul Bernhardt, the electrode preparation was revised to overcome the limitation of mass transport as well as assessing and comparing the enzyme activity of seven Ln-MDHs (Ln = La, Ce, Pr, Nd, Sm, Eu and Gd) electrochemically.

Initially, the 2019 method for electrode preparation was employed but with a significant modification: a rotating disk electrode (RDE) replaced the stationary one. The RDE is a hydrodynamic method that has several benefits: i) the rotation of the electrode induces a centripetal force towards the center of the electrode which increases the diffusion of the substrate across the membrane, overcoming the previously encountered mass transport limitations of the substrate, leading to the acquisition of more reliable kinetic parameters; ii) a steady state is achieved faster and iii) more precise and reproducible measurements are possible due to less sensitivity of the RDE to external vibrations and precise control of the rotation speed, respectively.[86] The RDE was prepared exactly as the stationary Au electrode and consists of a chitosan and MU-modified Au electrode with Ln-MDH and cyt c_{GJ} adsorbed on the electrode surface and constraint with a membrane. After the preparation of the RDE, the rotation was turned on and the blank sample with no addition of the substrate was measured until the cyt c_{GJ} wave

was stable (Figure III-16A). Without a membrane to constrain the proteins near the electrode surface, the proteins will gradually diffuse into the buffer solution with start of the rotation, resulting in a reduction of the observed signal as shown by continuous cyclic voltammetry (CV) measurements (Figure III-16B)
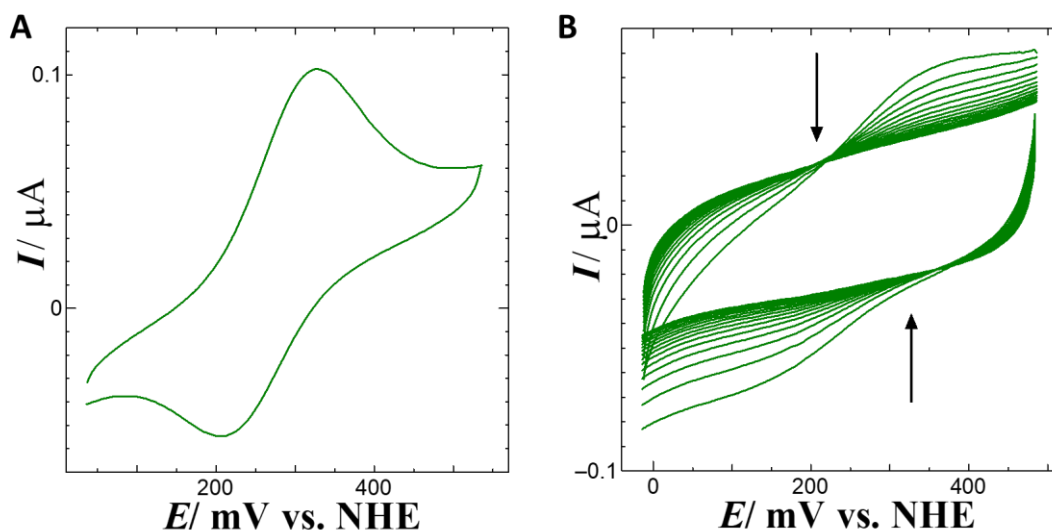
Figure III-16 A) Cyclic voltammogram (CV) obtained with membrane and B) continuous CV obtained without membrane for Au/MU/chitosan-cyt c_{GJ} electrode in 20 mM PIPES buffer (pH 7.2) at a scan rate of 20 mV s^{-1}. The data was kindly provided by Dr. Palraj Kalimuthu.

Once stabilized, an increasing amount of MeOH was added until saturation was reached. Figure III-17A exemplarily shows the results of the RDE voltammograms (RDEVs) with La-MDH and its respective electrochemical Michaelis-Menten plot. RDEVs and Michaelis-Menten plots of the other Ln-MDHs are shown in Chapter V.1.6.
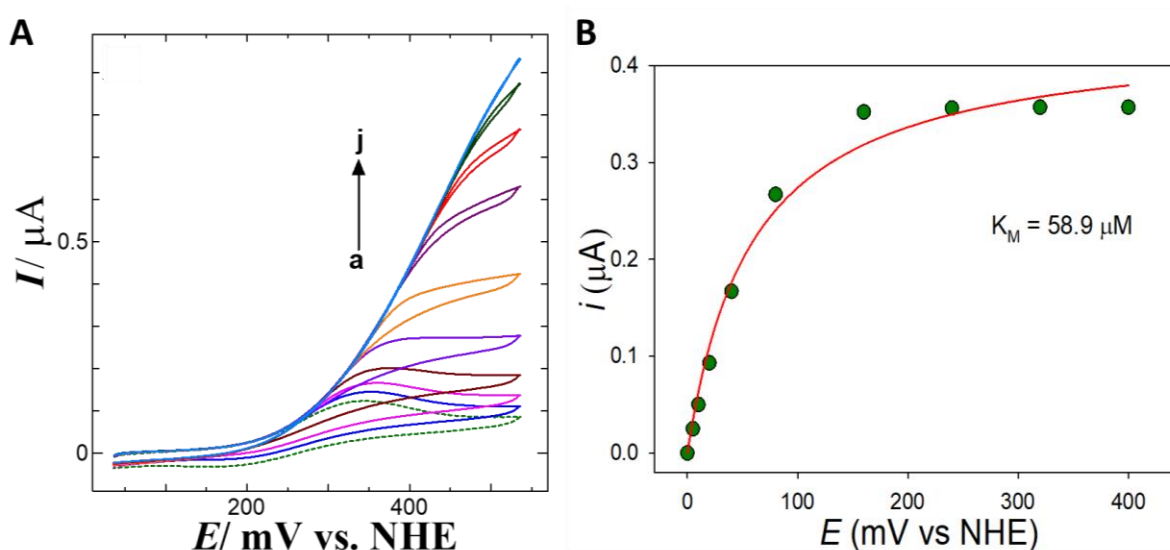
Figure III-17 A) Rotating disk electrode voltammograms (2000 RPM) obtained for Au/MU/chitosan-cyt c_{GJ}/La-MDH electrode for increasing concentration of methanol (a) 0, (b) 5, (c) 10, (d) 20, (e) 40, (f) 80, (g) 160, (h) 240, (i) 320 and (j) 400 µM in 20 mM PIPES buffer (pH 7.2) at a scan rate of 5 mV s^{-1}. B) Electrochemical Michaelis-Menten plot for the limiting currents at 400 mV as a function of methanol concentration. The data was kindly provided by Dr. Palraj Kalimuthu.

Initial experiments with Ln-MDHs containing the early Lns were promising but moving to the Ln-MDHs containing late Lns, increasing enzyme activity was observed for the blank sample after rotation of the RDE started. Without addition of any substrate, the signal of Gd-MDH measured after 8 min of rotation showed a very similar signal compared to the measurement when a saturating amount of substrate was added (Figure III-18), suggesting that nearly all of the measured signal of Gd-MDH originates from the cyt c_{GJ} signal.
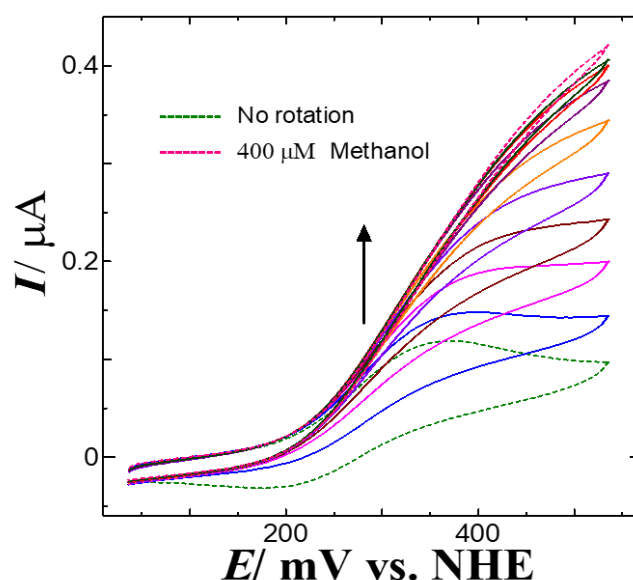
Figure III-18 Rotating disk electrode voltammograms (2000 RPM) obtained for Au/MU/chitosan-cyt c_{GJ}/Gd-MDH electrode recorded at every 1 min interval in 20 mM PIPES buffer (pH 7.2) at a scan rate of 5 mV s^{-1}. Once saturation was reached, 400 µM MeOH was added. The data was kindly provided by Dr. Palraj Kalimuthu.

After further investigation, the previously observed results obtained from RDE with Ln-MDHs containing early Lns consists of the Ln-MDH activity, but also include the activity from cyt c_{GJ}. Once the rotation started, an increasing amount of cyt c_{GJ} got pulled towards the surface of the electrode increasing the observed signal for cyt c_{GJ}. The relative contribution of cyt c_{GJ} signal to the total observed signal is relatively minor for Ln-MDHs containing early Lns, which explains why this was not identified initially. On the other hand, for Ln-MDHs containing late Lns, the relative contribution of cyt c_{GJ} signal is substantially higher, which lead to an increased signal in the blank sample when the RDE is in motion. Thus, the measured enzyme activity of Ln-MDHs containing late Lns mainly reflect the signal from cyt c_{GJ}. Therefore, the calculated K_M values should be considered very carefully. All calculated K_M values of the Ln-MDHs are in the same range of the previously reported value of 50(±8) µM.

To summarize, the procedure to prepare electrodes for the electrochemical assessment of the enzyme activity of Ln-MDHs was revised and rotating disk electrodes were selected instead of the previously used stationary electrodes. A semipermeable membrane is necessary to constrain the Ln-MDH and cyt c_{GJ} near the electrode surface, but leads to mass transport limitation. The rotation of the electrode generates a centripetal force towards the center of the electrode surface, mitigating the mass

transport limitation. Unfortunately, the rotation of the electrode also leads to an increased cyt c_{GJ} signal which contributes to the total observed signal. The relative contribution of the cyt c_{GJ} signal to the total observed signal increases across the Ln series and nearly all of the measured signal from Gd-MDH is created by the cyt c_{GJ} signal. Consequently, calculated K_M values from these experiments are not reliable and further studies are required to obtain conclusive results about the electrochemical assessment of the Ln-MDH enzyme activity. The challenge to overcome the mass transport limitation is still ongoing. Experiments reverting back to the stationary electrodes but using a shorter linker to anchor the proteins to the electrode surface like 5-(pyridine-4-yl)-1,3,4-oxadiazole-2-thiol instead of mercaptoundecanol are investigated. The shorter linkage leads to a more rigid structure of the biofilm and positions the proteins in closer proximity to the electrode surface, enhancing the efficiency of electron transfer from Ln-MDH to cyt c_{GJ} to electrode. A more rigid structure also provides better control over the orientation and positioning of Ln-MDH and cyt c_{GJ} ensuring that they are optimally aligned for interaction and electron transfer.[87] If promising results are obtained with the shorter linker, the method can be applied for the rotating disk electrode. The shorter linker length will help to minimize the contribution of the cyt c_{GJ} signal when rotation starts and the rotation of the electrode will decrease the mass transport limitation.

5. Kinetic Isotope Effect Studies of Lanthanide-Dependent Methanol Dehydrogenase

There are two rate-limiting steps in Ln-MDH enzyme activity: i) Substrate oxidation/turnover and ii) PQQ re-oxidation.[41a] The following experiments focused on i) substrate oxidation/turnover to understand the impact of this aspect on the overall enzyme activity. Kinetic isotope effect (KIE) experiments are a fundamental method in enzymology to elucidate the rate of substrate turnover and to get insights into the reaction mechanism. The replacement of atoms in the substrate molecules for their heavier isotopes, i.e. deuterium (D) for protium (H), allow to investigate the same reactions but will yield different reaction rates if the respective C-D bond is involved in the reaction mechanism. This effect occurs because chemical bonds with heavier isotopes are stronger and have lower zero-point vibrational energies compared to bonds with lighter isotopes like C-H bonds.[88] Measuring the KIE is therefore critical to understand the overall kinetics of the enzyme. Colleagues have previously completed KIE experiments utilizing the dye-coupled activity assay.[89] The substrate isotope effect was determined using either protiated (MeOH) or deuterated substrate (methanol-d4, henceforth MeOD) and the solvent isotope effect was examined using PIPES dissolved in H_2O or D_2O. The results show that the enzyme activity decreases linearly with higher concentration of MeOD in the assay mixture, displaying a large substrate isotope effect of 36 (100% MeOH compared to 100% MeOD). Similarly, the

enzyme activity declines with increasing concentration of D_2O-PIPES, revealing a solvent isotope effect too.

Herein, the substrate and solvent isotope effect were examined using the protein-coupled assay. Again, cyt c_{GJ} as the native electron acceptor and cyt *c* from equine heart as secondary cytochrome for the spectroscopic read-out were employed to investigate the KIE. The KIE was investigated across a range of pH, thus the multicomponent (MC) buffer containing equimolar amount of citric acid, Bis-Tris, Tris and CHES, that covers a wider pH range as each individual buffer, was used. The MC buffer was prepared in H_2O or D_2O and the pH/pD ranged from 6–8. MeOH and MeOD were used as substrates and added at saturating concentrations. For adjustment of pD values, the general formula pD = pH + 0.4 was applied.[90] For the calculation and assessment of the enzyme activity of Ln-MDH, the extinction coefficient ε of cyt *c* from equine heart is required. The extinction coefficient ε depends on parameters like buffer, buffer concentration and pH. Previous studies have determined the extinction coefficient in 10 mM PIPES buffer at pH 7.2 (19.5 mM^{-1} cm^{-1}) and 120 mM MOPS buffer at pH 7.0 (19.0 mM^{-1} cm^{-1}).[32, 39] Given that the extinction coefficients ε of cyt *c* in MC buffer were not known, determining these values was necessary. Considering the six different MC buffer conditions, spanning the pH and pD scale from 6 to 8, a total of six different ε values were determined. A serial dilution of cyt *c* with the respective MC buffer conditions were prepared and the absorption was measured by UV/Vis spectroscopy. Subsequently, the ε values were obtained through linear fitting and application of the Beer-Lambert law. An exemplary result of the serial dilution measurement is shown in Figure III-19 with the derived ε values are presented in Table III-3.
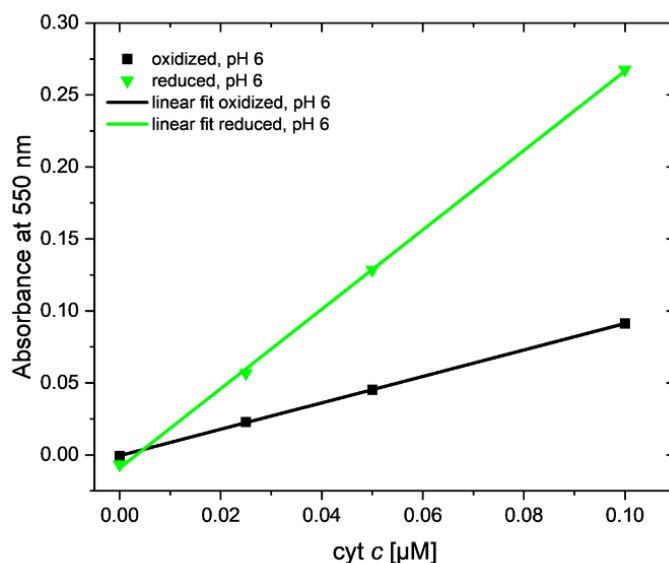
Figure III-19 Exemplary results from a dilution series of cyt *c* from equine heart in its oxidized and reduced state for the determination of the extinction coefficient ε.

Table III-3 Extinction coefficient ε of cyt *c* from equine heart in 10 mM H_2O- and D_2O-MC buffer (pH/pD 6–8), n = 2.

	pH 6	pH 7	pH 8	pD 6	pD 7	pD8
ε [mM^{-1} cm^{-1}]	18.4	18.6	16.4	17.8	18.2	17.0

With these values in hand, KIE studies using Pr-MDH and cyt c_{GJ} were conducted. The assay components consist of Pr-MDH, the secondary cyt *c* from equine heart, the substrate (MeOH or MeOD) and was initiated by the addition of cyt c_{GJ}. Enzyme activity was assessed using H_2O- and D_2O-MC buffer. The enzyme enzyme activities are shown in Figure III-20. The substrate isotope effect is shown in Table III-4 and the solvent isotope effect values are shown Table III-5.
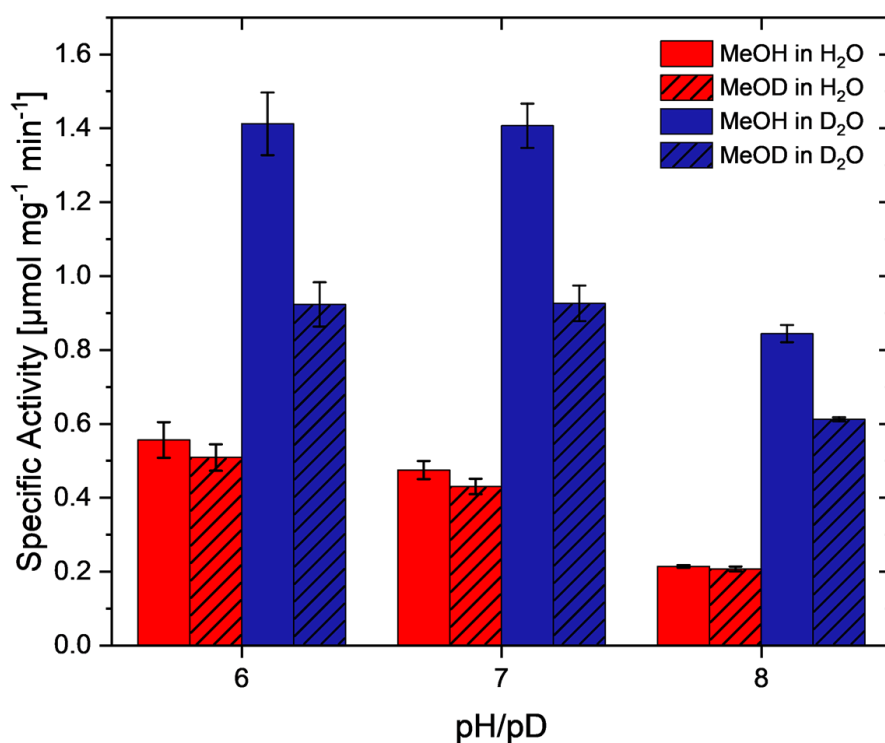
Figure III-20 Results of the kinetic isotope effect (KIE) experiments. The normalized specific activity for each condition is shown with the KIE regarding substrate (MeOH vs. MeOD) and buffer solvent (H_2O vs. D_2O). The assay mixture contains 100 nM Pr-MDH, 50 µM cyt *c* from equine heart, 20 mM MeOH or MeOD and 5 µM cyt c_{GJ}, n = 3.

Table III-4 Calculated substrate isotope effect of the KIE experiments.

	pH 6	pD 6	pH 7	pD 7	pH 8	pD 8
KIE (k_{MeOH}/k_{MeOD})	1.09	1.53	1.10	1.52	1.03	1.38

Table III-5 Calculated solvent isotope effect of the KIE experiments.

	pH/pD 6		pH/pD 7		pH/pD 8	
	MeOH	MeOD	MeOH	MeOD	MeOH	MeOD
KIE (k_{H2O}/k_{D2O})	2.54	1.81	2.96	2.15	3.94	2.95

The results show that the pH optimum for Pr-MDH is in the range of pH/pD 6–7 and declines towards pH/pD 8 which is in accordance with several reported studies.[12b, 20b, 32] Furthermore, the enzyme activity is higher when using MeOH instead of MeOD (substrate isotope effect > 1) in both H_2O- and D_2O-MC buffer across all three pH conditions. This demonstrates the importance of proton abstraction from the substrate for its turnover and its impact on total enzyme activity. This also reinforces previous experimental observation with the dye-coupled assay that the rate of bond breaking (specifically, breaking of a C-H is faster than breaking of a C-D bond) is the rate-limiting step, as reflected by a lower enzyme activity with deuterated MeOD as the substrate.[89] Unexpectedly, the enzyme activity in D_2O-MC buffer is more than two-fold higher (solvent isotope effect > 2) than their respective counterpart in H_2O across all three pH conditions. This contradicts the results obtained by the dye-coupled assay which showed a lower enzyme activity with higher D_2O concentration. The highest enzyme activity was obtained in D_2O-MC buffer at pD 6 and 7 with MeOH as the substrate.

Intrigued by the surprisingly substantial positive effect of D_2O on the enzyme activity, the effect was further investigated. H_2O-MC buffer (pH 7) with increasing amount of D_2O (0, 25, 50, 75 and 100% D_2O) were prepared to repeat the protein-coupled assays. The specific buffer was prepared by combining the respective amount of H_2O-MC buffer (pH 7) and D_2O-MC buffer (pD 7), e.g. 25% D_2O buffer contained 75% v/v H_2O-MC buffer and 25% v/v D_2O-MC buffer. Figure III-21 presents data that indicate a linear correlation between enzyme activity and D_2O concentration in the solution. The enzyme activity increases linearly with the D_2O-MC buffer concentration.
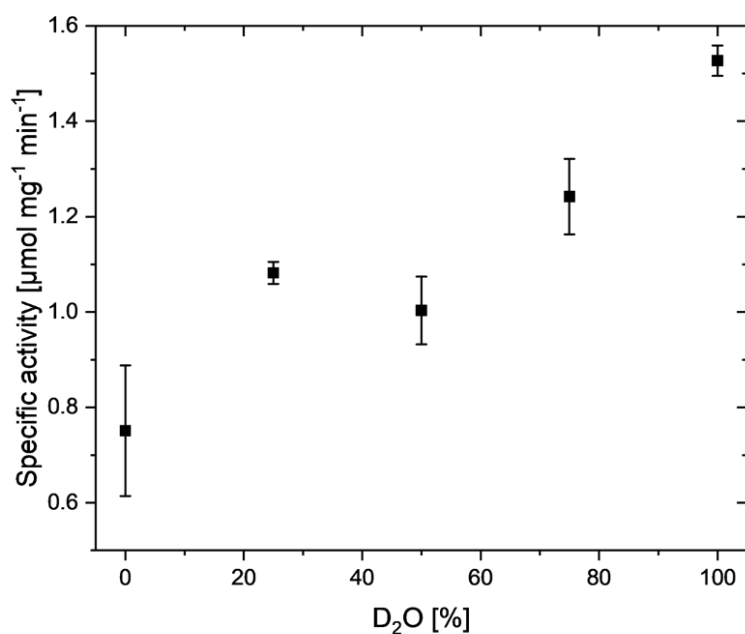
Figure III-21 Effect of D_2O content in buffer on specific activity of Pr-MDH. 100 nM Pr-MDH, 50 µM cyt *c*, 20 mM MeOH, 1 µM cyt *c_GJ* in 10 mM MC buffer (pH 7.0), n = 2.

Consistent with previous experiments, the enzyme activity in D_2O-MC buffer exceeds that of H_2O-MC by over two times (solvent isotope effect = 2.29). These results indicate that there is indeed a positive effect of D_2O on the total enzyme activity and shows the importance of hydrogen bonds in this system.

Cioni and Strambini investigated the effect of heavy water on protein integrity and reported that D_2O substantially enhances the rigidity of the native protein structure.[88] They argue that the deuterium bonds being marginally stronger than hydrogen bonds (by roughly 0.1 to 0.2 kcal mol^{-1}) thus leading to stronger intrapeptide deuterium bonds and increased protein stability. It could be argued that the increased protein stability of Ln-MDH and/or cyt c_{GJ} benefits the electron transfer by minimizing structural fluctuations und reducing protein dynamics.[88] Mie *et al.* reported that the electron transfer rate from myoglobin to an electrode was a magnitude higher in D_2O buffer compared to an H_2O buffer. Myoglobin is an O_2 storage hemoprotein that undergoes autooxidation. The conversion of reduced Fe^{2+}-containing myoglobin with O_2 to oxidized Fe^{3+}-containing myoglobin is a slow process, impeded by the slow dissociation and re-association of bound H_2O and high reorganization energy. They propose that the reorganization of the iron-water-His moiety, crucial for the electron transfer, is facilitated in D_2O. However, the exact underlying mechanism remains unknown.[91] Oubrie *et al.,* through crystal structures of a comparable alcohol dehydrogenase from *Comamonas testosteroni* containing Ca^{2+} and PQQ in its active site, along with its cytochrome, have demonstrated that a network of amino acid residues and water molecules are involved in transferring electrons from the enzyme's redox center to its cytochrome.[92] These findings are supported by molecular modelling for the Ca-MDH and its cytochrome from *Paracoccus denitrificans*. The huge distance, 17 Å edge-to-edge between PQQ and the haem moiety, also involves an intraprotein space jump from PQQ to the disulphide bridge above PQQ, passage through a series of 13 covalent bonds of amino acid residues and an interprotein space jump from Ca-MDH to the haem edge of the cytochrome.[93] A similar electron transfer pathway would be plausible for Ln-MDH and its cytochrome. The stronger intrapeptide bonds caused by D_2O and the involvement of D_2O molecule in the electron transfer pathway could enhance the re-oxidation process of PQQ and thus enhancing the total enzyme activity.[21d] These finding might suggest that in addition to substrate oxidation and PQQ re-oxidation, the electron transfer from Ln-MDH to its physiological cyt c_{GJ} contributes significantly to the total enzyme activity.

Investigation of the kinetic isotope effect (KIE) of enzymes can give valuable information about the reaction mechanism. Besides cofactor regeneration, substrate turnover is a key aspect influencing the total enzyme activity of Ln-MDH. The substrate and solvent isotope effect for Pr-MDH was examined through the protein-coupled assay and compared to previously conducted KIE experiments that employed the dye-coupled assay.[89] The trend for the substrate isotope effect was similar for both, showing that the enzyme activity declines when deuterated MeOD is used as a substrate instead of the protiated MeOH, underscoring the importance of proton abstraction of the substrate for its

turnover. Surprisingly, the outcome of the solvent isotope effect experiments showed contradictory results. KIE experiments with the dye-coupled assay indicate a decrease in enzyme activity with increasing amount of D_2O concentration. In contrast, the experiments with the protein-coupled assay showed that the enzyme activity is enhanced with increasing concentration of D_2O in solution. The electron transfer from Ln-MDH to cyt c_{GJ} requires association and dissociation of two proteins as well as interaction with solvent molecules (H_2O/D_2O). The replacement of H_2O by D_2O in the electron transfer pathway from the active site of Ln-MDH to cyt c_{GJ} could enhance the enzyme activity. Additionally, D_2O can impact the intramolecular peptide bonds which can result in higher stability and rigidity of proteins. The results suggest that the interactions between Ln-MDH and cyt c_{GJ} are facilitated and/or the electron transfer process from the active site to the cytochrome is enhanced in D_2O. Circular dichroism (CD) is a spectroscopic method that is used to study proteins, nucleic acids and other biomolecules, providing information about their secondary and tertiary structures and reveals changes in conformation, folding and interaction with other biomolecules. Employing CD to compare the protein structure of Ln-MDH and cyt c_{GJ} in H_2O and D_2O buffer will help to understand if D_2O induces significant structural changes that enhance the enzyme activity. Furthermore, performing temperature-dependent protein-coupled assays and generating the corresponding Arrhenius plot will reveal whether thermodynamic effects are involved in the increased enzyme activity. If the electron transfer process is positively impacted by D_2O, electrochemical experiments of Ln-MDH and cyt c_{GJ} in both H_2O and D_2O should be considered. The enzyme activity should be assessed in H_2O as previously shown and then repeated using the buffer prepared with D_2O. By comparing the electrochemical behavior in H_2O and D_2O, it would be possible to discern any alterations in reaction kinetic or electron transfer process that D_2O might induce and help to understand how D_2O impacts enzyme functionality. The combined results of all these experiments will provide a more thorough comprehension of how D_2O affects the total enzyme activity and helps identifying the specific mechanisms through which D_2O interacts with and influences enzymatic processes.

6. Purification of Methanol Dehydrogenase from *Methylorubrum Extorquens* AM1

Featherston *et al.* conducted kinetic assays with Ln-MDH from *M. extorquens* AM1 and its native cytochrome XoxG.[23] They showed that v_{max} is similar among three different Ln-MDH (Ln = La, Ce and Nd) but the Michaelis constant K_M for XoxG increased threefold from La to Nd. These values differ from their results obtained by dye-coupled assay which they argue is due to difference of mechanisms assessed by protein-coupled and dye-coupled assays. Furthermore, they postulate that "the increasing K_M values for XoxG reflect elevated reduction potentials of the Ln^{III}-PQQ cofactor, as Lewis acidity of the lanthanide ion increases from La^{III} to Nd^{III}".[23] They determined the rather low reduction potential

of XoxG as 172 mV. In combination with the results of the kinetic assays, they theorized that bacteria that can tolerate heavier lanthanides require cytochromes with higher reduction potentials.[23] Indeed, Versantvoort et *al.* showed for SolV that the native cyt c_{GJ} of Ln-MDH (tolerates Lns up to Tb^{3+}) has a reduction potential of 240 mV.[12b, 32] In short, Ln-MDH that prefer lighter lanthanides have cytochromes with lower reduction potential and Ln-MDH that can utilize heavier lanthanides could require cytochromes with higher reduction potential.

Studies have shown the isolation of La- and Ca-MDH from AM1 and assessed their activity with the dye-coupled assay.[20a, 23, 39, 43, 94] To the best of our knowledge, a systematic comparison of the enzyme activity of Ln- and Ca-MDH from AM1 across different pH, temperature and additives is yet to be conducted. The objective is to isolate and assess Ca-MDH and Ln-MDHs from AM1 and compare their enzyme activity across different conditions using the dye-coupled assay. Initially, AM1 was cultivated both with and without the addition of Lns. The addition of Ln will trigger the lanthanide switch and the expression of Ln-MDH is favored over the expression of Ca-MDH. Without the addition of any Ln, Ca-MDH will be expressed by AM1. Preliminary experiments with AM1 cells grown without Lns and cells grown with Nd^{3+} were harvested for the successive isolation of Ca- and Nd-MDH, respectively. After chemical lysis and enzymatic digestion by lysozyme and DNase, cell debris and small particles were removed by centrifugation and the cell-free extract was applied on a ÄKTA Go FPLC system. The purification procedure developed by Anthony and coworkers consists of four major steps: 1) purification with anion exchange column (DEAE FF Sepharose), 2) purification with hydroxyapatite column, 3) desalting by gel filtration and 4) purification with cation exchange column (SP FF Sepharose). A hydroxyapatite column was not available, therefore the protocol was adopted for the isolation of Ca- and Nd-MDH (Table III-6).[39] Again, addition of MeOH to the buffer is imperative to keep enzyme activity high.

Table III-6 Protocol for the purification of MDH from *M. extorquens* AM1.[39]

Column	Buffer	Method
DEAE Sepharose	A: 20 mM TRIS, 25 mM MeOH, pH 8.0 B: 20 mM TRIS, 25 mM MeOH, 1 M NaCl, pH 8.0	Gradient: 0% over 3.5 CVs, then 0 to 100% over 1.5 CVs Sample collection: 8.33 to 16.33 min
Desalting	25 mM MES, 25 mM MeOH, pH 5.5	Equilibrate 3 CVs, load up to 500 μL sample, elute with 1 mL buffer
SP Sepharose	A: 25 mM MES, 25 mM MeOH, pH 5.5 B: 25 mM MES, 25 mM MeOH, 0.25 M NaCl, pH 5.5	Gradient: 0 to 60% over 5 CVs Sample collection: 15.33 to 17.33 min, elution starts at 32% B*

*not reproducible

First, samples containing Ca-MDH were purified. Due to the high isoelectronic point of Ca-MDH, it will not bind to the anion exchange column and elutes immediately.[39] After the first purification step, three major peaks were observed (Figure III-22A). The first peak showed a red coloration, indicative of another protein. Thus, the second major peak was collected and buffer exchange was conducted from TRIS to MES by a desalting column. Subsequently, purification by cation exchange chromatography (Figure III-22B) was performed, resulting in Ca-MDH eluting as the sole peak at 32% B.
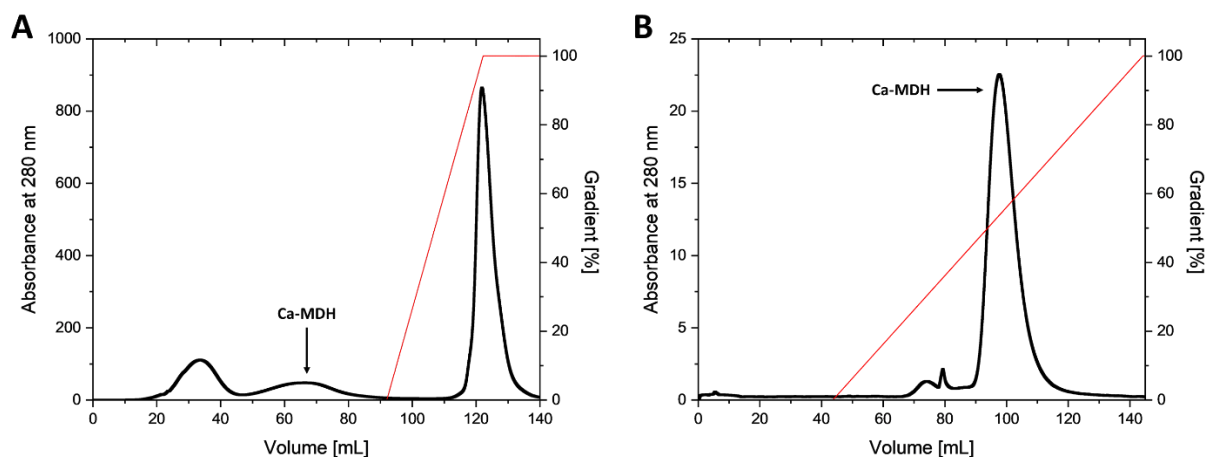
Figure III-22 A) Chromatogram of DEAE FF column. Buffer A: 20 mM TRIS with 25 mM MeOH (pH 8.0), buffer B: 20 mM TRIS with 25 mM MeOH and 1 M NaCl (pH 8.0), gradient: 0% B over 3.5 CVs, 0 to 100% B over 1.5 CVs, flow: 5 mL/min. B) Chromatogram of SP FF column. Buffer A: 25 mM MES with 25 mM MeOH (pH 5.5), buffer B: 25 mM MES with 25 mM MeOH and 0.25 M NaCl (pH 5.5), gradient: 0 to 100% B over 5 CVs, flow: 5 mL/min.

Given the high purity of Ca-MDH fractions from the first purification, only one purification step using the anion exchange column was used to isolate Nd-MDH. SDS-PAGE analysis of various samples taken along the purification process and of Ca- and Nd-MDH are shown in Figure III-23. A prominent band around the 63 kDa protein mark is observed, demonstrating the correct size of Ca- and Nd-MDH. Eu-MDH from SolV was used as a positive control and confirms that the size of the purified Ca- and Nd-MDH are correct.
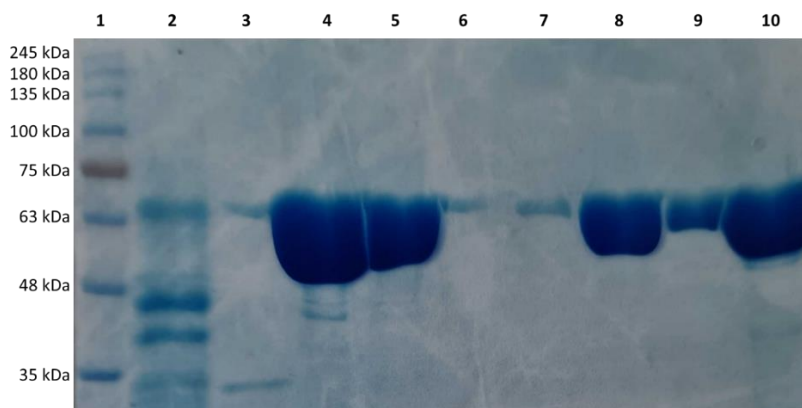
Figure III-23 SDS-PAGE analysis (12% w/v acrylamide) from the purification process of Ca- and Nd-MDH from AM1 (1: marker, 2: crude, 3: flow-through, 4: peak 2 of anion exchange column, 5: peak 2 after buffer exchange, peak 6: peak 1 of cation exchange column, peak 7: peak 2 of cation exchange column, peak 8: Ca-MDH, peak 9: Nd-MDH, peak 10: Eu-MDH from SolV). BlueEye prestained protein ladder (Jena Bioscience) was used as the marker.

The dye-coupled assay was utilized to determine and compare the enzyme activity of Ca-MDH and Nd-MDH. The results show that the enzyme activity of Ca-MDH is one order of magnitude higher than Nd-MDH (Figure III-24) with an averaged specific activity of 0.073±0.001 and 0.009±0.0005 µMol min^{-1} mg^{-1}, respectively.
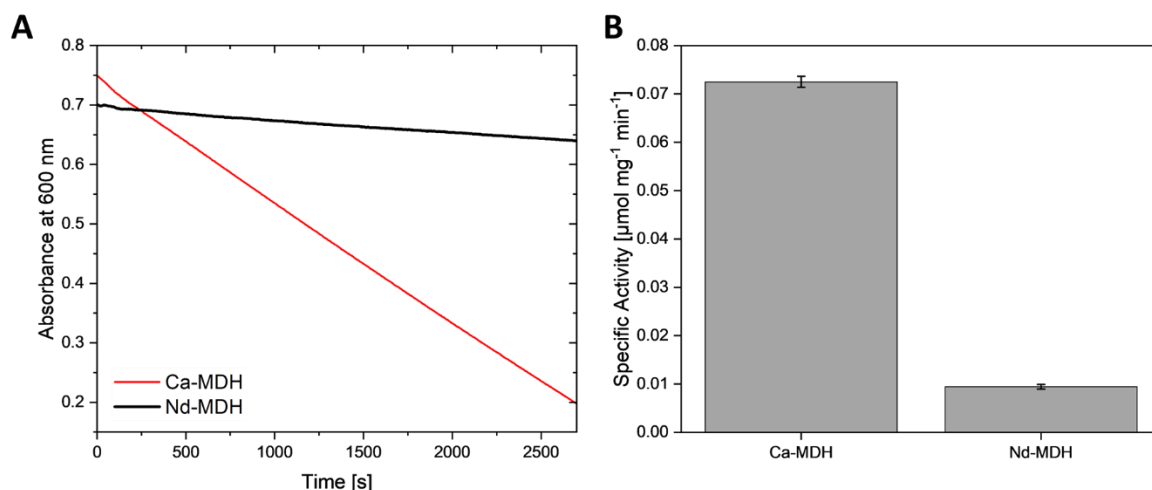
Figure III-24 Dye-coupled activity assay of Ca- and Nd-MDH from AM1 with artificial electron acceptor. Conditions: 1 mM PES, 100 µM DCPIP, 25 mM MeOH, 150 nM MDH in 25 mM MES buffer pH 5.5, n = 2.

These are only preliminary results and warrant cautious interpretation. It should be mentioned, that this particular Nd-MDH sample was only purified once with the DEAE column and not further with the desalting and SP column. It is very likely, that other protein impurities are present and thus falsify the correct amount of Nd-MDH. Nevertheless, further investigations regarding assay conditions should be conducted including pH and temperature optimization as well the impact of addition of NH$_4$Cl to properly assess if Ca-MDH has higher activity than Nd-MDH or if this is only the case under these certain conditions. More importantly, the purification is not reproducible. The purification of Ca- and Nd-MDH was only possible with one batch of cells. The growth of these cells was interrupted overnight. The incubator encountered a malfunction during operation, resulting in both shaking and temperature control being disabled for an unknown time. After restarting the incubator, the cells were treated as usual. The lack of aeration and loss of temperature probably induced stress in the cells, possibly triggering upregulation of critical metabolic functions including the expression of MDH. Subsequent attempts following this batch resulted in significantly lower MDH yield from the first column. Besides attempting to isolate MDH from freshly harvested cells, various lysozymes were tested including the increase of added lysozyme to enhance cell lysis, but no improvement in MDH yield was observed.

To conclude, there is no approach published that systematically compares the activity of Ca- and Ln-MDH from *M. extorquens* AM1. A three-step protocol based on a method established by Anthony and coworkers was modified for this purpose.[39] Ca- and Nd-MDH could be successfully purified and dye-coupled assay at pH 5.5 showed that the enzyme activity of Ca-MDH is a an order of magnitude

higher. Nonetheless, more experiments with varying pH and temperature as well as additives like NH$_4$Cl should be conducted. It should be noted that the metal content was not determined by ICP-MS and that Nd-MDH was used after one purification. Furthermore, the MDH yield is very low. Sufficient amount of MDH could be isolated only from one cell batch. While growing in the incubator, a malfunction caused the incubator to halt, stopping the shaking and temperature control for an unknown time. This probably induced stress to the cells, triggering the upregulation of MDH. This incident should be revisited before further attempts to purify Ca- and Ln-MDH from AM1 are considered.

7. Conclusion and Outlook

The strictly Ln-dependent *Methylacidiphilum fumariolicum* SolV is an extremophilic bacterium isolated from volcanic mudpot.[12b] SolV is able to thrive on different Lns and is able to incorporate various Lns in the active site of its Ln-MDH. Together with the second cofactor PQQ, Ln-MDH catalyzes the oxidation of methanol to formaldehyde which is crucial for its C1 metabolism and growth. Concurrently, PQQ is reduced to PQQH$_2$ which is re-oxidized after a step-wise single electron transfer to two separate molecules of its native electron acceptor cytochrome c_{GJ} (cyt c_{GJ}). By using the artificial dye-coupled activity assay, previous studies have shown that the enzyme activity of Ln-MDH containing early Lns increase towards Nd^{3+} and declines afterwards. We were interested in elucidating the mechanism of substrate oxidation in Ln-MDH by using cyt c_{GJ}. First, a custom-made 3.7 L bioreactor was built for the large-scale cultivation of SolV. Large-scale cultivation of SolV with nine different Lns (Lns = La, Ce, Pr, Nd, Sm, Eu, Gd, Tb and Lu) were performed und eight different Ln-MDHs (Ln = La, Ce, Pr, Nd, Sm, Eu, Gd and Tb) were successfully isolated by fast protein liquid chromatography. Only Tb- and Lu-SolV did not show exponential growth and ICP-MS measurement revealed that Lu-MDH did not contain any Lu^{3+} in the active site. Pure cyt c_{GJ} was obtained after size exclusion chromatography. A protein-coupled activity assay based on Anthony and coworkers was developed and optimized to assess the enzyme activity.[39] We discovered that spent cyt c_{GJ} is very stable and remains relatively active after storage at 4 °C for over two years. Additionally, cyt c_{GJ} can be recycled from protein-coupled assay mixtures, which reduces the workload to obtain cyt c_{GJ} in the long term. The enzyme activity of Ln-MDHs were assessed by the widely used dye-coupled and protein-coupled assay and the comparison of their results showed that the trend of enzyme activity across the Ln series differs. The trend using the dye-coupled assay is in accordance with literature (see above), but the results of the protein-coupled assay revealed that La-MDH has the highest enzyme activity, which decreases gradually across the Ln series. More steps are involved in transferring the electrons from Ln-MDH to the final electron acceptor, however La-, Ce- and Pr-MDH exhibit higher enzyme activity using the

protein-coupled assay. This suggests that the early Lns not only effect substrate oxidation, but also the electron transfer to cyt c_{GJ}.

Then, a new method was developed for isothermal titration calorimetry to assess the enzyme activity using cyt c_{GJ}. Reproducible results were obtained when filling the syringe with Ln-MDH and the substrate added to the sample cell. The results of Pr- and Eu-MDH measurements mirror the results obtained by dye-coupled and protein-coupled assay. Pr-MDH is able to oxidize the substrate twice as fast as Eu-MDH. These are only proof-of-concept experiments, thus should be repeated with more Ln-MDHs to obtain conclusive results.

Furthermore, the electrochemical assay published by Kalimuthu *et al*. was revisited to overcome previously encountered mass transport limitation of the substrate.[34] The stationary electrode was switched for a rotating disk electrode which induces a centripetal force towards the center of the electrode to increase the diffusion of the substrate through the membrane, reducing the mass transport limitation. The rotation of the electrode increased the cyt c_{GJ} signal which also contributes to the total observed signal. Without the addition of any substrate, the total observed signal from a Gd-MDH electrode gradually increases with the length of rotation. Addition of saturating amount of substrate only marginally increased the signal, indicating that relative contribution of the cyt c_{GJ} signal is really high. The relative contribution of cyt c_{GJ} to the total observed signal declines towards the early Lns. The calculated K_M values remain within the range observed in previous experiments, thus the mass transport limitation still persists. Replacing the long mercaptoundecanol linker with a shorter one will create a more rigid structure closer to the electrode surface, creating a more uniform biofilm and possibly reducing the observed effect. If proven correct, experiments using the rotating disk electrode can be picked up again to further overcome the mass transport limitation.

The substrate oxidation mechanism was further investigated by looking at the kinetic isotope effect (KIE). Investigating the substrate (MeOH vs. MeOD) and solvent (buffer prepared in H_2O vs. D_2O) isotope effect will reveal rate-limiting steps. Previous KIE experiments employed the dye-coupled assay and results showed that oxidation of MeOH is faster, indicating that proton abstraction of the substrate is a rate-limiting step. Likewise, the substrate oxidation decreases with increasing amount of D_2O in solution. Following on these experiments, the substrate and solvent isotope effect were investigated using the protein-coupled assay. Analogous to results obtained with the dye-coupled assay, the substrate turnover was faster with MeOH compared to MeOD. The use of deuterated buffer increased the substrate oxidation more than two-fold, proving an enhancing effect of D_2O on total enzyme activity, an effect undetected by the dye-coupled assay. Studies have reported that D_2O increases the protein stability (due to the stronger intrapeptide deuterium bonds), facilitates the reorganization of water-containing catalytic sites and improves long-distance electron transfers.[88, 91-92] These findings

are intriguing but further investigation is required to elucidate if the increase in enzyme activity by D_2O is a structural, thermodynamic or electrochemical phenomenon. The possibility that an interplay of several factors contributes to the increase enzyme activity in D_2O cannot be ruled out.

Lastly, Ca- and Nd-MDH from *M. extorquens* AM1 were purified and the enzyme activity assessed using the dye-coupled assay. At pH 5.5, Ca-MDH displayed an order of magnitude higher enzyme activity but was also purified to a higher degree. More experiments covering a wider pH range, different temperatures and addition of activators are crucial to obtain a better understanding. Further purifications were ineffective as only very low amount of MDH was detected. It should be noted that the cells that had high amount of MDH were interrupted during growth due to a malfunction of the incubator, possibly triggering a stress-induced upregulation of critical metabolic functions including the expression of MDH. This observation should be revisited.

To conclude, our investigation on the interaction between Ln-MDH from SolV with its physiological cyt c_G has revealed that factors influencing enzyme activity are far more complex and multifaceted than what a dye-coupled assay would reveal alone. Further studies are necessary to fully elucidate the mechanism and gain valuable insights for potential strategies in REE separation and bio-recovery of REE. The prevalence of Ln-utilizing biomolecules across a wide array of microorganisms and cellular processes firmly establishes the Lns as biological relevant. As research continues to uncover the biological role of Lns, it is increasingly evident that Lns are much more than substitutes for Ca-dependent enzymes.

IV.   Experimental Section

1. Chemical Experiments

1.1 General Considerations

If not stated otherwise, all reactions were performed using oven-dried glassware under an atmosphere of nitrogen. Volatiles were concentrated by rotary evaporation at 40 °C. Purification was performed *via* flash column chromatography with silica gel (ACROS Organics Si 60 Å, particle size 35-70 µm). All commercial reagents were used without further purification. Acetone, ethyl acetate methanol, dichloromethane, *iso*-hexane and diethyl ether were purchased from the LMU Munich chemical supply shop. Dichloromethane, *iso*-hexane and diethyl ether were distilled by rotary evaporation before use. TLC Silica gel (Merck, 0.25 mm, 60 Å pore size, 230–400 mesh) were used to track the progress of the reaction and visualized by UV absorption (254 nm).

1.2 Analytical Methods

NMR Spectroscopy

^{1}H NMR and ^{13}C NMR spectra were recorded at 25 °C on Bruker Avance III (400 MHz) by Brigitte Breitenstein or Christine Neumann and Bruker Avance III HD (800 MHz) by Claudia Ober. All chemical shifts are reported in units of δ (ppm) relative to residual solvent peak (CDCl$_3$: δ_H = 7.26, δ_C = 77.16; DMSO-d$_6$: δ_H = 3.3, δ_C = 39.52; MeOD-d$_4$: δ_H = 3.31, δ_C = 49.00 and D$_2$O: δ_H = 4.79). Multiplicity were shown as singlet (s), doublet (d), triplet (t), quartet (q), multiplet (m) and their combination. Coupling constants (J) are given in Hertz. MestreNova Version 14.1 was used for data processing.

Mass Spectrometry

Low resolution electrospray mass spectra were received from a liquid chromatograph system (Agilent 1100 SL system, G1312A BinPump, G1313A ALS, G1316A COLCOM) coupled to HCTultra PTM Discovery system mass spectrometer (Bruker Daltonik) in alternate ESI mode. A 1:1 acetonitrile/water mixture was used as carrier solvent.

High resolution ESI spectra of aerobactin complexes (Figure II-5) were received from LTQ FT Ultra Fourier Transform Ion Cyclotron Resonance mass spectrometer (Thermo Finnigan) by Dr. Werner Spahl with acetonitrile/water as carrier solvents. HPLC-ESI-HRMS measurements of rhodopetrobactin B (Figure II-16) were performed on an Agilent HPLC 1260 Infinity II system (G7115A 1260 DAD WR,

G7116A 1260 MCT, G7167A 1260 Multisampler, G7104C 1260 Flexible Pump) coupled to a 6530 C QTOF LC/MS system (G1958-65171). All measurements were performed at 30 °C on a C18 porous core column (Agilent Poroshell 120 EC-C18, 150 mm×3 mm, 2.7 µm) with a flow rate of 0.7 mL/min. As eluent system a mixture of water/acetonitrile with 0.1% formic was used. Samples were prepared in H_2O (<10 µg/mL). HPLC-ESI-HRMS data was obtained in positive mode. Data was analyzed with MassHunter Qualitative Analysis10.0HPLC.

High performance liquid chromatography (HPLC)

HPLC was performed on an Agilent 1260 II system (G1364E 1260 FCPS, G7165A 1260 MWD, G7161A Prep Bin Pump). Crude samples were filter through a 0.45 µM syringe filter prior to injection. The detection wavelength was set to 210 nm. Aerobactin (R_t = 26 min) was purified by semipreparative HPLC using a reverse-phase C18 column with the following method: A: H_2O + 0.1% TFA, B: MeCN + 0.1% TFA, 0 to 25% in 40 min and flow rate: 5 mL/min. Rhodopetrobactin (R_t = 27.7 min) was purified by preparative HPLC using a reverse-phase C18-AQ column with the following method: A: H_2O + 0.1% TFA, B: MeCN + 0.1% TFA, 5 to 32% in 45 min and flow rate: 20 mL/min.

Samples that contain product were lyophilized on a 1-2 LDplus lyophilisator (Christ Alpha) attached to a VACUU PURE® 10 screw pump (vacuubrand).

UV/Vis Spectroscopy

UV/Vis spectra were either recorded with a Cary 60 UV/Vis spectrophotometer (Agilent) with Peltier element or Epoch2 plate reader (BioTek). If not otherwise stated, the spectra were recorded using the "Scan" program at room temperature, from 200–800 nm, the scanning speed set to fast or medium, and sample spectra were baseline corrected by subtracting the buffer spectrum. Data were analyzed with Gen5 and Origin 2017.

Chrome Azurol S (CAS) Assay

CAS assay were performed according to Zytnick *et al.*[73] All assay components including CAS (Sigma-Aldrich), hexadecyltrimethylammonium bromide (>99%, ACROS Organics), $LaCl_3$ x 7 H_2O (99.999%, Sigma-Aldrich), $NdCl_3$ x 6 H_2O (99.9%, abcr) and $LuCl_3$ x 6 H_2O (99.999%, Sigma-Aldrich) were commercially obtained and used without further purification. Before measurement, the plate was incubated for 5 min at room temperature (180 rpm, orbital shake). Measurements were performed by

the Epoch2 plate reader (BioTek) using transparent 96-well plates (Corning) without the lid. The UV/Vis spectra were recorded from 350–750 nm in 1 nm intervals with the highest scan rate per data point. The obtained data was corrected for pathlength and baseline. Data were analyzed with Gen5 and Origin 2017.

1.3 Experimental Procedures

1.3.1 Aerobactin

2-hydroxy-4-methoxy-2-(2-methoxy-2-oxoethyl)-4-oxobutanoic acid (**1**)
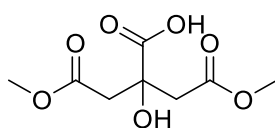
According to a modified literature procedure:[63] Citric acid (4.8 g, 25.0 mmol, 1.0 equiv.) and sodium iodide (1.1 g, 7.5 mmol, 0.3 equiv.) were dissolved in 75 mL MeOH. 10 g dried Dowex-H$^+$ resin* was added and the reaction mixture was stirred for 28 h at room temperature. After completion, the resin was filtered off and the volatiles were removed under reduced pressure. The residue was dissolved in 100 mL DCM and the reaction mixture was stirred overnight at room temperature. The product forms as a white precipitate that was collected by filtration. After addition of 100 mL DCM to the filtrate, the reaction mixture was stirred for 4 h at room temperature. The product was collected again and the process was repeated once more. Title compound was obtained as a yellowish solid (1.3 g, 6.0 mmol, 24%).

* 25 g of Dowex ion-exchange resin (50WX8, 16–40 mesh) was added to 50 mL 2 M HCl and stirred for 60 min at room temperature. The resin was collected and washed with H_2O until the filtrate reached a pH of 7. Then, the resin was dried in an oven for 16–24 h at 100 °C.

^{1}H NMR (400 MHz, MeOD-d$_4$) δ [ppm] = 3.68 (s, 6H), 2.96–2.80 (m, 4H).

^{13}C NMR (101 MHz, MeOD-d$_4$) δ [ppm] = 176.38, 171.85, 74.22, 52.17, 44.01.

Analytical data were consistent with those reported in literature.[63]

2-(tert-butyl) 1,3-dimethyl 2-hydroxypropane-1,2,3-tricarboxylate (**2**)
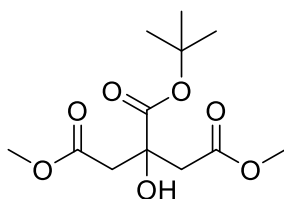
According to a modified literature procedure:[95] The reaction flask was charged with 10 mL *tert*-butyl acetate and **1** (1.1 g, 5.0 mmol, 1.0 equiv.). To the reaction mixture was added dropwise 200 µL perchloric acid. The reaction mixture was stirred for 3 days at room temperature. After completion, the reaction mixture was carefully poured into a saturated solution of 20 mL $NaHCO_3$ and extracted three times with Et_2O. Volatiles were removed under reduced pressure before 30 mL *iso*-hexane was added to the residue. The reaction mixture was stirred for 2 h and then stored at 4 °C overnight. The byproduct (white precipitate) was filtered off and the volatiles were removed under reduced pressure. Title compound was obtained as a colorless oil (0.55 g, 2.0 mmol, 40%).

^{1}H NMR (400 MHz, $CDCl_3$) δ [ppm] = 3.68 (s, 6H), 2.89–2.74 (m, 4H), 1.50 (s, 9H).

Analytical data were consistent with those reported in literature.[95]

3-(*tert*-butoxycarbonyl)-3-hydroxypentanedioic acid (**3**)
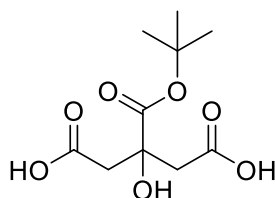
According to a modified literature procedure:[95] **2** (0.49 g, 1.77 mmol, 1 equiv.) was dissolved in 2.5 mL MeOH. The reaction mixture was cooled down to 0 °C before 2.5 mL of cooled 2 M NaOH was added. The reaction mixture was stirred for 30 min at 0 °C. The cooling was removed and the reaction was stirred for 24 h at room temperature. After completion, the reaction mixture was acidified with 2 M HCl and extracted three times with EtOAc. The volatiles were removed under reduced pressure. Title compound was obtained as a white solid (0.42 g, 1.68 mmol, 95%).

^{1}H NMR (400 MHz, MeOD-d_4) δ [ppm] = 2.89–2.70 (m, 4H), 1.48 (s, 9H).

^{13}C NMR (101 MHz, MeOD-d_4) δ [ppm] = 173.84, 173.37, 83.49, 74.35, 44.13, 28.05.

Analytical data were consistent with those reported in literature.[95]

Ethyl ((benzyloxy)carbonyl)-*L*-lysinate (**6**)
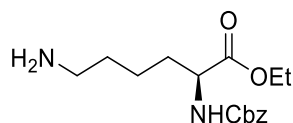
According to a modified literature procedure:[62] The reaction flask was charged with 30 mL ethanol and cooled to 0 °C. After dropwise addition of 5 mL thionyl chloride to the solution, the reaction mixture was stirred at 0 °C for 30 min. Commercially available Cbz-Lys(Boc)-OH (2.24 g, 5.89 mmol, 1.0 equiv.) was added to the solution and stirred at 0 °C for 2 h before the cooling was removed. After warming to room temperature, the reaction mixture was stirred for 20 h. After completion, volatiles were removed under reduced pressure and the crude **6** was used without further purification.

Ethyl N^6-(benzoyloxy)-N^2-((benzyloxy)carbonyl)-*L*-lysinate
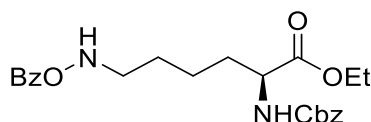
According to a modified literature procedure:[62] The crude product **6** was dissolved in 100 mL DCM and cooled to 0 °C. Then, 100 mL of a cooled sodium bicarbonate buffer solution (0.75 M NaHCO$_3$/NaOH, pH 10.5) was added. Dibenzoyl peroxide (2.85 g, 8.83 mmol, 1.5 equiv., 75 wt%) was added and the biphasic reaction mixture was stirred at 0 °C for 8 h and then at room temperature for 12 h. After completion, the reaction mixture was extracted three times with DCM. The combined organic layers were washed with 10% v/v Na$_2$SO$_3$ solution, brine and dried over MgSO$_4$. The volatiles were removed under reduced pressure and purified *via* flash column chromatography (0 → 5% EtOAc in DCM). Title compound was obtained as a colorless oil (1.47 g, 3.42 mmol, 58% after two steps).

¹H NMR (400 MHz, CDCl$_3$) δ [ppm] = 8.04–7.99 (m, 2H), 7.61–7.56 (m, 1H), 7.49–7.43 (m, 2H), 7.38–7.28 (m, 6H), 5.34–5.27 (m, 1H), 5.11 (s, 2H), 4.38 (q, *J* = 7.1 Hz, 1H), 4.20 (q, *J* = 7.2 Hz, 2H), 3.12 (t, *J* = 7.0 Hz, 2H), 1.94–1.83 (m, 1H), 1.76–1.58 (m, 3H), 1.55–1.41 (m, 2H), 1.27 (t, *J* = 7.0 Hz, 3H).

¹³C NMR (101 MHz, CDCl$_3$) δ [ppm] = 172.48, 167.06, 156.01, 136.41, 133.51, 129.49, 128.69, 128.53, 128.34, 128.26, 67.14, 61.65, 53.91, 52.37, 32.77, 27.04, 22.84, 14.32.

TLC: R_f = 0.45 (DCM/EtOAc, 9:1).

LR-MS (ESI⁺): *m/z* calc. for [C$_{23}$H$_{29}$N$_2$O$_6$]⁺ 429.2; found 429.3.

Analytical data were consistent with those reported in literature.[62]

Ethyl N^6-acetyl-N^6-(benzoyloxy)-N^2-((benzyloxy)carbonyl)-L-lysinate (**7**)
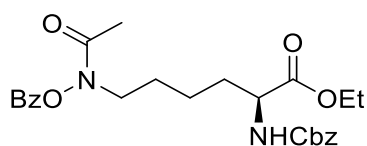
According to a modified literature procedure:[62] **6** (0.370 g, 0.864 mmol, 1.0 equiv.) was dissolved in 3 mL acetic anhydride followed by addition of 300 μL pyridine. The reaction mixture was stirred at 50 °C for 4 h and then at room temperature for 18 h. The volatiles were removed under reduced pressure. The residue was diluted with DCM and the organic layer was washed with 1 M HCl, saturated NaHCO₃ solution, brine and then dried over MgSO₄. The volatiles were removed under reduced pressure and purified *via* flash column chromatography (0 → 20% EtOAc in DCM). Title compound was obtained as a colorless oil (0.387 g, 0.822 mmol, 95%) which crystallized after several hours.

¹H NMR (400 MHz, CDCl₃) δ [ppm] = 8.15–8.02 (m, 2H), 7.67 (t, J = 7.7 Hz, 1H), 7.52 (t, J = 7.8 Hz, 2H), 7.37–7.28 (m, 5H), 5.34 (d, J = 8.2 Hz, 1H), 5.09 (s, 2H), 4.34 (q, J = 7.8 Hz, 1H), 4.18 (q, J = 7.1 Hz, 2H), 3.87–3.74 (m, 2H), 2.04 (s, 3H), 1.92–1.81 (m, 1H), 1.70–1.61 (m, 3H), 1.50–1.35 (m, 2H), 1.26 (t, J = 7.1 Hz, 3H).

¹³C NMR (101 MHz, CDCl₃) δ [ppm] = 173.82, 163.94, 156.04, 135.99, 134.67, 130.16, 129.09, 128.66, 128.30, 128.22, 126.85, 77.36, 67.09, 61.63, 53.87, 32.36, 26.74, 22.40, 20.49, 14.29.

TLC: R_f = 0.40 (DCM/EtOAc, 9:1).

LR-MS (ESI⁺): *m/z* calc. for $[C_{25}H_{31}N_2O_7]^+$ 471.2; found 471.3.

Analytical data were consistent with those reported in literature.[62]

NH₂-Lys(Boc)(Ac)-OEt hydrobromide (**8**)
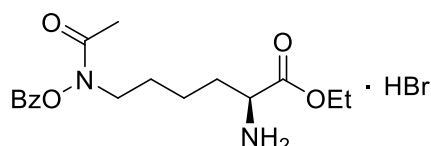
According to a modified literature procedure:[62] **7** (193 mg, 0.41 mmol) was dissolved in 25 mL DCM followed by slow addition of 25 mL HBr (33 wt% in AcOH). The reaction mixture was stirred at room temperature for 2.5 h. After completion, the volatiles were removed under reduced pressure. Title compound has to be prepared right before use to avoid decomposition and was used without further purification.

12-(*tert*-butyl) 16,8-diethyl 3,21-diacetyl-12-hydroxy-1,10,14,23-tetraoxo-1,23-diphenyl-2,22-dioxa-3,9,15,21-tetraazatricosane-8,12,16-tricarboxylate (**9**)
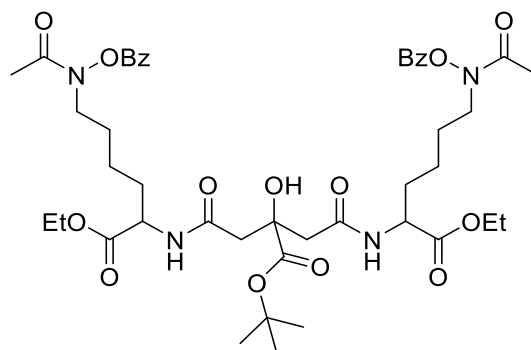
According to a modified literature procedure:[62] **3** was synthesized according to protocols described previously.[95] **3** (50 mg, 0.20 mmol, 1.0 equiv.) and *N*-Hydroxysuccinimide (55 mg, 0.48 mmol, 2.4 equiv.) were dissolved in 3 mL THF, followed by addition of *N,N'*-Dicyclohexylcarbodiimide (124 mg, 0.60 mmol, 3.0 equiv.). The formation of a white precipitate was observed after 2 min stirring. After 30 min of stirring at room temperature, 1.5 mL H_2O was added to the reaction and the reaction mixture was stirred for 10 min at room temperature. Then, $NaHCO_3$ (1.680 g, 20.0 mmol, 100.0 equiv.) was added to the reaction mixture followed by freshly prepared **8** (0.41 mmol, 2.1 equiv.) dissolved in 9 mL THF. The reaction mixture was stirred at room temperature for 18 h. After completion, the solids were filtered off and the volatiles were removed under reduced pressure. The residue was diluted with EtOAc and the organic layer was washed with H_2O, brine and then dried over $MgSO_4$. The volatiles were removed under reduced pressure und purified *via* flash column chromatography (50 → 65% EtOAc in *iso*-hexane, then 5 → 10% MeOH in DCM). Title compound was obtained as a colorless oil (78 mg, 0.09 mmol. 44%).

^{1}H NMR (400 MHz, CDCl$_3$) δ [ppm] = 8.08 (dt, *J* = 7.1, 1.4 Hz, 4H), 7.71–7.64 (m, 2H), 7.56–7.49 (m, 4H), 7.46–7.38 (m, 2H), 4.57–4.45 (m, 2H), 4.19–4.13 (m, 4H), 3.86–3.71 (m, 4H), 2.81 (d, *J* = 14.4 Hz, 1H), 2.70 (d, *J* = 2.7 Hz, 2H), 2.59 (d, *J* = 14.4 Hz, 1H), 2.04 (s, 6H), 1.90–1.78 (m, 3H), 1.71–1.60 (m, 6H), 1.49–1.43 (m, 12H), 1.27–1.23 (m, 6H).

^{13}C NMR (101 MHz, CDCl$_3$) δ [ppm] = 173.64, 173.27, 171.48, 171.42, 170.08, 169.62, 164.62, 134.72, 130.15, 130.14, 129.68, 129.12, 129.10, 128.55, 128.52, 128.48, 128.46, 126.78, 82.68, 74.44, 61.93, 61.83, 61.60, 52.41, 52.21, 52.13, 44.51, 41.95, 31.47, 31.29, 27.95, 26.66, 23.27, 22.87, 22.82, 22.2 8, 20.50, 14.29, 14.24, 14.22.

TLC: R_f = 0.50 (DCM/MeOH, 19:1).

LR-MS (ESI$^+$): *m/z* calc. for $[C_{44}H_{60}N_4O_{15}+Na]^+$ 907.4; found 907.5.

Analytical data were consistent with those reported in literature.[62]

Aerobactin
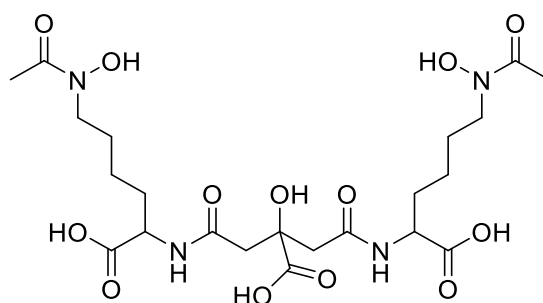
According to a modified literature procedure:[62] **9** (78 mg, 0.088 mmol, 1.0 equiv.) was dissolved in 15 mL DCM, followed by addition of 8 mL trifluoroacetic acid. The reaction mixture was stirred at room temperature for 3 h. Then, volatiles were removed under reduced pressure. The residue was diluted with 10 mL THF, 5 mL of 0.5 M NaOH was added and the reaction mixture was stirred at room temperature for 3.5 h. After completion, 10% HCl was added to bring the pH to 2. The volatiles were removed under reduced pressure und purified by semi-preparative HPLC (Dr. Maisch ReproSil-Pur 120 reverse-phase C18-AQ column, A: H_2O (0.1% TFA), B: MeCN (0.1% TFA), 0 → 25% in 40 min). Title compound was obtained as a white solid (24 mg, 0.043 mmol, 48%).

HPLC: R_t = 26 min (H_2O/MeCN with 0.1% TFA).

^{1}H NMR (400 MHz, D_2O) δ [ppm] = 4.43–4.32 (m, 2H), 3.69–3.57 (m, 4H), 2.95 (dd, J = 14.9, 7.4 Hz, 2H), 2.80 (dd, J = 14.9, 6.5 Hz, 2H), 2.15 (s, 6H), 1.98–1.85 (m, 2H), 1.84–1.60 (m, 6H), 1.49–1.34 (m, 4H).

^{13}C NMR (101 MHz, D_2O) δ [ppm] = 176.42, 175.75, 173.69, 171.34, 171.27, 73.92, 52.64, 52.57, 51.27, 47.45, 44.10, 30.01, 29.97, 25.17, 21.95, 19.24.

HR-MS (ESI$^-$): m/z calc. for $[C_{22}H_{35}N_4O_{13}]^-$ 563.2206; found 563.2202.

HR-MS (ESI$^-$): m/z calc. for $[C_{22}H_{32}N_4O_{13}Fe]^-$ 616.1321; found 616.1318.

HR-MS (ESI$^-$): m/z calc. for $[C_{22}H_{32}N_4O_{13}Lu]^-$ 735.1379; found 735.1379.

Analytical data were consistent with those reported in literature.[62]

1.3.2 Deoxyschizokinen

tert-butyl (3-aminopropyl)carbamate (**12**)
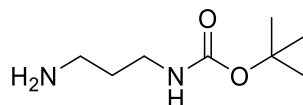
According to a modified literature procedure:[77] 1,3-Diaminopropane (3.6 g, 48.0 mmol, 3 equiv.) was dissolved in 100 mL MeOH, followed by the addition of 10 mL TEA. Di-*tert*-butyldicarbonate (3.5 g, 16.0 mmol, 1 equiv.) was dissolved in 6 mL MeOH and added to the solution. The reaction mixture was stirred for 2.5 h at 80 °C. After completion, the volatiles were removed under reduced pressure. After the addition of 25 mL H_2O, the insoluble di-Boc-amine precipitated and was filtered off. The filtrate was extracted three times with DCM and the combined organic layers were dried over Na_2SO_4. The volatiles were removed under reduced pressure and title compound was obtained as a colorless oil (2.4 g, 13.5 mmol, 84%).

¹H NMR (400 MHz, CDCl₃) δ [ppm] = 4.83 (s, 1H), 3.27 − 3.12 (m, 2H), 2.78 (t, J = 6.6 Hz, 2H), 1.66 − 1.57 (m, 4H), 1.44 (s, 9H).

¹³C NMR (101 MHz, CDCl₃) δ [ppm] = 156.35, 39.80, 38.53, 33.42, 29.85, 28.57.

LC-MS (ESI⁺): *m/z* calc. for $[C_8H_{19}N_2O_2]^+$ 175.1441; found 175.1.

Analytical data were consistent with those reported in literature.[77]

tert-butyl (3-acetamidopropyl)carbamate (**10**)
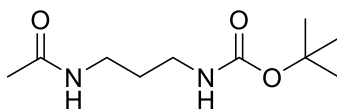
According to a modified literature procedure:[68] **12** (0.27 g, 1.6 mmol, 1.0 equiv.) was dissolved in 20 mL DCM. Acetic anhydride (0.32 g, 3.2 mmol, 2.0 equiv.) was slowly added, followed by the addition of pyridine (0.25 g, 3.1 mmol, 2.0 equiv.). The reaction mixture was stirred for 16 h at room temperature. After completion, the volatiles were removed under reduced pressure. The residue was re-dissolved in 10 mL H_2O, extracted three times with DCM and the combined organic layers were dried over Na_2SO_4. The volatiles were removed under reduced pressure and title compound was obtained as a yellow oil (0.34 g, 1.6 mmol, 100%).

¹H NMR (400 MHz, CDCl₃) δ [ppm] = 6.24 (s, 1H), 4.88 (s, 1H), 3.28 (q, J = 6.3 Hz, 2H), 3.17 (q, J = 6.3 Hz, 2H), 1.99 (s, 3H), 1.66–1.56 (m, 2H), 1.44 (s, 9H).

13C NMR (101 MHz, CDCl$_3$) δ [ppm] = 170.66, 149.76, 123.95, 37.19, 36.09, 30.36, 28.53, 23.50.

LC-MS (ESI+): *m/z* calc. for [C$_{10}$H$_{21}$N$_2$O$_3$]$^+$ 217.1547; found 217.2.

Analytical data were consistent with those reported in literature.[68]

tert-butyl (3-((benzoyloxy)amino)propyl)carbamate
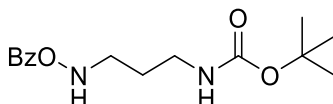
According to a modified literature procedure:[68] After cooling 100 mL of an aqueous sodium bicarbonate buffer solution (NaHCO$_3$/NaOH, pH 10.5) to 0 °C, **12** (1.74 g, 10.0 mmol, 1 equiv.) was added. Dibenzoyl peroxide (6.5 g, 20.0 mmol, 2.0 equiv., 75 wt%) was dissolved in 75 mL DCM and added portion wise to the biphasic solution. The cooling was removed and the reaction mixture was stirred for 4 h at room temperature. LC-MS measurement shows the *N*-oxidation product as the major product. Acetyl chloride (0.78 g, 10.0 mmol, 1 equiv.) was dissolved in 10 mL DCM and added dropwise to the solution. The reaction mixture was stirred for 18 h at room temperature. After completion, the reaction mixture was extracted three times with DCM. The combined organic layers were washed once with 10% Na$_2$SO$_3$ solution and dried over Na$_2$SO$_4$. The volatiles were removed under reduced pressure and purified with *via* flash column chromatography (DCM/EtOAC, 0 → 10%). Title compound was obtained as a colorless oil (2.01 g, 6.9 mmol, 69%) which crystalizes upon storage at 4 °C.

TLC: *R*$_f$ = 0.65 (DCM/EtOAc, 6:4).

1H NMR (400 MHz, CDCl$_3$) δ [ppm] = 8.05–7.98 (m, 2H), 7.59 (m, 1H), 7.50–7.41 (m, 2H), 4.79 (s, 1H), 3.29 (q, J = 6.5 Hz, 2H), 3.19 (t, J = 6.7 Hz, 2H), 1.83 (p, J = 6.7 Hz, 2H), 1.44 (s, 9H).

13C NMR (101 MHz, CDCl$_3$) δ [ppm] = 166.97, 156.21, 133.54, 129.50, 128.69, 128.49, 50.32, 38.61, 28.54, 27.90.

LC-MS (ESI+): *m/z* calc. for [C$_{15}$H$_{23}$N$_2$O$_4$]$^+$ 295.1652; found 295.2.

Analytical data were consistent with those reported in literature.[68]

tert-butyl (3-(*N*-(benzoyloxy)acetamido)propyl)carbamate (**11**)
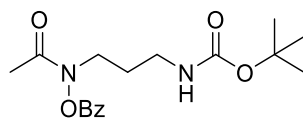
According to a modified literature procedure:[68] Precursor-6 (0.78 g, 2.66 mmol) was dissolved in 10 mL acetic anhydride, followed by the addition of 1 mL dry pyridine. The reaction mixture was stirred at room temperature for 18 h. After completion, the reaction mixture was diluted with DCM and the organic layer was washed once with 2 M HCl, saturated $NaHCO_3$, brine and then dried over Na_2SO_4. The volatiles were removed under reduced pressure and purified *via* flash column chromatography (DCM/EtOAc, 0 → 5%). Title compound was obtained as a colorless oil (0.86 g, 2.57 mmol, 97%).

TLC: R_f = 0.60 (DCM/EtOAc, 4:1).

¹H NMR (400 MHz, $CDCl_3$) δ [ppm] = 8.13–8.05 (m, 2H), 7.73–7.64 (m, 1H), 7.57–7.48 (m, 2H), 5.08 (s, 1H), 3.88 (t, J = 6.5 Hz, 2H), 3.22 (t, J = 6.4 Hz, 2H), 2.07 (s, 3H), 1.79 (p, J = 6.5 Hz, 2H), 1.43 (s, 9H).

¹³C NMR (101 MHz, $CDCl_3$) δ [ppm] = 174.13, 164.68, 156.21, 134.77, 130.18, 129.11, 126.68, 37.47, 28.55, 27.51, 26.76, 20.39.

LC-MS (ESI⁺): *m/z* calc. for $[C_{17}H_{24}N_2O_5+Na]^+$ 359.1577; found 359.1.

Analytical data were consistent with those reported in literature.[68]

N-(3-aminopropyl)acetamide (**13**)
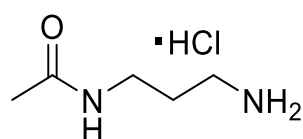
According to a modified literature procedure:[68] For the Boc deprotection the setup depicted in Figure II-3 was prepared. **5** (0.19 g, 0.87 mmol, 1 equiv.) was dissolved in 25 mL dry Et_2O and dry HCl was generated by the slow addition of 20 mL concentrated H_2SO_4 into 30 g NaCl. After 2 h, the volatiles were removed under reduced pressure. Title compound was obtained as an off-white solid (0.13 g, 0.87 mmol, quant. yield).

¹H NMR (400 MHz, $CDCl_3$) δ [ppm] = 3.30–3.25 (m, 2H), 2.94 (t, J = 7.4 Hz, 2H), 1.98 (s, 3H), 1.90–1.78 (m, 2H).

LC-MS (ESI⁺): *m/z* calc. for $[C_5H_{13}N_2O]^+$ 117.1022; found 117.2

Analytical data were consistent with those reported in literature.[68]

N-(3-aminopropyl)-*N*-(benzoyloxy)acetamide (**14**)
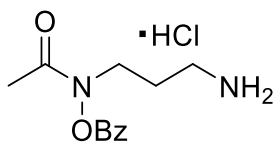
According to a modified literature procedure: [68] For the Boc deprotection the setup depicted in Figure II-3 was prepared. **6** (0.30 g, 0.89 mmol, 1 equiv.) were dissolved in 25 mL dry Et_2O and dry HCl was generated by the slow addition of 20 mL concentrated H_2SO_4 into 40 g NaCl. After 2 h, the volatiles were removed under reduced pressure. Title compound was obtained as a white solid (0.20 g, 0.73 mmol, 82%).

^{1}H NMR (400 MHz, $CDCl_3$) δ [ppm] = 8.19–8.11 (m, 2H), 7.83–7.74 (m, 1H), 7.72–7.45 (m, 2H), 3.98 (t, J = 6.6 Hz, 2H), 3.10 (t, J = 7.5 Hz, 2H), 2.11 (s, 3H), 2.08–2.00 (m, 2H).

LC-MS (ESI$^+$): *m/z* calc. for $[C_{12}H_{18}N_2O_3]^+$ 237.1234; found 237.3

Analytical data were consistent with those reported in literature.[68]

tert-butyl 4-hydroxy-2,6-dioxotetrahydro-2H-pyran-4-carboxylate (**16**)
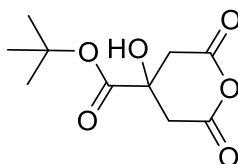
According to a modified literature procedure:[68] DCC (185 mg, 0.9 mmol, 1 equiv.) was dissolved in 16 mL of EtOAC/DCM (1:3). **3** (223 mg, 0.9 mmol, 1 equiv.) was dissolved in 20 mL DCM and slowly added to the solution with DCC. The formation of white precipitate was observed after a few minutes. The reaction mixture was stirred for 30 min at room temperature. After completion, the precipitate was filtered off and volatiles were removed under reduced pressure. The residue was recrystallized with 20 mL of EtOAC/*iso*-hexane (1:4) and title compound was obtained as a pinkish solid (114 mg, 0.5 mmol, 55%).

^{1}H NMR (400 MHz, $CDCl_3$) δ [ppm] = 3.65 (s, 1H), 3.07–2.91 (q, 4H), 1.51 (s, 9H).

^{13}C NMR (101 MHz, $CDCl_3$) δ [ppm] = 171.05, 163.74, 86.71, 69.83, 40.60, 27.87.

Analytical data were consistent with those reported in literature.[68]

tert-butyl 4-((3-acetamidopropyl)amino)-2-(2-((3-(*N*-(benzoyloxy)acetamido)propyl)amino)-2-oxoethyl)-2-hydroxy-4-oxobutanoate (**15**)
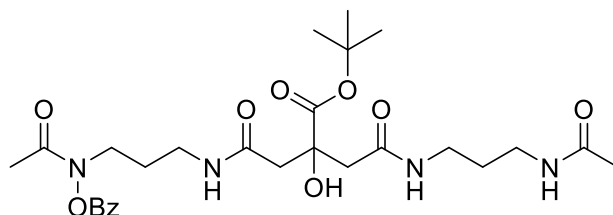
According to a modified literature procedure:[68] **16** (92 mg, 0.34 mmol, 1.3 equiv.) was dissolved in 5 mL DCM and slowly added to a solution of **14** (60 mg, 0.26 mmol, 1.0 equiv.) dissolved in 5 mL DCM and stirred for 10 min at room temperature. After completion, the reaction mixture was repeatedly washed with an aqueous HCl solution (pH 2) and the organic phase was dried over Na_2SO_4. The volatiles were removed under reduced pressure. The crude product (86 mg, 0.18 mmol, 1 equiv.) was re-dissolved in 5 mL DCM, followed by the addition of NHS (21 mg, 0.18 mmol, 1 equiv.) and DCC (38 mg, 0.18 mmol, 1 equiv.). The reaction mixture was stirred for 15 min at room temperature. After completion, **13** (28 mg, 0.18 mmol, 1 equiv.) was added followed by 60 μL triethylamine. The reaction mixture was stirred for 15 min at room temperature. Then, solids were filtered off, volatiles were removed under reduced pressure und purified via flash column chromatography (DCM/MeOH, 0 → 5%). Title compound was obtained as a yellow solid (25 mg, 0.04 mmol, 6%).

LC-MS (ESI⁺): *m/z* calc. for $[C_{27}H_{41}N_4O_9]^+$ 565.2868; found 565.3.

1.3.3 Rhodopetrobactin B
tert-butyl (4-aminobutyl)carbamate (**22**)
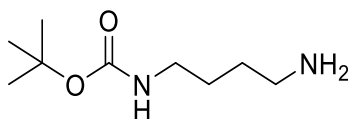
According to a modified literature procedure:[77] 1,4-Diaminobutane (6.1 g, 70.0 mmol, 3 equiv.) was dissolved in a solution of 135 mL MeOH and 15 mL TEA. Di-*tert*-butyldicarbonate (5.1 g, 23.2 mmol, 1 equiv.) was dissolved in 15 mL MeOH and added portionwise to the solution. The reaction mixture was stirred for 18 h at room temperature. After completion, the volatiles were removed under reduced pressure. The residue was dissolved in 150 mL DCM and washed four times with 150 mL saturated Na_2CO_3 solution and the combined organic layers were dried over Na_2SO_4. The volatiles were removed

under reduced pressure and purified with *via* flash column chromatography (DCM/MeOH, 0 → 10% + 1% TEA). Title compound was obtained as a colorless oil (3.1 g, 16.6 mmol, 72%).

^{1}H NMR (400 MHz, CDCl$_3$) δ [ppm] = 4.71 (s, 1H), 3.10 (q, J = 6.5 Hz, 2H), 2.68 (t, J = 6.6 Hz, 2H), 1.56 – 1.42 (m, 4H), 1.41 (s, 9H), 1.22 (s, 2H).

^{13}C NMR (101 MHz, CDCl$_3$) δ [ppm] = 156.12, 79.12, 41.94, 40.55, 31.02, 28.53, 27.61.

LC-MS (ESI$^+$): *m/z* calc. for [C$_9$H$_{21}$N$_2$O$_2$]$^+$ 189.1598; found 189.2.

Analytical data were consistent with those reported in literature.[77]

tert-butyl (3-((2-cyanoethyl)amino)propyl)carbamate (**23**)
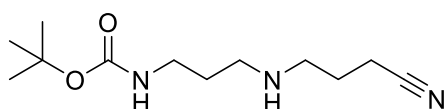
According to a modified literature procedure:[77] **22** (1.33 g, 7.1 mmol, 1.0 equiv.) was dissolved in 25 mL MeCN and 2.5 g K$_2$CO$_3$ was added to the solution. The reaction mixture was stirred for 10 min at room temperature. 4-Bromobutyronitrile (1.15 g, 7.8 mmol, 1.1 equiv.) was dissolved in 10 mL MeCN and the solution was slowly added to **22**. The reaction mixture was stirred for 16 h at room temperature. After completion, solids were removed by filtration. The volatiles were removed under reduced pressure and purified with *via* flash column chromatography (DCM/MeOH, 5% + 1% TEA). Title compound was obtained as a yellow oil (1.25 g, 4.9 mmol, 70%).

TLC: R$_f$ = 0.25 (DCM/MeOH/TEA 94:5:1, *p*-Anisaldehyde).

^{1}H NMR (400 MHz, CDCl$_3$) δ [ppm] = 4.76 (s, 1H), 3.15 (dd, J = 20.8, 6.8 Hz, 2H), 2.74 (t, J = 6.7 Hz, 2H), 2.66 – 2.58 (m, 2H), 2.45 (t, J = 7.1 Hz, 2H), 1.82 (p, J = 7.0 Hz, 2H), 1.56 – 1.47 (m, 4H), 1.44 (s, 9H).

LC-MS (ESI$^+$): *m/z* calc. for [C$_{13}$H$_{26}$N$_3$O$_2$]$^+$ 256.2020; found 256.2.

Analytical data were consistent with those reported in literature.[77]

tert-butyl (4-(*N*-(3-cyanopropyl)acetamido)butyl)carbamate (**24**)
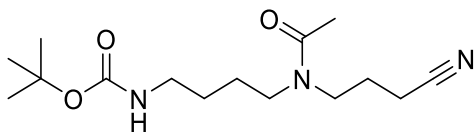
According to a modified literature procedure:[77] **23** (1.00 g, 3.9 mmol, 1 equiv.) was dissolved in 20 mL acetic anhydride and 1.5 mL pyridine was added. The reaction mixture was stirred for 4.5 h at room temperature. After completion, the reaction mixture was diluted with 50 mL DCM. The organic layer was washed once with saturated $NaHCO_3$ solution, once with brine and dried over Na_2SO_4. The volatiles were removed under reduced pressure and purified with *via* flash column chromatography (DCM/MeOH, 0 → 5%). Title compound was obtained as a colorless oil (0.86 g, 2.9 mmol, 73%).

TLC: R_f = 0.25 (DCM/MeOH 98:2, *p*-Anisaldehyde).

¹H NMR (400 MHz, CDCl₃) δ [ppm] = 4.64 (s, 1H), 3.39 (q, J = 8.0, 7.5 Hz, 2H), 3.34 − 3.20 (m, 2H), 3.18 − 3.06 (m, 2H), 2.37 (dt, J = 14.2, 7.0 Hz, 2H), 2.07 (s, 3H), 1.96 − 1.83 (m, 2H), 1.62 − 1.43 (m, 4H), 1.41 (d, J = 2.3 Hz, 9H).

LC-MS (ESI⁺): *m/z* calc. for $[C_{15}H_{27}N_3O_3Na]^+$ 320.1945; found 320.2.

Analytical data were consistent with those reported in literature.[77]

tert-butyl (4-(*N*-(4-aminobutyl)acetamido)butyl)carbamate (**19**)
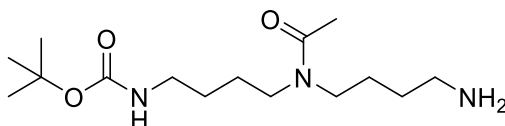
According to a modified literature procedure:[78] **24** (0.86 g, 2.9 mmol, 1 equiv.) was dissolved in 30 mL EtOH and CoCl₂·6 H₂O (1.37 g, 5.8 mmol, 2 equiv.) was added. The blue reaction mixture was stirred for 5 min at room temperature. Then, NaBH₄ (1.09 g, 28.8 mmol, 10 equiv.) was added and the reaction mixture was stirred for 6 h at room temperature. The volatiles were removed under reduced pressure and the residues was re-dissolved in 50 mL DCM and 25 mL 0.1 M NH₄OH. The reaction mixture was stirred for 1 h at room temperature. After completion, the solids were filtered off with Celite and washed with DCM. The organic layer was washed three times with saturated $NaHCO_3$ solution and dried over Na_2SO_4. The volatiles were removed under reduced pressure and title compound was obtained as a colorless oil (0.52 g, 1.7 mmol, 60%).

¹H NMR (400 MHz, CDCl₃) δ [ppm] = 3.34 – 3.28 (m, 2H), 3.27 – 3.20 (m, 2H), 3.18 – 3.10 (m, 2H), 2.07 (t, J = 2.1 Hz, 3H), 1.71 – 1.52 (m, 8H), 1.51 – 1.41 (m, 11H), 1.29 – 1.23 (m, 2H).

LC-MS (ESI⁺): *m/z* calc. for $[C_{15}H_{32}N_3O_3]^+$ 302.2438; found 302.2.

Analytical data were consistent with those reported in literature.[77]

3,4-bis(benzyloxy)benzoic acid (**21**)
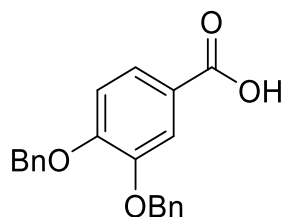
According to a modified literature procedure:[77] 3,4-Dihydroxybenzoic acid (2.0 g, 13.0 mmol, 1 equiv.) was dissolved in 50 mL acetone and 5 g K₂CO₃ was added. Then, benzyl chloride (9.9 g, 78.2 mmol, 6 equiv.) was added and the reaction was stirred for 1 d at 70 °C. After completion, solids were filtered off and volatiles were removed under reduced pressure. The residue was re-dissolved in a solution of 50 mL MeOH and 25 mL 6 M NaOH. The reaction mixture was stirred for 2 h at 80 °C., then for 16 h at room temperature. After completion, the volatiles were removed under reduced pressure and 150 mL H₂O was added to the residues. The emulsion was washed three times with 100 mL *iso*-hexane. After acidification of the aqueous layer with 2 M HCl, title compound precipitated as a white solid (2.3 g, 6.9 mmol, 53%).

¹H NMR (400 MHz, DMSO-d₆) δ [ppm] = 12.67 (s, 1H), 7.59–7.51 (m, 2H), 7.50–7.44 (m, 4H), 7.43–7.31 (m, 6H), 7.20–7.15 (m, 1H), 5.21 (d, J = 18.2 Hz, 4H).

¹³C NMR (101 MHz, DMSO-d₆) δ [ppm] = 166.92, 152.08, 147.62, 137.02, 136.72, 128.44, 128.39, 127.90, 127.79, 127.53, 127.42, 123.46, 123.27, 114.60, 113.13, 70.00, 69.86, 25.48.

LC-MS (ESI⁺): *m/z* calc. for $[C_{21}H_{18}O_4Na]^+$ 357.1097; found 357.1.

Analytical data were consistent with those reported in literature.[77]

3,4-bis(benzyloxy)benzoyl chloride (**18**)
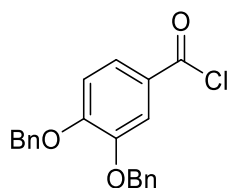
According to a modified literature procedure:[77] **21** (260 mg, 0.78 mmol, 1 equiv.) was dissolved in solution of 6 mL DCM and 3 mL benzene and the reaction mixture was stirred for 15 min at 0 °C. Then, three drops of DMF and oxalyl chloride (740 mg, 5.83 mmol, 7.5 equiv.) were added to the solution. The reaction mixture was stirred for 30 min at 0 °C. After completion, the volatiles were removed under reduced pressure and the crude was used without further purification.

tert-butyl (4-(*N*-(4-(3,4-bis(benzyloxy)benzamido)butyl)acetamido)butyl)carbamate (**25**)
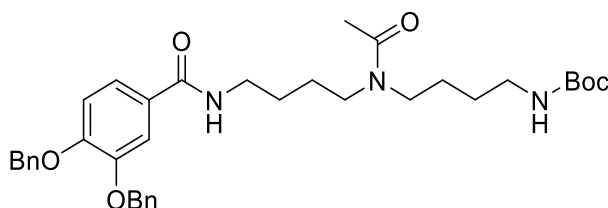
According to a modified literature procedure:[77] **19** (281 mg, 0.93 mmol, 1.2 equiv.) was dissolved in a solution of 6 mL DCM and 2 mL TEA. The reaction mixture was stirred at 0 °C for 20 min. The crude of **18** was dissolved in 5 mL DCM and was added dropwise to the solution of **19**. The reaction mixture was stirred for 24 h at room temperature. After completion, the reaction was extracted three times with DCM and dried over Na_2SO_4. The volatiles were removed under reduced pressure and purified with *via* flash column chromatography (DCM/MeOH, 0 → 5%). Title compound was obtained as a colorless oil (240 mg, 0.39 mmol, 50%).

TLC: R_f = 0.45 (DCM/MeOH 95:5, UV/Vis)

^{1}H NMR (400 MHz, CDCl$_3$) δ [ppm] = 7.59 (d, J = 2.1 Hz, 1H), 7.50–7.41 (m, 4H), 7.40–7.29 (m, 7H), 6.92 (dd, J = 8.4, 1.8 Hz, 1H), 5.24–5.16 (m, 4H), 3.52 – 3.43 (m, 2H), 3.38–3.21 (m, 4H), 3.17–3.08 (m, 2H), 2.07 (d, J = 5.6 Hz, 3H), 1.67–1.46 (m, 13H), 1.44 (s, 9H).

LC-MS (ESI⁺): *m/z* calc. for $[C_{36}H_{48}N_3O_6]^+$ 618.3538; found 618.3.

Analytical data were consistent with those reported in literature.[77]

3,4-Rhodopetrobactin *tert*-Butyl Ester (**26**)
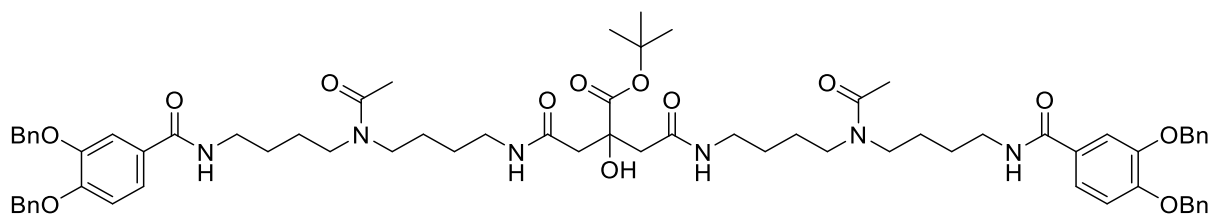
According to a modified literature procedure:[77] For Boc deprotection, **25** (210 mg, 0.34 mmol, 2.2 equiv.) was dissolved in 5 mL DCM and stirred for 15 min at 0 °C. Then, 1 mL TFA was dissolved in 5 mL DCM and added dropwise to **25**. The cooling was removed and the reaction mixture was stirred for 2 h at room temperature. After completion, the volatiles were removed under reduced pressure and the crude was used without further purification.

Tert-butyl citrate **3** (39 mg, 0.16 mmol, 1.0 equiv.) was dissolved in 5 mL THF, followed by the addition of *N*-Hydroxysuccinimide (50 mg, 0.43 mmol, 2.8 equiv.) and *N,N'*-Dicyclohexylcarbodiimide (96 mg, 0.47 mmol, 3.0 equiv.). The reaction mixture was stirred for 3 h at room temperature. After completion, the volatiles were removed under reduced pressure. Then, 5 mL dioxane was added to the residue and the reaction mixture was stirred for 15 min at 10 °C. Crude **25** was dissolved in 5 mL DCM and 1 mL TEA and the reaction mixture was stirred for 30 min at 0 °C. Then, the reaction mixture with **25** was added dropwise to **3**. The cooling was removed and the reaction mixture was stirred for 16 h at room temperature. After completion, the solids were filtered off and the volatiles were removed under reduced pressure. The residue was re-dissolved in 20 mL DCM and the organic layer was washed three times with saturated Na_2CO_3 solution and dried over Na_2SO_4. The volatiles were removed under reduced pressure and purified with *via* flash column chromatography (DCM/MeOH, 0 → 5% + 1% TEA). Title compound was obtained as a colorless oil (90 mg, 0.07 mmol, 47%).

TLC: R_f = 0.45 (DCM/MeOH 95:5, UV/Vis)

LC-MS (ESI⁺): *m/z* calc. for $[C_{72}H_{91}N_6O_{13}]^+$ 1247.6639; found 1247.3.

3,4-Rhodopetrobactin B
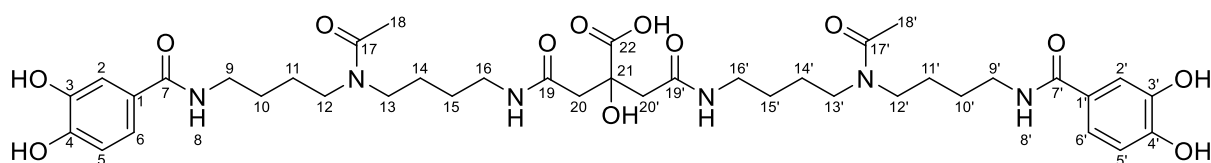
According to a modified literature procedure:[77] **26** (45 mg, 36 μmol) was dissolved in 2 mL glacial acetic acid. Then, 2 mL concentrated HCl was dissolved in 3 mL glacial acetic acid and added dropwise to **26**. The reaction mixture was stirred for 2 h at room temperature. After completion, the volatiles were removed under reduced pressure and residual acid was removed by co-evaporation with DCM. The residue was re-dissolved in 5 mL EtOH and 10 mg Pd/C was added. The reaction mixture was saturated with H_2 for 15 min and stirred for 2 h at room temperature. After completion, the solids were filtered off with Celite and washed with EtOH. The volatiles were removed under reduced pressure. The residue was re-dissolved in 5% MeCN in H_2O and purified by preparative HPLC (reverse-phase C18-AQ column, A: H_2O + 0.1% TFA, B: MeCN + 0.1% TFA, 5 → 32% in 45 min). Title compound was obtained as a white solid (3 mg, 4 μmol, 11%).

HPLC: R_t = 27.7 min

^{1}H (800 MHz) and ^{13}C NMR (201 MHz):

Group	C/H	δ_H	Multiplicity J (Hz)	δ_C	HMBC
DHBA*	1, 1'			125.95	
	2, 2'	7.26	d (2.2)	115.06	C1, C3, C4, C6, C7
	3, 3'			144.77	
	4, 4'			148.15	
	5, 5'	6.74	ddd (8.2, 4.3, 1.3)	114.78	C1, C2, C3, C4, C6, C7
	6, 6'	7.16	dd (8.2, 2.1)	118.83	C2, C3, C4, C7
	7, 7'			166.10	
Putrescine	8, 8'	8.13	m		C7
	9, 9'	3.19, 3.22	m	38.59, 38.64	C7, C9, C10, C11
	10, 10'	1.35/1.47	m	25.43/25.99	C8, C10, C11
	11, 11'	1.35/1.47	m	25.43/25.99	C8, C9, C11
	12, 12'	3.19, 3.22	m	44.25, 47.31	C9, C10, C12, C16
Acetyl	17, 17'			169.10	
	18, 18'	1.96	m	21.32	C11, C12, C16
Putrescine	13, 13'	3.19, 3.22	m	44.25, 47.31	C11, C13, C14, C16
	14, 14'	1.30/1.41/1.47	m	24.70/26.17/26.36/26.54	C12, C14, C15
	15, 15'	1.30/1.41/1.47	m	24.70/26.17/26.36/26.54	C12, C13, C15
	16, 16'	3.00, 3.04	m	37.85	C13, C14
Citrate	19, 19'			169.54	
	20, 20'	2.48, 2.57	m	43.13	C18, C19, C20
	21			73.52	
	22			174.98	

* 3,4-dihydroxybenzoic acid

HR-MS (ESI⁺): *m/z* calc. for $[C_{40}H_{59}N_6O_{13}]^+$ 831.4135; found 831.4142.

Analytical data were consistent with those reported in literature.[80]

1.3.4 Petrobactin

tert-butyl (4-((2-cyanoethyl)amino)butyl)carbamate (**28**)
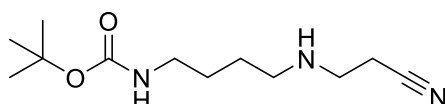
According to a modified literature procedure:[77] **22** (585 mg, 3.11 mmol, 1.0 equiv.) was dissolved in 40 mL dry acetonitrile and 2.5 mL dry triethylamine were added. Afterwards 3-bromopropanenitrile (1.03 mL, 12.4 mmol, 4.0 equiv.) was added slowly to the solution and heated for 18 h at 60°C. The initially clear solution turned orange/brownish overnight and after cooling to room temperature, precipitation of a white solid was observed. The precipitate was separated by filtration and the solvent was removed under reduced pressure. The crude product was purified *via* flash column chromatography (DCM/MeOH, 2% + 1% TEA). Title compound was obtained as an orange oil (558 mg, 2.312 mmol, 74%).

¹H NMR (400 MHz, CDCl₃) δ [ppm] = 4.80 (s, 1H), 3.08 (q, J = 6.3 Hz, 2H), 2.87 (t, J = 6.6 Hz, 2H), 2.62 (d, J = 6.7 Hz, 2H), 2.48 (t, J = 6.6 Hz, 2H), 1.48 (m, 4H), 1.39 (s, 9H).

¹³C NMR (101 MHz, CDCl₃) δ [ppm] = 156.06, 118.77, 79.04, 48.74, 45.03, 40.36, 28.46, 27.78, 27.26, 18.72.

LC-MS (ESI⁺): *m/z* calc. for $[C_{12}H_{24}N_3O_2]^+$ 242.1863; found 242.2.

Analytical data were consistent with those reported in literature.[77]

tert-butyl (4-((3-aminopropyl)amino)butyl)carbamate (**27**)
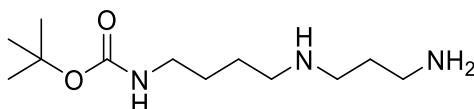
According to a modified literature procedure:[77] **28** (558 mg, 2.31 mmol, 1.0 equiv.) was dissolved in 50 mL dry Et₂O. Afterwards 3 mL of LiAlH₄ (1.0 M in THF) was added dropwise to the solution with strong gas development. The reaction mixture was stirred for 18 h at room temperature. After completion, 50 mL of 6 M NaOH was added. The organic phase was removed and the aqueous phase

was extracted three times with DCM. The combined organic phases were dried over Na_2SO_4 and the volatiles were removed under reduced pressure. The crude compound was obtained as a colorless oil (489 mg, 1.99 mmol, 86%) and was used without further purification.

LC-MS (ESI⁺): *m/z* calc. for $[C_{12}H_{28}N_3O_2]^+$ 246.2176; found 246.2.

tert-butyl (4-((3-(3,4-bis(benzyloxy)benzamido)propyl)amino)butyl)carbamate (**29**)
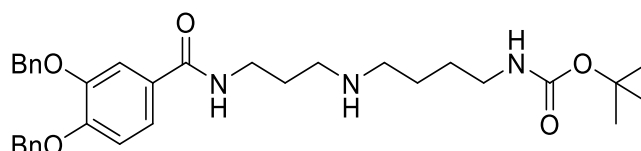
According to a modified literature procedure:[77] **27** (350 mg, 1.43 mmol, 1.0 equiv.) was dissolved in a solution of 10 mL DCM and 10 mL 10% NaOH. The reaction mixture was stirred for 1 h at 0 °C. The crude of **18** was dissolved in 20 mL DCM and was added dropwise to the solution of **27**. The reaction mixture was stirred for 16 h at room temperature. After completion, the reaction mixture was extracted three times with DCM and dried over Na_2SO_4. The volatiles were removed under reduced pressure and purified with *via* flash column chromatography (DCM/MeOH, 0 → 5%). Title compound was obtained as a colorless oil (340 mg, 0.61 mmol, 42%).

LC-MS (ESI⁺): *m/z* calc. for $[C_{33}H_{44}N_3O_5]^+$ 562.3275; found 562.2.

N-(3-((4-aminobutyl)amino)propyl)-3,4-bis(benzyloxy)benzamide
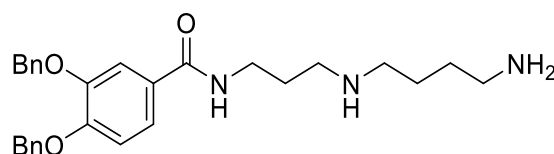
According to a modified literature procedure:[77] For Boc deprotection, **29** (300 mg, 0.53 mmol, 2.2 equiv.) was dissolved in 8 mL DCM and stirred for 15 min at 0 °C. Then, 2 mL TFA was dissolved in 10 mL DCM and added dropwise to **29**. The cooling was removed and the reaction mixture was stirred for 3 h at room temperature. After completion, the volatiles were removed under reduced pressure and the crude was used without further purification.

N-(3-((4-aminobutyl)amino)propyl)-3,4-bis(benzyloxy)benzamide (**30**)
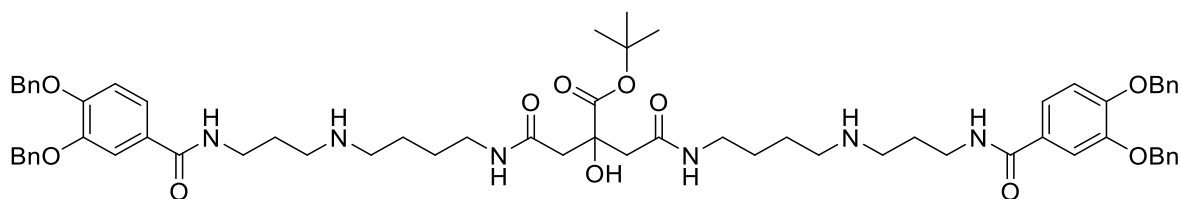
According to a modified literature procedure:[77] **3** (60 mg, 0.24 mmol, 1.0 equiv.) was dissolved in 20 mL THF, followed by the addition of *N*-hydroxysuccinimide (78 mg, 0.68 mmol, 2.8 equiv.) and *N,N'*-dicyclohexylcarbodiimide (150 mg, 0.73 mmol, 3.0 equiv.). The reaction mixture was stirred for 2 h at room temperature. After completion, the volatiles were removed under reduced pressure. Then, 20 mL dioxane was added to the residue and the reaction mixture was stirred for 15 min at 10 °C. Crude **29** was dissolved in 20 mL DCM and 3 mL TEA and the reaction mixture was stirred for 30 min at 0 °C. Then, the reaction mixture with **29** was added dropwise to **3**. The cooling was removed and the reaction mixture was stirred for 16 h at room temperature. After completion, the solids were filtered off and the volatiles were removed under reduced pressure. The residue was re-dissolved in 20 mL DCM and the organic layer was washed three times with saturated Na_2CO_3 solution and dried over Na_2SO_4. The volatiles were removed under reduced pressure and purified with *via* flash column chromatography (DCM/MeOH, 0 → 5% + 1% TEA). Title compound was obtained as a colorless oil (42 mg, 0.04 mmol, 15%).

LC-MS (ESI⁺): *m/z* calc. for $[C_{72}H_{91}N_6O_{13}]^+$ 1247.6639; found 1247.3.

2. Biochemical Experiments

Methylacidiphilum fumariolicum SolV Cultivation

The cultivation of *M. fumariolicum* SolV (La–Eu) was performed by using a modified protocol as previously reported.[12b, 24, 96] For the composition of the growth medium see Table IV-1. SolV was grown with the desired lanthanide (La–Eu) in single-use polypropylene plastic cultivation flasks to an optical density at 600 nm (OD_{600}) of 0.5. A gas atmosphere of 85% air, 10% CH_4 and 5% CO_2 was provided. The flask was incubated in an incubator at 55 °C and 250 rpm. Around 100–200 mL of SolV culture was used to inoculate the large-scale (3.7 L) bioreactor (non-commercial, custom-made) to obtain a starting OD_{600} of 0.05.[96] Throughout the cultivation, CO_2 (600 mL/min), CH_4 (750 mL/min) and air (1000 mL/min) was sparged through the medium. The temperature was kept at 55 °C and a stirring bar was used to ensure homogeneity and even distribution of gases.

The inoculants for Gd- and Tb-SolV were obtained by starvation of La-SolV through two cycles:

To a 1 L cultivation flask 100 mL minimal medium was added and La-SolV to a starting OD_{600} of 0.05. For incubation, a gas atmosphere of 85% air, 10% CH_4 and 5% CO_2 was provided. The flask was incubated in a shaker at 55 °C and 250 rpm for 4 days until an OD_{600} of around 0.25 was reached (cycle 1). 100 mL of this starved La-SolV was used to repeat the same procedure once more until an OD_{600} of 0.125 was reached (cycle 2). In the third round, 100 nM $GdCl_3$ or $TbCl_3$ was added to the starved SolV culture and further incubated until the desired OD_{600} was reached and then used as inoculant for the bioreactor.

Table IV-1 Composition of SolV growth medium.[19]

Solution	Composition
Minimal medium solution (10x)	2 mM $MgCl_2 \cdot 6\ H_2O$, 10 mM Na_2SO_4, 20 mM K_2SO_4, 10 mM NaH_2PO_4, 2 mM $CaCl_2$ **Note:** All components except $CaCl_2$ were mixed and adjusted to pH 2.7 with 1 M H_2SO_4. $CaCl_2$ was autoclaved separately and added afterwards to prevent the precipitation of calcium phosphates.
Trace element (TE) solution	200 mM $FeSO_4 \cdot 7\ H_2O$, 200 mM $MnCl_2 \cdot 4\ H_2O$, 300 mM $CuSO_4 \cdot 5\ H_2O$, 10 mM $NiCl_2 \cdot 6\ H_2O$, 10 mM $ZnSO_4 \cdot 7\ H_2O$, 10 mM $CoCl_2 \cdot 6\ H_2O$, 10 mM $Na_2MoO_4 \cdot 2\ H_2O$ **Note:** All components were dissolved one after the other in 1.5 % v/v H_2SO_4. Solution will occur blue immediately after preparation but turns green after a few days.
Growth medium for *M. fumariolicum* SolV	Prepared according to Pol *et al.*[12b] 1x Minimal medium, 20 μL/L TE, 8 mM NH_4^+ for cultivation in bottles, for the bioreactor experiments the TE concentration was increased to 80 μL/L and 30 mM NH_4^+. All stock solutions were mixed and autoclaved. **Note:** NH_4^+ available from a 2 M $(NH_4)_2SO_4$ solution in MilliQ water.

Cell Lysis of SolV

SolV cells were harvested by centrifugation at 8000 rpm for 10 min (Avanti JXN-26, Beckman Coulter). The cells were resuspended in 10 mM PIPES supplemented with 1 mM MeOH (pH 7.2) and chemically lysed by commercially available BugBuster Protein Extraction Reagent (Merck, product code 70921). 10XBugBuster Protein Extraction Reagent was diluted to 1X with 10 mM PIPES and 1 mM MeOH (pH 7.2). The reagent was added to frozen or thawed cell pellet (2 mL 1X BugBuster per 1 g resuspended cells), followed by the addition of 0.5–1.0 mg/mL lysozyme from chicken egg white (Sigma-Aldrich, CAS 12650-88-3), 0.2-0.5 mg/mL DNase I (PanReac AppliChem, product code A3778,0100) and incubated on a shaking platform for 30–45 min at room temperature. Afterwards, insoluble cell debris were removed by centrifugation (17 000 rpm, 20 min, 4 °C) and the supernatant was filtered through a filter paper (VWR, 5–13 μm particle retention).

Purification of Ln-MDH and cyt c_{GJ} from SolV

The sample was applied on a HiPrep^TM SP Sepharose FF 16/10 cation exchange column (Cytiva, product code 28936544). The column was equilibrated with 10 mM PIPES, 1 mM MeOH (pH 7.2) and bound proteins were eluted using 10 mM PIPES, 1 M NaCl, 1 mM MeOH (pH 7.2). Cyt c_{GJ} eluted at 2% (20 mM NaCl) and Ln-MDH at 25% (250 mM NaCl). Cyt c_{GJ} was further concentrated using an Amicon® Ultra Centrifugal Unit (Merck, product code UFC901024) with a molecular weight cut-off of 10 kDa and applied on a HiLoad^TM 16/600 Superdex^TM 75 pg size exclusion column (Cytiva, product code 28989333). The column was equilibrated with 10 mM PIPES, 0.2 M NaCl (pH 7.2) and cyt c_{GJ} started to elute after 65 mL at a flowrate of 0.3 mL/min. The NaCl concentration was reduced to less than 1 mM with an Amicon® Ultra Centrifugal Unit (Merck, UFC201024) with a molecular weight cut-off of 10 kDa and 10 mM PIPES (pH 7.2).

Methylorubrum extorquens AM1 Cultivation

Cultivations of *M. extorquens* AM1 were started from a frozen stock which was streaked out on MP+S (Table IV-2) agar plates and incubated for seven days. Overnight cultures (3 mL) were grown in MP medium supplemented with 15 mM succinate. For the inoculation 7–10 single colonies were used (12 h, 29 °C, 250 rpm). Ten overnight cultures were combined to inoculate a seed culture with a starting OD_{600} of 0.08 (250 mL, MP+S medium, 29 °C, 250 rpm, 20 h). The cells were separated by centrifugation at an OD_{600} of 2.0 (7 min, 4000 rpm, room temperature) and washed three times with MP+M medium supplemented with 125 mM MeOH. Then, the cells were resuspended in 5 mL of the same medium, the OD_{600} determined and 250 mL cultures (MP+M, 125 mM MeOH, triplicates of 2 μM NdCl₃, no Ln, 29°C, 200 rpm, 44 h) were inoculated with a starting OD_{600} of 0.1.

Table IV-2 Composition of AM1 growth medium.[97]

Solution	Composition
Phosphate (P) solution (100x)	145 mM KH$_2$PO$_4$ · 3 H$_2$O and 188 mM NaH$_2$PO$_4$, adjusted to pH 6.75 with KOH
C7 metal solution (1000x)	45.5 mM sodium citrate · 2 H$_2$O, 1.2 mM ZnSO$_4$ · 7 H$_2$O, 1.0 mM MnCl$_2$ · 4 H$_2$O, 18 mM FeSO$_4$ · 7 H$_2$O, 2 mM (NH$_4$)$_6$Mo$_7$O$_{24}$ · 4 H$_2$O, 1.0 mM CuSO$_4$ · 5 H$_2$O, 2 mM CoCl$_2$ · 6 H$_2$O and 0.33 mM Na$_2$WO$_4$ · 2 H$_2$O. **Note:** All salts need to be dissolved in this exact order.
PIPES solution (10x)	300 mM PIPES, adjusted to pH 6.75 with KOH
Growth medium for *M. extorquens* AM1	Prepared according to Delaney *et al.*[97] Final concentration in 1 L: 1x PIPES solution, 1x P solution, 500 μM MgCl$_2$, 8 mM (NH$_4$)$_2$SO$_4$, 20 μM CaCl$_2$ and 1X C7 **Note:** All stock solutions were mixed and autoclaved separately. Mix all components for growth medium except CaCl$_2$, autoclave and then add CaCl$_2$ afterwards to avoid precipitation of calcium phosphates. For MP + S medium, add 15 mM sodium succinate · 6 H$_2$O For MP + M medium, add 50 mM MeOH

Cell Lysis of AM1

AM1 cells were harvested by centrifugation (7 min, 8000 rpm, room temperature) and resuspended in 20 mM TRIS supplemented with 25 mM MeOH (pH 8.0). Cell lysis of AM1 was performed as mentioned above for SolV but instead of 10 mM PIPES and 1 mM MeOH (pH 7.2), 20 mM TRIS and 25 mM MeOH (pH 8.0) was used for the preparation of 1X BugBuster reagent.

Purification of Ca- and Nd-MDH from AM1

The sample was applied on a HiPrep^{TM} DEAE FF Sepharose 16/10 anion exchange column (Cytiva, product code 28936541). The column was equilibrated with 20 mM TRIS and 25 mM MeOH (pH 8.0). MDH did not bind to the column and elutes immediately at 0 %. Fractions containing MDH were concentrated to 500 µL sample volume using Amicon® Ultra Centrifugal Unit (Merck, product code UFC903024) with a molecular weight cut-off of 30 kDa. Secondly, buffer exchange was performed using a PD MiniTrap^{TM} G-25 (Cytiva, product code 28918007) which was equilibrated with 3 CVs of 25 mM MES buffer containing 25 mM MeOH (pH 5.5). The sample was applied and eluted with 1 mL of 25 mM MES buffer containing 25 mM MeOH (pH 5.5). Then, the sample was purified with a HiPrep^{TM} SP Sepharose FF 16/10 cation exchange column (Cytiva, product code 28936544) using 25 mM MES and 25 mM MeOH (pH 5.5) as buffer A and 25 mM MES and 25 mM MeOH with 0.25 M NaCl (pH 5.5) as buffer B. MDH fractions start eluting around 32% buffer B. MDH fractions were pooled and concentrated using Amicon® Ultra Centrifugal Unit Merck, product code UFC903024) with a molecular weight cut-off of 30 kDa.

Sodium Dodecyl Sulfate–Polyacrylamide Gel Electrophoresis (SDS-PAGE)

Proteins were separated by molecular weight using electrophoresis.[98] Gels were casted using commercially available casting chambers. The resolving and stacking gel were prepared according to Table IV-3. For sample preparation, mPAGE® 4X LDS sample buffer (Merck, product code MPSB-10ML) containing 2% β-mercaptoethanol was added to samples and then heated at 70 °C for 5–7 min. The samples were loaded on a 12% SDS-PAGE gel. The gel was then stained with Coomassie Blue Stain for 1 h and subsequently treated with a destaining solution (10% v/v acetic acid and 20% v/v EtOH in MilliQ water).

Table IV-3 Composition of resolving and stacking gel for SDS-PAGE. APS, ammonium persulfate. TEMED, tetramethylethylendiamine.

	MilliQ H_2O	Rotiphorese (37.5:1)	1.5 M Tris (pH 8.8)	0.5 M Tris (pH 6.8)	10% SDS	10% APS	TEMED
12% v/v resolving gel	4.4 mL	3 mL	2.5 mL	-	100 µL	50 µL	10 µL
4% v/v stacking gel	3.2 mL	0.5 mL	-	1.25 mL	50 µL	25 µL	7.5 µL

Protein Concentration Determination

UV/Vis Traycell (Hellma)

The protein concentration was calculated with the following equation:

$$\text{Concentration (mg/mL)} = \frac{1}{\text{sample specific factor}} \times \text{absorbance} \times \text{dilution factor}$$

The absorbance at 280 nm was measured with a Cary60 spectrophotometer (Agilent) and a TrayCell (Hellma) with a dilution factor of 10. The specific factor was determined for each Ln-MDH and cyt c_{GJ} batch.

UV/Vis cuvette

The protein concentration was calculated using the Beer-Lambert law:

$$A_{280} = c \times \varepsilon \times d$$

The absorbance A_{280} was either recorded with a Cary60 spectrophotometer (Agilent) and a 10 mm pathlength Quartz suprasil cuvette (Hellma) or a 10 mm pathlength disposable cuvette micro (Brand). The molar extinction coefficient of MDH was previously determined at 158 mM^{-1} cm^{-1}.[12b] If not stated otherwise, measurements with a Cary 60 UV/Vis spectrophotometer (Agilent) were recorded from 200–800 nm, the scanning speed was set to fast and sample spectra were baseline corrected by subtracting the buffer spectrum. Data were analyzed with Gen5 and Origin 2023.

Metal Analysis by ICP-MS

The Ln-content of each Ln-MDH was determined by addition of the samples to 3% nitric acid (Suprapur®, Supelco) and heating for 1 h at 90 °C. The samples were submitted to Christine Benning (Haisch Lab, TUM) for measurement using an Inductively Coupled Plasma Mass Spectrometer (NexION 350D, Perkin Elmer) and the Aristar® ICP-MS Calibration Standard 10 µg/mL (VWR). Protein

concentration were determined spectrophotometrically at 280 nm using an extinction coefficient of 158 cm^{-1} mM^{-1}.[12b]

Protein-Coupled Activity Assay

The protein-coupled activity assays with cyt c_{GJ} are based on the protocols reported by Gutenthaler *et al.* and Phi *et al.*[19, 40] The enzymatic activity of Ln-MDH was assessed through the reduction of secondary cyt *c* from equine heart cytochrome *c* (Sigma, CAS 9007-43-6). The reaction was monitored with an Epoch2 plate reader (BioTek) at 45 °C through the increase of A$_{550}$. All experiments were conducted in 96-well plates without the lid and each assay mixture usually contains a total volume of 100 µL with 50 µM equine heart cyt *c*, 0–10 µM cyt c_{GJ}, 0–200 nM Ln-MDH and 0–50 mM MeOH in a buffer solution. Experimental details are found in the description of each figure. Everything but Ln-MDH were mixed and incubated for 2 min at 45 °C before the reaction was initiated with addition of Ln-MDH which was also incubated for 2 min at 45 °C. The extinction coefficient of cyt *c* from equine heart was previously determined at 19.5 mM^{-1} cm^{-1} for 10 mM PIPES pH 7.2 and in MC buffer as shown in Table III-3.[32] The specific activity was calculated using the initial slope (usually 30–120 s) after Ln-MDH addition. If specified, the specific activity of each experiment was adjusted according to the metal content of the Ln-MDH.

$$enzyme\ unit\ U\ [\mu mol\ min^{-1}] = \frac{initial\ rate\ of\ slope\ of\ measurement}{\varepsilon\ [cm^{-1}M^{-1}] \cdot pathlength\ of\ cell\ [cm]} \cdot 10^6 \cdot volume\ of\ assay\ [L]$$

$$specific\ activity\ [\mu mol\ min^{-1}\ mg^{-1}] = \frac{enzyme\ unit\ U\ [\mu mol\ min^{-1}]}{amount\ of\ enzyme\ [mg]}$$

$$specific\ activity_{adjusted}\ [\mu mol\ min^{-1}\ mg^{-1}] = \frac{enzyme\ unit\ U\ [\mu mol\ min^{-1}]}{amount\ of\ enzyme\ [mg] \cdot \frac{metal\ content\ [\%]}{100}}$$

Dye-coupled Activity Assay

The dye-coupled activity assays with PES and DCPIP are based on the protocols reported by Gutenthaler *et al.* and Phi *et al.*[19, 40] The activity assay with the artificial electron acceptor DCPIP (Honeywell, CAS: 1266615-56-8) and PES (Sigma-Aldrich, CAS 10510-77-7) was assessed through the reduction of DCPIP. The reaction was monitored with an Epoch2 plate reader (BioTek) through the decrease of A$_{600}$. All experiments were conducted in 96-well plates without the lid and each assay mixture usually contains a total volume of 100 µL with 1 mM PES, 100 µM DCPIP, 100 nM Ln-MDH, 50 mM MeOH in a buffer solution. Everything but Ln-MDH were mixed and incubated for 2 min at 45 °C in the dark before the reaction was initiated with addition of MDH which was also incubated for 2 min at 45 °C. The extinction coefficient of DCPIP was determined at 19.8 mM^{-1} cm^{-1} for 10 mM PIPES (pH

7.2). The specific activity was calculated using the initial slope (usually 30–120 s) after Ln-MDH addition. If specified, the specific activity of each experiment was adjusted according to the metal content of the Ln-MDH.

$$enzyme\ unit\ U\ [\mu mol\ min^{-1}] = \frac{-1 \cdot initial\ rate\ of\ slope\ of\ measurement}{\varepsilon\ [cm^{-1}M^{-1}] \cdot pathlength\ of\ cell\ [cm]} \cdot 10^6 \cdot volume\ of\ assay\ [L]$$

$$specific\ activity\ [\mu mol\ min^{-1}\ mg^{-1}] = \frac{enzyme\ unit\ U\ [\mu mol\ min^{-1}]}{amount\ of\ enzyme\ [mg]}$$

$$specific\ activity_{adjusted}\ [\mu mol\ min^{-1}\ mg^{-1}] = \frac{enzyme\ unit\ U\ [\mu mol\ min^{-1}]}{amount\ of\ enzyme\ [mg] \cdot \frac{metal\ content\ [\%]}{100}}$$

Michael-Menten Kinetics

The Michaelis-Menten constant K_M and the maximum turnover speed v_{max} of the protein-coupled activity assay (0–30 µM) with 100 nM Nd-MDH were calculated with the Michaelis-Menten equation using the slope of the initial 2 min after initiation:

$$v_0 = \frac{v_{max}[S]}{K_M + [S]}$$

With v_0 representing the initial velocity and [S] the substrate concentration. The specific activity of each experiment was adjusted according to the metal content of Nd-MDH (47.8%).

Isothermal Titration Calorimetry

ITC experiments were conducted using the MicroCal PEAQ-ITC (Malvern Panalytical). The reference cell was filled with H_2O, the temperature set to 45 °C, the stirring speed set to 750 rpm, feedback set to high, the initial delay set to 60 s and the single injection mode was used. The cell contained 5 µM cyt c_{GJ}, 50 µM cyt *c* from equine heart and 20 mM MeOH. The syringe was filled 10 µM Pr- or Eu-MDH and 5 µL was injected over 5 s into the cell. The raw data was processed with Origin 2023 and the area under the curve was calculated using its integration tool.

Electrochemical Assay

The electrochemical assessment of Ln-MDH is based on the protocol reported by Kalimuthu *et al*. with minor adjustments.[34] CV experiments were conducted with a BAS 100B/W electrochemical workstation at room temperature. The buffer was changed to 20 mM PIPES (pH 7.2), but the Au RDE

(3 mm diameter) was otherwise prepared identical to the stationary electrode: incubation of the electrode surface for 16 h in 10 mM mercaptoundecanol (dissolved in EtOH), addition of 2 μL cyt c_{GJ} and 2 μL of 0.25% chitosan (dissolved in 1% acetic acid) mixture onto the electrode surface (drying for 3 h at 4 °C) and finally addition of 3 μL of Ln-MDH (drying for 2 h at 4 °C). A dialysis membrane with a MWCO of 3.5 kDa (Serva, product code 44310.01) was used to constrain the proteins close to the electrode surface. The concentration of cyt c_{GJ} was not determined and further experimental details are found in the description of each figure.

Determination of Extinction Coefficient ε

The extinction coefficients (Table III-3) were calculated by subtracting the absorbance of the oxidized cyt *c* equine heart from the absorbance of its fully reduced form. A dilution series of cyt *c* (0, 25, 50 and 100 μM) for every condition was prepared (Figure V-33). The oxidized cyt *c* was purchased and used at is it, while the reduced cyt *c* was obtained by the addition of 100 equivalents of reductant $Na_2S_2O_4$ to cyt *c*. The absorbance at 550 nm for every sample was measured with Cary 60 UV/Vis spectrophotometer (Agilent). The absorbance was plotted against the concentration of cyt *c* and linear regression was applied to obtain a slope. The slope was divided by the path length (d = 0.1 cm) to obtain the extinction coefficient value for cyt *c* in its oxidized and reduced form.

Kinetic Isotope Effect Studies

10 mM MC (2.5 mM of citric acid, Bis-Tris, Tris and CHES each) buffer was prepared in either H_2O or D_2O. The pH was adjusted with a pH-meter using HCl or NaOH. The pD was adjusted with the formula pD = pH + 0.4 and DCl or NaOD.[90] When H_2O-MC buffer was used, all assay components were prepared in either H_2O or H_2O-MC. Proteins were washed in H_2O-MC as well. Similarly, when D_2O-MC was used as buffer, all assay components were prepared in either D_2O or D_2O-MC and washed in D_2O-MC. H_2O-MC buffer (pH 7) with increasing amount of D_2O (0, 25, 50, 75 and 100% D_2O) were prepared by combining the respective amount of H_2O-MC buffer (pH 7) and D_2O-MC buffer (pD 7), e.g. 25% D_2O buffer contained 75% v/v H_2O-MC buffer and 25% v/v D_2O-MC buffer. The final assay mixture contained 100 nM Pr-MDH, 50 μM cyt *c* from equine heart, 20 μM MeOH/MeOD and 5 μM cyt c_{GJ}. Samples were prepared in a micro-cuvette (Hellma, product code 104002B-10-40). Buffer and assay mixture (Pr-MDH, cyt *c* from equine heart and MeOH/MeOD) were mixed and incubated at 45 °C for 1 min. If no background reaction was observed, the reaction was initiated with cyt c_{GJ}. The initial slope (after addition of cyt c_{GJ}) was measured to calculate the specific activity. Spectra were recorded with Cary 60 UV/Vis spectrophotometer (Agilent) using the "Kinetics" program.

V. Appendix

1. Supporting Information

1.1 Supporting Information for Chapter II.2
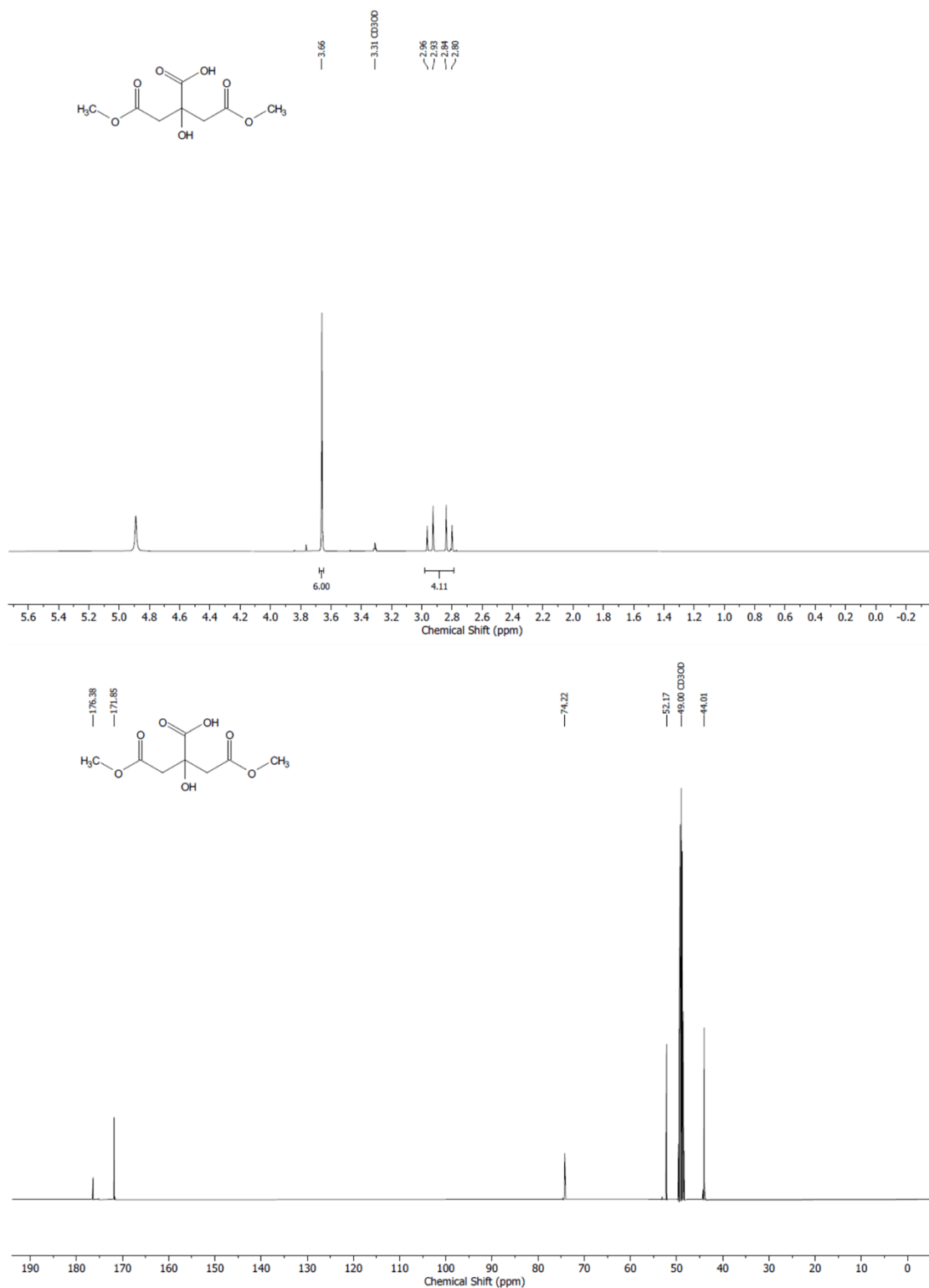
Figure V-1 ^{1}H and ^{13}C NMR spectra of **1** in MeOD-d$_4$.
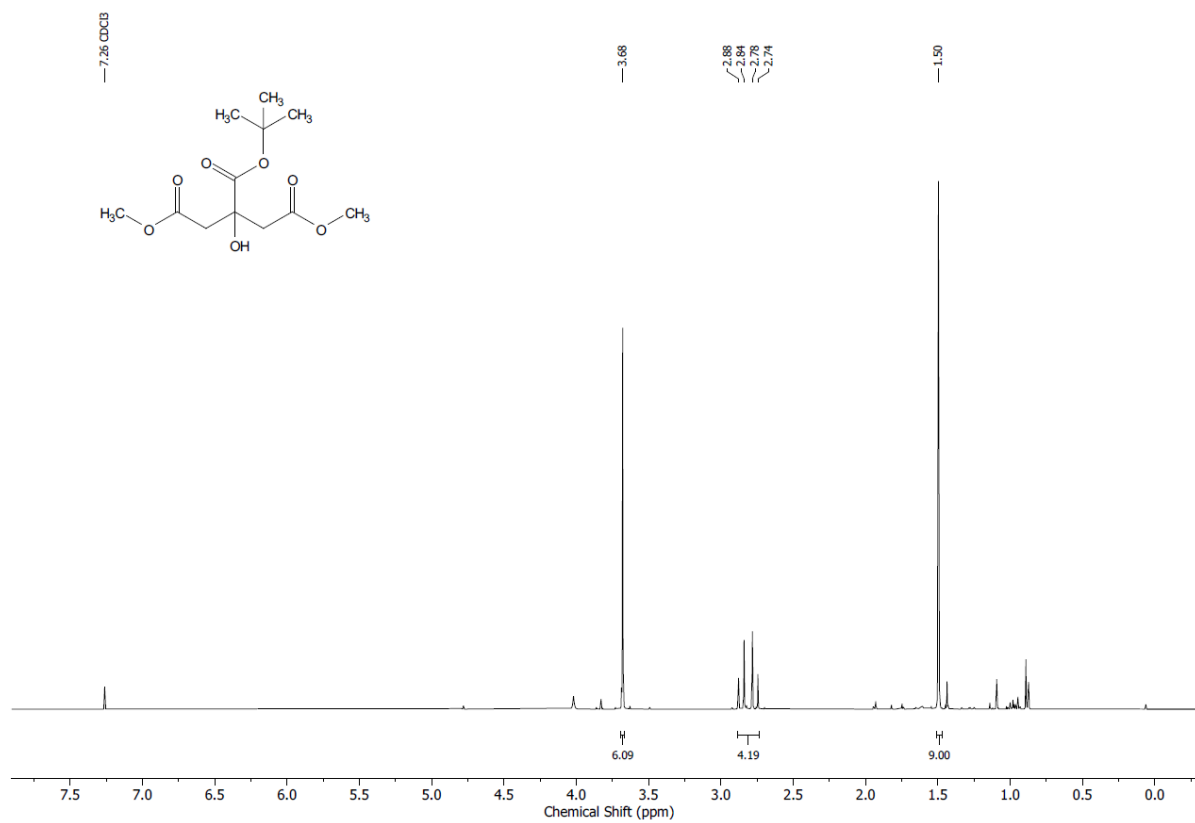
Figure V-2 ^{1}H spectrum of **2** in CDCl$_3$.
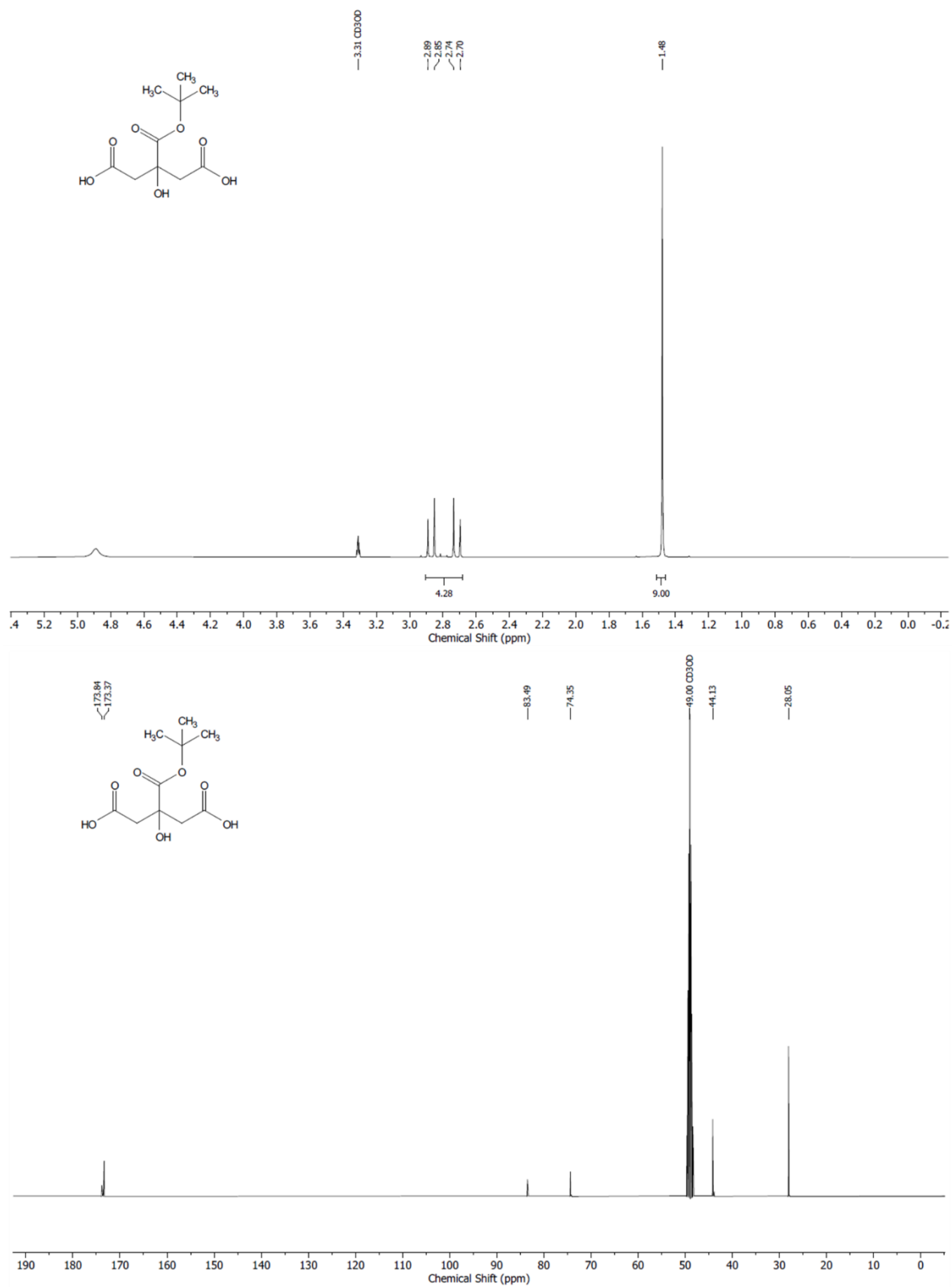
Figure V-3 ^{1}H and ^{13}C NMR spectra of **3** in MeOD-d$_4$.
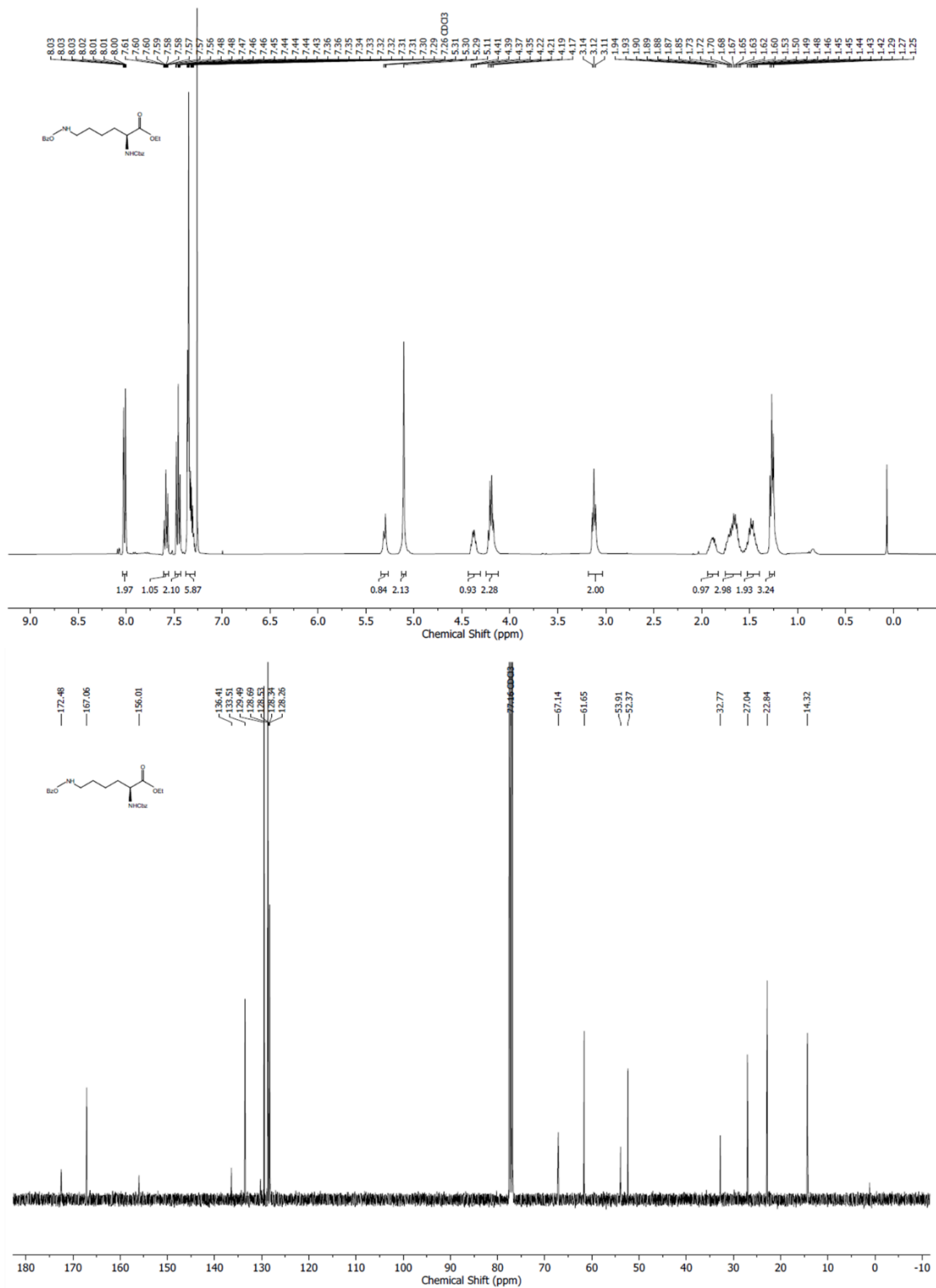
Figure V-4 ^{1}H and ^{13}C NMR spectra of intermediate towards **7** in CDCl$_3$.
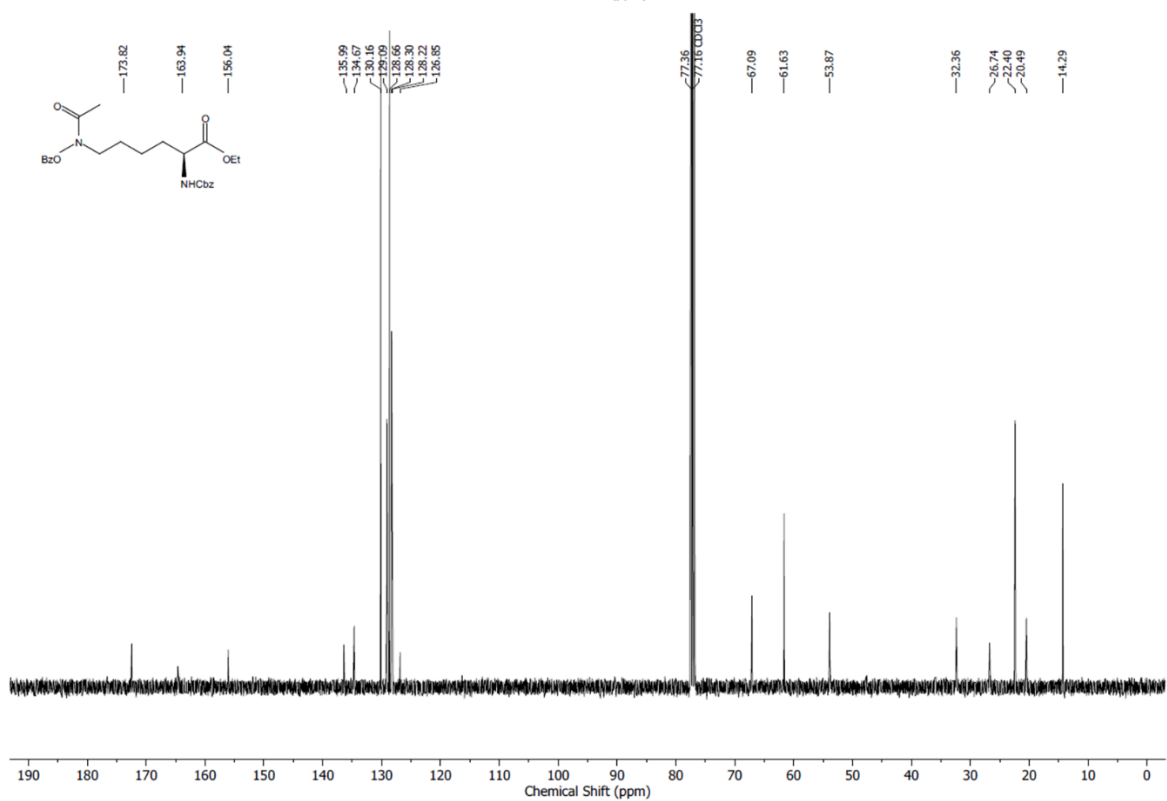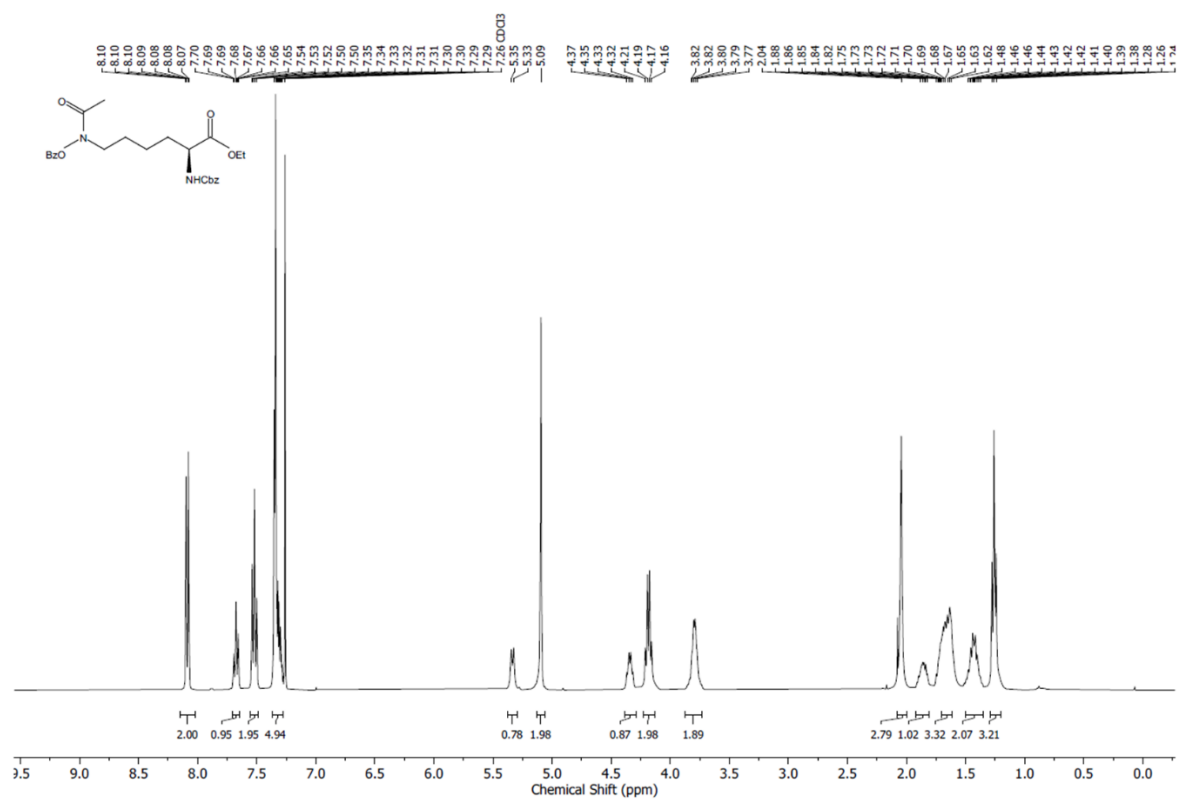
Figure V-5 ¹H and ¹³C NMR spectra of **7** in CDCl₃.
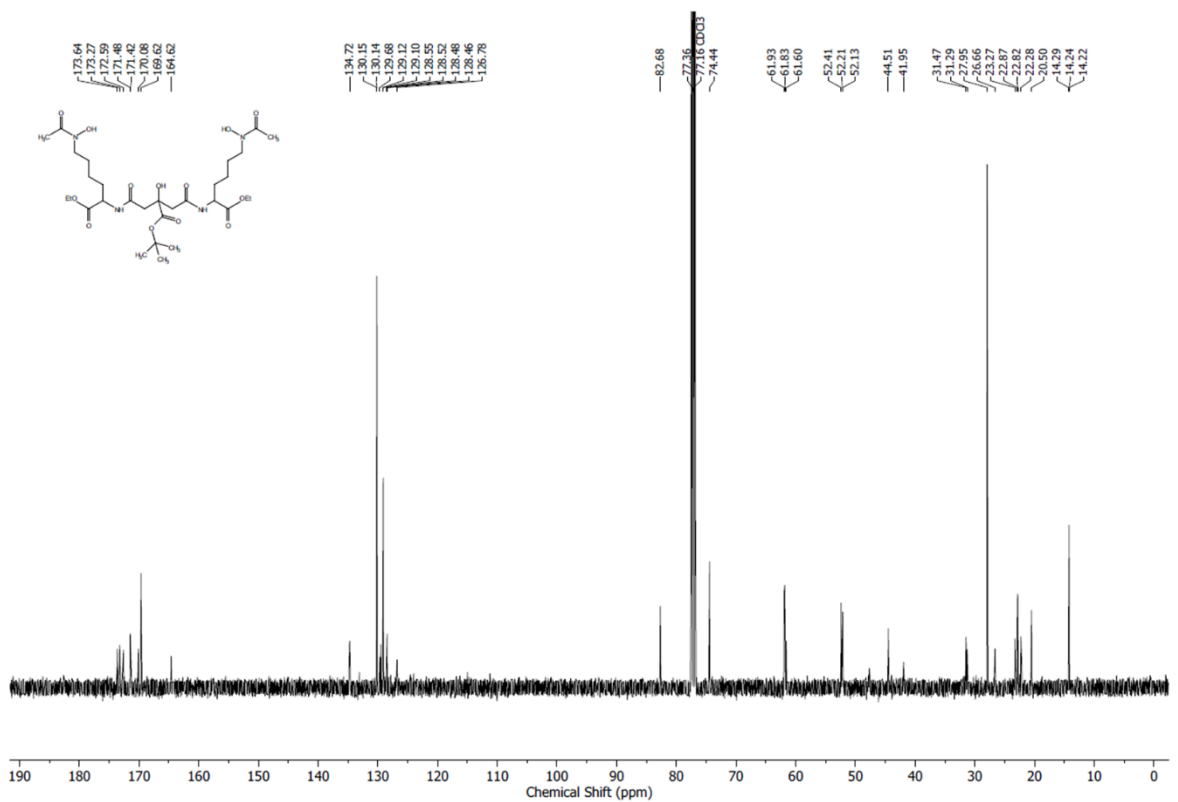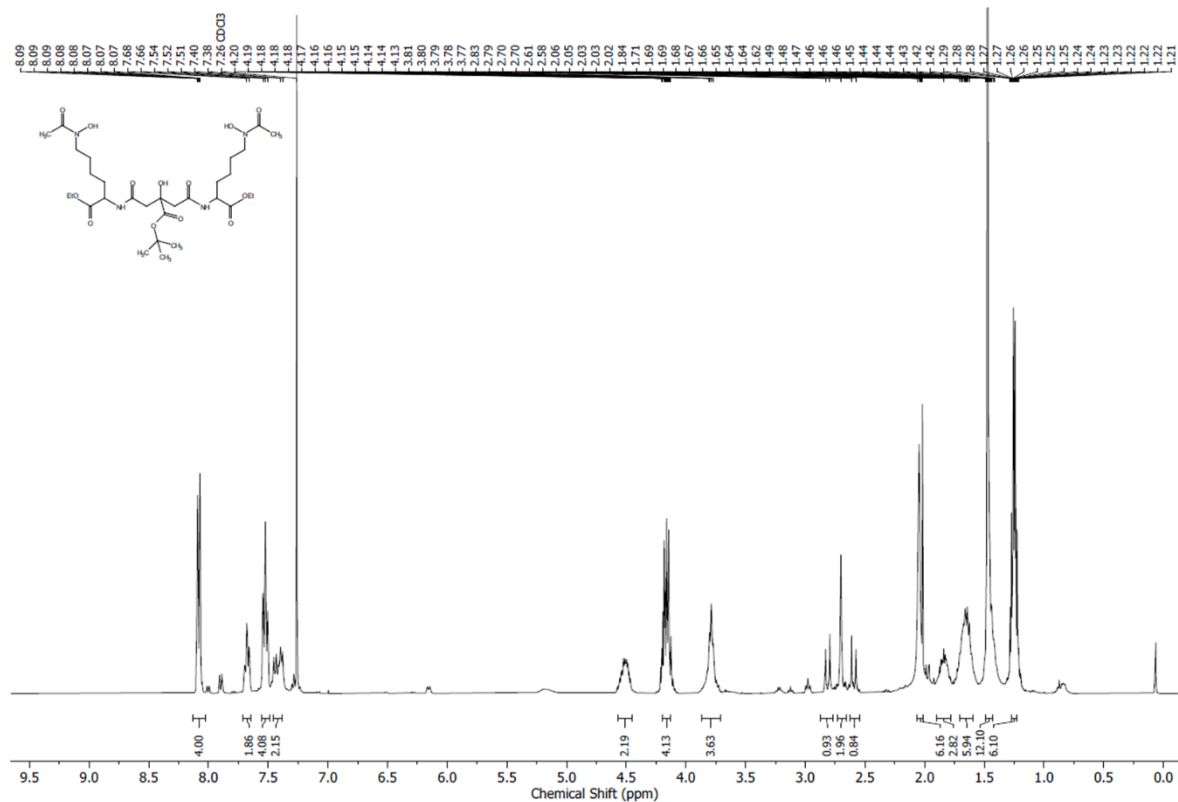
Figure V-6 ^{1}H and ^{13}C NMR spectra of **9** in CDCl$_3$.
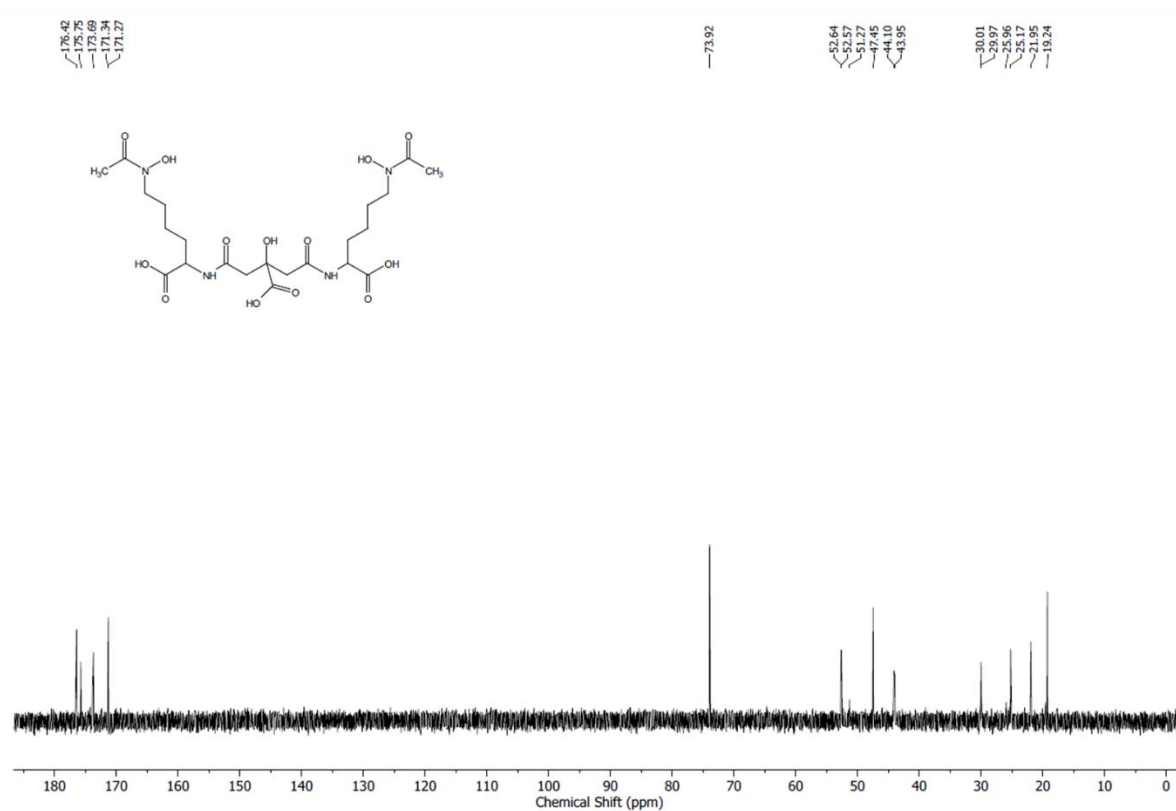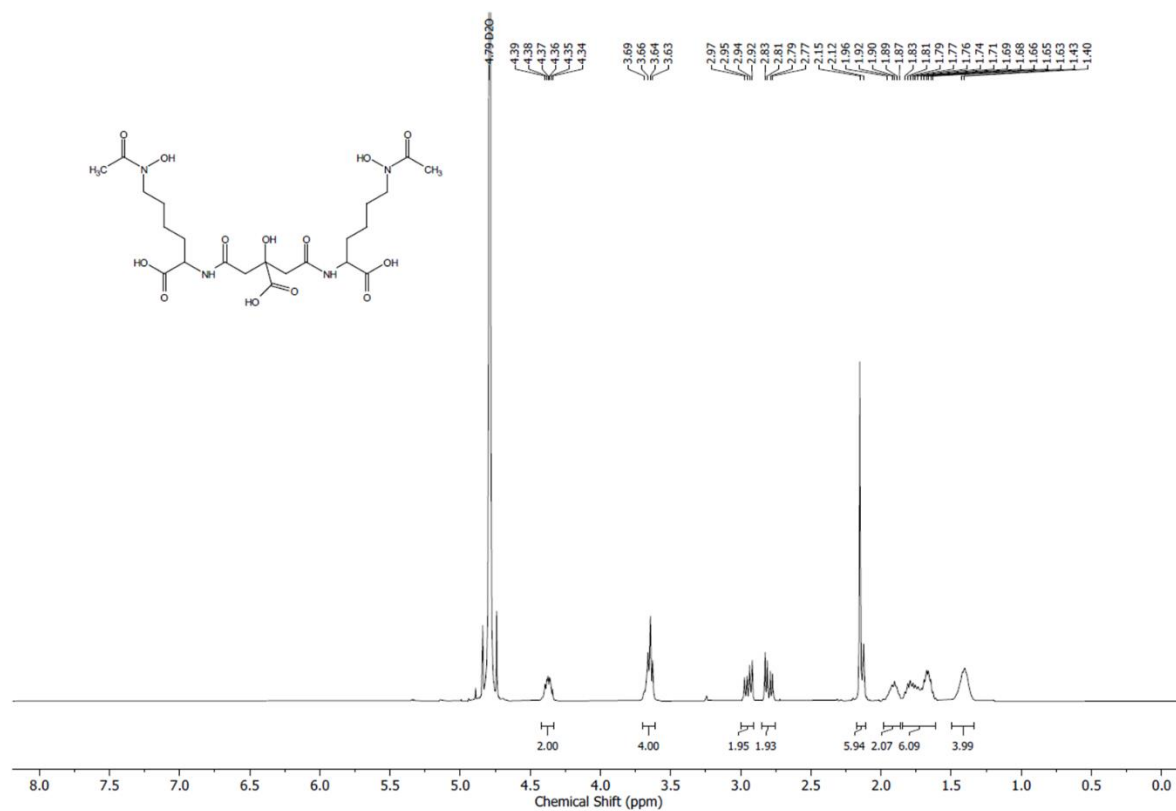
Figure V-7 ^{1}H and ^{13}C NMR spectra of aerobactin in D$_2$O.

1.2 Supporting Information for Chapter II.3
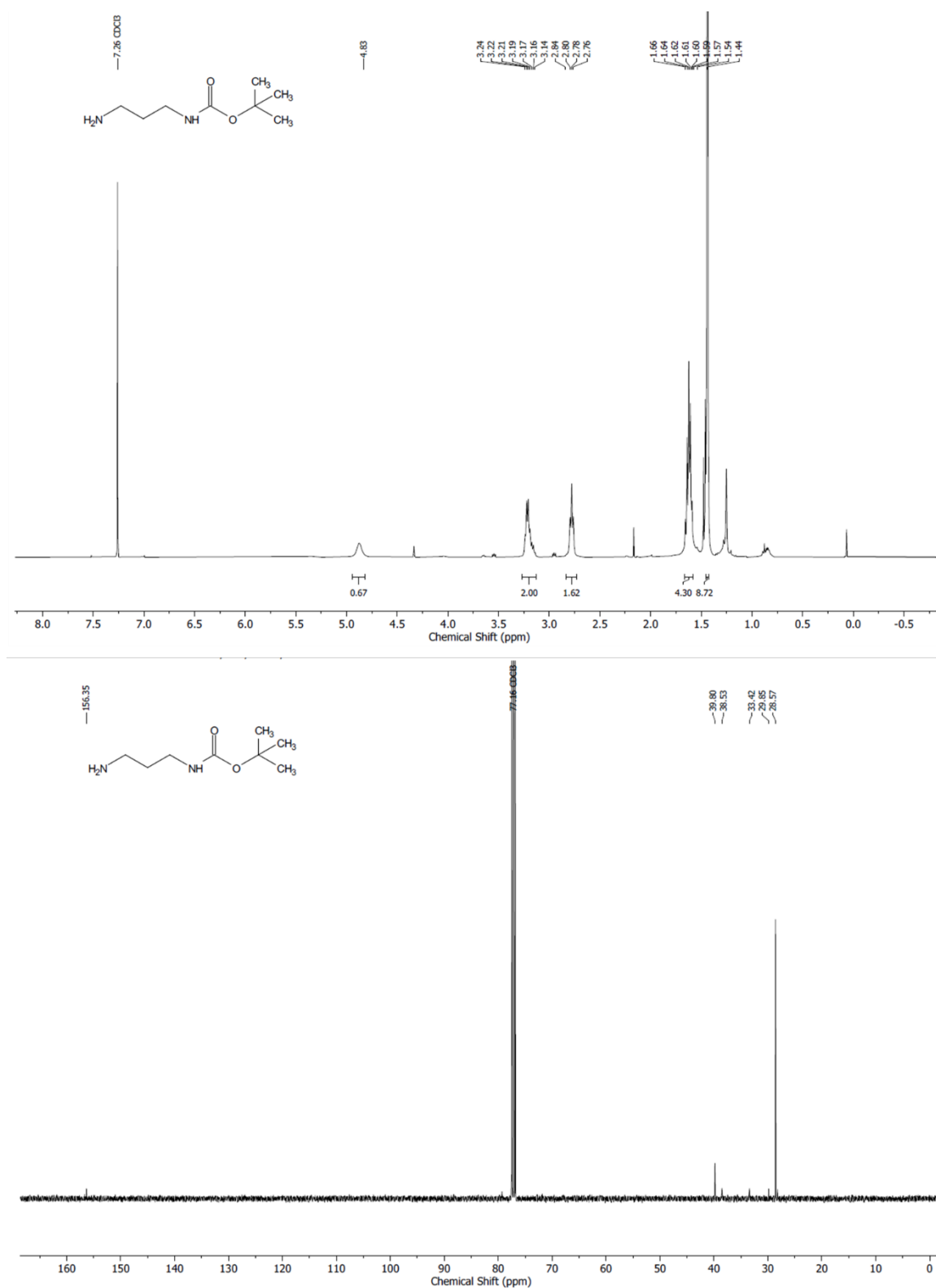
Figure V-8 ^{1}H and ^{13}C NMR spectra of **12** in CDCl$_3$.
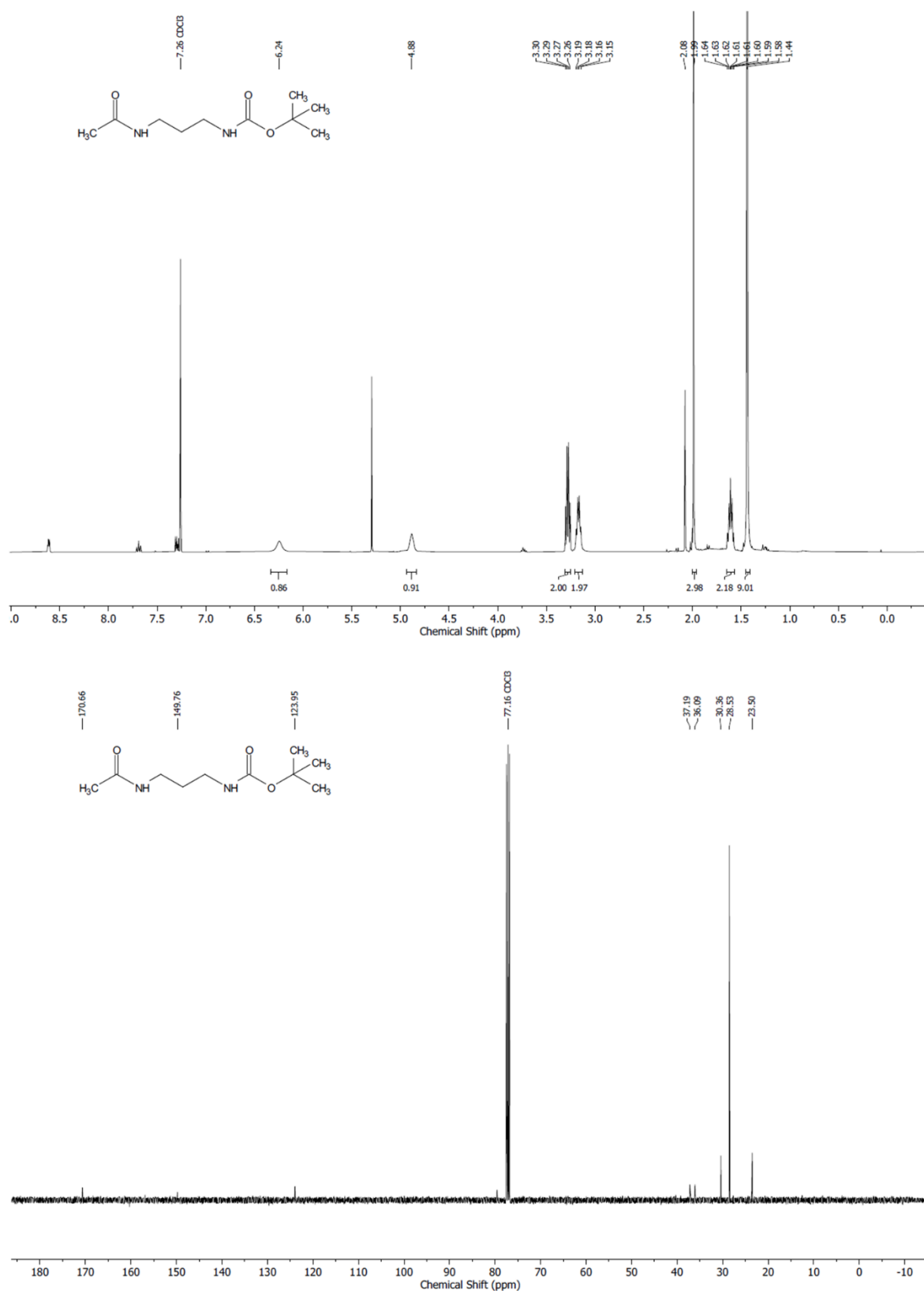
Figure V-9 ^{1}H and ^{13}C NMR spectra of **10** in CDCl[3].
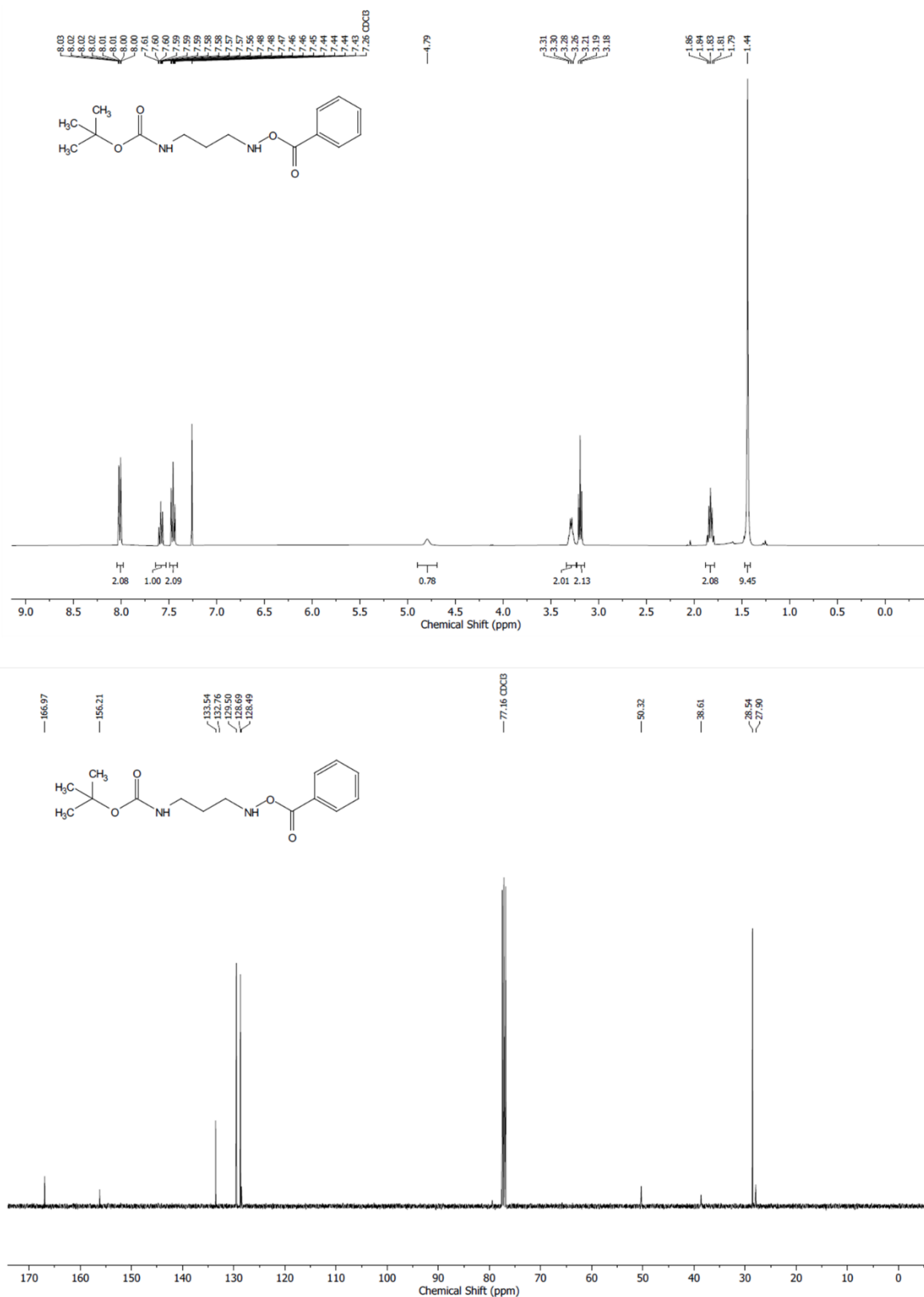
Figure V-10 ^{1}H and ^{13}C NMR spectra of intermediate towards **11** in CDCl$_3$.
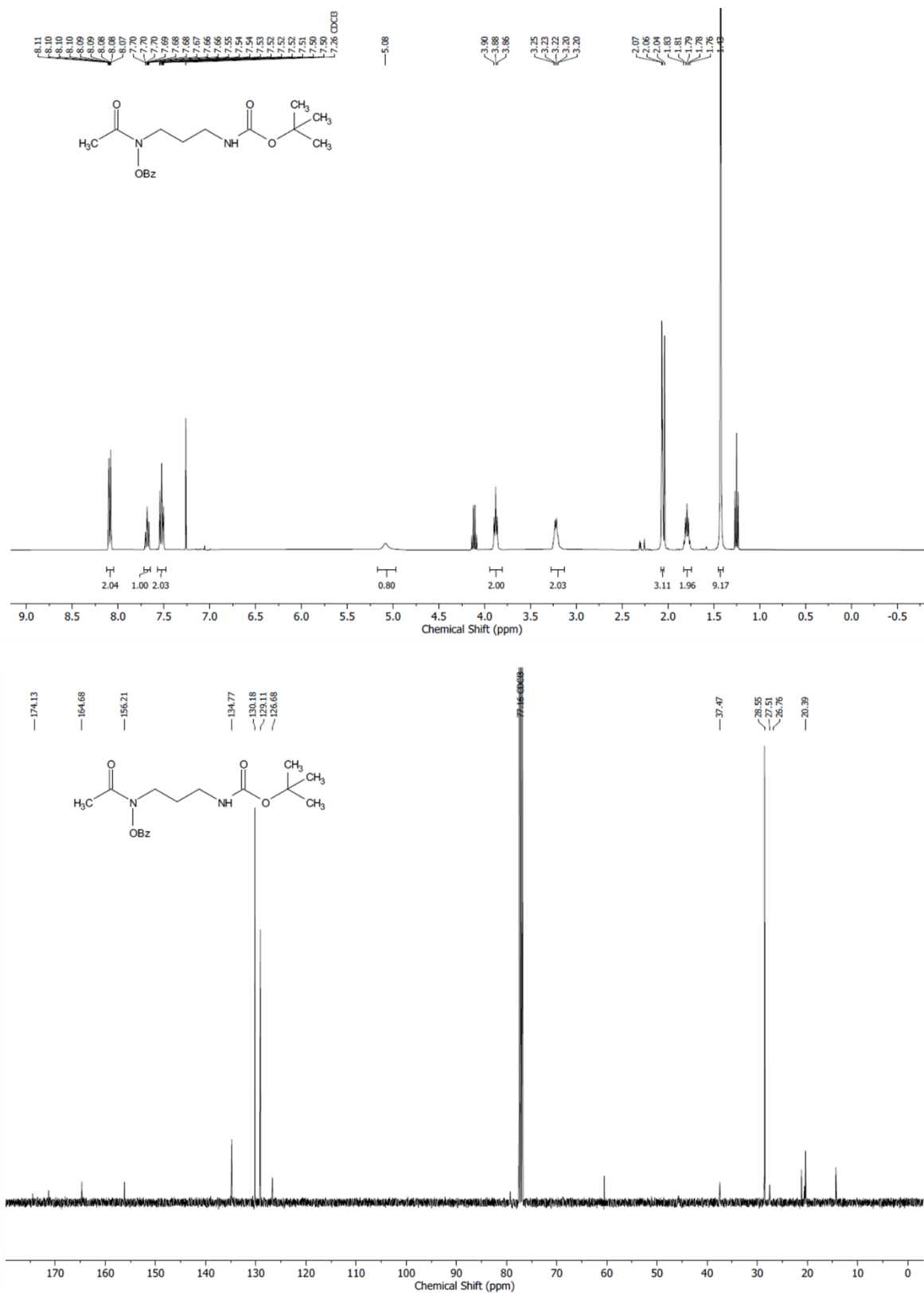
Figure V-11 ^{1}H and ^{13}C NMR spectra of **11** in CDCl$_3$.
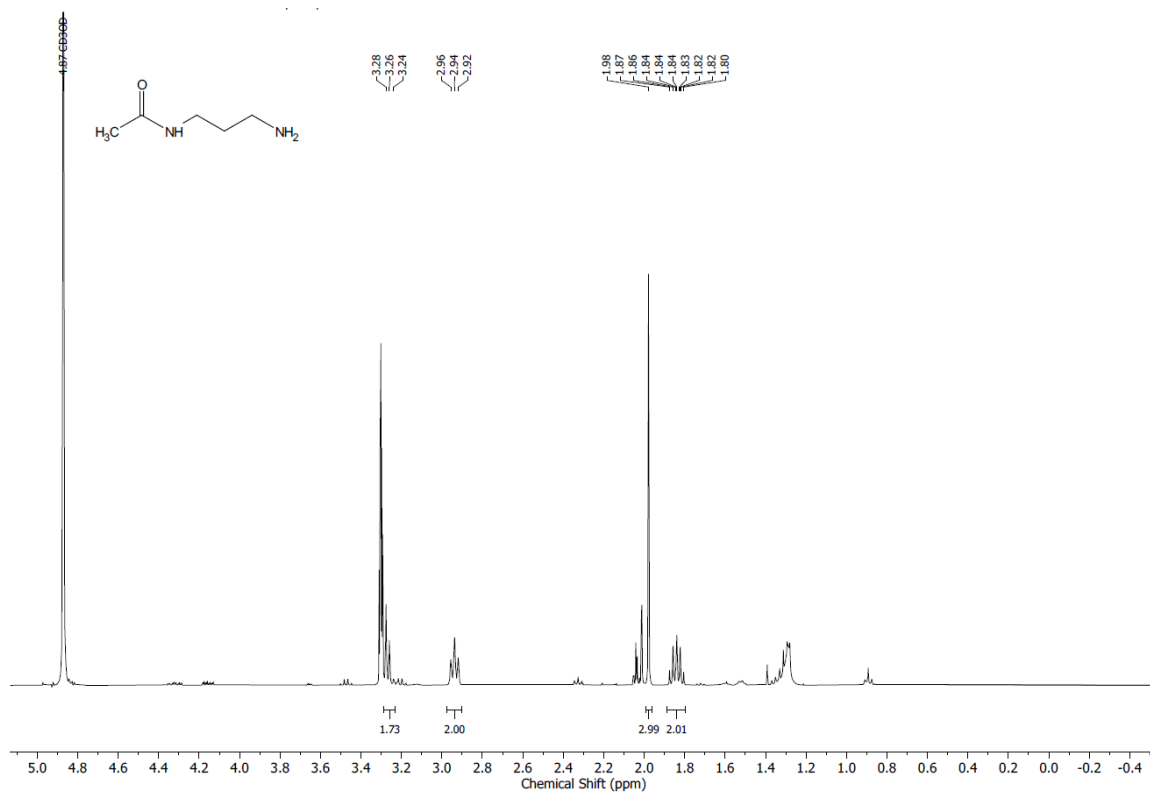
Figure V-12 ^{1}H NMR spectrum of **13** in CDCl$_3$.
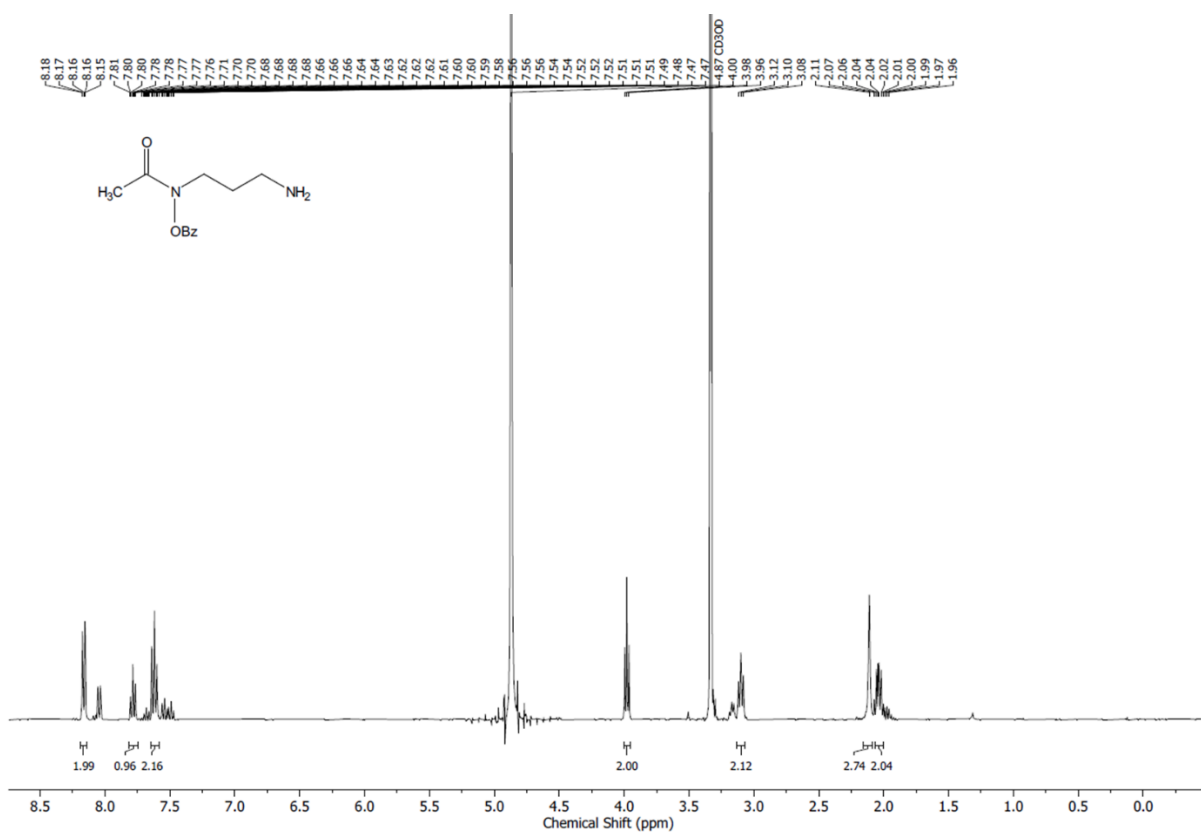
Figure V-13 ^{1}H NMR spectrum of **14** in CDCl$_3$.
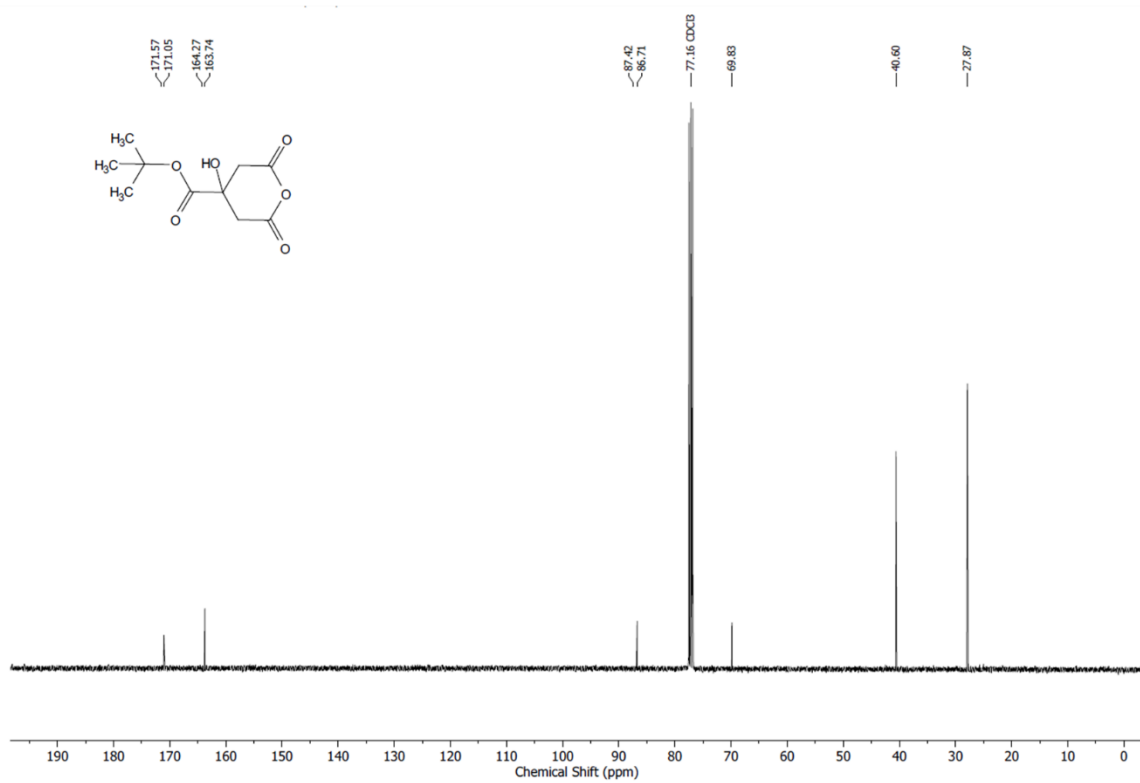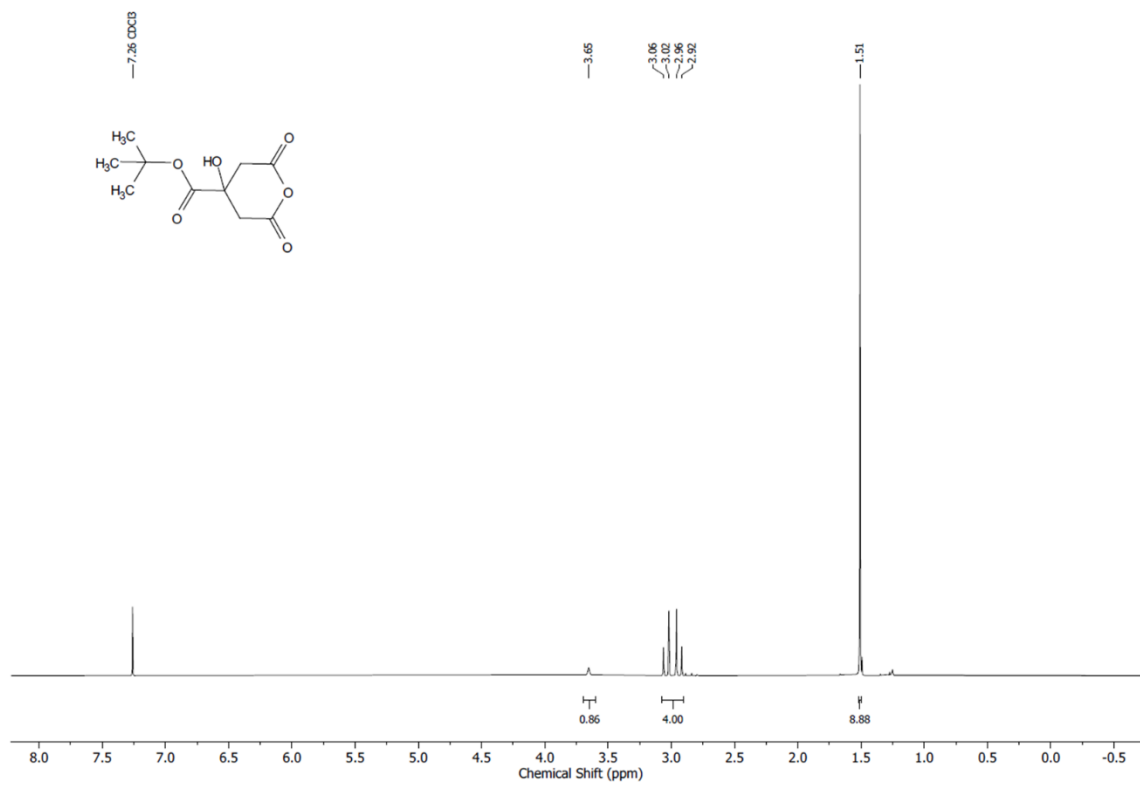
Figure V-14 ^{1}H and ^{13}C NMR spectra of **16** in CDCl$_3$.

1.3 Supporting Information for Chapter III.5
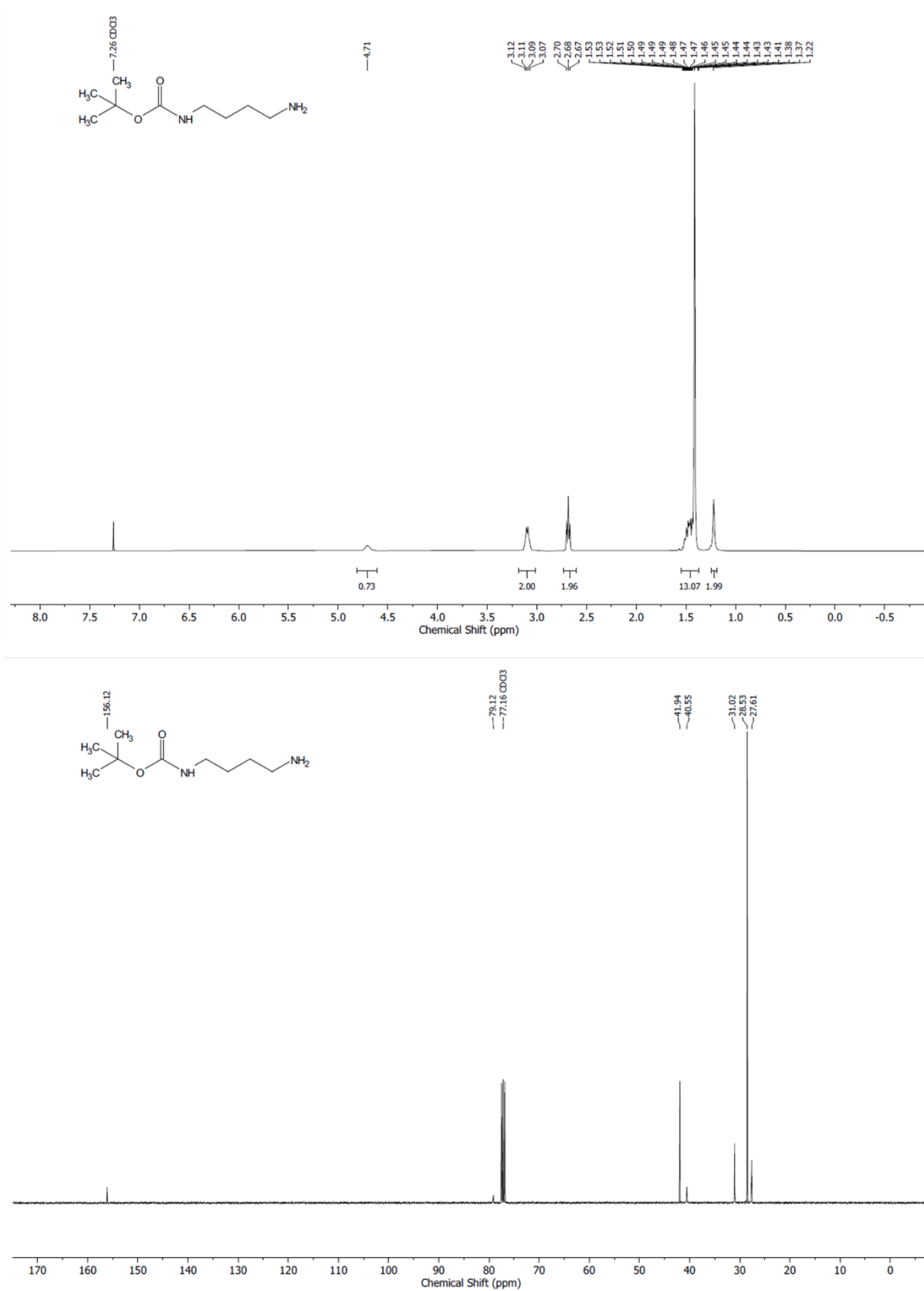
Figure V-15 ^{1}H and ^{13}C NMR spectra of **22** in CDCl$_3$.
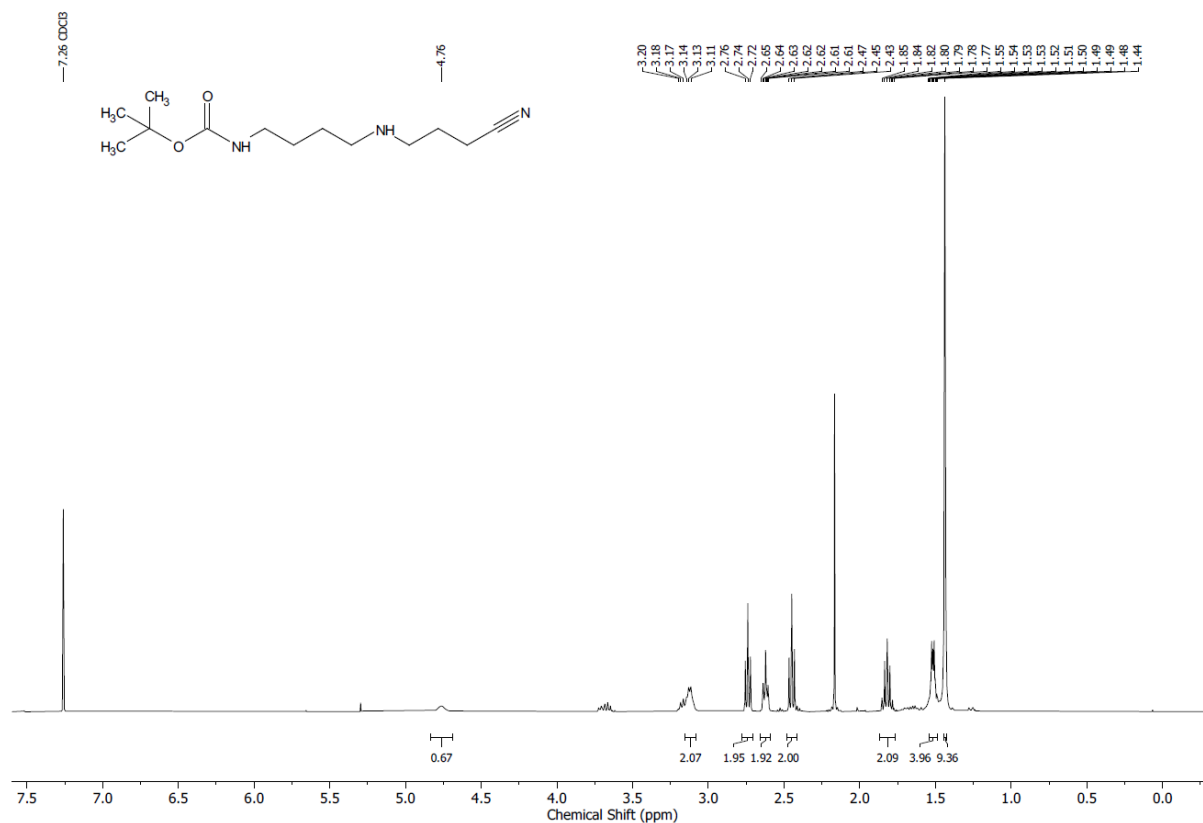
Figure V-16 ^{1}H NMR spectrum of **23** in CDCl$_3$.
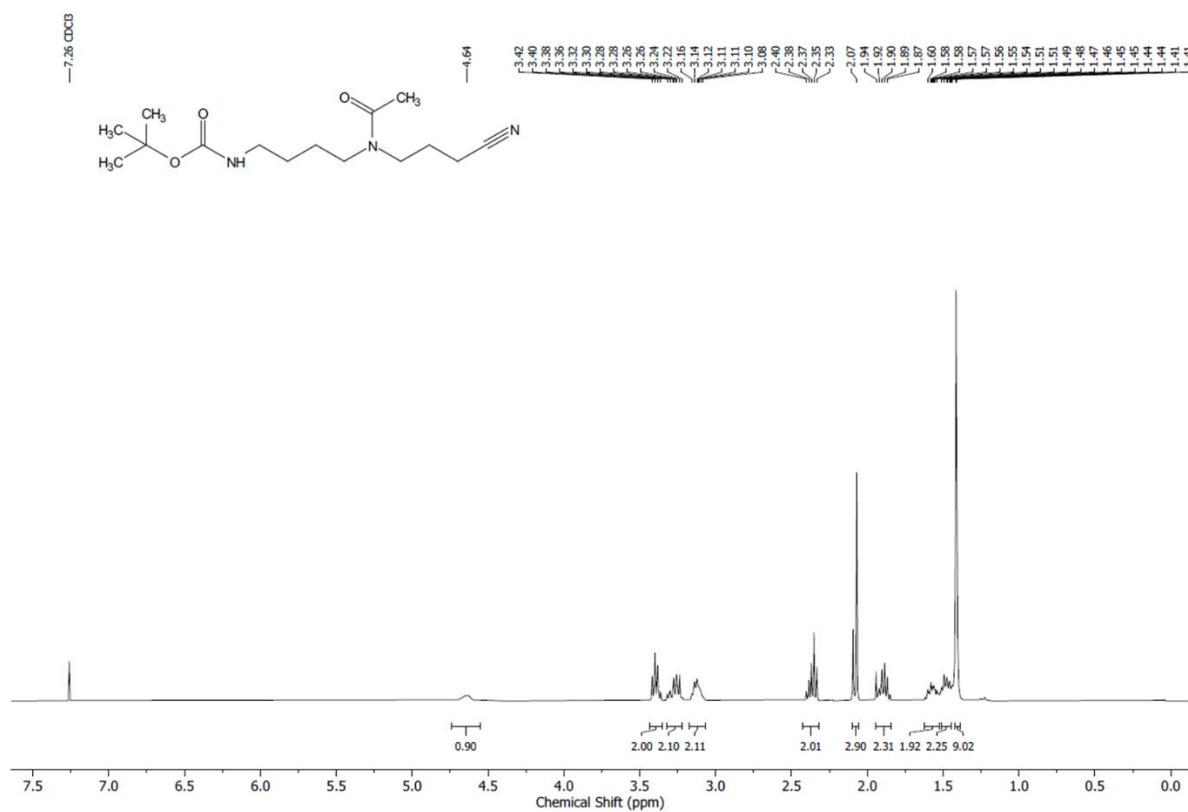
Figure V-17 ^{1}H NMR spectrum of **24** in CDCl$_3$.
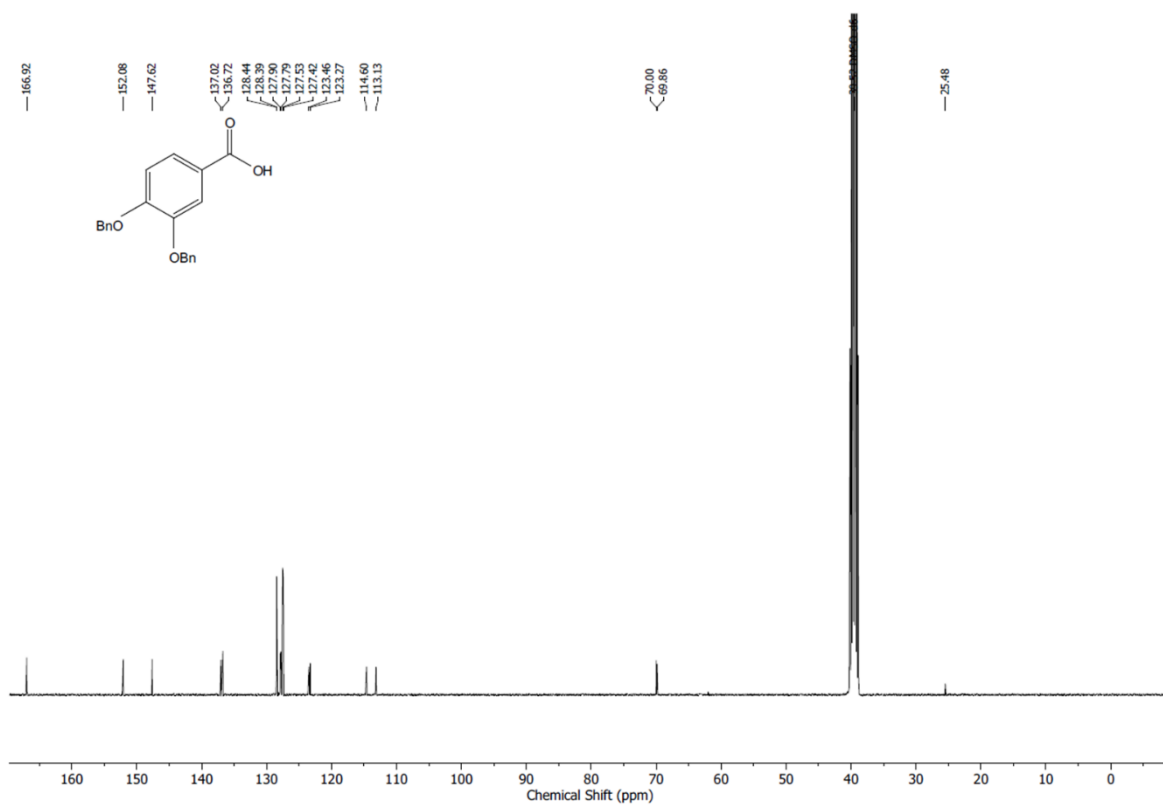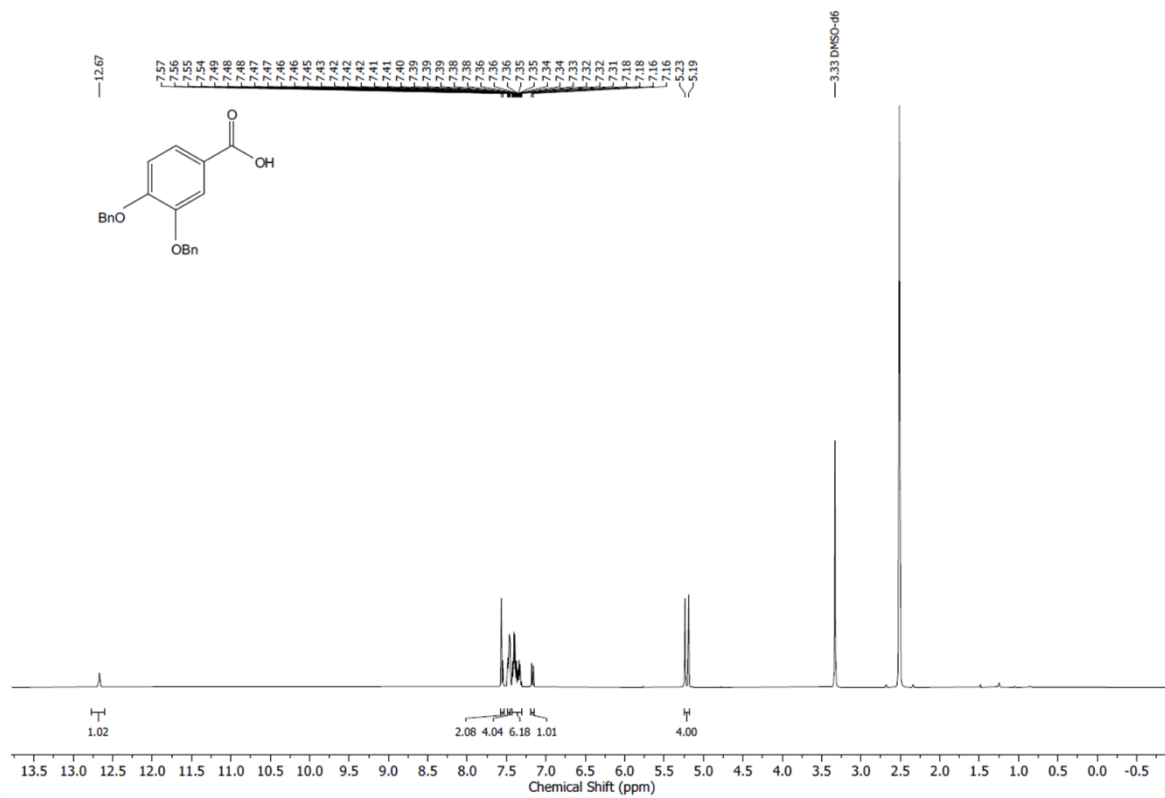
Figure V-18 ^{1}H and ^{13}C NMR spectra of **21** in DMSO-d$_6$.
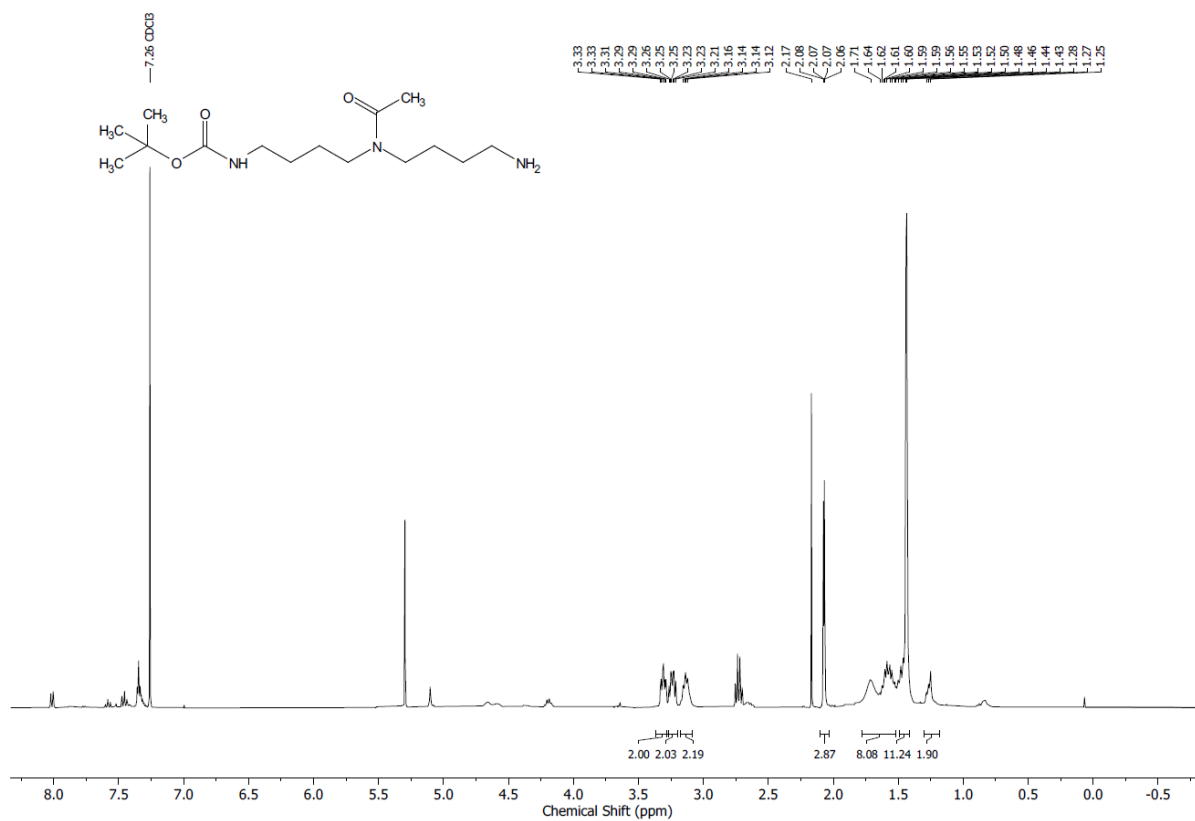
Figure V-19 ^{1}H NMR spectrum of **19** in CDCl$_3$.
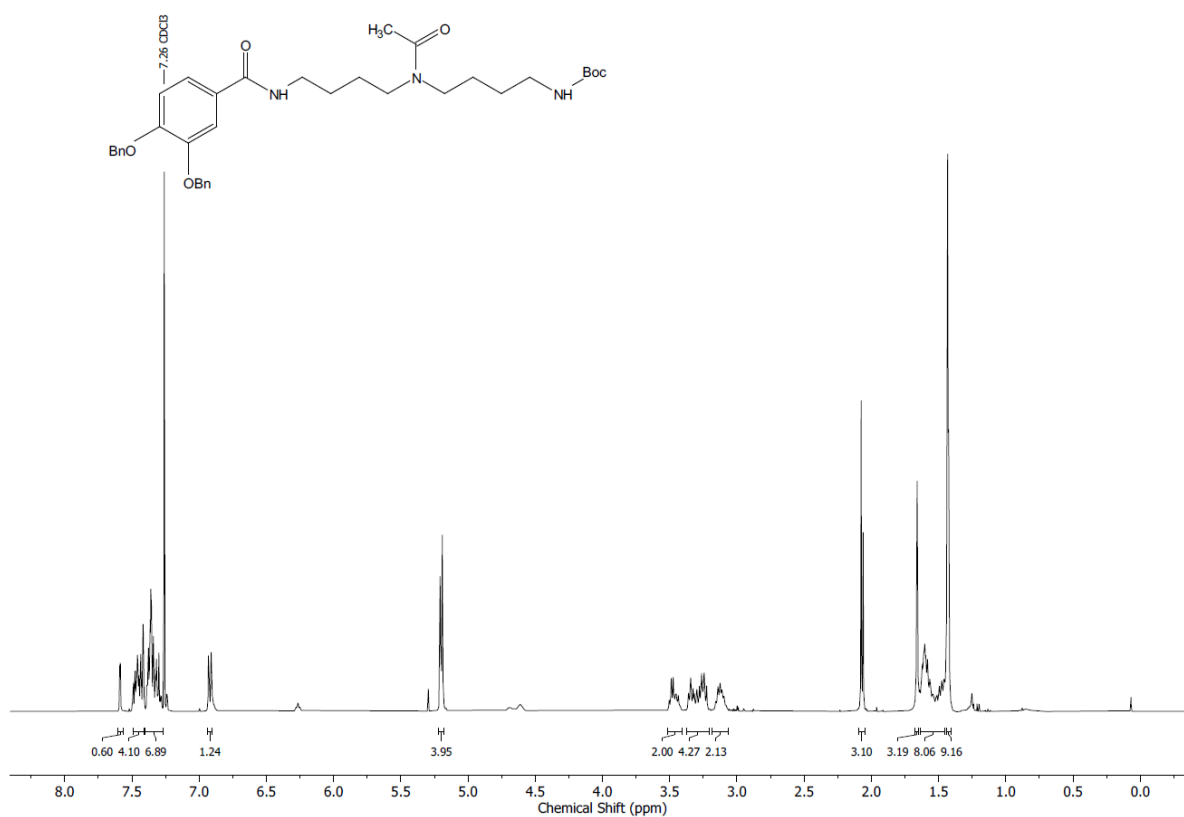
Figure V-20 ^{1}H NMR spectrum of **25** in CDCl$_3$.
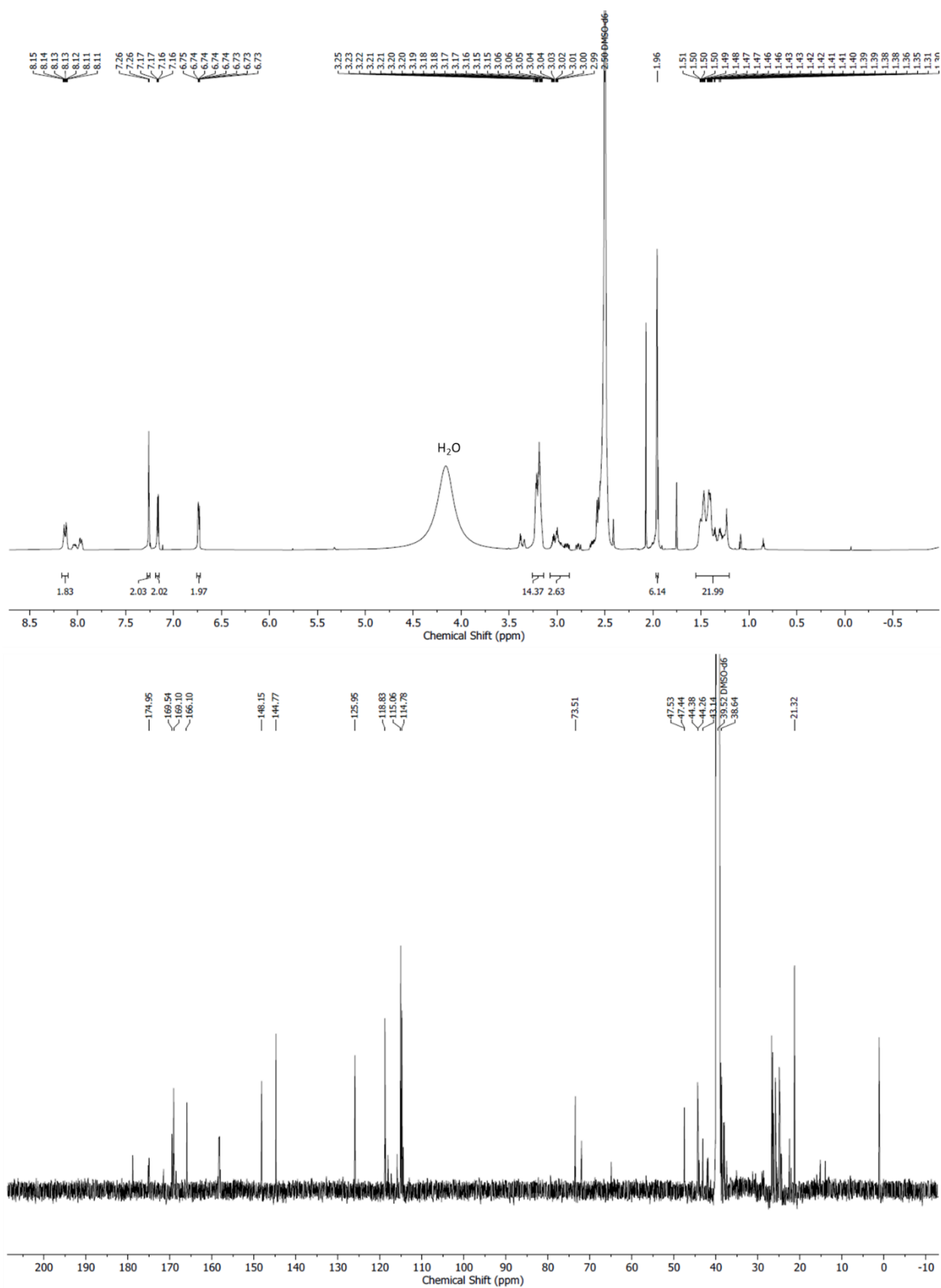
Figure V-21 ^{1}H and ^{13}C NMR spectra of rhodopetrobactin B in DMSO-d$_6$.
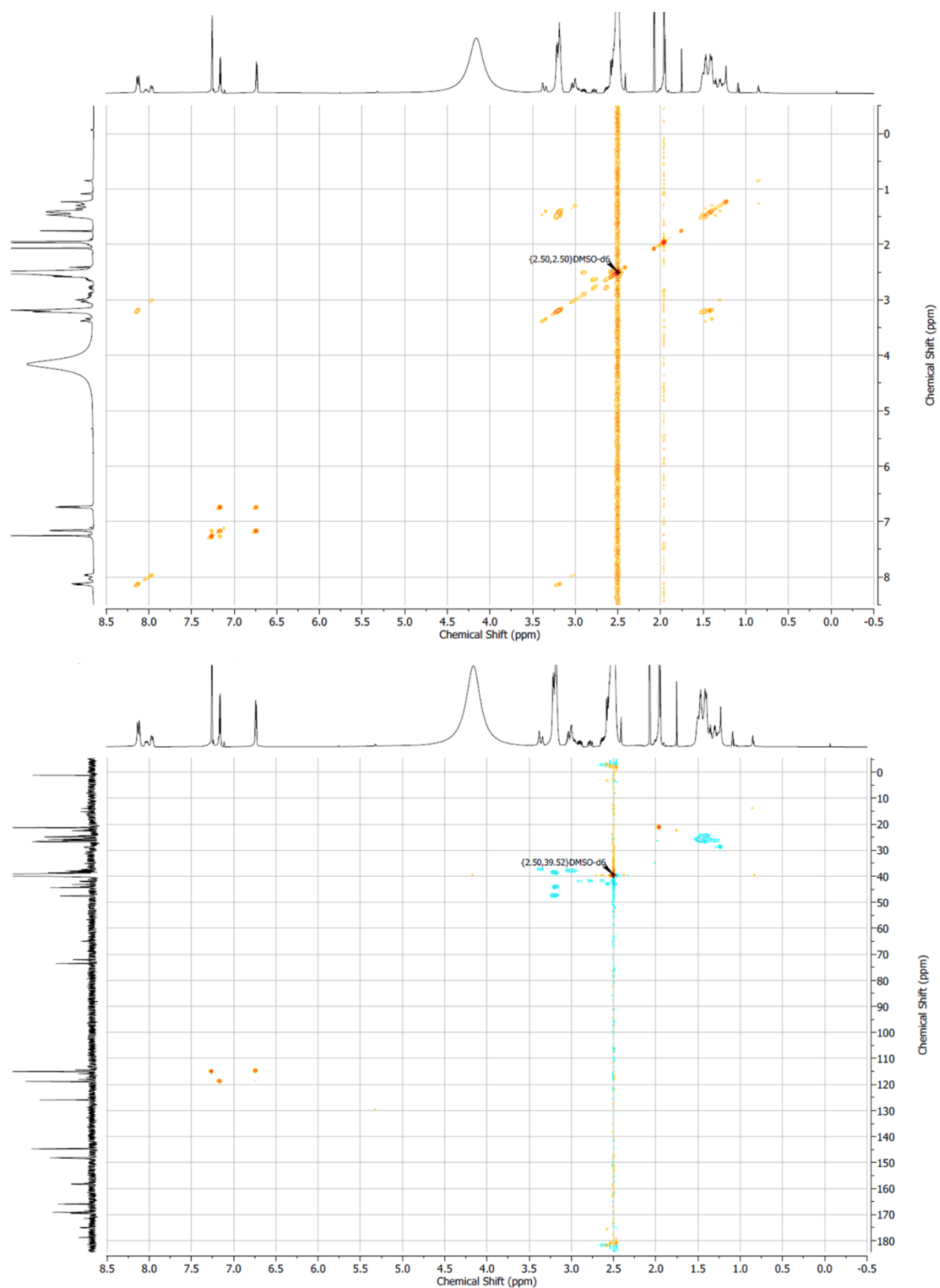
Figure V-22 COSY and HSQC NMR spectra of rhodopetrobactin B in DMSO-d$_6$. Correlations of -CH2- and -CH- are shown in blue and red, respectively.
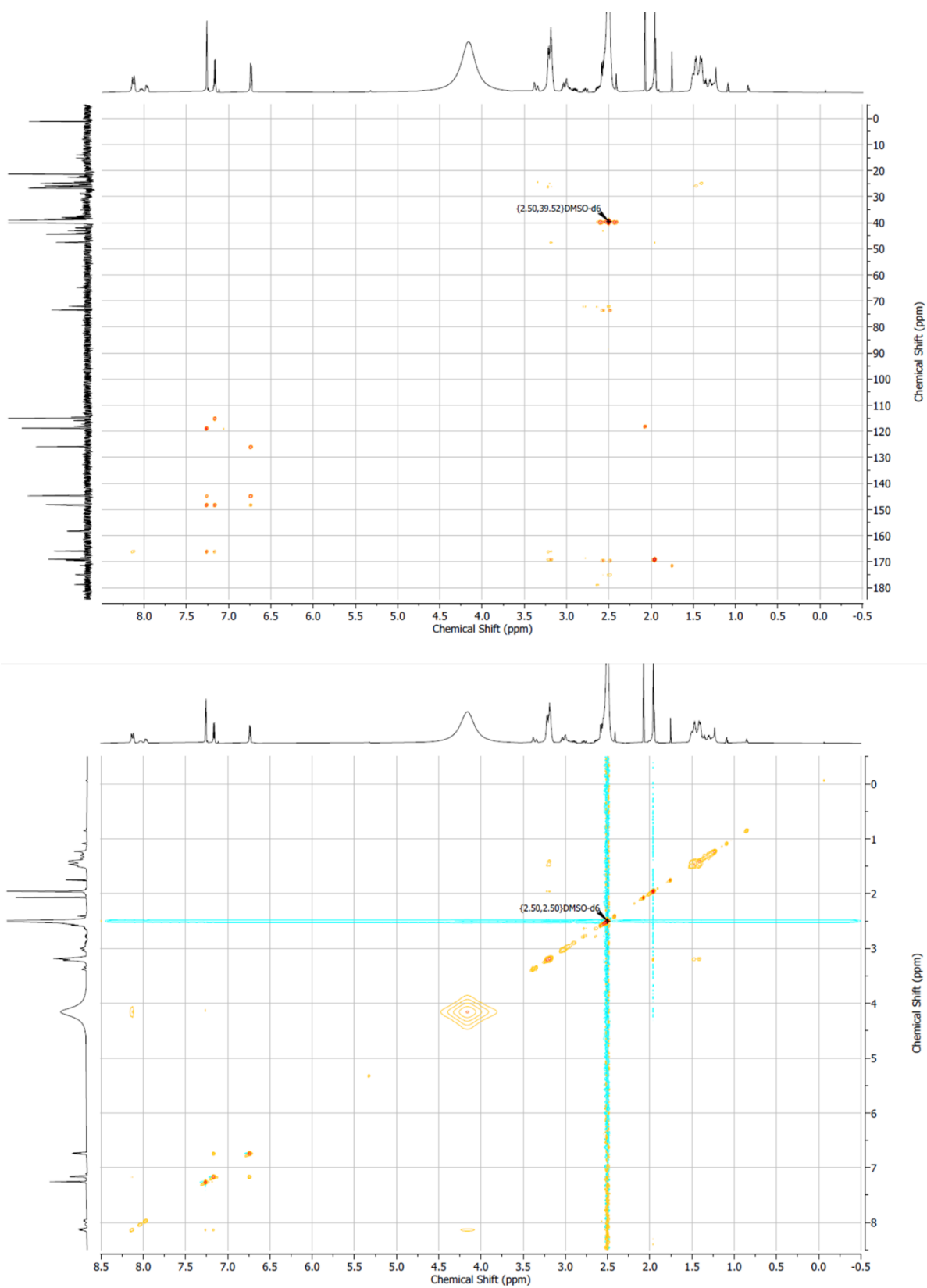
Figure V-23 HMBC and NOESY NMR spectra of rhodopetrobactin B in DMSO-d$_6$.
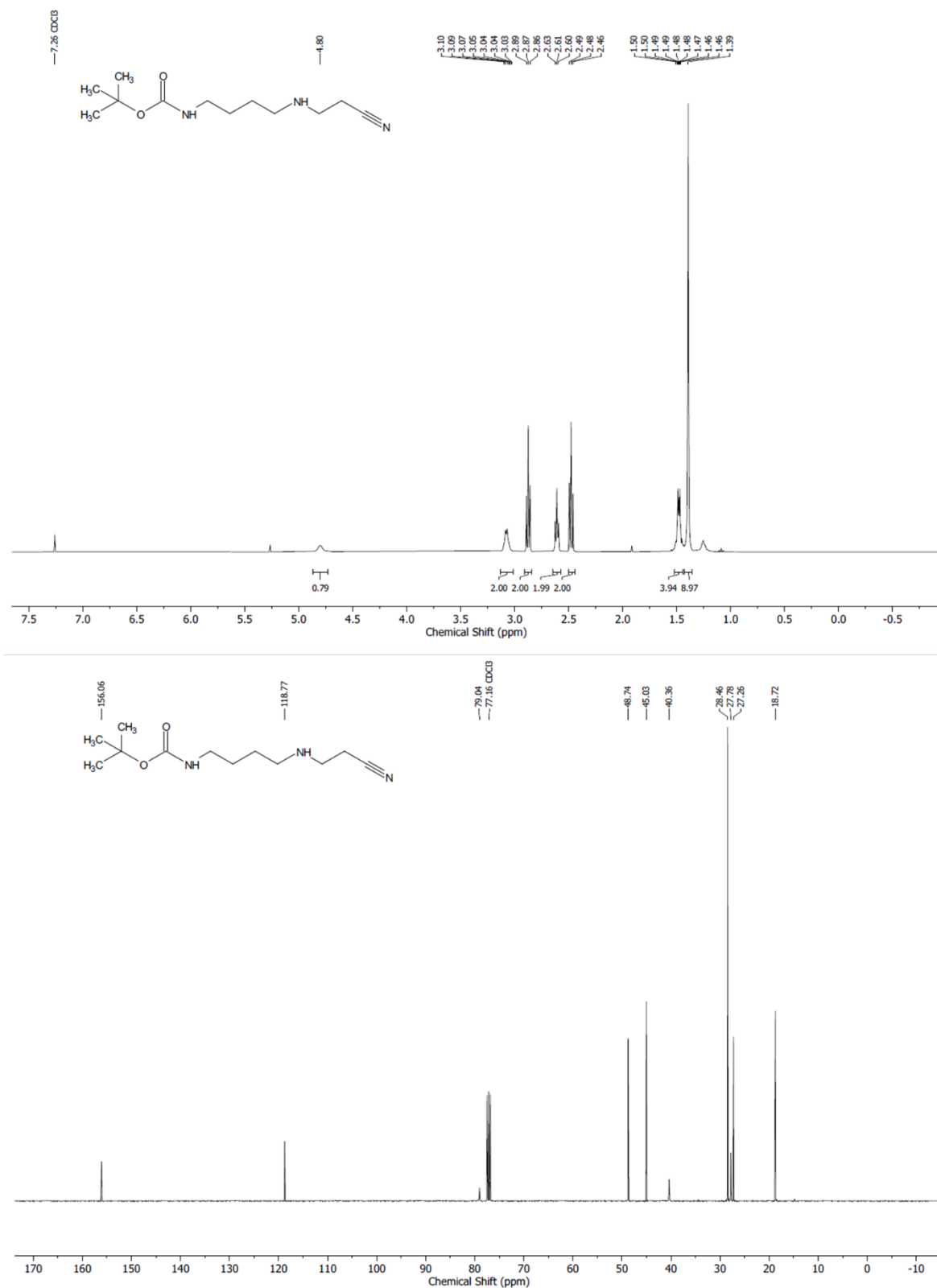
Figure V-24 ^{1}H and ^{13}C NMR spectra of **28** in CDCl₃.

1.4 Supporting Information for Chapter III.3.1
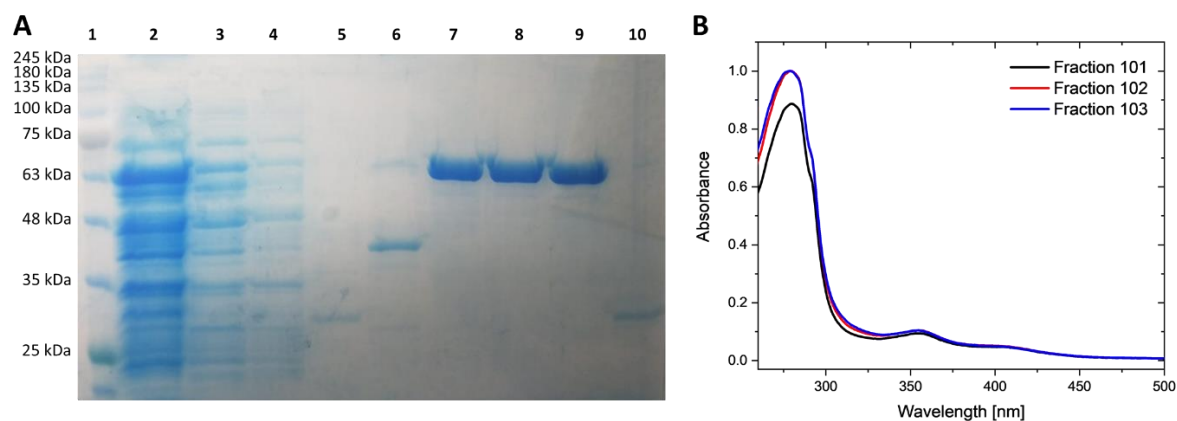
Figure V-25 A) SDS-PAGE analysis (12% w/v acrylamide) of Sm-MDH purification. (1: marker, 2: crude, 3: flow-through, 4: column wash, 5: cyt c_{GJ}, 6: hydroxylamine oxidoreductase, 7: Sm-MDH (fraction 101), 8: Sm-MDH (fraction 102), 9: Sm-MDH (fraction 103), 10: cyt c_{GJ} from previous purification as positive control). BlueEye prestained protein ladder (Jena Bioscience) was used as the marker. B) UV/Vis spectrum of Sm-MDH fractions normalized to 1.
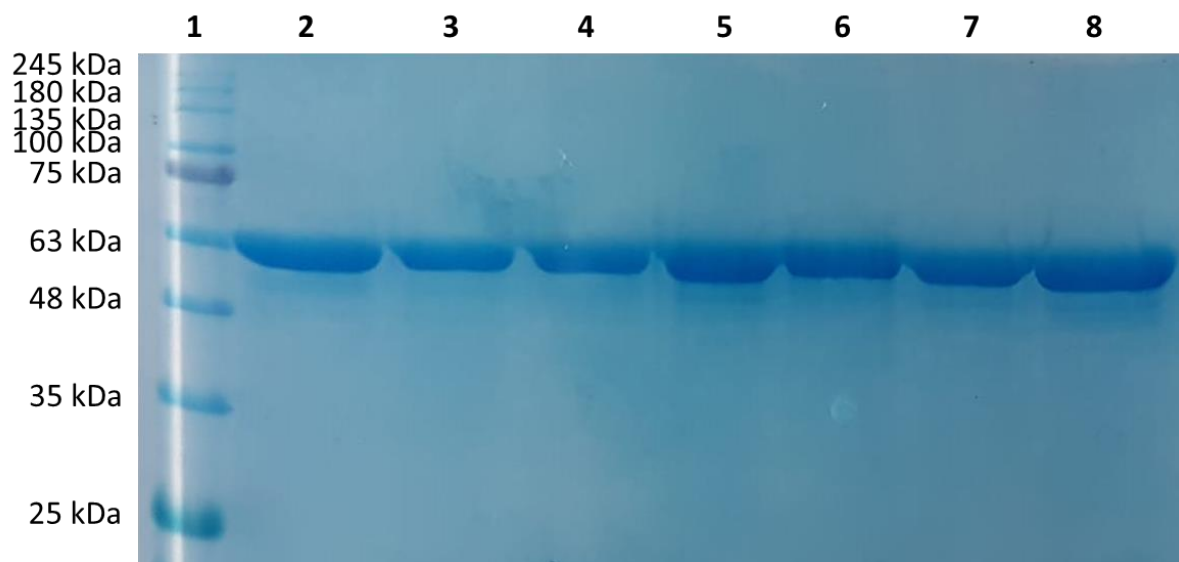
Figure V-26 SDS-PAGE analysis (12% w/v acrylamide) of purified Ln-MDH (10 µg each) (1: marker, 2: La-MDH, 3: Ce-MDH, 4: Pr-MDH, 5: Nd-MDH, 6: Sm-MDH, 7: Eu-MDH, 8: Lu-MDH). BlueEye prestained protein ladder (Jena Bioscience) was used as the marker.

1.5 Supporting Information for Chapter III.3.2
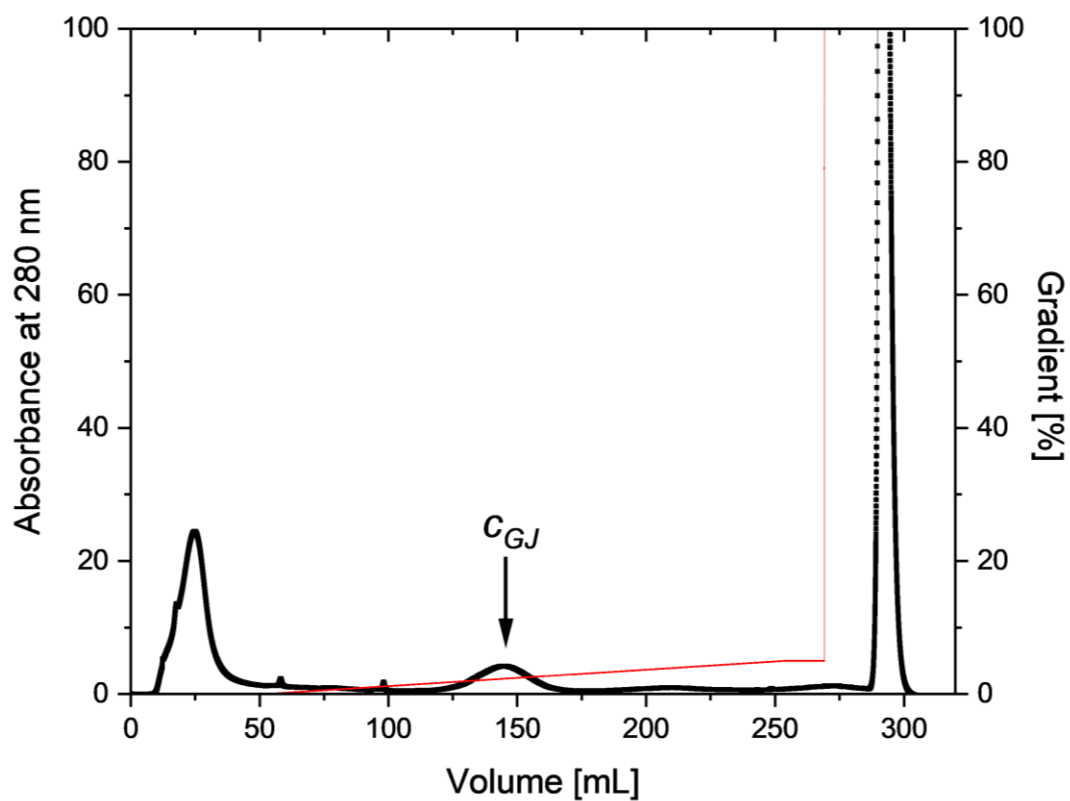
Figure V-27 Chromatogram of the purification of protein-coupled assay mixtures. Buffer A: 10 mM PIPES with 1 mM MeOH (pH 7); buffer B: 10 mM PIPES with 1 mM MeOH and 1 M NaCl (pH 7). Gradient: 0 to 5% B over 10 CV. Flow: 5 mL/min.

1.6 Supporting Information for Chapter III.4.2

ChemBioChem

Supporting Information

Assessing Lanthanide-Dependent Methanol Dehydrogenase Activity: The Assay Matters

Manh Tri Phi, Helena Singer, Felix Zäh, Christoph Haisch, Sabine Schneider, Huub J. M. Op den Camp, and Lena J. Daumann*

ChemBioChem

Supporting Information

Assessing Lanthanide-Dependent Methanol Dehydrogenase Activity: The Assay Matters

Manh Tri Phi,[a] Helena Singer,[a] Felix Zäh,[a] Christoph Haisch,[b] Sabine Schneider,[a] Huub J. M. Op den Camp,[c] Lena J. Daumann*[a, d]

lena.daumann@hhu.de
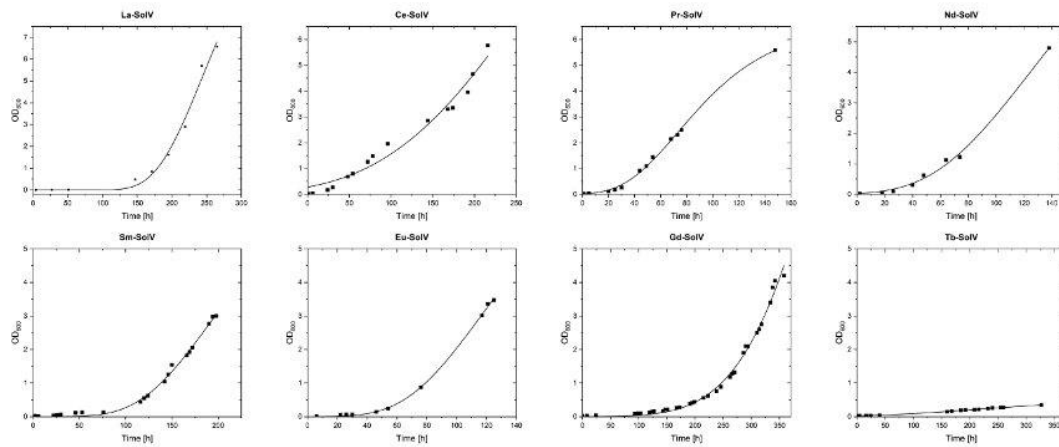
Figure S1 Growth curve of SolV cultivated with different Ln (2 µM) at 55 °C. For composition of medium see Table S1. Protocol was followed as previously reported.[1]
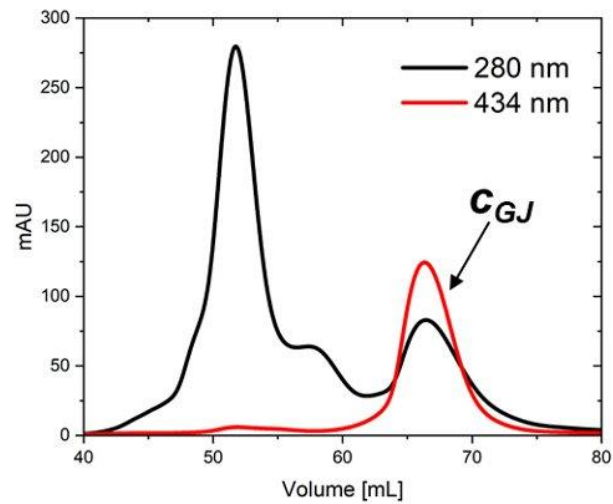
Figure S2 Chromatogram of cyt c_{GJ} purification by size exclusion chromatography (SEC). Conditions: 10 mM PIPES with 0.2 M NaCl, pH 7.2 at 4 °C.
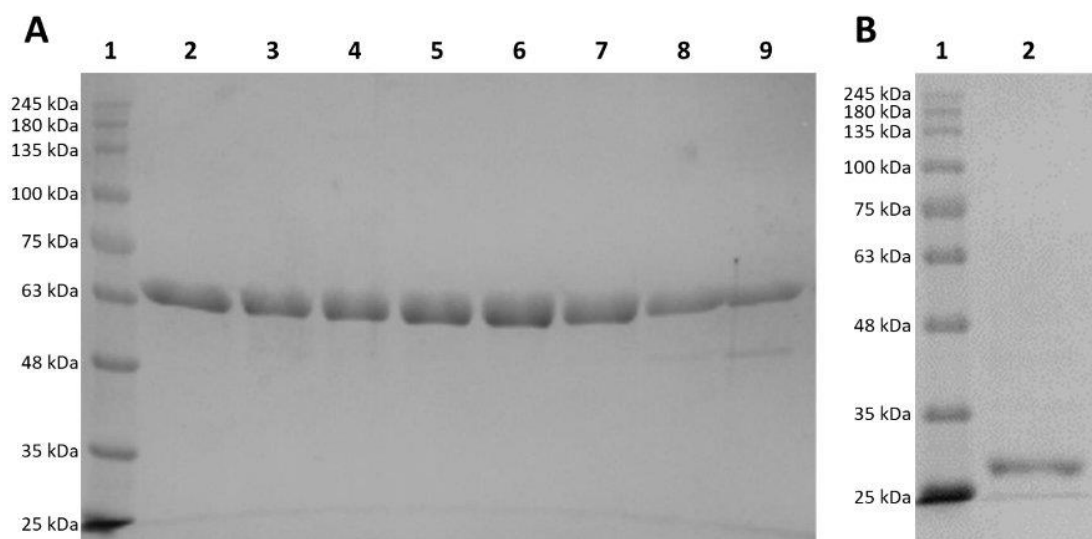
Figure S3 SDS-PAGE analysis (12% w/v acrylamid) of (A) purified XoxF-MDHs (1: marker, 2: La-MDH, 3: Ce-MDH, 4: Pr-MDH, 5: Nd-MDH, 6: Sm-MDH, 7: Eu-MDH, 8: Gd-MDH, 9: Tb-MDH) and (B) purified cyt c_{GJ} after size exclusion chromatography (1: marker, 2: cyt c_{GJ}). BlueEye prestained protein ladder (Jena Bioscience) was used as the marker.
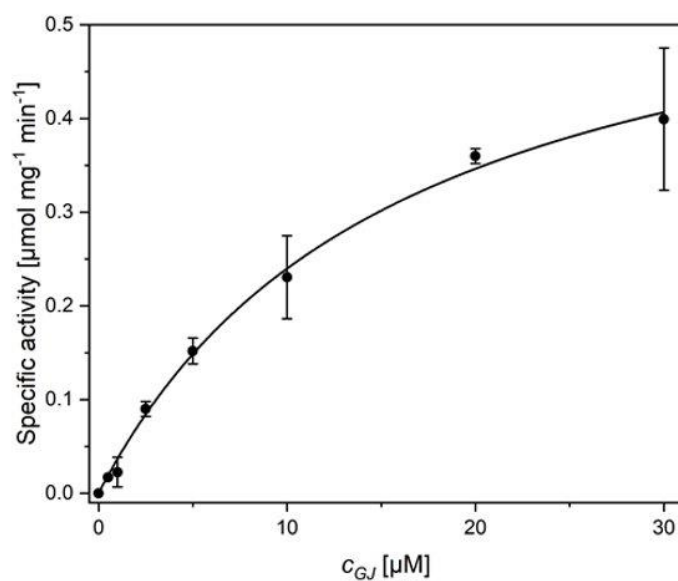
Figure S4 Specific activity of Nd-MDH with increasing concentration of cyt c_{GJ}. Conditions: 100 nM Nd-MDH, 0–30 µM cyt c_{GJ}, 50 µM cytochrome c from equine heart, 50 mM MeOH in 10 mM PIPES with 1 mM MeOH, pH 7.2, 45 °C. Each dot represents the average of three technical replicates. K_M= 16.0 ± 1.9 µM, v_{max}= 0.62 ± 0.04.

Table S1 Medium composition for the SolV growth medium.

Solution	Composition
Minimal medium (10x)	2 mM MgCl$_2$ · 6 H$_2$O, 10 mM Na$_2$SO$_4$, 20 mM K$_2$SO$_4$, 10 mM NaH$_2$PO$_4$, 2 mM CaCl$_2$ **Note:** All components except CaCl$_2$ were mixed and adjusted to pH 2.7 with 1 M H$_2$SO$_4$. CaCl$_2$ was autoclaved separately and added afterwards to prevent the precipitation of calcium phosphates.
Trace element (TE) solution	200 mM FeSO$_4$ · 7 H$_2$O, 200 mM MnCl$_2$ · 4 H$_2$O, 300 mM CuSO$_4$ · 5 H$_2$O, 10 mM NiCl$_2$ · 6 H$_2$O, 10 mM ZnSO$_4$ · 7 H$_2$O, 10 mM CoCl$_2$ · 6 H$_2$O, 10 mM Na$_2$MoO$_4$ · 2 H$_2$O **Note:** All components were dissolved one after the other in 1.5 % v/v H$_2$SO$_4$. Solution will occur blue immediately after preparation but turns green after a few days.
Growth medium for *M. fumariolicum* SolV	Prepared according to Pol *et al.*[2] 1x Minimal medium, 20 μL/L TE, 8 mM NH$_4^+$ for cultivation in bottles, for the bioreactor experiments the TE concentration was increased to 80 μL/L and 30 mM NH$_4^+$. All components were mixed and autoclaved. **Note:** NH$_4^+$ available from a 2 M (NH$_4$)$_2$SO$_4$ solution in MilliQ water.

References

[1]   H. Singer, R. Steudtner, I. Sottorff, B. Drobot, A. Pol, H. J. M. Op den Camp, L. J. Daumann, *Chem. Comm.* **2023**, *59*, 9066-9069.

[2]   A. Pol, T. R. M. Barends, A. Dietl, A. F. Khadem, J. Eygensteyn, M. S. M. Jetten, H. J. M. Op den Camp, *Environ. Microbiol.* **2014**, *16*, 255-264.

1.7 Supporting Information for Chapter III.4.4
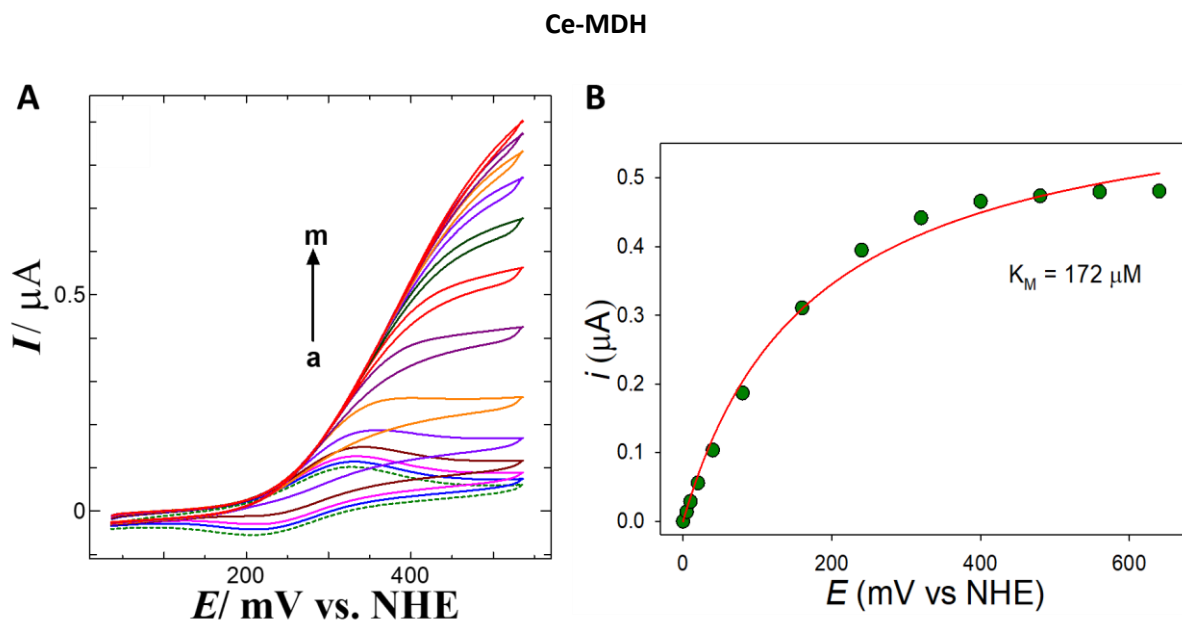
Ce-MDH

Figure V-28 A) RDEVs (2000 RPM) obtained for Au/MU/chitosan-cyt c_{GJ}/Ce-MDH electrode for increasing concentration of methanol (a) 0, (b) 5, (c) 10, (d) 20, (e) 40, (f) 80, (g) 160, (h) 240, (i) 320, (j) 400, (k) 480, (l) 560 and (m) 640 μM in 20 mM PIPES buffer (pH 7.2) at a scan rate of 5 mV s^{-1}. B) Electrochemical Michaelis-Menten plot for the limiting currents at 400 mV as a function of methanol concentration. The data was kindly provided by Dr. Palraj Kalimuthu.
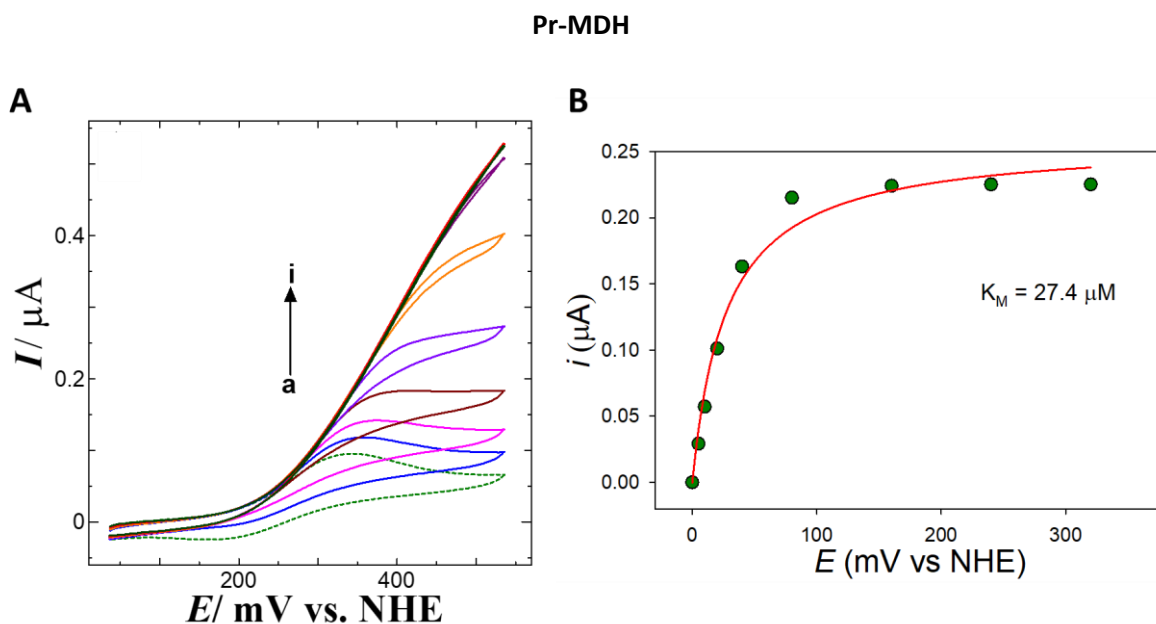
Pr-MDH

Figure V-29 A) RDEVs (2000 RPM) obtained for Au/MU/chitosan-cyt c_{GJ}/Pr-MDH electrode for increasing concentration of methanol (a) 0, (b) 5, (c) 10, (d) 20, (e) 40, (f) 80, (g) 160, (h) 240 and (i) 320 μM in 20 mM PIPES buffer (pH 7.2) at a scan rate of 5 mV s^{-1}. B) Electrochemical Michaelis-Menten plot for the limiting currents at 400 mV as a function of methanol concentration. The data was kindly provided by Dr. Palraj Kalimuthu.

Nd-MDH
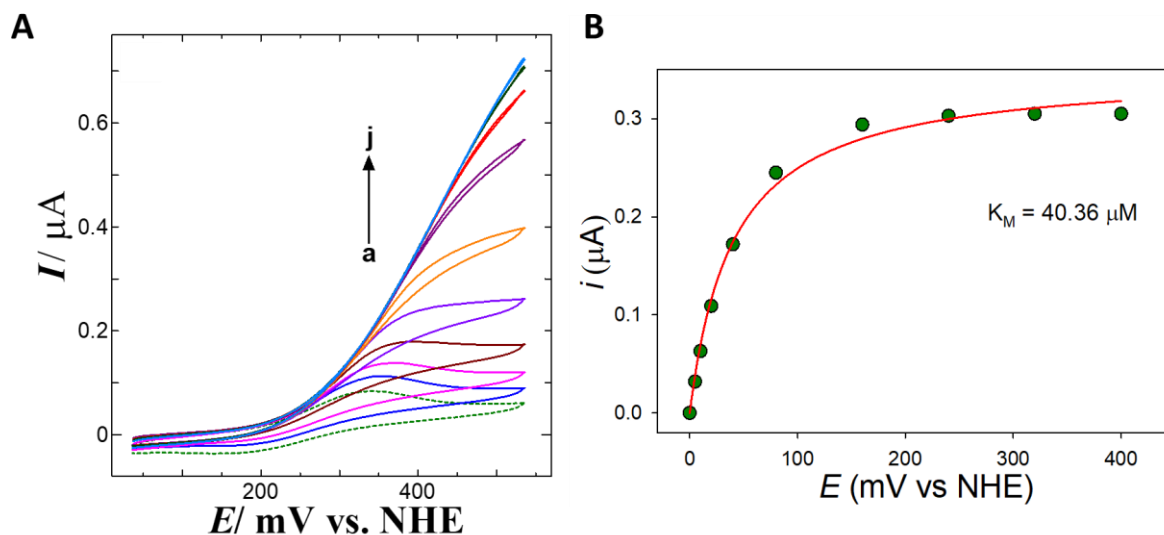
Figure V-30 A) RDEVs (2000 RPM) obtained for Au/MU/chitosan-cyt c_{GJ}/Nd-MDH electrode for increasing concentration of methanol (a) 0, (b) 5, (c) 10, (d) 20, (e) 40, (f) 80, (g) 160, (h) 240, (i) 320 and (j) 400 μM in 20 mM PIPES buffer (pH 7.2) at a scan rate of 5 mV s^{-1}. B) Electrochemical Michaelis-Menten plot for the limiting currents at 400 mV as a function of methanol concentration. The data was kindly provided by Dr. Palraj Kalimuthu.

Sm-MDH
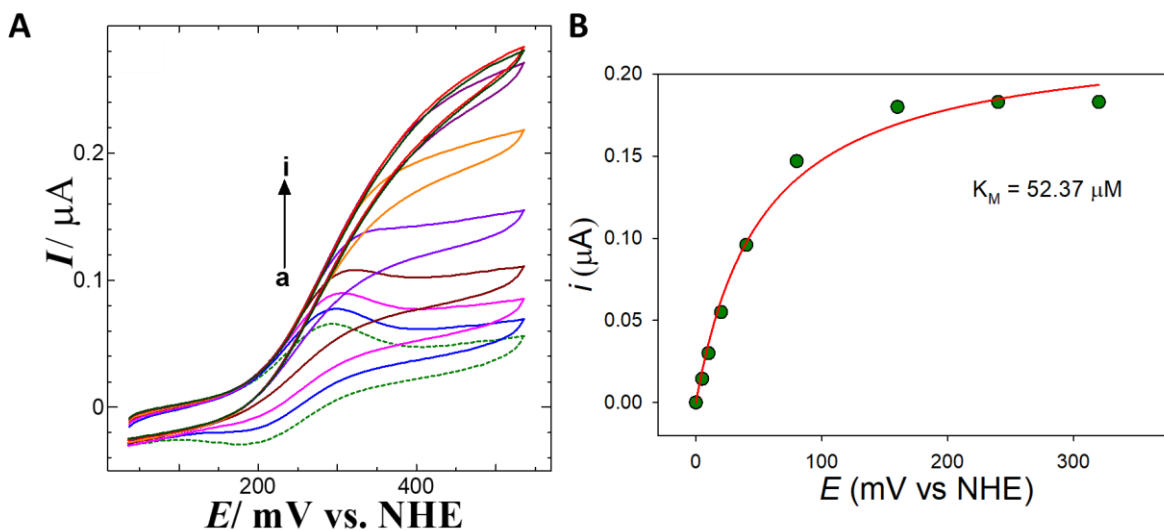
Figure V-31 A) RDEVs (2000 RPM) obtained for Au/MU/chitosan-cyt c_{GJ}/Sm-MDH electrode for increasing concentration of methanol (a) 0, (b) 5, (c) 10, (d) 20, (e) 40, (f) 80, (g) 160, (h) 240, (i) 320, (j) 400, (k) 480, (l) 560 and (m) 640 μM in 20 mM PIPES buffer (pH 7.2) at a scan rate of 5 mV s^{-1}. B) Electrochemical Michaelis-Menten plot for the limiting currents at 400 mV as a function of methanol concentration. The data was kindly provided by Dr. Palraj Kalimuthu.
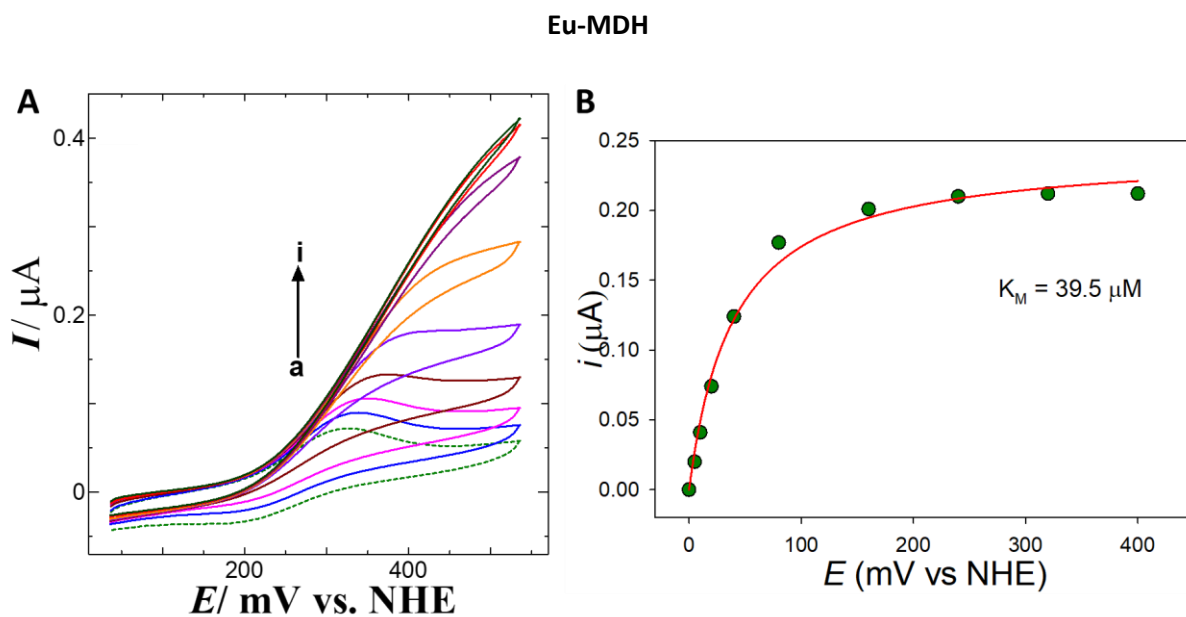
Eu-MDH

Figure V-32 A) RDEVs (2000 RPM) obtained for Au/MU/chitosan-cyt c_{GJ}/Eu-MDH electrode for increasing concentration of methanol (a) 0, (b) 5, (c) 10, (d) 20, (e) 40, (f) 80, (g) 160, (h) 240 and (i) 320 µM in 20 mM PIPES buffer (pH 7.2) at a scan rate of 5 mV s^{-1}. B) Electrochemical Michaelis-Menten plot for the limiting currents at 400 mV as a function of methanol concentration. The data was kindly provided by Dr. Palraj Kalimuthu.

1.8 Supporting Information for Chapter III.5
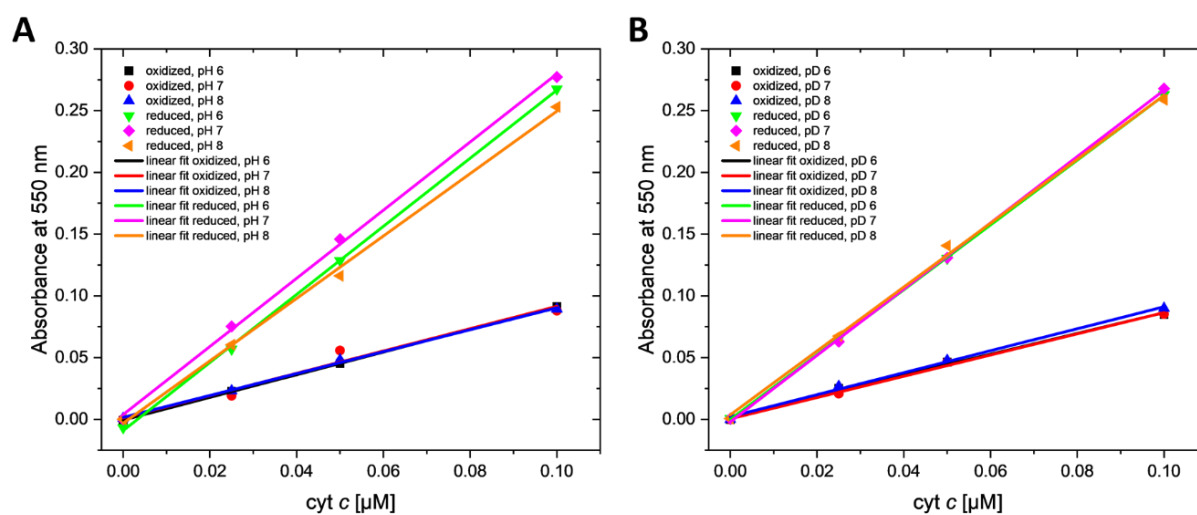
Figure V-33 Results of the dilution series of cyt c from equine heart in its oxidized and reduced state for the determination of the extinction coefficient ε.

2. List of Abbreviations

Å	Ångstrom
A_{280}	Absorbance at 280 nm
AB	Aerobactin
AM1	*Methylorubrum extorquens* AM1
Ce-MDH	Cerium-containing methanol dehydrogenase
CHES	*N*-cyclohexyl-2-aminoethanesulfonic acid
cm	Centimeter
CN	Coordination number
COSY	Correlation spectroscopy
CV	Cyclic voltammetry/voltammogram
cyt	Cytochrome
d	Pathlength of cell or cuvette
DCC	*N,N'*-dicyclohexylcarbodiimide
DCM	Dichloromethane
DCPIP	2,6-Dichlorophenolindophenol
DS	Deoxyschizokinen
DFO	Desferrioxamine
EDC	1-Ethyl-3-(3-dimethylaminopropyl)carbodiimide
ESI	Electrospray ionization
equiv.	Equivalent(s)
Eu-MDH	Europium-containing methanol dehydrogenase
FPLC	Fast protein liquid chromatography
Gd-MDH	Gadolinium-containing methanol dehydrogenase
h	hour
HEPES	4-(2-hydroxyethyl)-1-piperazineethanesulfonic acid

HMBC	Heteronuclear multiple bond correlation
HOBT	1-hydroxybenzotriazol
HPLC	High-performance liquid chromatography
HREE	Heavy rare earth elements (Gd–Lu)
HR-MS	High resolution mass spectrometry
HSQC	Heteronuclear single quantum correlation
ICP-MS	Inductively coupled plasma mass spectrometry
ITC	Isothermal titration calorimetry
K_d	Metal binding constant
K_D	Reaction rate constant wit with heavy isotope
K_H	Reaction rate constant wit with light isotope
K_M	Michaelis constant
kDa	Kilodalton
KIE	Kinetic isotope effect
La-MDH	Lanthanum-containing methanol dehydrogenase
LanM	Lanmodulin
LC-MS	Liquid chromatography mass spectrometry
Ln-MDH	Lanthanide-containing methanol dehydrogenase
LREE	Light rare earth elements (La–Eu)
Lu-MDH	Lutetium-containing methanol dehydrogenase
M	Molar
mAU	Milli absorbance unit
MC	Multicomponent buffer
MDH	Methanol dehydrogenase
MeOD	Deuterated methanol-d_4

MeOH	Methanol
MES	2-(N-morpholino)ethanesulfonic acid
min	Minute
mg	Milligram
mL	Milliliter
mm	Millimeter
mM	Millimolar
MOPSO	2-Hydroxy-3-morpholinopropanesulfonic acid
MW	Molecular weight
MWCO	Molecular weight cut-off
MxaI	Small subunit of Ca^{2+}-dependent methanol dehydrogenase
MxaF	Big subunit of Ca^{2+}-dependent methanol dehydrogenase
µg	Microgram
µL	Microliter
µM	Micromolar
Nd-MDH	Neodymium-containing methanol dehydrogenase
NHS	N-hydroxysuccinimide
nm	Nanometer
nM	Nanomolar
NMR	Nuclear magnetic resonance spectroscopy
NOESY	Nuclear Overhauser effect spectroscopy
PDB	Protein Data Bank
PES	Phenazine ethosulfate
pI	Isoelectronic point
PIPES	Piperazine-N,N'-bis(2-ethanesulfonic acid)

PQQ	Pyrroloquinoline quinone
PQQH$_2$	Reduced form of pyrroloquinoline quinone
Pr-MDH	Praseodymium-containing methanol dehydrogenase
QTOF-MS	Quadrupole time-of-flight mass spectrometry
RDE	Rotating disk electrode
RDEV	Rotating disk electrode voltammogram
REE(s)	Rare earth element(s)
RPB	Rhodopetrobactin B
rpm	Revolutions per minute
RT	Room temperature
s	Second
[S]	Substrate concentration
SDS-PAGE	Sodium dodecyl sulfate–polyacrylamide gel electrophoresis
NHE	Normal hydrogen electrode
Sm-MDH	Samarium-containing methanol dehydrogenase
SolV	*Methylacidiphilum fumariolicum* SolV
SP	Sulphopropyl resin
Tb-MDH	Terbium-containing methanol dehydrogenase
TEA	Triethylamine
TEMED	Tetramethylethylenediamine
TLC	Thin layer chromatography
TMPD	*N,N,N',N'*-Tetramethyl-*p*-phenylenediamine
TRIS	Tris(hydroxymethyl)aminomethane
TRLFS	Time-resolved laser-induced fluorescence spectroscopy
U	Enzyme unit

UV/Vis	Ultraviolet-visible
v_0	Initial velocity of an enzyme reaction
v_{max}	Maximum velocity of an enzyme reaction
WB	Wurster's Blue
xoxF	Gene encoding the lanthanide-dependent methanol dehydrogenase
XoxF	Lanthanide-dependent methanol dehydrogenase

3. Materials

Buffers, chemicals, reagents and instruments that were used for chapter III.

Table V-1 Overview of chemicals and reagents.

Chemical/Reagent	Purity	Supplier
β-Mercaptoethanol	For synthesis	Merck
Ammonium persulfate (APS)	For electrophoresis, ≥95%	Sigma-Aldrich
Bromophenol blue sodium salt	for electrophoresis	GE Healthcare
BugBuster 10X Protein Extraction Reagent	-	Merck
Chitosan (from shrimp shells)	≥75% (deacetylated)	Sigma-Aldrich
Coomassie Brilliant Blue (CBB) G250	-	Sigma-Aldrich
Cytochrome c from equine heart	≥95%	Sigma-Aldrich
2,6-Dichlorophenol indophenol sodium salt hydrate (DCPIP)	≥90%	Sigma-Aldrich
Deuterium chloride (35 wt. % in D2O)	≥99 atom % D	Sigma-Aldrich
Deuterium oxide	99.9 atom % D	Sigma-Aldrich
DNAse	-	PanReac AppliChem
11-Mercapto-1-undecanol	97%	Sigma-Aldrich
Methanol	For HPLC, ≥99.9%	Sigma-Aldrich
Methanol-d_4	99.8%	Deutero
Lanthanide chloride (Ln = La, Ce, Pr, Nd, Sm, Eu, Gd, Tb, Lu)	≥99.9%	abcr
Lysozym (≥40 000 U/mg)	≥90%	Sigma-Aldrich
N,N,N',N'- Tetramethylethylenediamine (TEMED)	≥99%	Sigma-Aldrich
Phenazine ethosulfate (PES)	≥95%	Sigma-Aldrich
Rotiphorese (37.5:1, Acrylamide/Bisacrylmide)	40% solution	Carl Roth
Sodium dithionite	Technical	LMU chemical supply shop

Table V-2 Overview of buffers.

Buffer	Purity	Supplier
1,4-Piperazinediethanesulfonic acid (PIPES)	≥99 %	Sigma-Aldrich
2-Amino-2-(hydroxymethyl)propane-1,3-diol hydrochloride (Tris-HCl)	molecular biology grade	Sigma-Aldrich
2,2-Bis(hydroxymethyl)-2,2',2"-nitrilotriethanol (Bis-Tris)	≥98%	Sigma-Aldrich
2-(Cyclohexylamino)ethanesulfonic acid (CHES)	≥99%	Sigma-Aldrich
2-(N-Morpholino)ethanesulfonic acid (MES)	≥99.5%	Sigma-Aldrich
3-Morpholino-2-hydroxypropanesulfonic acid (MOPSO)	≥99%	Sigma-Aldrich
4-(2-hydroxyethyl)-1-piperazine-ethanesulfonic acid (HEPES)	≥99.5%	Carl Roth
Sodium citrate tribasic dihydrate	≥99.5%	Sigma-Aldrich

Table V-3 Overview of instruments.

Instrument	Manufacturer
ÄKTA Go FPLC system	Cytiva
BAS 100B/W electrochemical workstation	BASi
Cary 60 spectrophotometer with Peltier element	Agilent
Centrifuge (Avanti JXN-26)	Beckman Coulter
Centrifuge (Heraeus Megafuge 8R)	Thermo Fisher
Epoch2 plate reader	BioTek
NexION 350D ICP-MS	Perkin Elmer
MicroCal PEAQ-ITC	Malvern Panalytical
Mini-PROTEAN Electrophoresis Cell	BioRad
pH meter	Mettler-Toledo

4. Disclosure of Participation

The following people contributed to the practical laboratory work of this thesis as part of their research internships or thesis:

For a research internship, **Daniel Bejko** performed initial experiments to investigate the kinetic isotope effect of the substrate and solvent on the enzyme activity of Pr-MDH with cytochrome c_{GJ}. Daniel also investigated the interaction of PQQ and Ln-MDH with cytochrome c_{GJ} that are not presented in this work.

For the Bachelor's thesis, **Isabella Heinzelmann** asisssted with the large-scale cultivation of Lu-SolV, the purification of Ln-MDH and conducted dye-coupled activity assay to assess the enzyme activity of Ln-MDHs. Only the growth curve of Lu-SolV is presented in this thesis.

VI.   References

[1]   N. Haque, A. Hughes, S. Lim, C. Vernon, *Resources* **2014**, *3*, 614-635.

[2]   a) L. J. Daumann, *Angew. Chem. Int. Ed.* **2019**, *58*, 12795-12802; b) Z. Hu, S. Gao, *Chem. Geol.* **2008**, *253*, 205-221.

[3]   A. L. Knasin, E. J. Schelter, in *Methods Enzymol., Vol. 650* (Ed.: J. A. Cotruvo), Academic Press, **2021**, pp. 19-55.

[4]   a) T. Cheisson, E. J. Schelter, *Science* **2019**, *363*, 489-493; b) V. Balaram, *Geosci. Front.* **2019**, *10*, 1285-1303.

[5]   a) G. A. Molander, *Chem. Rev.* **1992**, *92*, 29-68; b) N. C. Martinez-Gomez, H. N. Vu, E. Skovran, *Inorg. Chem.* **2016**, *55*, 10083-10089; c) F. Barmettler, C. Castelberg, C. Fabbri, H. Brandl, *AIMS Microbiol.* **2016**, *2*, 190-204; d) T. I. Kostelnik, C. Orvig, *Chem. Rev.* **2019**, *119*, 902-956.

[6]   a) U. S. Geological Survey: *Mineral Commodity Summaries* **2004**, p. 133; b) U. S. Geological Survey: *Mineral Commodity Summaries*, Reston, VA, **2024**, p. 145.

[7]   S. Lim, S. J. Franklin, *Cell. Mol. Life Sci.* **2004**, *61*, 2184-2188.

[8]   C. H. Evans, *Biochemistry of the Lanthanides, Vol. 8*, Springer Science & Business Media, New York, **1990**.

[9]   Y. Hibi, K. Asai, H. Arafuka, M. Hamajima, T. Iwama, K. Kawai, *J. Biosci. Bioeng.* **2011**, *111*, 547-549.

[10]   T. Nakagawa, R. Mitsui, A. Tani, K. Sasa, S. Tashiro, T. Iwama, T. Hayakawa, K. Kawai, *PLOS ONE* **2012**, *7*, e50480.

[11]   a) D. Chaudhuri, W. D. Horrocks, J. C. Amburgey, D. J. Weber, *Biochemistry* **1997**, *36*, 9674-9680; b) J. D. Walters, J. D. Johnson, *J. Biol. Chem.* **1990**, *265*, 4223-4226; c) K. J. Franz, M. Nitz, B. Imperiali, *ChemBioChem* **2003**, *4*, 265-271; d) M. D. McCreary, D. W. Lewis, D. L. Wernick, G. M. Whitesides, *J. Am. Chem. Soc.* **1974**, *96*, 1038-1054; e) K. N. Allen, B. Imperiali, *Curr. Opin. Chem. Biol.* **2010**, *14*, 247-254.

[12]   a) B. Vekeman, D. Speth, J. Wille, G. Cremers, P. De Vos, H. J. M. Op den Camp, K. Heylen, *Microb. Ecol.* **2016**, *72*, 503-509; b) A. Pol, T. R. M. Barends, A. Dietl, A. F. Khadem, J. Eygensteyn, M. S. M. Jetten, H. J. M. Op den Camp, *Environ. Microbiol.* **2014**, *16*, 255-264.

[13]   L. Chistoserdova, *Environ. Microbiol.* **2011**, *13*, 2603-2622.

[14]   a) H. In Yeub, L. Seung Hwan, C. Yoo Seong, P. Si Jae, N. Jeong Geol, C. In Seop, K. Choongik, K. Hyun Cheol, K. Yong Hwan, L. Jin Won, *J. Microbiol. Biotechnol.* **2014**, *24*, 1597-1605; b) A. S. Hakemian, A. C. Rosenzweig, *Annu. Rev. Biochem.* **2007**, *76*, 223-241.

[15]   N. Delmotte, C. Knief, S. Chaffron, G. Innerebner, B. Roschitzki, R. Schlapbach, C. von Mering, J. A. Vorholt, *PNAS* **2009**, *106*, 16428-16433.

[16]   L. Chistoserdova, *J. Microbiol. Biotechnol.* **2016**, *32*, 138.

[17]   J. T. Keltjens, A. Pol, J. Reimann, H. J. M. Op den Camp, *Appl. Microbiol. Biotechnol.* **2014**, *98*, 6163-6183.

[18]   a) H. N. Vu, G. A. Subuyuj, S. Vijayakumar, N. M. Good, N. C. Martinez-Gomez, E. Skovran, *J. Bacteriol.* **2016**, *198*, 1250-1259; b) F. Chu, M. E. Lidstrom, *J. Bacteriol.* **2016**, *198*, 1317-1325; c) N. M. Good, H. N. Vu, C. J. Suriano, G. A. Subuyuj, E. Skovran, N. C. Martinez-Gomez, *J. Bacteriol.* **2016**, *198*, 3109-3118.

[19]   M. T. Phi, H. Singer, F. Zäh, C. Haisch, S. Schneider, H. J. M. Op den Camp, L. J. Daumann, *ChemBioChem* **2024**, *25*, e202300811.

[20]   a) N. M. Good, M. Fellner, K. Demirer, J. Hu, R. P. Hausinger, N. C. Martinez-Gomez, *J. Biol. Chem.* **2020**; b) B. Jahn, A. Pol, H. Lumpe, T. R. M. Barends, A. Dietl, C. Hogendoorn, H. J. M. Op den Camp, L. J. Daumann, *ChemBioChem* **2018**, *19*, 1147-1153.

[21]   a) M. Prejanò, T. Marino, N. Russo, *Chem. Eur. J.* **2017**, *23*, 8652-8657; b) M. Prejanò, N. Russo, T. Marino, *Chem. Eur. J.* **2020**, *26*, 11334-11339; c) M. Leopoldini, N. Russo, M. Toscano, *Chem. Eur. J.* **2007**, *13*, 2109-2117; d) C. Anthony, *Arch. Biochem. Biophys.* **2004**, *428*, 2-9.

[22]   C. Anthony, in *Enzyme-Catalyzed Electron and Radical Transfer: Subcellular Biochemistry* (Eds.: A. Holzenburg, N. S. Scrutton), Springer US, Boston, MA, **2000**, pp. 73-117.

[23]   E. R. Featherston, H. R. Rose, M. J. McBride, E. M. Taylor, A. K. Boal, J. A. Cotruvo Jr., *ChemBioChem* **2019**, *20*, 2360-2372.

[24]   H. Singer, R. Steudtner, A. S. Klein, C. Rulofs, C. Zeymer, B. Drobot, A. Pol, N. C. Martinez-Gomez, H. J. M. Op den Camp, L. Daumann, *Angew. Chem. Int. Ed.* **2023**, e202303669.

[25]   J. A. Cotruvo, E. R. Featherston, J. A. Mattocks, J. V. Ho, T. N. Laremore, *J. Am. Chem. Soc.* **2018**, *140*, 15056-15061.

[26]   a) G. J. P. Deblonde, J. A. Mattocks, D. M. Park, D. W. Reed, J. A. Cotruvo, Y. Jiao, *Inorg. Chem.* **2020**; b) Q. Ye, X. Jin, B. Zhu, H. Gao, N. Wei, *Environ. Sci. Technol.* **2023**.

[27]   J. L. Hemmann, P. Keller, L. Hemmerle, T. Vonderach, A. M. Ochsner, M. Bortfeld-Miller, D. Günther, J. A. Vorholt, *J. Biol. Chem.* **2023**, *299*.

[28]   A. M. Zytnick, S. M. Gutenthaler-Tietze, A. T. Aron, Z. L. Reitz, M. T. Phi, N. M. Good, D. Petras, L. J. Daumann, N. C. Martinez-Gomez, *bioRxiv* **2023**, 2022.2001.2019.476857.

[29]   A. Pol, K. Heijmans, H. R. Harhangi, D. Tedesco, M. S. M. Jetten, H. J. M. Op den Camp, *Nature* **2007**, *450*, 874-878.

[30]   S. Castaldi, D. Tedesco, *Chemosphere* **2005**, *58*, 131-139.

[31]   C. Anthony, *Biochim. Biophys. Acta* **1992**, *1099*, 1-15.

[32]   W. Versantvoort, A. Pol, L. J. Daumann, J. A. Larrabee, A. H. Strayer, M. S. M. Jetten, L. van Niftrik, J. Reimann, H. J. M. Op den Camp, *Biochim. Biophys. Acta* **2019**, *1867*, 595-603.

[33]   W. D. Butt, D. Keilin, *Proc. R. Soc. B* **1962**, *156*, 429-458.

[34]   P. Kalimuthu, L. J. Daumann, A. Pol, H. J. M. Op den Camp, P. V. Bernhardt, *Chem. Eur. J.* **2019**, *25*, 8760-8768.

[35]   H. Singer, R. Steudtner, I. Sottorff, B. Drobot, A. Pol, H. J. M. Op den Camp, L. J. Daumann, *Chem. Commun.* **2023**, *59*, 9066-9069.

[36]   C. Anthony, *Sci. Prog.* **2011**, *94*, 109-137.

[37]   J. A. Mattocks, J. J. Jung, C.-Y. Lin, Z. Dong, N. H. Yennawar, E. R. Featherston, C. S. Kang-Yun, T. A. Hamilton, D. M. Park, A. K. Boal, J. A. Cotruvo, *Nature* **2023**, *618*, 87-93.

[38]   a) C. Anthony, L. Zatman, *Biochem. J.* **1965**, *96*, 808-812; b) D. Widdowson, C. Anthony, *Biochem. J.* **1975**, *152*, 349-356; c) D. T. O'Keeffe, C. Anthony, *Biochem. J.* **1980**, *190*, 481-484; d) S. L. Dales, C. Anthony, *Biochem. J.* **1995**, *312*, 261-265.

[39]   D. J. Day, C. Anthony, in *Methods Enzymol., Vol. 188*, Academic Press, **1990**, pp. 210-216.

[40]   S. M. Gutenthaler, M. T. Phi, H. Singer, L. J. Daumann, in *Methods Enzymol., Vol. 650* (Ed.: J. A. Cotruvo), Academic Press, **2021**, pp. 57-79.

[41]   a) M. Dijkstra, J. Frank, Jr., J. A. Duine, *Biochem J* **1989**, *257*, 87-94; b) T. Harris, V. L. Davidson, *Biochemistry* **1993**, *32*, 4362-4368.

[42]   B. Jahn, N. S. W. Jonasson, H. Hu, H. Singer, A. Pol, N. M. Good, H. J. M. O. den Camp, N. C. Martinez-Gomez, L. J. Daumann, *J. Biol. Inorg. Chem.* **2020**, 199-212.

[43]   M. Beardmore-Gray, D. T. O'Keeffe, C. Anthony, *Microbiology* **1983**, *129*, 923-933.

[44]   a) H. Lv, N. Sahin, A. Tani, *Environ. Microbiol.* **2018**, *20*, 1204-1223; b) S. Kato, M. Takashino, K. Igarashi, W. Kitagawa, *Microbes Environ.* **2020**, *35*; 19128 c) H. Lv, N. Sahin, A. Tani, *Int. J. Syst. Evol. Microbiol.* **2020**.

[45]   a) P. Roszczenko-Jasińska, H. N. Vu, G. A. Subuyuj, R. V. Crisostomo, J. Cai, C. Raghuraman, E. M. Ayala, E. J. Clippard, N. F. Lien, R. T. Ngo, F. Yarza, C. A. Hoeber, N. C. Martinez-Gomez, E. Skovran, *bioRxiv* **2019**, 647677; b) Y. Zhang, S. Sen, D. P. Giedroc, *ChemBioChem* **2020**, *21*, 1955-1967; c) M. Wehrmann, C. Berthelot, P. Billard, J. Klebensberger, *bioRxiv* **2019**, 670216; d) A. M. Ochsner, L. Hemmerle, T. Vonderach, R. Nüssli, M. Bortfeld-Miller, B. Hattendorf, J. A. Vorholt, *Mol. Microbiol.* **2019**, *111*, 1152-1166.

[46]   P. Roszczenko-Jasińska, H. N. Vu, G. A. Subuyuj, R. V. Crisostomo, J. Cai, N. F. Lien, E. J. Clippard, E. M. Ayala, R. T. Ngo, F. Yarza, J. P. Wingett, C. Raghuraman, C. A. Hoeber, N. C. Martinez-Gomez, E. Skovran, *Sci. Rep.* **2020**, *10*, 12663-12663.

[47]   H.-X. Zheng, W.-S. Liu, D. Sun, S.-C. Zhu, Y. Li, Y.-L. Yang, R.-R. Liu, H.-Y. Feng, X. Cai, Y. Cao, G.-H. Xu, J. L. Morel, A. van der Ent, L. Q. Ma, Y.-G. Liu, E. L. Rylott, R.-L. Qiu, Y.-T. Tang, *Environ. Sci. Technol.* **2023**.

[48]   W. Gu, M. Farhan Ul Haque, A. A. DiSpirito, J. D. Semrau, *FEMS Microbiol. Lett.* **2016**, *363*.

[49]   a) W. Gu, J. D. Semrau, *Appl. Microbiol. Biotechnol.* **2017**, *101*, 8499-8516; b) Y. Zheng, J. Huang, F. Zhao, L. Chistoserdova, *mBio* **2018**, *9*, e02430-02417.

[50]   a) S. Masuda, Y. Suzuki, Y. Fujitani, R. Mitsui, T. Nakagawa, M. Shintani, A. Tani, *mSphere* **2018**, *3*, 00462-17; b) E. Skovran, A. D. Palmer, A. M. Rountree, N. M. Good, M. E. Lidstrom, *J. Bacteriol.* **2011**, *193*, 6032-6038.

[51]   L. Gorniak, J. Bechwar, M. Westermann, F. Steiniger, C.-E. Wegner, *Microbiol. spectr.* **2023**, *11*, e00867-00823.

[52]   a) C. J. Coates, H. Decker, *Cell. Mol. Life Sci.* **2017**, *74*, 293-317; b) S. Puig, L. Ramos-Alonso, A. M. Romero, M. T. Martínez-Pastor, *Metallomics* **2017**, *9*, 1483-1500; c) J. Liu, S. Chakraborty, P. Hosseinzadeh, Y. Yu, S. Tian, I. Petrik, A. Bhagi, Y. Lu, *Chem. Rev.* **2014**, *114*, 4366-4469; d) L. Hu, Z. Li, J. Cheng, Q. Rao, W. Gong, M. Liu, Y. G. Shi, J. Zhu, P. Wang, Y. Xu, *Cell* **2013**, *155*, 1545-1555; e) J. J. D. Voss, K. Rutter, B. G. Schroeder, C. E. Barry, *J. Bacteriol.* **1999**, *181*, 4443-4451; f) M. Raschke, L. Bürkle, N. Müller, A. Nunes-Nesi, A. R. Fernie, D. Arigoni, N. Amrhein, T. B. Fitzpatrick, *PNAS* **2007**, *104*, 19637-19642.

[53]   V. Braun, K. Hantke, *Curr. Opin. Chem. Biol.* **2011**, *15*, 328-334.

[54]   a) V. I. Holden, M. A. Bachman, *Metallomics* **2015**, *7*, 986-995; b) C. Ratledge, L. G. Dover, *Annu. Rev. Microbiol.* **2000**, *54*, 881-941; c) J. Francis, H. M. Macturk, J. Madinaveitia, G. A. Snow, *Biochem. J.* **1953**, *55*, 596-607.

[55]   R. C. Hider, X. Kong, *Nat. Prod. Rep.* **2010**, *27*, 637-657.

[56]   a) J.-M. Meyer, D. Hohnadel, F. Hallé, *Microbiology* **1989**, *135*, 1479-1487; b) J. Brandel, N. Humbert, M. Elhabiri, I. J. Schalk, G. L. A. Mislin, A.-M. Albrecht-Gary, *Dalton Trans.* **2012**, *41*, 2820-2834.

[57]   I. Captain, G. J. P. Deblonde, P. B. Rupert, D. D. An, M.-C. Illy, E. Rostan, C. Y. Ralston, R. K. Strong, R. J. Abergel, *Inorg. Chem.* **2016**, *55*, 11930-11936.

[58]   C. D. Hardy, A. Butler, *J. Nat. Prod.* **2019**, *82*, 990-997.

[59]   a) V. Braun, A. Pramanik, T. Gwinner, M. Köberle, E. Bohn, *BioMetals* **2009**, *22*, 3-13; b) M. G. P. Page, *Clin. Infect. Dis.* **2019**, *69*, S529-S537.

[60]   M. Wehrmann, C. Berthelot, P. Billard, J. Klebensberger, *Front. Microbiol.* **2019**, *10*.

[61]   a) F. Gibson, D. I. Magrath, *Biochim. Biophys. Acta - Gen. Subj.* **1969**, *192*, 175-184; b) P. J. Maurer, M. J. Miller, *J. Am. Chem. Soc.* **1982**, *104*, 3096-3101.

[62]   Y.-H. Ho, S.-Y. Ho, C.-C. Hsu, J.-J. Shie, T.-S. A. Wang, *Chem. Commun.* **2017**, *53*, 9265-9268.

[63]   P. A. Turhanen, J. Leppänen, J. J. Vepsäläinen, *ACS Omega* **2019**, *4*, 8974-8984.

[64]   Q. X. Wang, J. King, Phanstiel, *J. Org. Chem.* **1997**, *62*, 8104-8108.

[65]   X. Hu, G. L. Boyer, *BioMetals* **1995**, *8*, 357-364.

[66]   a) M. J. Milewska, A. Chimiak, Z. Głowacki, *J. prakt. Chem.* **1987**, *329*, 447-456; b) E. A. Fadeev, M. Luo, J. T. Groves, *J. Am. Chem. Soc.* **2004**, *126*, 12065-12075.

[67]   R. H. Verschueren, P. Gilles, S. Van Mileghem, W. M. De Borggraeve, *Org. Biomol. Chem.* **2021**, *19*, 5782-5787.

[68]   E. A. Fadeev, M. Luo, J. T. Groves, *Bioorg. Med. Chem. Lett.* **2005**, *15*, 3771-3774.

[69]   W. R. Harris, C. J. Carrano, K. N. Raymond, *J. Am. Chem. Soc.* **1979**, *101*, 2722-2727.

[70]   a) M. Bau, N. Tepe, D. Mohwinkel, *Earth. Planet. Sci. Lett.* **2013**, *364*, 30-36; b) D. Bellotti, M. Remelli, *Molecules* **2021**, *26*.

[71]   W. Cheung, M. Patel, Y. Ma, Y. Chen, Q. Xie, J. V. Lockard, Y. Gao, H. He, *Chem. Sci.* **2016**, *7*, 5192-5199.

[72]   a) B. Schwyn, J. B. Neilands, *Anal. Biochem.* **1987**, *160*, 47-56; b) D. B. Gladilovich, V. Kubáň, L. Sommer, *Talanta* **1988**, *35*, 259-265; c) D. B. Gladilovich, V. Kuban, *Chem. Pap.* **1988**, *42*, 607-620.

[73]   A. M. Zytnick, N. M. Good, C. C. Barber, M. T. Phi, S. M. Gutenthaler, W. Zhang, L. J. Daumann, N. C. Martinez-Gomez, *bioRxiv* **2022**, 2022.2001.2019.476857.

[74]   M. Y. Andrews, O. Duckworth, *BioMetals* **2016**, *29*, 1085-1095.
[75]   K. Barbeau, G. Zhang, D. H. Live, A. Butler, *J. Am. Chem. Soc.* **2002**, *124*, 378-379.
[76]   R. J. Bergeron, G. Huang, R. E. Smith, N. Bharti, J. S. McManis, A. Butler, *Tetrahedron* **2003**, *59*, 2007-2014.
[77]   R. A. Gardner, R. Kinkade, C. Wang, Phanstiel, *J. Org. Chem.* **2004**, *69*, 3530-3537.
[78]   R. Goswami, M. G. Moloney, *Chem. Commun.* **1999**, 2333-2334.
[79]   L. J. Daumann, D. S. Tatum, C. M. Andolina, J. I. Pacold, A. D'Aléo, G.-l. Law, J. Xu, K. N. Raymond, *Inorg. Chem.* **2016**, *55*, 114-124.
[80]   O. Baars, F. M. M. Morel, X. Zhang, *Environ. Microbiol.* **2018**, *20*, 1667-1676.
[81]   M. Wehrmann, P. Billard, A. Martin-Meriadec, A. Zegeye, J. Klebensberger, X. Zhang, D. K. Newman, *mBio* **2017**, *8*, e00570-00517.
[82]   M. S. Islam, A. Aryasomayajula, P. R. Selvaganapathy, *Micromachines* **2017**, *8,* 83.
[83]   N. A. Danaf, J. Kretzschmar, B. Jahn, H. Singer, A. Pol, H. J. M. Op den Camp, R. Steudtner, D. C. Lamb, B. Drobot, L. J. Daumann, *PCCP* **2022**, *24*, 15397-15405.
[84]   J. A. Cotruvo, in *Methods Enzymol., Vol. 650* (Ed.: J. A. Cotruvo), Academic Press, **2021**, pp. xiii-xv.
[85]   M. J. Todd, J. Gomez, *Anal. Biochem.* **2001**, *296*, 179-187.
[86]   a) A. J. Bard, L. R. Faulkner, *Electrochemical methods: fundamentals and applications*, John Wiley & Sons, **2000**; b) S. Treimer, A. Tang, D. C. Johnson, *Electroanalysis* **2002**, *14*, 165-171.
[87]   B. J. Taft, M. O'Keefe, J. T. Fourkas, S. O. Kelley, *Anal. Chim. Acta* **2003**, *496*, 81-91.
[88]   P. Cioni, G. B. Strambini, *Biophys. J.* **2002**, *82*, 3246-3253.
[89]   B. Jahn, Functional investigation of the lanthanide-dependent methanol dehydrogenase from methylacidiphilum fumariolicum SolV, LMU München, **2020**.
[90]   A. Krężel, W. Bal, *J. Inorg. Biochem.* **2004**, *98*, 161-166.
[91]   Y. Mie, C. Yamada, T. Uno, S. Neya, F. Mizutani, K. Nishiyama, I. Taniguchi, *Chem. Commun.* **2005**, 250-252.
[92]   A. Oubrie, H. J. Rozeboom, K. H. Kalk, E. G. Huizinga, B. W. Dijkstra, *J. Biol. Chem.* **2002**, *277*, 3727-3732.
[93]   Z.-X. Xia, W.-W. Dai, Y.-N. He, S. A. White, F. S. Mathews, V. L. Davidson, *J. Biol. Inorg. Chem.* **2003**, *8*, 843-854.
[94]   a) N. M. Good, R. S. Moore, C. J. Suriano, N. C. Martinez-Gomez, *Sci. Rep.* **2019**, *9*, 4248; b) J. M. Cox, D. J. Day, C. Anthony, *Biochim. Biophys. Acta* **1992**, *1119*, 97-106.
[95]   H. Guo, S. A. Naser, G. Ghobrial, Phanstiel, *J. Med. Chem.* **2002**, *45*, 2056-2063.
[96]   H. Singer, R. Steudtner, I. Sottorff, B. Drobot, A. Pol, H. J. M. Op den Camp, L. J. Daumann, *Chem. Commun.* **2023**.
[97]   N. F. Delaney, M. E. Kaczmarek, L. M. Ward, P. K. Swanson, M. C. Lee, C. J. Marx, *PLoS One* **2013**, *8*, e62957.
[98]   U. K. Laemmli, *Nature* **1970**, *227*, 680-685.